Leibniz-Institut für Ostseeforschung Warnemünde

Universität Rostock Traditio et Innovatio

Exploring the Nitrogen cycle of the Amazon shelf and river plume

Cumulative dissertation for the award of the academic degree Doctor rerum naturalium (Dr. rer. nat.) of the Faculty of Mathematics and Natural Sciences of the University of Rostock

Submitted by

Noémie Joseph dit Choisnard

Supervisor:
Prof. Dr. Maren Voß

Thesis committee:

Prof. Dr. Heide Schulz-Vogt,
Prof. Dr. Joseph Montoya,
Dr. Nicolas N. Duprey

Rostock, 2024

https://doi.org/10.18453/rosdok_id00005020

Date of submission: 19.02.2024

Date of public defense: 28.06.2024

1. Referee:

Prof. Dr. Maren Voss

Leibniz Institute for Baltic Sea Research Warnemuende

2. Referee:

Prof. Dr. Bess B. Ward

Princeton University

3. Referee:

Prof. Dr. Jack Middelburg

Utrecht University

Table of content

Acknowledgments

First of all, I'd like to thank my supervisor, Maren Voss, for giving me the opportunity to join her working group as a PhD student. Your guidance throughout my journey, and your constant enthusiasm for new results made working with you thrilling. I am extremely grateful for all the freedom you gave me within the project. You gave me the chance to be part of four incredible expeditions, across the Atlantic to the Amazon estuary, twice in the Baltic Sea and as far as Patagonia and I will never thank you enough for that. Here, also a big thanks goes to Solveig Kühl, for moving heavens and earth to make it possible for me to change at the last minute the plane ticket to Chile that I had wrongly booked. I would also like to thank my thesis committee, Heide Schulz-Vogt, Joseph Montoya and Nicolas Duprey, for their advice and their support any time I needed it. A special thanks to Nicolas, and Anne Lorrain; thank you sharing with me your passion for science, which motivated me to do a PhD.

To the N-cycle working group, thank you for welcoming me, and for all the fruitful discussions professional of course, but also personal. Here, I'd like to give some special thanks to Iris Liskow, whose technical expertise was invaluable. Thank you for your help, in the lab, during all the endless cruise preps, and for always making sure that we would have enough liquid nitrogen for the mass spectrometer! I would also like to thank Jacqueline Umbricht, for helping me settle in Rostock, for always answering my last-minute questions, and for all the discussions at the office. An office that wouldn't have been the same without Joachim Dippner, whom I'd like to thank for all of the ideas he had to help me get around obstacles. Also, thanks for letting Jacqueline and I decorate the office.

I want to thank Christian Burmeister for helping me with all the nutrient measurements, and also for being an amazing friend. Going on cruises and working with you in the lab was the highlight of my day. Also, thanks to Natalie Loick-Wilde, Anne Köhler, Christian Meeske, Volker Mohrlhoz, Toralf Heene, Uwe Hehl, Vincent, Sören, Mira, Ina, Josi and all the people who made going at sea unique and so much fun each time. A special thanks to Ajit Subramaniam, for always being in a good mood and for staying up all night to keep me company as I was finishing an experiment, and for all the valuable initiating me to the basics of ocean color and attenuation coefficient data processing.

I also want to thank my co-authors of the publications that were part of this thesis: Claudia Frey, Emma Burtscher, Stefan Foster, Matthias Moros, Theodor Sperlea, Michael Böttcher, Iris Schmiedinger, Moacyr Araujo. I also thank Christiane Hassenrück, who was never tired of discussing statistics with me, and for keeping me company when we were staying late at the institute. A big thank you to Ana Fernandez Carrera, for all your mental support throughout my PhD, for the coffee breaks, and for all the ideas we shared.

This acknowledgment section wouldn't be complete without mentioning Heike, Kaylim, Gabriela, Gizem, Nadya, Anna, Erik, Conor, Connor, and all the members of the coffee at late three group, for all the fun we had at the Pleitergeier. I have laughed so much thanks to you, I will never forget the time we've had together here in Rostock. Connor, Josephine, and of course Rosie, Winston, and Dela, for being such good friends here. Elise, Guillaume, and Magali, thank you for being yourself, you are among the funniest people I know and I am extremely glad that this adventure we started during our master's degree continues today. Thanks to you, this PhD was "not the ocean to drink". Most importantly I want to thank my parents for giving me the strength to do this PhD, Agathe Jeanne and Zoé, for all the memes and senseless hilarious calls. And thanks to my partner, David for your love, patience, and support, thank you for being there for me, even late at night. Thank you all for your encouragement in hard times, which made this thesis possible.

Summary

Nitrogen (N) plays a crucial role in the biochemical processes that sustain ecosystems, making its cycle relevant for comprehending global biogeochemistry and climate dynamics. Human activities, especially since the advent of the Haber-Bosch process, have significantly altered the global N cycle, leading to increased N fluxes into reservoirs such as the ocean. Coastal zones are particularly vulnerable to these increased N fluxes, which may have profound implications for the ecosystem's health. In this context, the cycling of N in regions influenced by the Amazon River, the world's largest river by water discharge, remains largely understudied despite its far-reaching impact. However, the Amazon Basin is undergoing drastic changes due to climate change, deforestation, and damming, raising concerns about the potential impact on dissolved inorganic nitrogen (DIN) and organic matter (OM) loads to the estuary. In response to these challenges, the German Research Foundation (DFG) funded the MeNARP (metabolism of nitrogen in the Amazon River Plume) Project, with the aim of establishing baseline knowledge about N forms' use and transformation along the plume. Sediments on the shelf are a crucial component, potentially acting as either a source or sink of DIN based on OM preservation and remineralization pathways. Previous studies indicated that the Amazon shelf sediments primarily acted as a sink for N, with denitrification as the main loss process. The analysis of short sediment cores, together with cores incubations, revealed intense recycling of terrestrial material most likely via ammonification and nitrification of organic N. Despite changes in the Amazon Basin since previous studies, nitrification remains balanced by denitrification in the sediments, preventing DIN or nitrous oxide from diffusing out. In the water column, nitrification is also likely a dominant pathway for N, as confirmed by the analysis of nitrate and water N and oxygen (O) isotopes. While denitrification might be at play at the sediment-water interface, it does not appear to be significant in the plume layer. The highest nitrification rates are observed at the river mouth, coinciding with elevated turbidity, nitrite, and phosphate concentrations. Within 200 km from the river mouth, nitrification rates decline, accompanied by nitrate depletion, likely because of phytoplankton uptake. The acquired knowledge in this thesis allowed us to draw the first N budget for the Amazon and neighboring Pará river mouths, based on rates of N cycle processes. N budgeting highlighted the relevance of N export to plume regions with reduced light limitations for carbon uptake. This comprehensive exploration of nitrogen dynamics in the Amazon Basin sheds light on the intricacies of the nitrogen cycle in one of the world's most critical ecosystems.

1 | Introduction

Nitrogen cycle overview

In the late 18th century, Lavoisier suggested naming the 7th element of the periodic table "azote", or "no life", as it usually seems unreactive. Centuries of research later, we now know that nitrogen (N) is an essential element for life. Required in a large array of biomolecules including proteins, nucleic acids, and even chlorophyll, N is the fourth most abundant element in biomass. N is everywhere and yet, in the ocean, more than 90 % of all N is inert dissolved dinitrogen (N_2; Gruber 2008), and biologically available N is a paramount limiting nutrient (Moore et al. 2013). In the sunlit ocean, phytoplankton uses N and carbon dioxide (CO_2) for growth (Falkowski 1997; Gruber and Sarmiento 2002), and the biomass produced can be later transferred to the deep ocean. This carbon flux, referred to as the biological pump, is estimated to represent more than three times the atmospheric carbon pool (Gruber and Sarmiento 2002). Processes controlling the amount and form of N available for life are thus fundamentally impacting global biogeochemistry and climate (Fowler et al. 2013). Such biogeochemical processes are part of the N cycle and can be divided between budgetary pathways, which encompass transformations governing inputs and output of biologically available N, and internal cycling, which groups processes ruling the speciation of N (Table 1) without altering the size of the N pool.

Table 1. N forms in the N cycle.

Form	Formula	Oxidation state
Organic N, ammonia, ammonium	R-NH_3, NH_3 ,NH_4^+	-III
Hydrazine	N_2H_4	-II
Hydroxylamine	NH_2OH	-I
Dinitrogen	N_2	0
Nitrous oxide	N_2O	+I
Nitric oxide	NO	+II
Nitrite, nitrous acid	NO_2^-, HNO_2	+III
Nitrogen dioxide	NO_2	+IV
Nitrate, nitric acid	NO_3^-, HNO_3	+V

N_2 fixation

In contrast to nutrients that originate from geochemical processes such as weathering, most biologically available N also derives from biological N_2 fixation (step 1, Figure 1). During this process, N_2 fixers (diazotrophs) reduce N_2 to ammonia and ammonium (NH_3, NH_4^+; Gruber and Sarmiento 1997; Gruber 2004). Because the triple bond of N_2 is very stable N_2 fixation is a high energy-requiring process that depends upon the nitrogenase, a complex metalloenzyme with high iron requirements (Hutchins and Sañudo-Wilhelmy 2022). The nitrogenase is usually composed of two proteins: the molybdenum-iron protein (dinitrogenase, encoded in the *nifDK* genes; Table 2) and the iron protein (dinitrogenase reductase, encoded in the *nifH* gene). It can occur in several other forms: the iron-only nitrogenase (encoded in the *anf* gene) and the vanadium nitrogenase (encoded in the *vnf* gene; Eady 1996; Seefeldt et al. 2009; Rees et al. 2015; Sippel and Einsle 2017), although only a few diazotrophs possess these alternative forms (McRose et al. 2017). The composition of the nitrogenases results in the limitation of N_2 fixation by a variety of factors such as trace metals availability, temperature, oxygen, and nutrient concentrations (Pajares and Ramos 2019).

But even though N_2 essentially represents an unlimited reservoir of N, only a small group of diverse bacteria and archaea are capable of diazotrophy. They typically have a low abundance (Gaby and Buckley 2015), and metagenome studies suggest that only about 15 % of prokaryotic species are known to be or could be N_2 fixers. *Trichodesmium*, a bloom-forming non-heterocystous filamentous cyanobacteria has been studied for decades (Dugdale et al. 1961), and represents the most important currently known diazotroph community in marine systems together with other cyanobacteria, such as heterocystous filamentous cyanobacteria (e.g., *Aphanizomenon*, *Nodularia*), diatom symbiotic cyanobacteria (e.g., *Richelia*), and unicellular cyanobacteria (Zehr and Turner 2001; Capone et al. 2005; Foster et al. 2011). These organisms are typically found in N-poor waters, although other non-cyanobacterial diazotrophs, predominantly heterotrophic Proteobacteria, have been found in aphotic, N-rich, and cold environments, expanding the ecological niche of N_2 fixation to the deep-ocean, sediments, and coastal waters in addition to open ocean surface waters (Sohm et al. 2011; Bonnet et al. 2013; Bentzon-Tilia et al. 2015; Gier et al. 2017). Amongst these are sulfate-reducing bacteria that are long known to be potential N_2 fixers (Gandy and Yoch 1988; Zehr et al. 1995).

N assimilation

Despite the low abundance of N_2 fixers, N_2 fixation can supply up to 50 % of the new N in oligotrophic environments (Karl et al. 1997), providing an invaluable N source, which along with nitrate (NO_3^-), NH_4^+, or some organic species (R-NH_3), can be assimilated into phytoplankton or microbe biomass (step 2, Figure 1). NO_3^- assimilation is more energetically costly than NH_4^+ assimilation because of the oxidation state of the former (Table 1). Instead of simple diffusion or transport into the cell and incorporation into the biomass (Leigh and Dodsworth 2007), NO_3^- first needs to be reduced to NH_4^+, a two-step process carried out by nitrate and nitrite reductases. Consequently, NH_4^+ is usually the preferred form of inorganic N for growth (Glibert et al. 2016), and involves the incorporation of NH_3 into amino acids by the enzymes glutamine synthetase and glutamate synthase following NH_4^+ transport into the cell (Table 2).

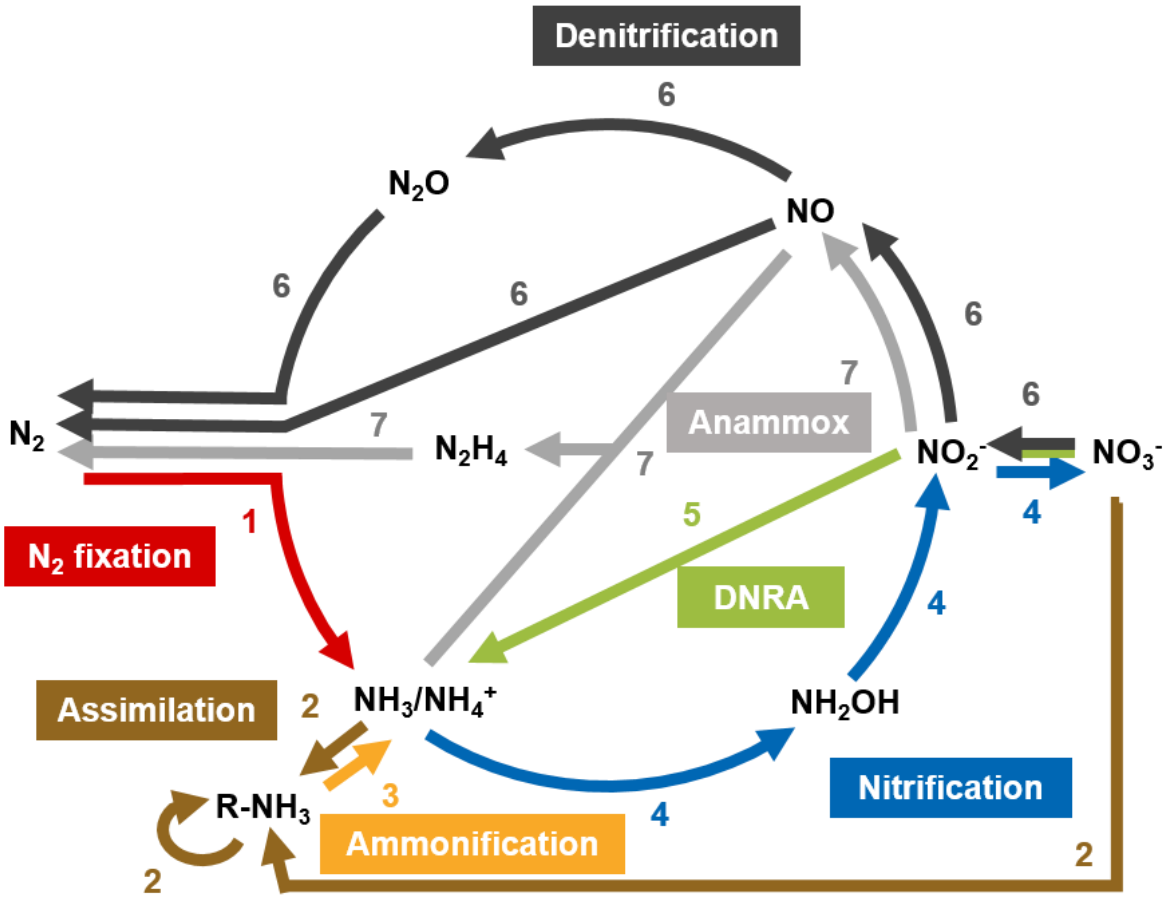

Figure 1. Schematics of the N cycle. Dinitrogen fixation (step 1) constitutes the main step for the creation of biologically available N. Together with N assimilation pathways (step 2), it represents anabolic processes, whereas ammonification (step 3) nitrification (step 4), DNRA (step 5) denitrification (step 6), and anammox (step 7) derive from catabolic processes. Modified from Zhang et al. (2020).

Table 2. Main marine N-cycling pathways, chemical reactions, and relevant genes. Adapted from Zehr and Kudela (2011), Pajares and Ramos (2019), and Zhang et al. (2020) and references therein.

Reaction name	Chemical reaction	Genes
Dinitrogen fixation	$N_2 + 8H^+ + 8e^- + 16ATP \rightarrow 2NH_3 + H_2 + 16ADP + 16P_i$	*nifH*, *nifDK,* anf, vnf
Ammonium assimilation	$NH_3/NH_4^+ \rightarrow R\text{-}NH_3$	*gdhA*,*gdhA*
Assimilatory nitrate and nitrite reduction	$NAD(P)H + H^+ + NO_3^- + 2e^- \rightarrow NO_2^- + NAD(P)^+ + H_2O$	*nasA, nasB, narB*
	6 ferredoxin (red) + 8 H^+ + 6 e^- + $NO_2^- \rightarrow NH_4^+$ + 6 ferredoxin (ox) + $2H_2O$	*nirA*
Ammonification	$R\text{-}NH_3 \rightarrow NH_3/NH_4^+$	*gltB*
Ammonium oxidation	$NH_3 + O_2 + 2H^+ + 2e^- \rightarrow NH_2OH + H_2O$	*amoC*, *amoA, amoB*
	$NH_2OH + H_2O \rightarrow HNO_2 + 4H^+ + 4e^-$	hao
	$0.5O_2 + 2H^+ + 2e^- \rightarrow H_2O$	
Nitrite oxidation	$2NO_2^- + H_2O \rightarrow NO_3^- + 2H^+ + 2e^-$	*nxrAB*
	$2H^+ + 2e^- + 0.5O_2 \rightarrow H_2O$	
Dissimilatory nitrate reduction to ammonia	$NO_3^- + 2H^+ + 4H_2 \rightarrow NH_4^+ + 3H_2O$	*nir*, nar, *nap*, *nrfABCDE*
	$NO_3 \rightarrow NO_2^-$	*narG, napA*
	$NO_2 \rightarrow NH_4^+$	*nrfA*
Denitrification	$(CH_2O)_{106}(NH_3)_{13}+H_3PO_4 + 94.4HNO_3 \rightarrow 106CO_2 + 39.2N_2 + 16NH_3 + 16HNO_2+H_3PO_4+145.2H_2O$	
	$NO_3 \rightarrow NO_2^-$	*narDGHIJ, napABDE*
	$NO_2^- \rightarrow NO$	*nirK, nirS*
	$NO \rightarrow N_2O$	*cnorB, qnorB*
	$N_2O \rightarrow N_2$	*nosZ*
Anaerobic ammonia oxidation	$NH_4^+ + 1.146NO_2^- + 0.071HCO_3^- + 0.0057H^+ \rightarrow 0.986N_2 + 0.161NO_3^- + 2.003H_2O + 0.071CH_{1.74}O_{0.31}N_{0.20}$	Over 200 genes involved in anammox metabolism (Strous et al. 2006)
	$NO_2^- + 2H^+ + e^- \rightleftarrows NO + H_2O$	*NirS*
	$NO + NH_4^+ + 2H^+ + 3e^- \rightleftarrows N_2H_4 + H_2O$	
	$N_2H_4 \rightleftarrows N_2 + 4H^+ + 4e^-$	

Mineralization and nitrification

The biomass-derived N introduced to the system as particulate organic nitrogen (PON) is eventually returned into the dissolved N pool as NH_4^+ via remineralization, or ammonification (step 3, Figure 1). This process is carried out by heterotrophic microbes and can occur in both oxic and anoxic environments. The PON is first transformed into dissolved organic nitrogen (DON), which is ultimately broken down further to NH_4^+. In the presence of dioxygen (O_2), this NH_4^+ can be further oxidized to NO_3^- as part of the nitrification pathway (step 4, Figure 1).

The first step of this process is itself split in three, where first, NH_3 is converted to hydroxylamine (NH_2OH; Table 1), a process catalyzed by the ammonia monooxygenase (AMO, encoded in the *amoA, B* and *C* genes; Table 2). The NH_2OH is then converted to nitric oxide (NO; Table 1), a step catalyzed by the hydroxylamine oxidoreductase (HAO, encoded in the *hao* gene; Table 2), and ultimately to NO_2^- (Kozlowski et al. 2016; Caranto and Lancaster 2017). For long, ammonia-oxidizing bacteria (AOB, e.g. proteobacteria *Nitrosomonas* and *Nitrosospira*) were thought to be the main ammonia-oxidizers, until the discovery of ammonia-oxidizing archaea (AOA, e.g. thaumarchaeon *Nitrosopumilus maritimus*), a much more abundant and widespread group of ammonia-oxidizers (Ward 1996; Könneke et al. 2005; Wuchter et al. 2006). The pathways for NH_3 oxidation to NO_2^- by AOA still lack understanding, as no *hao* gene has been identified in AOA genomes, suggesting that AOA might use an unknown enzyme for NH_2OH oxidation (Vajrala et al. 2013; Kozlowski et al. 2016), or that NH_2OH is not the intermediate product in archaeal NH_3 oxidation (Walker et al. 2010).

Nitrite oxidizing bacteria (NOB, e.g., *Chloroflexi*, *Nitrospirae*, *Nitrospinae*, proteobacteria *Nitrobacter*; Daims et al. 2016) drive the second step, to oxidize NO_2^- to NO_3^-. This step is catalyzed by the nitrite oxidoreductase (NXR, encoded in the *nxrAB* genes; Table 2). Some marine NOB are mixotrophs also capable of using urea to produce NH_3 (Koch et al. 2015). Until recently, no organism was known to be capable of performing both steps (Ward 2008). However, a group of proteobacteria named Comammox (*Nitrospira spp.*) that fully oxidize NH_4^+ to NO_3^- was discovered in marine wetlands, estuaries, and coastal waters (Xia et al. 2018; Sun et al. 2020). As an alternative to NH_3, some nitrifiers can also use organic N as a substrate (Kitzinger et al. 2019; Damashek et al. 2019). Many species have also been demonstrated to be capable of heterotrophic nitrification, using organic carbon instead of CO_2

as a carbon source, though the mechanistic of this process still lacks understanding (Qin et al. 2014; Martikainen 2022).

Nitrification is one of the most dominant processes in the dark mid-depths of the ocean, and usually peaks just below the euphotic zone (Wuchter et al. 2006; Bristow et al. 2015) or in the most turbid part of estuaries and river plumes (Damashek et al. 2016). As it is a recycling pathway, nitrification only influences the net N pool of the ocean by small losses to the gaseous pool of nitrous oxide (N_2O) under low oxygen availability (Stein 2019), and mainly transforms N among different forms, providing substrate for other N cycling pathways.

Dissimilatory Nitrate Reduction to Ammonium

In anoxic environments, NO_3^- can be reduced to NO_2^- and ultimately NH_4^+ during dissimilatory nitrate reduction to ammonium (DNRA; step 5, Figure 1). This process is mainly driven by chemoheterotrophs, although some studies suggest that it can be autotrophic via the use of sulfide or ferrous iron (Robertson et al. 2016; Slobodkina et al. 2017). It thus constitutes another recycling pathway for N, although incomplete DNRA may also produce N_2O (Kelso et al. 1997). The first step is the reduction of NO_3^- to NO_2^-. It can be catalyzed by two enzymes, the NarGHI (encoded in the *narG* gene; Table 2), or the periplasmic nitrate reductase complex (NapAB, encoded in the *napA* gene; Table 2), although the latter one is mainly present in Gram-negative bacteria (Moreno-Vivián et al. 1999; Simon and Klotz 2013). The heterotrophic reduction of NO_2^- to NH_4^+ is catalyzed by the cytochrome C nitrite reductase (ccNIR, encoded in the *nrfA* gene; Table 2), while the chemolithotrophic pathway can be catalyzed by two enzymes, the octaheme tetrathionate reductase (OTR) or the octaheme cytochrome C nitrite reductase (ONR; Tikhonova et al. 2006; Atkinson et al. 2007).

A variety of prokaryotes and eukaryotes can perform DNRA (Kamp et al. 2015; Kuypers et al. 2018). Diatoms are known to perform DNRA to survive in anoxic sediments (Kamp et al. 2011). In sulfide-rich sediment, nitrate-accumulating sulfur bacteria (e.g., *Thioploca spp.*, *Thiomargarita spp.*, and *Beggiatoa spp.*) are also capable of carrying out DNRA (Jørgensen and Nelson 2004; Preisler et al. 2007). DNRA is usually favored over denitrification (an N removal pathway, discussed below) in environments with high organic C/NO_3^- ratios (King and Nedwell 1985) and sulfidic conditions (Caffrey et al. 2019). DNRA might also be less sensitive to oxygen than denitrification, allowing for the spatial distribution of both processes along the oxygen gradient (Yang et al. 2015). DNRA is thus often

predominant in eutrophic environments (e.g., coastal waters and sediments) where it can account for up to 92 % of the total NO_3^- reduction (Jäntti and Hietanen 2012; Hylén et al. 2022).

Denitrification

In contrast to DNRA, denitrification converts NO_3^- and NO_2^- to N_2 (step 6, Figure 1), thus constituting the proximate N loss pathway from marine ecosystems. Most denitrifiers are heterotrophic bacteria (such as the genera *Pseudomonas* and *Marinobacter*), and while most denitrification occurs under anoxic conditions, most denitrifiers can be aerobe (Ji et al. 2015). During denitrification, denitrifiers use NO_3^- as an electron acceptor for respiration to NO_2^- (see the DNRA section), which is, in the case of complete denitrification, followed by the stepwise reduction of NO_2^- to NO, N_2O, and N_2 (Zumft 1997). While the complete pathway exists in many cultivated denitrifying bacteria, many microorganisms only possess part of the denitrification genes (Graf et al. 2014).

NO_2^- reduction to NO is performed by two enzymes, which are isofunctional, although structurally unrelated (Simon and Klotz 2013): an oxygen-sensitive copper-containing nitrite reductase (CuNIR, encoded in the *NirK* gene; MacPherson 2007) and a cytochrome-containing iron protein (cdNIR, encoded by the *NirS* gene; Table 2). The subsequent conversion of NO to N_2O is mainly catalyzed by the nitric oxide reductases (cNOR or qNOR, encoded in the *cnorB* and *qnorB* gene, respectively; Simon and Klotz 2013). Due to the toxicity of NO, many organisms are capable of NO reduction, including non-denitrifying ones, probably using it as a detoxifying pathway, some of them leading to N_2O production (Jones et al. 2008; Wu et al. 2020). The conversion of N_2O to N_2 is the final step of denitrification, which requires a complex copper enzyme, the nitrous oxide reductase (N_2OR, encoded in the *nosZ* gene). Interestingly, this enzyme is found in two clades (Jones et al. 2013): clade I mainly includes Proteobacteria, and Clade II consists of a more diverse group of archaea and other microorganisms, many of which lack complete denitrification pathways (Sanford et al. 2012; Jones et al. 2013).

Although it is mainly known as a heterotrophic process, complete denitrification is also coupled to a cryptic sulfur cycle performed by autotrophic sulfide oxidizing bacteria. The current understanding is that this process likely plays a significant role in benthic microbial mats (Bowles et al. 2012), and ongoing discussions exist surrounding the broader implications of this process in other environments, such as oxygen minimum zones (Johnston et al. 2014). The partial denitrification pathway performed by AOA and AOB is referred to as nitrifier-denitrification, where NO_2^- is reduced to N_2O via NO under suboxic or anoxic conditions

(Goreau et al. 1980; Wrage et al. 2001). This process has been observed in the lower euphotic zone of the open ocean (Wilson et al. 2014) and oxygen minimum zones (Löscher et al. 2012; Bourbonnais et al. 2017). Denitrification was also discovered in eukaryotic microbes in marine sediments (Risgaard-Petersen et al. 2006) where rates attributed to foraminiferan equal those of bacterial denitrification (Piña-Ochoa et al. 2010; Prokopenko et al. 2011; Bernhard et al. 2012). In the water column, fungal N_2O production has been discovered (Peng and Valentine 2021), but remains to be confirmed for other eukaryotes.

Denitrification is, to date, the only known pathway for biological N_2O removal, although similarly to DNRA, incomplete denitrification under anoxic or low-O_2 conditions can release N_2O into the environment (Dalsgaard et al. 2014). Because denitrification is a modular process, the microbial community composition may be one of the main drivers of the fate of N and the yield or removal of N_2O. Sulfidic conditions are also known to lead to high N_2O accumulation (Senga et al. 2006), as sulfide inhibits the final steps of denitrification. Other factors, such as oxygen concentrations and the quantity and quality of the organic matter supply control the denitrifiers' distribution and subsequent denitrification rates (Ward 2008; Eyre et al. 2013). As mentioned above, low sulfide concentrations and low C/NO_3^- ratios favor denitrification over DNRA, and fresh organic matter with high C/N ratios favor denitrification over anammox (see below; Babbin and Ward 2013; Chang et al. 2014). As a result, denitrification is usually restricted to suboxic and anoxic environments, such as oxygen minimum zones (Ward et al. 2009), sediments (Voss et al. 2023, and references therein), and groundwater (Harris et al. 2022), making it a major N removal process in coastal zones (Damashek and Francis 2018, and references therein).

Anammox

The second pathway for loss of biologically available N is anaerobic ammonium oxidation, or "anammox", which converts NH_4^+ and NO_2^- to N_2 under low O_2 conditions (step 7, Figure 1; Table 2). NO_2^- is reduced first to NO, a step likely catalyzed by the enzymes encoded in the *NirS* gene (Strous et al. 2006; Van De Vossenberg et al. 2008). The subsequent production of hydrazine (N_2H_4; Table 1) from NH_4^+ and NO is catalyzed by the hydrazine synthase (HZS). Finally, the N_2H_4 is oxidized to N_2 by the hydrazine dehydrogenase (HDH), also known as hydrazine oxidase (HZO) (Jetten et al. 2009; Kartal et al. 2011; Simon and Klotz 2013).

This process, initially discovered in wastewater treatment plants (van de Graaf et al. 1995), is widespread in coastal sediment and the great depths in the water column (Trimmer and Engström 2011; Thamdrup 2012). Anammox bacteria are chemoautotrophs belonging to the phylum *Planctomycetes* and rely on remineralization to obtain their substrate, a substrate that they partly share with DNRA and denitrification organisms. Anammox should also indirectly depend on the supply of organic matter (Ward 2013; Babbin et al. 2014), although the regulating mechanisms of this process still lack understanding. Anammox bacteria are found to be present in a variety of environments, such as oxygen minimum zones (Bandekar et al. 2018), eutrophic bays (Lisa et al. 2014), estuarine sediments (Nicholls and Trimmer 2009), fjord sediments (Brandsma et al. 2011), Arctic sediments (Rysgaard et al. 2004), deep-sea sediments (Hong et al. 2011), and hydrothermal vents (Byrne et al. 2009). Anammox coupled with the reduction of sulfate (Sulfammox) and ferric iron (Feammox) has also been recently reported in coastal sediments (Rios-Del Toro et al. 2018).

Nitrogen inputs in coastal zones

Nitrogen sources - the role of rivers

All biotic and abiotic transformations among the multiple forms of N drive the N cycling between various reservoirs. In the marine environment, there is often a strong difference in N availability between the surface and the deep ocean, as well as between coastal zones and the open ocean, with greater N concentrations in coastal ecosystems. This is due to several additional N sources driven by physical processes (e.g. river and groundwater runoff, upwelling, tidal and wind-driven mixing), which together with the relative shallowness of the coastal zone in comparison to oceanic systems, allows for a much easier N resupply from sinking organic matter remineralization (Sarmiento and Gruber 2006). As such, coastal zones are often referred to as productive ecosystems that can host at least a quarter of annual global primary production (Sharples et al. 2017).

Coastal ecosystems are influenced by at least six allochthonous sources of N (Figure 2), aside from the autochthonous N derived from primary production. Atmospheric deposition and N_2 fixation are sources that can also be found in oceanic environments estimated to supply globally ~30 and up to 160 Tg N y^{-1} (Jickells et al. 2017). Inputs from groundwater and intertidal wetlands are much smaller, about 0.4 and up to 1.5 Tg N y^{-1}, respectively (Alongi 2013; Santos et al. 2021). Riverine inputs are estimated to be larger, at least 40 Tg N y^{-1}

(Seitzinger et al. 2010). While this input is mostly geographically constrained at the river mouth, large river plumes can be globally important sources of nutrients and particles for regions far beyond the estuary (Subramaniam et al. 2008; Weber et al. 2017). However, the magnitude of the riverine N input is largely determined by the extent of remineralization processes within coastal zones (Mulholland et al. 2008; Asmala et al. 2017; Wells et al. 2018), which in turn strongly influences primary production and subsequent CO_2 sequestration (Bernhardt et al. 2017). As the balance between sources, recycling, and consumption underlies whether an estuary is a sink or a source of N (and of carbon) for the open ocean, studying riverine-derived N becomes relevant to understanding the productivity of adjacent marine ecosystems.

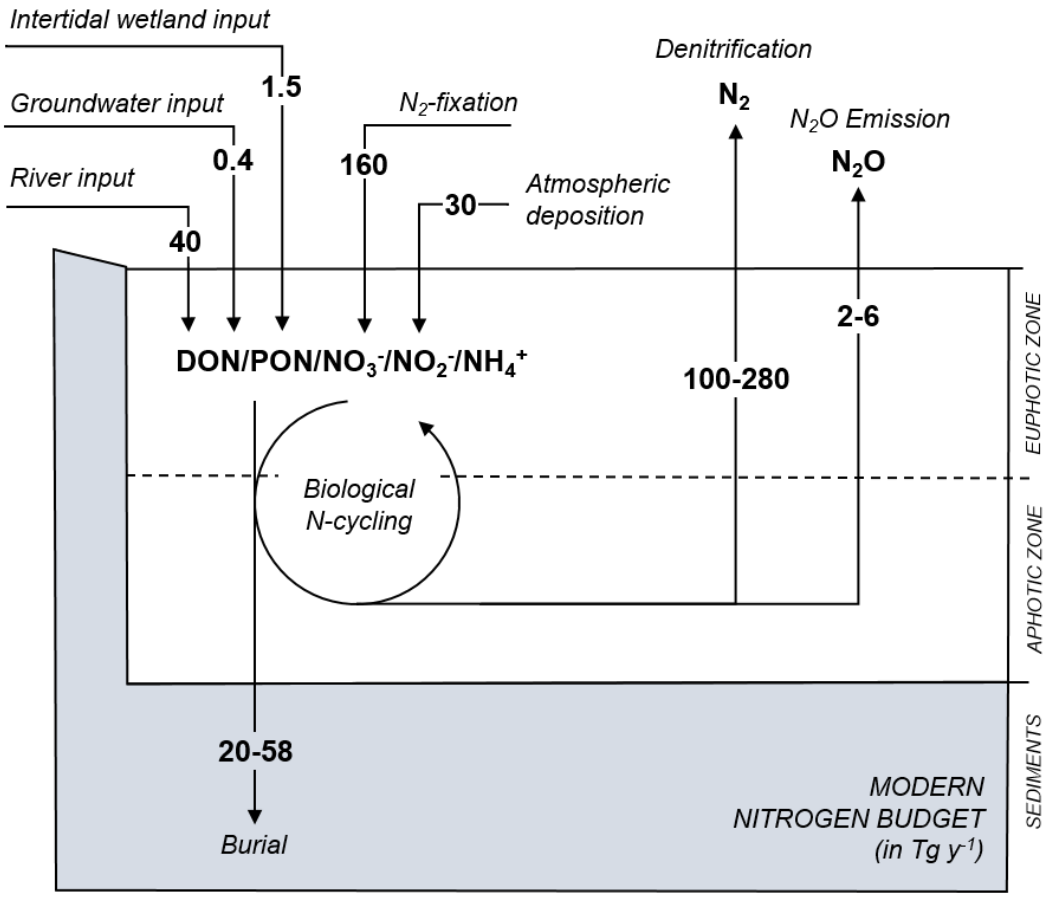

Figure 2. N fluxes to coastal zones, adapted from Gruber (2008). Fluxes are given in Tg N y^{-1}. Inputs to coastal zones encompass intertidal wetland inputs (Alongi 2013), groundwater (Santos et al. 2021), and river inputs (Seitzinger et al. 2010; Jickells et al. 2017), rivers usually supplying 44 % of dissolved inorganic nitrogen (DIN), 25% of dissolved organic nitrogen (DON) and 32% of particulate organic nitrogen (PON) (Seitzinger et al. 2010). N_2-fixation and atmospheric deposition are also major sources of N for surface waters. While the internal N-cycle recycles N among its various forms, burial, denitrification, and N_2O emission represent sinks of N for the marine environment (Fowler et al. 2013; Jickells et al. 2017).

Asmala et al (2017) described four major pathways for N processing in the coastal zone: bypassing, transformation, retention and removal (Figure 3). The first one is referred to as bypassing, and describes the export of N without biogeochemical alterations, in contrast to the transformation pathway, which changes the chemical composition of the processed N. Alternatively, N can be retained through the combination of assimilation and mineralization pathways discussed above, or be permanently removed (Figure 3). Thus, how the coastal zone modulates the N reaching the marine ecosystem depends on different features of this organic matter and N reactor. Aside from the quantity of material delivered to the coastal zone, the most evident aspect is the depth of the water column, as it allows for a tight benthic-pelagic coupling and subsequent exchange of PON, DON, and remineralized DIN between the sediment and the water reservoirs (Figure 3).

In coastal zones, the seabed is long known as a hotspot for the remineralization of organic matter (Jørgensen and Revsbech 1989). In fact, in high sediment accumulation zones, the input of dissolved oxygen into the sediment via benthic macrofauna burrows and resuspension promotes ammonification and nitrification pathways (see Figure 1). The DIN produced from these reactions in the seabed may be supplied to the water column via diffusion, or reworking. In shallow water columns, the seafloor may thus be a source of dissolved N available to primary producers (Figure 3; Dugdale and Goering 1967; Nixon 1981). When the depth of the water column increases, in some cases, the strong salinity gradients generated by the river discharge may result in a strong vertical stratification as well as salinity fronts, both of which affect the mixing of different water masses. As a result, the N resupply from the seabed below the halocline to the euphotic zone or from the river to the open ocean is limited, and surface communities become more reliant on forms of N regenerated within the euphotic zone for their growth (Pomeroy 1974; Eppley and Peterson 1979; Azam et al. 1983).

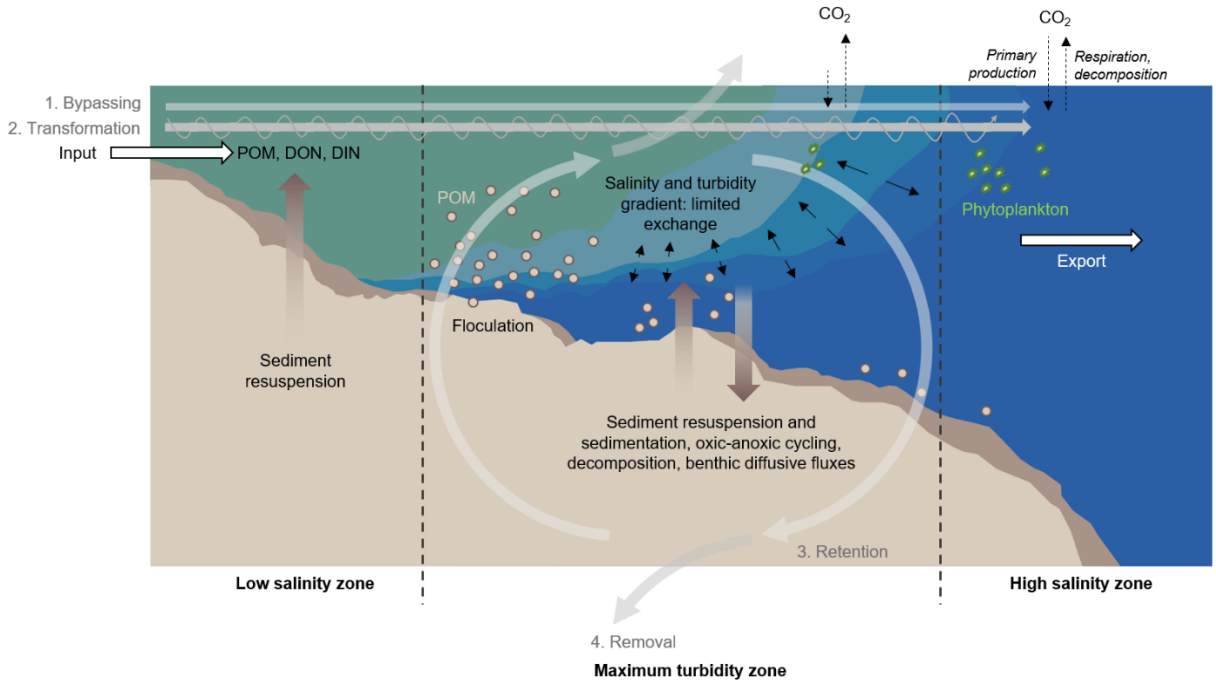

Figure 3. Conceptual figure of the fates of organic matter and N along the estuarine salinity gradient. Four major pathways may be at play: bypassing, transformation, retention, and removal (grey arrows). Adapted from (Canuel and Hardison 2016; Asmala et al. 2017).

Studies have shown that estuaries are often respiration-dominated systems, where remineralization processes are fueled by allochthonous material (Figure 2) and local primary production (Caffrey 2004). Autochthonous dissolved and particulate material is more labile and, thus more easily mineralized than allochthonous matter (Ittekkot 1988; Smith and Benner 2005; Lin et al. 2019). As a result, the efficiency of the burial and removal pathways (Figure 2; Figure 3) depends partly on the proportion of allochthonous versus autochthonous material. An example of this is the Changjiang estuary, where the decrease in allochthonous organic matter inputs following damming in the river catchment has resulted in a cascade of feedback: the reduced inputs of suspended sediments increased water transparency in the estuary, which enhanced primary production and consequently increased the fraction of labile compounds in the organic matter. As mentioned above, this organic matter is easily decomposable and not preserved (Ittekkot 1988; Galy et al. 2015), resulting in a strong decrease in organic carbon burial in the Changjiang estuary (Wang et al. 2022).

The general estuarine N cycling picture portrayed here can become more complex, as estuaries are distinct from one another, in terms of biochemical properties (e.g. nutrient levels, productivity) as well as physical properties (e.g. river discharge, turbidity, tidal range). The relationship between N-supply and productivity is thus not straightforward (Nixon et al. 1986;

Paerl et al. 2014), yet, its understanding at a local level is critical for coastal management, as ecosystems as we know them today are undergoing rapid change.

Anthropogenic impacts

Human activities have been altering the global N cycle for almost two centuries with dramatic consequences (Galloway et al. 2003), the last century marking the beginning of a new period referred to as the Anthropocene. A notable development during this period is the Haber-Bosch process, which converts N_2 and hydrogen into ammonia (Galloway et al. 2004) for fertilizer production. The transformation of inert N to reactive N is not without consequences for the environment. The yearly fixed industrial N_2 is of similar magnitude as the amount of N fixed biologically [~130-140 TgN y^{-1} ;(Galloway et al. 1995, 2004; Falkowski et al. 2000)], which together with inefficiencies in agriculture and water treatment, leads to greater fluxes of reactive N to the environment. These increased N inputs trigger harmful consequences, including acidification, eutrophication, and human health problems (Galloway et al. 1995, 2004; Falkowski et al. 2000), a succession of negative feedback defined by Galloway et al. (2003) as the N cascade. Since rivers are primary and rapid exporters of land-derived material to the coastal sea (Sharples et al. 2017), anthropogenic activities led to an increase in N and organic matter concentrations (i.e. eutrophication) in the rivers and hence in the loads draining into coastal zones (Seitzinger et al. 2010).

Because of their elevated nutrient concentrations compared to the open ocean, coastal zones are naturally highly productive, but today, are severely affected by eutrophication. The net effect of the greater N inputs and excessive primary production (summarized in Figure 4) results in decreased water transparency, a build-up of epiphytes communities, and an associated decrease in macrophyte communities abundance (Kennish and de Jonge 2011). Ultimately, these ecosystems often become dominated by harmful algal species. The increased amounts of organic matter produced lead to greater remineralization rates, which subsequently draws down O_2 levels. The development of such low O_2 regions is not only associated with loss of biodiversity (Galloway et al. 2003; Malone and Newton 2020) but also with acidification via CO_2 release during organic matter decomposition (Cai et al. 2011; Sunda and Cai 2012).

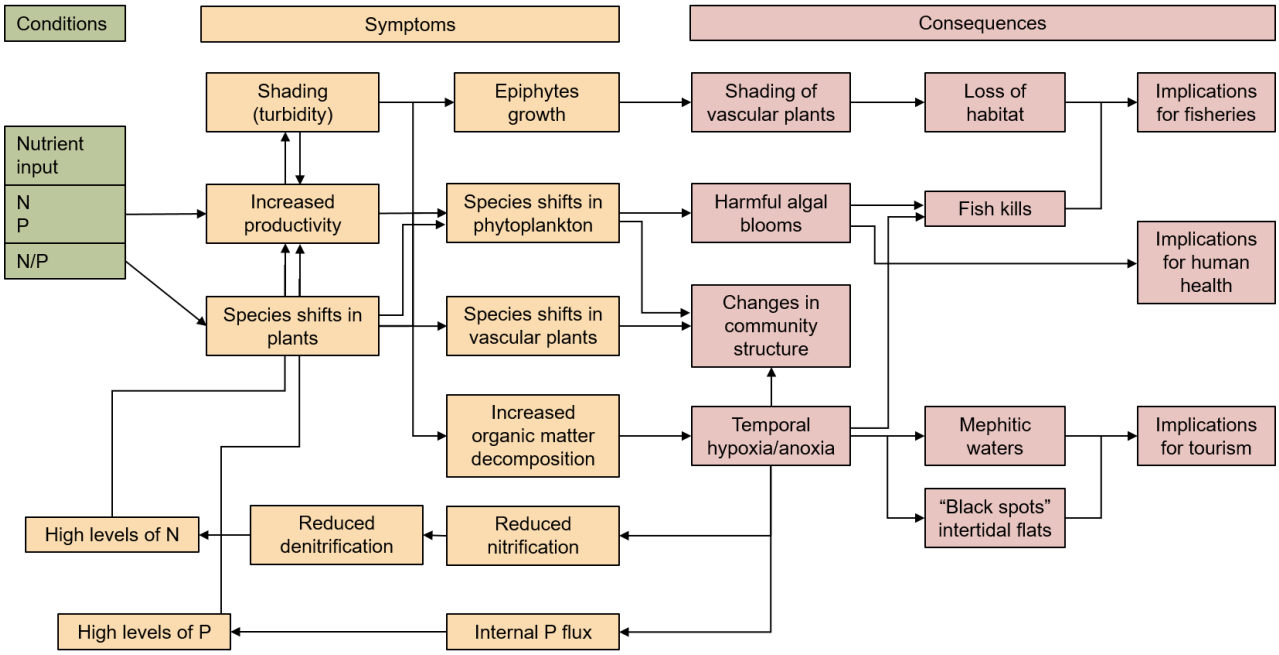

Figure 4. Overview of the potential effects of N, P enrichments, and N/P ratios in estuaries. Flowchart adapted from Kennish and de Jonge (2011).

Many studies have shown that controlling N and phosphorus (P) levels was key to mitigating coastal eutrophication (Howarth and Marino 2006; Paerl 2009), and denitrification has been estimated to remove a significant fraction of riverine N (Seitzinger and Kroeze 1998; Jickells et al. 2017). However, denitrification rates are quite variable between systems (Ward et al. 2009; Martínez-Espinosa et al. 2021), and N balance studies are only available for a limited number of coastal zones, while system-specific understanding of controlling factors of N inputs and N cycling is important in designing coastal management strategies.

The Amazon River Plume

Characteristics of the Amazon River and its plume

In marine ecosystems influenced by the Amazon River, the world's largest river by freshwater discharge, the role of riverine N for primary production is still largely unresolved. Yet, the fate of N along the Amazon River Plume is thought to contribute to the occurrence of massive *Sargassum* blooms in regions as far as the Caribbean Sea (Wang et al. 2019; Aquino et al. 2022). Constraining the sources and fate of N is therefore crucial to understanding the global biogeochemistry of this highly dynamic environment. In fact, the Amazon River contributes nearly one-fifth of the global riverine freshwater input to the ocean ($>5\times10^{12}$ m^3 y^-

[1]; Gibbs 1967). It is also the largest river in terms of particulate discharge, as it releases up to 1,200 Mt of particles into the ocean per year (Milliman and Farnsworth 2013).

The large amount of water, particles, and associated dissolved compounds originate from the catchment of the Amazon River, the largest drainage basin in the world, with an area of about 7×10^6 km^2 (Sioli 1984), extending from the East side of the Andes Cordillera to the Atlantic coast. Precipitations in the region are driven by the seasonality of the Intertropical Convergence Zone, with higher rainfall in the most southern (northern) part of the drainage basin in January (June). As a consequence, the Amazon discharge displays limited seasonal fluctuations, with a difference between high flow (May-June; Figure 5a) and low flow (October-November; Figure 5a) of less than a factor 4 (Richey et al. 1986; Nittrouer and DeMaster 1996; Fricke et al. 2019). Near Óbidos, approximately 800 km away from the coast, the tidal river starts and the tidal range progressively increases with distance downstream from about ten cm in Óbidos to 5 m at the river mouth (Kosuth et al. 2009). Tides are semidiurnal and bimonthly modulated, causing peak current velocities greater than 200 (80) cm s^{-1} during spring (neap) tides (Geyer and Kineke 1995).

The Amazon water reaching the estuary, both from the Amazon and neighboring Pará channels, moves northwestward along the shelf (Geyer et al. 1996) and mixes gradually with oceanic waters. The front between these two water masses appears as a strong halocline at around 10 m depth in the water column and between the 10 m and 20 m isobaths cross-shelf. As the freshwater follows the North Brazil Current, forming the Amazon River Plume (Figure 5b), surface salinities reach brackish values (between 20 and 30 of salinity), causing the vertical stratification to weaken and the surface mixed layer depth to get deeper. Consequently, the Amazon River Plume extends from the river mouth to the Caribbean Sea (Coles et al. 2013) and covers much of the continental shelf seawards, depending on the season. In fact, because of the temporal variability of the North Brazil Current, the tides or the wind, the Amazon River Plume is dynamic. From January to April, the Amazon River Plume is entrained northward, in a relatively slim band along the shelf. During maximum discharge, from April to June, Amazon waters can reach the Caribbean Sea, and from August to December, the Amazon water follows the North Brazil Current, which retroflex eastward into the Equatorial Atlantic Ocean following the migration of the Intertropical Convergence Zone (Gouveia et al. 2019 and references therein).

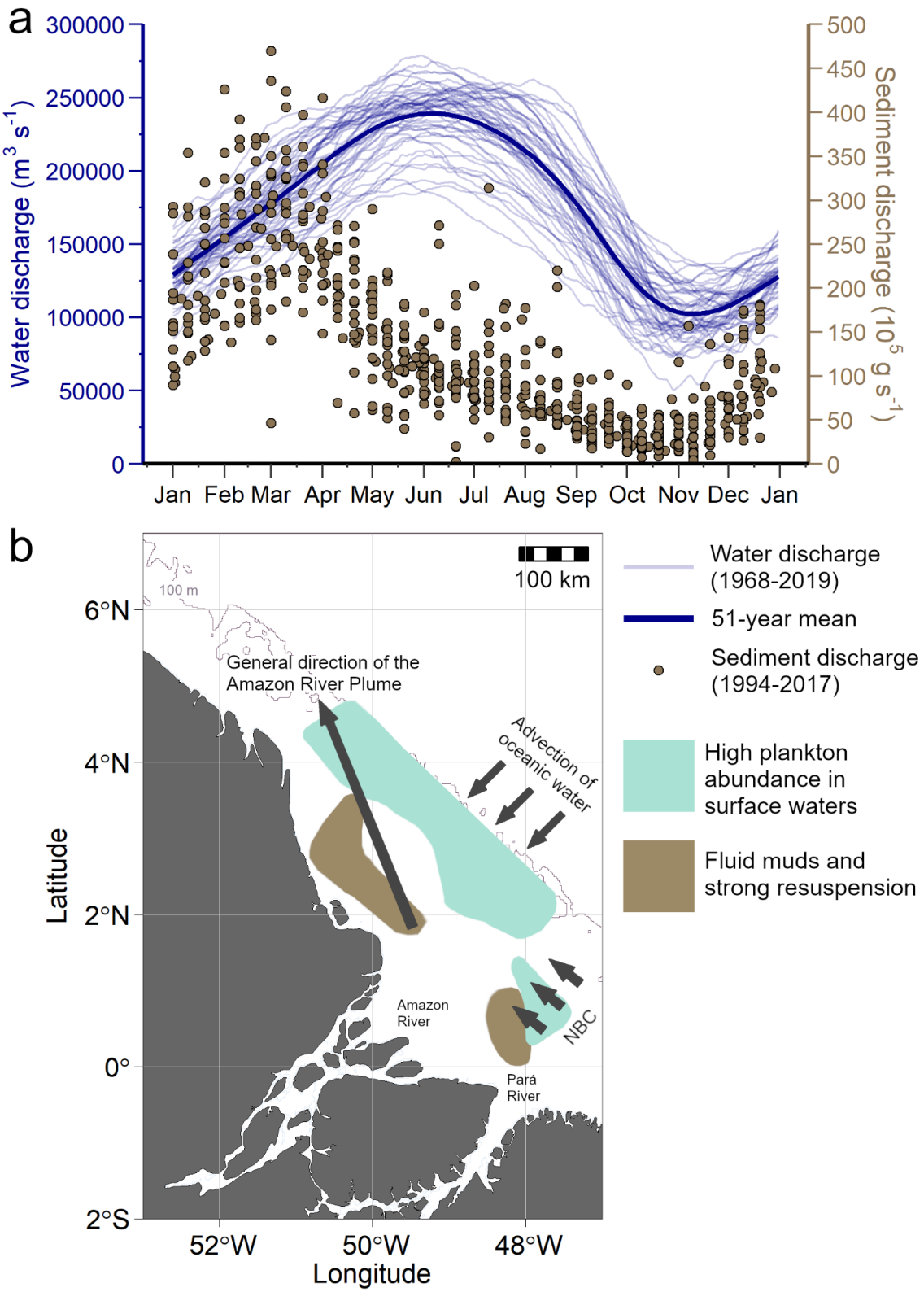

Figure 5. (**a**) The seasonal hydrograph for the Amazon River at Óbidos. The water discharge reaches a maximum in May–June and a minimum in October–November. The peak sediment discharge occurs in February–March. (**b**) Once it reaches the estuary, the riverine plume follows the North Brazilian Current (NBC). On the shelf, it creates zones of intense sediment reworking (brown areas) and zones of high plankton abundance (light blue areas). Panel a was generated with data from the HYBAM database, and panel b was adapted from (DeMaster and Aller 2001).

Where the river meets the ocean, the mixing of water and suspended sediment is thus driven by the river discharge, trade winds-induced surface waves, and tidal currents (Beardsley et al. 1995). Fresh water fills the entire water column as far as 150 km from the river mouth (10 m isobaths; Geyer et al. 1996) and the strong spring tides resuspend muddy sediment into the water column. As a result, the first 2 m of the seabed is regularly reworked, and both surface and bottom suspended sediment concentrations of at least 100 mg L^{-1} (Kuehl et al. 1986). The fluid muds formed at the bottom cause a water column stratification (Trowbridge and Kineke 1994), which in addition to the salinity stratification, hampers the mixing of riverine and oceanic waters in the estuary.

The Amazon River and its plume, aside from the tremendous amount of particles, convey large amounts of dissolved organic and inorganic N forms. Near the river mouth, NO_3^- concentrations range between 8 and 16 μM (Table 3; Araujo et al. 2014). Dissolved organic nitrogen is present in similar concentrations, although its bioavailability varies between its different forms. NH_4^+ and NO_2^- are present in much lower quantities, averaging 0.6 and 0.15 μM respectively (Table 3), making NO_3^- the dominant source of biologically available N in the estuary. In comparison, the NO_3^- concentrations in the euphotic zone of the North Brazil Current do not exceed 1 μM (Demaster and Pope 1996).

Table 3. Typical N concentrations in the Amazon River mouth.

N form	Concentration	Reference
Particulate organic nitrogen	64 μmol g^{-1}	Aller et al. unpublished
NO_3^-	8-16 μM	(Araujo et al. 2014)
NO_2^-	0.15 μM	(Edmond et al. 1981)
NH_4^+	0.6 μM	(Demaster and Pope 1996)
Dissolved organic nitrogen	14 μM	(Richey et al. 1990)

As for water and sediment, N concentrations are ruled by the seasonal variability of the Amazon River, with higher concentrations generally occurring at high discharge. Since the 1990s however, this system has undergone substantial transformations. The difference between high and low riverine flows has increased under the pressures of climate change, leading to stronger floods and droughts (Gloor et al. 2013; Gouveia et al. 2019). There are still uncertainties regarding the consequences of these changes on sediment discharge, as studies have demonstrated both an increase of 20 % (1995–2007; Martinez et al. 2009) and no

significant change (1984–2015; Montanher et al. 2018). Dissolved N concentrations have also been shown to increase over the last decade, but this change was demonstrated to not be caused by fluctuations in river discharge (Aquino et al. 2022).

Instead, land use change and anthropogenic activities are perceived as the main drivers of changes in both sediment and N fluxes to the estuaries. Deforestation in the Amazon River basin is probably the most studied factor and has received much attention since about 1970. In 2004, an action plan was launched and led to a reduction of 80 % in deforestation in the Amazon by 2012 (Toledo et al. 2017). Unfortunately, deforestation has increased again since then (West and Fearnside 2021; Barbosa et al. 2023), leading to increased potential for soil erosion. However, the direct effects of deforestation on sediment fluxes are countered by damming for hydropower development and mining. Before 2000, few dams existed in the Amazon Basin (Fearnside 2015), but more than a hundred dams have been built since then and many more are already planned for construction (Latrubesse et al. 2017). As a result of dams construction, sediment discharge of large rivers has globally decreased despite increased land erosion (Syvitski et al. 2005) and in the Amazon, a 20 % drop in suspended sediment concentration has been observed downstream of a major dam on the Madeira River (Latrubesse et al. 2017). Increased deforestation and damming have occurred in conjunction with population and agriculture growth. In the neighboring Pará River catchment, 81 % of sewage water remains untreated (IBGE 2018). Altogether, these factors result in new inputs of organic matter which have been linked to increased biochemical oxygen demand by 42 % as well as an increase in dissolved N forms in the Pará River (Aquino et al. 2022).

Significance for adjacent ecosystems and current knowledge

Many studies explored parts of the N cycling on the Amazon shelf or in the river plume. The great sediment discharge and associated turbidity in the estuary motivated large scale studies of benthic processes on the shelf (DeMaster and Aller 2001 and references therein). In the water column, primary production has been studied close to the river mouth, but studies of N_2 fixation and nitrification only focused on the Northern Amazon River plume (Smith and Demaster 1996; Cooley et al. 2007; Subramaniam et al. 2008; Starr et al. 2022). The variety of N cycling pathways described earlier thus remain largely unexplored, even though some work on N concentrations in the river and along the plume has been done (Araujo et al. 2017; Drake et al. 2021; Aquino et al. 2022).

As a result, the fate of riverine-dissolved inorganic N in the Amazon region still raises some questions. Some studies suggest all of it is consumed at the mouth, whereas others suggest 70-80 % reaches the ocean (Duce et al. 2008; Sharples et al. 2017). Depending on the distance from the river mouth, the cycling of N may vary, along with its significance for the ecosystem. Weber et al. (2019) highlighted the importance of NO_3^- availability for shaping phytoplankton community composition along the Amazon River Plume. In the river mouth and the most turbid parts of the Amazon River Plume, NO_3^- is abundantly available, though not consumed by phytoplankton as phototrophic production is light-limited here (Demaster and Pope 1996; Smith and Demaster 1996). With increasing light availability as turbid riverine waters mix with oceanic water and particles sediment to the seafloor, NH_4^+ and NO_3^- concentrations are sufficiently high to support phytoplankton (mainly diatoms) growth and there is limited N_2-fixation (Subramaniam et al. 2008; Loick-Wilde et al. 2016). As the plume extends, N is assimilated and the surface plume is continuously mixed with low-N seawater, and N becomes limiting (Subramaniam et al. 2008). There, where biological available N originates from N_2-fixation, diatom diazotroph associations (DDAs) become a significant component of the phototroph community. Finally, in N-deplete oceanic waters adjacent to the Amazon River Plume, cyanobacteria *Trichodesmium* are particularly abundant, and N_2-fixation occurs (Goes et al. 2014; Weber et al. 2017).

While it is currently undergoing drastic changes (Wang et al. 2019), present observations indicate that the Amazon estuary is not yet strongly impacted by the increasing damming, deforestation or urbanization in its catchment area unlike many other large deltas in the world, such as the Mississippi (Day et al. 2019). This relatively pristine state is favored by the unique discharge, equatorial location, and relatively small population of the Amazon basin, which contribute to buffer and delay the consequences of human activities. This offers an invaluable opportunity for establishing baseline knowledge about the use and transformation of N species at the Amazon River mouth and along the Amazon River Plume. A more detailed knowledge of N-cycling in the Amazon River Plume is essential for our understanding of the future of primary productivity in large regions of the Atlantic Ocean, as well as for future ecosystem management and protection.

Objectives of the study

For this purpose, the German Research Foundation (DFG) funded the MeNARP Project (Metabolism of Nitrogen in the Amazon River Plume and Tropical North Atlantic), with the main objective of studying the impact of riverine N on the cycling and turnover of N along the Amazon River Plume, in relation to the carbon cycle and functional biodiversity of primary producers and higher trophic levels. As previously mentioned, the N cycle is driven by several processes. In estuaries, the exchanges between the seabed and the water column and remineralization processes can be dominant in determining how much and which N form is made bioavailable. As such, this thesis aimed at resolving the origin of riverine N and the significance of its regeneration as a source of N for the Amazon River Plume, in the water column as well as at the water-sediment interface (Figure 6). This work is based on results from the M174 research cruise, which took place in April/May 2021, during rising to high river flow, and thus represent a snapshot of the studied processes during these specific conditions.

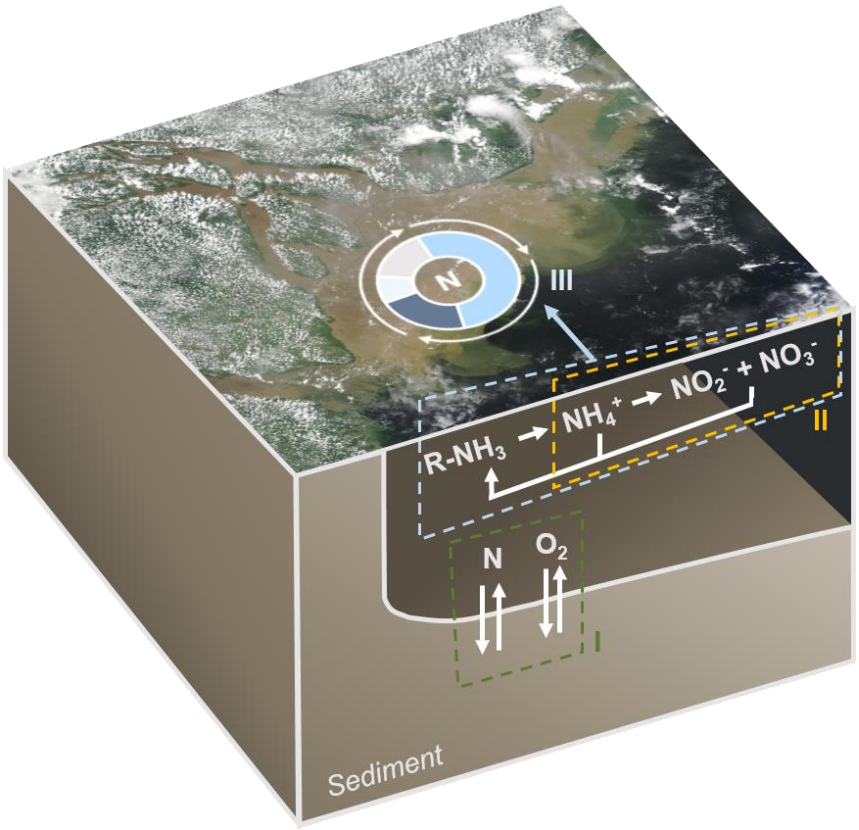

Figure 6. Summary of the research objectives detailed in this thesis: (I), explore N fluxes and associated respiration rates at the water-sediment interface, (II) provide first measurements of nitrification rates in the water column along the Amazon River Plume, and (III) provide an updated N-budget for the Amazon River mouth region—image from NASA Worldview.

The role of sediment as a reactor for riverine organic matter and its potential as a source of dissolved N for the water column have been largely documented in the early 2000s (Aller et al. 1996; DeMaster and Aller 2001). Nevertheless, the continuous changes that the Amazon catchment has faced since these last studies call for a re-examination of the N processes at the sediment-water interface, as sediment discharge and the associated N cycle may have been impacted. The second chapter of this thesis re-evaluates the role of sediment as a source of DIN for overlying waters on the Amazon shelf. This study can be regarded as a monitoring experiment, which largely confirms previously discussed that the fingerprints of human activities in the Amazon River are countered or delayed so far. A new facet to N processes at the sediment-water interface is highlighted in this chapter, as it provides the first measurements of greenhouse gas N_2O in overlying waters on the Amazon Shelf.

Regeneration of N is a major process in many turbid river estuaries and is also thought to be happening at high rates in the Amazon River mouth and along the Amazon River Plume (DeMaster and Aller 2001). However, to date, the only data available for the Amazon River and its plume do not cover the estuarine part of the plume (Starr et al. 2022). In Chapter 3, N regeneration was studied by measuring bulk nitrification rates at sites covering the Amazon and Pará River mouths, and the Amazon River Plume as far as Bajan waters, 15°N. Here, the aim was to provide the first extended data set of nitrification rates in the region and together with a cutting-edge statistical approach, to give an accurate description of sites with high nitrification rates. The results of this study provide a basis for future modelling-based work in the region, essential for predicting the future of the Amazon River Plume.

The acquired knowledge on regeneration in the plume layer is put into context with the overall N cycling in at the Amazon and neighboring Pará river mouths in Chapter 4 of this thesis, to provide insights on the fate of N in the Amazon River Plume. N budgets have been previously calculated for the Amazon Shelf, but in Chapter 4, they are for the first time integrated with new rate measurements of major N processes occurring in the estuary, such as nitrification and dissolved inorganic and organic nitrogen uptake by phytoplankton. Additionally, the potential for denitrification in the plume layer at the river mouth was investigated using NO_3^- and H_2O N and O isotopes. As such, this chapter provides the first estimates of N sources and processes using a combination of NO_3^- and H_2O stable isotopes in the region.

As mentioned in the author contribution statement at the end of this thesis, the three scientific papers that are part of this thesis are either accepted or submitted to peer-reviewed journals. Chapters 2 and 3 are first-author papers, where I conceived and designed the research, and contributed to the data collection and interpretation. Chapter 4 is a shared first authorship, I contributed 50 % to the study design, data collection, and interpretation. I authored the initial drafts for all three manuscripts.

2 | The Amazon shelf sediments, a reactor that fuels intense N cycling at the seabed

Authors: Choisnard Noémie, Burtscher Emma, Forster Stefan, Frey Claudia, Moros Matthias, Voss Maren.

Limnology and Oceanography Volume 68, issue 10, p. 2211-2226 (DOI:10.1002/lno.12416).

Author Contribution Statement: NC, MV, CF, and EB conceived and designed the research. All authors contributed to the collection and compilation of data. NC, MM, CF, EB, and MV wrote the manuscript. NC, MM, CF, EB, and MV analyzed the data. All authors contributed to content revisions and approved the final text.

Abstract

Large river plumes such as the Amazon River Plume are known as regions of intense biological, chemical, and physical forcing affecting the delivery and speciation of nutrients. On the shelf, sediments may act as a net source or sink of dissolved inorganic nitrogen (DIN) for the water column depending on the preservation of organic matter (OM) and its remineralization pathways in benthic environments. Previous studies on sediments of the Amazon shelf suggested that the seabed mainly acted as a sink of DIN, with denitrification as the main loss process. However, the Amazon Basin faced drastic changes over the past decades, with climate change, deforestation, and damming potentially impacting the DIN and OM loads to the estuary. These perturbations might have led to changes in benthic remineralization, calling for updates of previously studied benthic remineralization processes on the Amazon shelf. Our analysis of eight short cores confirmed the occurrence of intense recycling of mostly terrestrial material (>60 %) in the river mouth, and little organic carbon was remaining in shelf sediments. We measured a sediment oxygen demand of ~23 mmol m^{-2} d^{-1}, which can explain the ammonification and nitrification of all the organic nitrogen (N) reaching the sediment, underlining the importance of the seabed as a sink for organic N species. Therefore, in spite of the changes in the Amazon Basin, nitrification still seems to be balanced by denitrification, as, similarly to previous results, no DIN diffused out of the sediment.

Introduction

Pelagic primary productivity in most ecosystems on Earth is limited by nitrogen (N) (Howarth 1988), which indirectly controls the amount of carbon that can be exported to the deep sea, known as the biological carbon pump (Eppley and Peterson 1979). Primary production can be supported by various autochthonous and allochthonous sources, with the latter largely represented by rivers (Lohrenz et al., 1990). The Amazon River is fed by the largest drainage basin in the world, from the Andes to the Brazilian coast. Together with the Pará River outflow, it delivers high concentrations of dissolved organic and inorganic N (DON, 14 μM or 1.1 Tg N y^{-1} and DIN, 16.8 μM, resulting in 1.3 to 2.8 Tg N y^{-1}) to the Western Tropical North Atlantic (Demaster and Pope 1996; Martinelli et al. 2012), influencing primary production in the estuary and beyond. As 65 % of the Amazon River plume follows the North Brazil Current along the north-eastern coast of South America, it impacts the biochemistry of surface water as far as the Caribbean during periods of maximum discharge in winter and spring (January to May) (Froelich Jr et al. 1978; Coles et al. 2013).

However, the large freshwater load is only one of multiple factors influencing the N-cycle of the Amazon shelf. Annually, the Amazon River also discharges roughly a billion tons of sedimentary particles into the estuary (Meade et al. 1985), most of which originate from the Andes, a region that covers less than 1/8 of the drainage basin, but the steep slopes of the riverbank favor erosion (Meade et al. 1985; Filizola and Guyot 2009). In contrast, the Guiana and Brazilian shorelines contribute to approximately 7 % of the suspended sediment load to the estuary (Filizola and Guyot 2009). The fate of these suspended sediments is mostly determined by the density stratification of the water column formed by the strong semi-diurnal tides on the shelf (tidal range up to 10 m; Geyer et al., 1996).

The strong spring-neap modulation of the tides generates variation in the stratification: during neap tides, it is more pronounced and results in an accumulation of suspended sediments near the seabed (Geyer et al. 1996; Kineke et al. 1996). Of the 7.5×10^{14} g yr^{-1} of particles delivered by the Amazon (Molinier et al. 1996; DeMaster and Aller 2001), half settles on the seafloor (Kuehl et al., 1986), while another part moves northwestward in the form of suspended sediments and as migrating mudbanks (Kineke et al. 1996; Sternberg et al. 1996). Conversely, the occurrence of greater current speed during spring tides creates more mixing, resulting in weaker stratification of the water column (Geyer 1995; Kineke et al. 1996), potentially

impacting the stability of the seabed. The Amazon shelf is therefore a highly dynamic environment, where the upper 50 to 150 cm of the sediments are reworked once to twice a year (Kuehl et al., 1986; Kuehl et al., 1995), which could influence the release or trapping of N by the sediments by forcing benthic remineralization of organic matter (OM).

Diagenesis is partly driven by the microbial degradation of OM, a process that can significantly affect oxygen concentrations (O_2) and N speciation in coastal waters (Nixon 1981). Ammonification leads to a production of ammonium (NH_4^+) (Abril et al. 2000; Tobias et al. 2003), while subsequent nitrification-denitrification can be a major pathway of DIN removal from the estuarine system (Crowe et al. 2012). Nitrification alone is also central, as it consumes NH_4^+ from ammonification within the sediments and provides the majority of the available nitrate (NO_3^-) for either primary production in oxic environments, or for denitrification to occur in deeper anoxic sediments (Tobias et al. 2003). Depending on the preservation versus remineralization of OM, the Amazon sediments may act as a net source or sink for DIN in the coastal environment. Thus, it could either foster primary production, stress the ecosystem by contributing to aquatic eutrophication, or contribute to N-limitation (Tyrrell 1999; Paerl and Piehler 2008).

Earlier studies, conducted in the late 1900s to early 2000 showed that the Amazon shelf sediments released little or no DIN via diffusion into the overlying water because of coupled nitrification and denitrification of remineralized N changes(Kuehl et al. 1986; Aller et al. 1996; Demaster and Pope 1996; DeMaster and Aller 2001; Aller and Blair 2006). However, the Amazon drainage basin has undergone continuous changes over the past 30 to 40 years, including increased damming, deforestation, mining (Ometto et al., 2011) as well as a changes in its hydrological cycle (Gloor et al., 2013; Gouveia et al., 2019). It is likely that these perturbations lead to significant changes in sediment load and nutrient concentrations, and (Aquino et al. 2022) already detected a significant increase in riverine DIN loads in the last decade. These changes could potentially impact the fluxes of OM to the seabed and its degradation. Therefore, updating our knowledge of DIN fluxes at the seabed on the Amazon shelf would be valuable for future ecosystem management.

As sediments and pore water profiles can record the sequence and rate of OM degradation (Froelich et al. 1979; Goloway and Bender 1982; Schulz and Zabel 2006), they are valuable tools for studying the diagenetic reactions influencing the benthic DIN pool. Here, we revisit these processes on the Amazon shelf and present updated fluxes estimates based on a

new data set. We sampled sediment cores along an alongshore transect from the Amazon River mouth to French Guyana waters to address the pathways by which OM and DIN are transformed and to characterize the fluxes of DIN at the water-sediment interface, in comparison with earlier studies of the region.

Materials

Study site and sample collection

To account for the role of high Amazon riverine discharge on sediment geochemistry, short multicorer sediment cores (10 cm internal diameter, < 60 cm long) were recovered at 6 sites in the Amazon River estuaries and along the Amazon River Plume, during the cruise M-174 in April and May 2021 (Figure 7; Table 4), which corresponds to rising to peak river flow during spring (Liang et al. 2020). Stations were selected based upon the plume extension as validated by satellite imagery. Sediment cores were retrieved in triplicate for porewater and incubation experiments and at each station, one core was sampled for solid phase analysis. Two stations (13-3 and 17-24) were located on the inner shelf, at a water depth of 16 m and 33 m respectively. Stations 19-5 and 21-14 were located 300 km off the river mouth (60 m and 90 m depth respectively), at location where sedimentation rates were found to be the highest (Kuehl et al., 1986). At station 24-5 and 26-9, situated more than 500 km away from the river mouth and along a cross shelf transect (30 m and 80 m depth respectively), cores were retrieved as references for environments with weaker Amazon River impact. Two sites (10-6 and 9-6; Figure 7, Table 4) were also sampled in the Pará River mouth to check for potential contribution of this river to the Amazon shelf N-pool.

Only cores with clear overlying water and straight sediment-water interface were selected for further processing. The cores retrieved close to the river mouths (10-6, 13-3 and 17-24) did not show any sign of perturbation. Cores from stations 9-6, 19-5 and 21-14 probably had communities of burrowing fauna, as small burrows could be seen in the first 5 cm of the cores. Cores from the most distant locations (21-14, 24-5 and 26-9) were inhabited by small shrimps and crabs. At stations 10-6 and 19-5, not enough cores could be retrieved to perform incubation experiments.

Table 4. Site description and main sediments characteristics. Water content and porosity were averaged for the entire core. The sediment type was described from the grain size analysis, following Shepard's nomenclature (Shepard 1954).

Station	Latitude	Longitude	Sampling date	Water depth (m)	Bottom water $[O_2]$ (μM)	Porosity	Water content (%wt)	Sediment type
9-6	00°07,308'S	047°43,890'W	23/04/2021	36	170.03	0.80	61	Silt, fluffy
10-6	00°35,854'S	048°15,631'W	23/04/2021	15	170.31	0.83	66	Silt, fluffy
13-3	01°03,049'N	048°35,052'W	24/04/2021	16	114.61	0.75	52	Silt, fluffy
17-24	01°20,745'N	048°21,193'W	27/04/2021	33	174.88	0.76	55	Silt, fluffy
19-5	03°25,107'N	049°58,339'W	29/04/2021	60	165.79	0.82	63	Silt, fluffy
21-14	03°33,486'N	049°53,059'W	01/05/2021	77	183.40	0.65	43	Silty sand
24-5	05°27,224'N	052°33,473'W	04/05/2021	30	110.91	0.43	22	Sand
26-9	05°59,886'N	052°01,201'W	05/05/2021	82	188.03	0.43	22	Sand

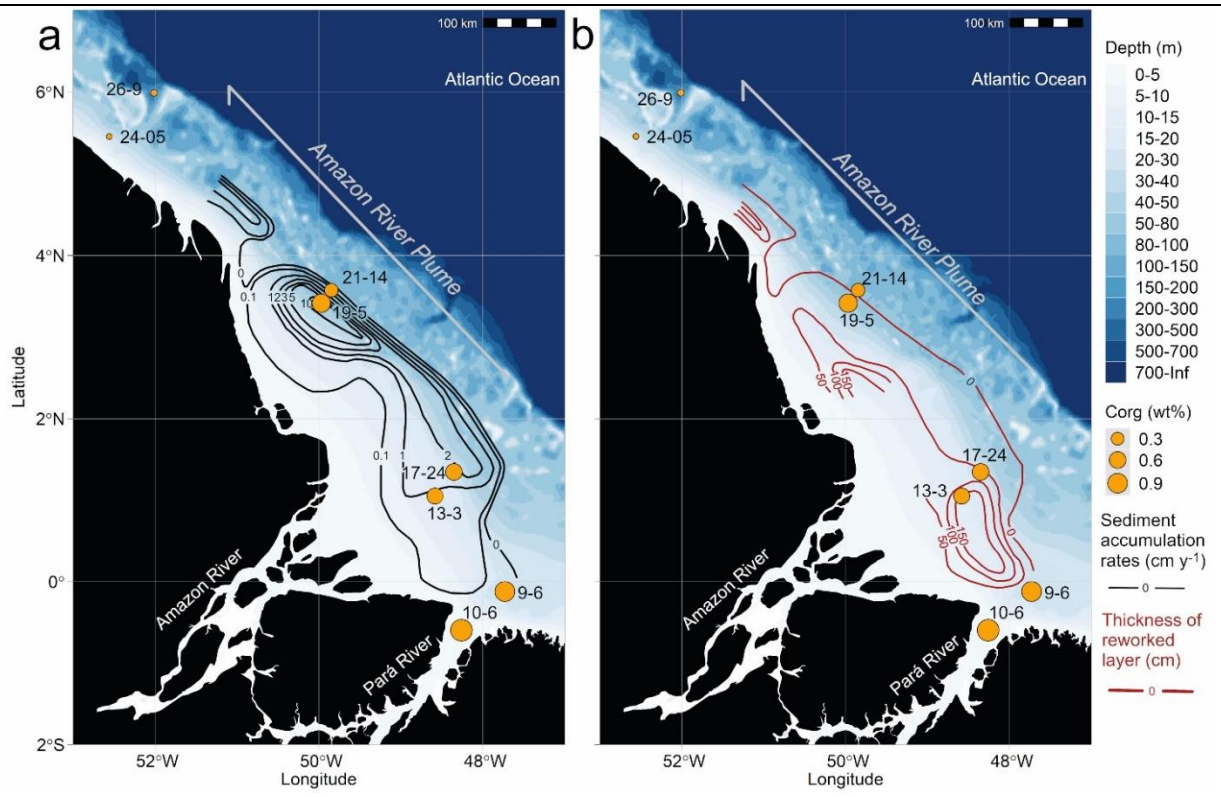

Figure 7. This study focuses on the Amazon shelf, an area influenced by the outflow of the Pará and Amazon River. Kuehl et al., (1986) demonstrated that the particles delivered by the two rivers are transported along the Amazon River Plume and accumulate at high rates (black line, in cm y^{-1}) around 3°N relative to the rest of the shelf (**a**). Their study also highlighted the dynamicity of the seabed, with maximum reworked layer thicknesses (red line) of at least 150 cm on the Amazon shelf (**b**). The surface sediment of small cores collected in both river's estuaries and along the Amazon River Plume presented different C_{org} content (%wt), as represented by the point area.

Porewater collection

To constrain the mechanisms by which OM and N are transformed in the sediments, 3 cores per stations were retrieved for pore water analysis and sampled at 0.5-3 cm intervals. The pore water was sampled using rhizons (Seeberg-Elverfeldt et al. 2005) inserted through pre-drilled holes in the core tube, which were covered with electrical tap prior to coring. Five mL plastic syringes were attached to the rhizons to extract pore water. The first milliliter drawn was used to condition both the rhizon and the syringe. A sample volume of approximately 2 mL was then collected and transferred into 2 mL Eppendorf tubes. Samples were analyzed for nutrient content on board shortly after collection.

Incubation experiment

Incubation experiments were performed in a non-aerated settings to characterize the O_2 consumption and fluxes of DIN at the water-sediment interface. As a comparison between nutrient fluxes from incubated cores and in situ chambers showed that both techniques provide similar flux estimates (about 65 % to 100 % of in situ fluxes; Hammond et al., 2004), we used here the core incubation technique to simplify sample collection. Three liners were sealed with a PVC plug at the bottom, and a movable PVC piston at the top, taking care to avoid trapping air bubbles. The piston was pushed down until 20 cm above the sediment, to ensure the presence of enough water above the sediments for the entire incubation. To simulate water circulation above the core, a magnetic stir bar was inserted below the piston. The cores were placed in a dark cold room (12 °C), to simulate the seafloor temperature conditions at the sampling stations. Samples for nutrient analysis were collected at the beginning of the experiment, after 6 h of incubation, and after 12 h. Samples were retrieved by pushing the piston down to fill a pre-weighed 10 mL Winkler titration flask for O_2 analysis, and a 25 mL plastic syringe for nutrient analysis. The nutrient sample was then filtered through a 0.2 μm cellulose acetate syringe filter (Whatman), collected in 15 mL Falcon tubes and analysed on board shortly after collection.

Nutrients and oxygen analysis

Dissolved silica ($Si(OH)_4$), NO_3^-, nitrite (NO_2^-) and NH_4^+ concentrations were determined on a continuous flow autoanalyser (Quatro, Seal analytics) following Grasshoff et al. (1999) with a precision of 0.3 μM ($Si(OH)_4$), 0.02 μM (NO_3^-), 0.01 μM (NO_2^-) and 0.02 μM (NH_4^+). Dissolved O_2 in the sediment overlying water was measured according to the protocol

described in Grasshoff et al. (1999), using an automated titration device (TiTouch 916, Metrohm), with a precision of 0.13 μM.

Concentration measurements of N_2O

Samples for nitrous oxide (N_2O) concentration were collected to identify potential sources or sinks at the sediment-water interface. As soon as the cores were secured, samples were drawn bubble-free directly from the sediment overlaying water using a gas-tight tygon tubing into a 160 mL glass serum bottles. Water was allowed to overflow the bottle to avoid gas exchange with the atmosphere and closed with a butyl rubber septum and an aluminum crimp. For measurement purposes in the laboratory, a 10 mL headspace was taken from all serum bottles. The samples were immediately preserved with 100 μL of saturated mercury chloride solution ($HgCl_2$).

Total N_2O was extracted from 150 mL liquid using a custom - build purge-trap system with a GC column coupled with an open split ConflowIV interface to an Isotope - Ratio Mass Spectrometer (GC-IRMS; Delta V Plus, Thermo) according to Frey et al. (2020) at the University of Basel, Switzerland. In short, serum bottles were flushed with helium gas for 35 min (60 mL min^{-1}) and N_2O was trapped by liquid nitrogen. Water was removed with an ethanol cold trap and a $Mg(ClO_4)_2$ trap and carbon dioxide (CO_2) was removed with an Ascarite CO_2 absorbance column. N_2O was detected by analyzing *m/z* 44, 45, and 46. With each sample run, different concentration of a N_2O standard from a reference N_2O tank were run to calibrate the peak areas for N_2O concentrations.

N_2O saturation disequilibrium (ΔN_2O, expressed in nmol L^{-1}) was calculated as the difference between measured N_2O concentration and N_2O concentration at atmospheric equilibrium using the equation by Weiss and Price's (1980). This was compared to the Apparent Oxygen Utilization (AOU), calculated as the difference between measured O_2 concentration and O_2 concentrations at atmospheric equilibrium according to Benson and Krause Jr., (1984).

Solid phase properties, $\delta^{15}N$ and $\delta^{13}C$ analysis

One additional core per station was sectioned in a maximum of 1 cm interval over the first few cm and in 2 cm to 4 cm intervals along the deeper part of the core (3 to 16 samples per core). A sediment aliquot from each slice was collected and stored frozen in a plastic bag

for the determination of water content and porosity as well as for solid phase analyses after the cruise.

The wet weight (ww) and dry weight (dw) of each sediment aliquot was measured before and after freeze-drying of the sediment samples for 2.5 days respectively, to determine the water content (in %ww). The wet weight was then used to calculate the porosity of the sediment following:

$$\varphi = \frac{\frac{m_w}{\rho_w}}{\frac{m_w}{\rho_w} + \frac{m_s}{\rho_s}} \quad (1)$$

With m_w and m_d as the mass fraction of water and dried sediment, respectively, ρ_w and ρ_s being the densities of the ambient seawater and sediment (2.65 g cm^{-3}).

$\delta^{15}N$ and $\delta^{13}C$ analysis were performed on approximately 30 mg of each freeze-dried and homogenized sediment samples on a Flash EA Isolink CN elemental analyzer (Thermo scientific) coupled via a ConFlo IV (Thermo scientific) interface to a Delta V advantage (Thermo scientific) isotope ratio mass spectrometer. An internal standard was used for the calibration of the measurement (Acetanilide, Merck), and 6 international standards were used as reference materials to ensure the quality of the analysis (IAEA-N1, IAEA-N2, IAEA-N3, NBS 22, IAEA-CH-3 and IAEA-CH-6). The analytical reproducibility for $\delta^{15}N$ and $\delta^{13}C$ is <0.2 ‰. To prevent any bias from the presence of inorganic carbon, the $\delta^{13}C$ of OM ($\delta^{13}C_{org}$) was measured after acidification of the sediment sample using hydrochloric acid (HCl, 10 %).

Radionuclides and pollutants

Analyses of radionuclides and pollutant were performed to check for signs of high sedimentation rates and reworking of sediment. ^{226}Ra, ^{210}Pb and ^{137}Cs were carried out by gamma spectrometry with a Ge-detector BE3830-7500SL-RDC-6-ULB and well detector (GCW4021-7500SL-RDC-6-ULB) and processed with GENIE 2000 software (Canberra Industries Inc., USA). Counting statistics were better than 5–10 %. The radionuclide activities were calculated using standard reference materials (decay corrected): IAEA-447 (^{137}Cs, ^{210}Pb, ^{226}Ra). The following nuclides and energies were used for quantification of isotopes: ^{210}Pb: 46.5 keV, ^{226}Ra: 295 and 351 keV and ^{137}Cs: 661 keV.

For mercury (Hg) measurements, samples were analyzed on a DMA-80 Analyzer from MLS Company. Data were calibrated against CRM (BCR) 142R certified reference material and the SRM 2709 soil standard using five concentration steps covering a range from 5 to 500 ng Hg. Sample weights were between 20 and 100 mg. For further analytical details and details regarding quality assurance see Leipe et al., (2013).

Particulate Silica analysis

Particulate silica (PSi) content was analyzed on 4 cores from the Amazon River mouth and the River Plume, following the protocol described in Ragueneau and Tréguer, (1994). 50 mg of freeze dried and homogenized sample were incubated for 40 min at 100 °C in 4 mL of sodium hydroxide (NaOH, 0.2 M). After cooling, 1 mL of HCl (1 M) was added. After centrifugation, 0.5 mL of the supernatant were withdrawn and diluted to 10 mL using Milli-Q water. PSi content of each sample was then determined at 810 nm on a fluorimeter (Shimadzu UVmini 1240) after reaction of the sample with 0.2mL of an acid/molybdate reagent (Mullin and Riley 1955).

Grain size analysis

Grain size analysis was performed using a Mastersizer 3000 at the Leibniz Institute for Baltic Sea Research (IOW), on an aliquot of freeze dried and homogenized sediment samples cleaned using HCl (10 %) and hydrogen peroxide (30 %). The type of sediment was later estimated using a Shepard's diagram for sediments grain size (Shepard 1954).

Sources contributions to the sediment δ^{13}C-C_{org}

The influence of different sources on sediments δ^{13}C-C_{org} was calculated using a simple mixing model (Fry 2006), making the assumption that the shelf exposed to a fraction of terrestrial OM ($f_{terrestrial}$) is also exposed to a fraction of marine OM (f_{marine}):

$$f_{terrestrial} = \frac{\delta^{13}C_{sediment} - \delta^{13}C_{marine}}{\delta^{13}C_{terrestrial} - \delta^{13}C_{marine}} \times 100 \quad (2)$$

$$f_{marine} = 100 - f_{terrestrial} \quad (3)$$

Where $\delta^{13}C_{sediment}$ is the $\delta^{13}C$-C_{org} observed at the surface of the sediments at each station, $\delta^{13}C_{terrestrial}$ is the $\delta^{13}C$-C_{org} of terrestrial OM measured in the lower Amazon River (-31.3 ± 3.2 ‰, Mortillaro et al. 2011), which was supposed to be similar to the one of surface particulate OM (POM) at the river mouth, and $\delta^{13}C_{marine}$ is the $\delta^{13}C$-C_{org} of marine OM (-20 ‰, Boutton 1991; Aller and Blair 2006).

Sediment $\delta^{15}N$ and $\delta^{13}C$ values were also compared with the isotopic composition of surface water POM at each site. To do so, 5 L of surface water, collected using a rosette, were filtered on precombusted (450 °C for 4 hours) 25 mm GF/F filters. Filters were oven dried (50 °C) until analysis, as previously described for sediment samples.

Incubation experiment

The rate of concentration change in the overlying water of a core was calculated from the incubation experiment. The O_2 decrease overtime ranged between 15 and 30 %, except at stations 9-6 and 13-3, were the O_2 decrease by up to 55 %. But although many experiments had substantial concentration changes, the increase or decrease of each nutrient over time was steady. Consequently, it was assumed that the O_2 decrease did not significantly impact the nutrient concentrations, and fluxes were calculated using linear regressions versus time (in the case of O_2 from the first and last points only). A positive flux symbolizes a flux out of the sediments.

Porewater profiles

Diffusive fluxes (in mmol m^{-2} d^{-1}) were calculated from the pore water profiles to compare with the incubation fluxes, according to Fick´s first law, as presented in Schulz and Zabel., (2006). The nutrient fluxes were calculated from the first 5 cm of each core, where a steady increase or decrease was found, enabling the application of a fit. As for incubation-derived fluxes, a positive flux symbolizes a flux out of the sediments.

Statistical analyses

To discriminate differences among the means of each incubation, we used Tukey's test for multiple comparisons. One sample t-tests (two-tailed) were also performed to check whether fluxes were significantly different from 0.

Results

Solid phase analysis

In the estuary, sediments were mostly fluffy, fine-grained and composed of silt. The PSi content was overall low (less than 0.6 wt%, Figure S1). The sediment type of each station sampled is reported in (Table 4). The proportion of sand in the sediment increased with distance from the river mouth (Table 4), while the PSi content decreased to nearly 0 wt% (Figure S1). Little or no downcore change was measured, except at station 21-14, where a layer of fine-grained sediments was found between 2 and 5 cm depth, in a core otherwise coarse-grained (Figure S1, Figure S2).

Hg concentration were high (60 μg kg^{-1}, Figure S1, Figure S2) from the river mouths to station 19-5 and low (less than 10μg/kg) at distal stations. Hg and ^{210}Pb exhibited a uniform downcore profile, while ^{137}Cs was detectable and highly variable with sediment depth. Distal stations (24-05 and 26-9) however, showed no ^{137}Cs activity. Unlike other stations, station 21-14 presented a peak in Hg co-occurring with a minimum in ^{210}Pb activity between 1 and 5 cm depth (Figure S1).

δ^{13}C-C_{org} in the sediments and mixing of two sources

The δ^{13}C-C_{org} of sediments increased from -26.7 ± 0.2 ‰ at the Pará and Amazon River mouth to -21.2 ± 0.2 ‰ at more distal stations (Figure 8a) and was related to a decrease in the sediment C_{org}-content, from 1.2 (wt%) to 0.1 (wt%) (Figure 8a). A simple mixing model between a marine and a terrestrial component showed an increasing contribution of marine OM to the sediment C_{org}-content with increasing distance from the river mouth (from 39 to 89 %, Figure 8b). However, stations 13-3 and 17-24, located at less than a 100 km of the Amazon River mouth, presented a lower C_{org}-content compared to stations with similar δ^{13}C-C_{org} (0.40 to 0.60 wt% instead of 0.9 wt%, at a δ^{13}C-C_{org} of ~-26.0 ‰; Table 5). The specific characteristic of these stations also seemed to be found in some parts of the core retrieved at station 21-14. Station 19-5 on the other hand presented the opposite trend, with a C_{org} content up to 0.3 %wt higher than expected for its range of δ^{13}C-C_{org} (Figure 8a).

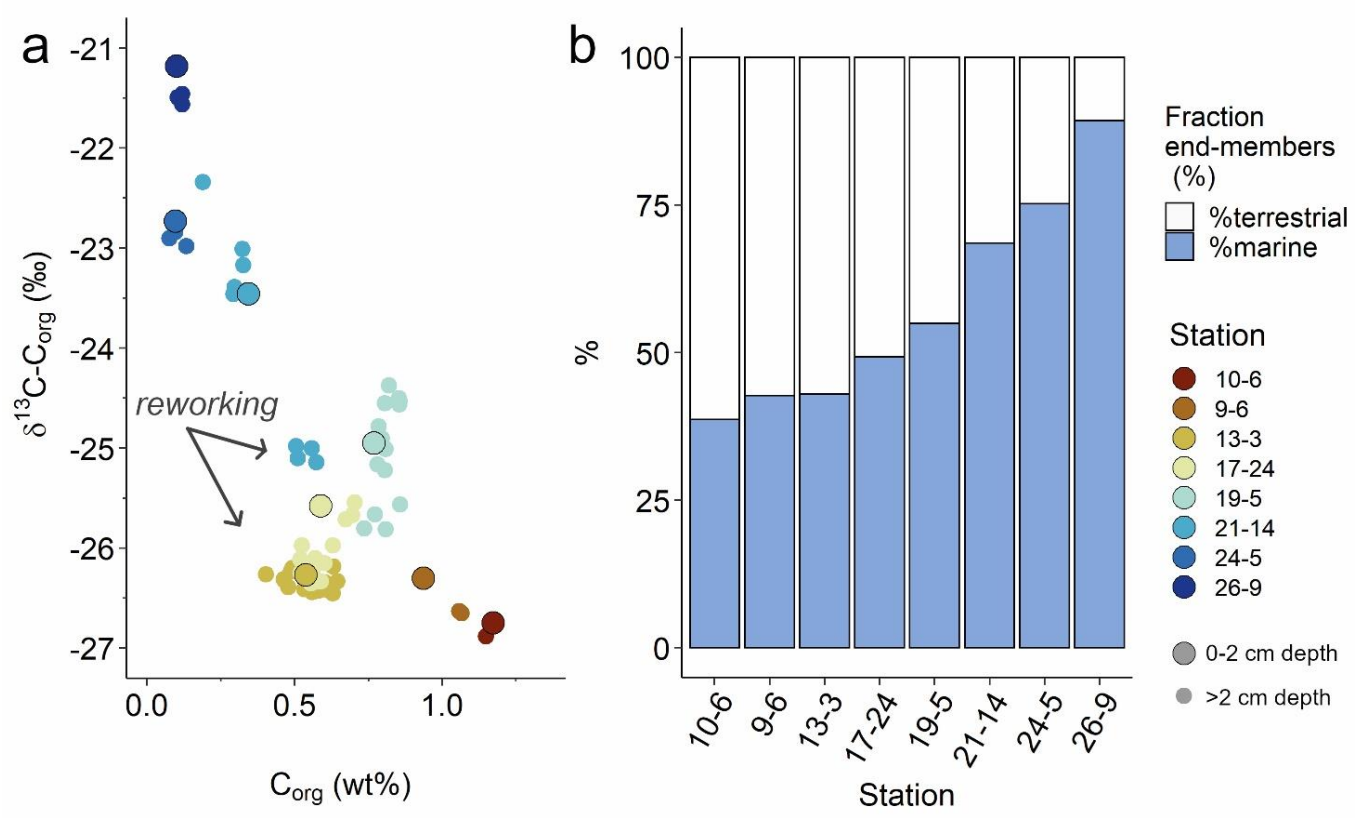

Figure 8. The δ^{13}C-C_{org} versus sediments C_{org}-content (wt%) revealed the gradient in C_{org} sources between river mouth and distal sites (**a**). Using the δ^{13}C-C_{org} values of the top 2 cm of the sediment at each station (highlighted with bigger markers in the first panel), we could estimate the (**b**) potential contribution of terrestrial and marine C_{org} to the surface sediments along the transect. The small markers in panel (**a**) represent values from individual sediment depths.

Table 5. Surface δ^{13}C- and δ^{15}N-POM at each station and downcore averages and standard deviation of C and N related analyses.

Station	δ^{13}C-POM (‰)	δ^{15}N-POM (‰)	δ^{15}N-N_{tot} (‰)	δ^{13}C-C_{org} (‰)	N_{tot} (μmol mg^{-1})	C_{org} (μmol mg^{-1})	C_{org}/N_{tot}
9-6	-28.2	7.3	4.4 ± 0.1	-26.5 ± 0.2	0.09 ± 0.01	0.85 ± 0.06	9.3 ± 0.2
10-6	-25.3	6.6	4.4 ± 0.1	-26.9 ± 0.3	0.11 ± 0.01	0.97 ± 0.02	8.7 ± 0.7
13-3	-28.3	7.7	4.7 ± 0.4	-26.3 ± 0.1	0.07 ± 0.01	0.45 ± 0.06	6.4 ± 0.2
17-24	-29.1	5.5	4.4 ± 0.3	-26.0 ± 0.3	0.06 ± 0.01	0.49 ± 0.05	7.9 ± 0.2
19-5			4.5 ± 0.4	-25.0 ± 0.5	0.08 ± 0.01	0.67 ± 0.03	8.0 ± 0.3
21-14	-21.5	5.6	4.4 ± 0.2	-23.9 ± 1.0	0.04 ± 0.02	0.33 ± 0.11	7.7 ± 0.4
24-5	-19.4	4.7		-22.9 ± 0.1	0.01	0.08	12.6
26-9	-22.9	2.9	3.5 ± 0.3	-21.4 ± 0.2	0.01	0.09 ± 0.01	9.5 ± 0.9

With distance from the Pará and the Amazon River mouths, δ^{13}C-C_{org} increased, while C_{org}/N_{tot} remained relatively constant, between 7.7 and 8.0 as far as station 21-14 (Figure 9a, Table 5). δ^{15}N-N_{tot} presented little variation on the shelf (ranging between 4.4 and 4.7 ‰; Table 5, Figure S1). Only at the most distal stations (24-5 and 26-9), C_{org}/N_{tot} ratios seemed to increase, reaching values of up to 12.6 (Figure 9a, Table 5) while δ^{15}N-N_{tot} exhibited the slightly lower value of 3.5 ± 0.3 ‰ (Table 5). The distribution of δ^{13}C-C_{org} versus C_{org}/N_{tot} gave more information regarding the source of marine and terrestrial OM to the sediment, station 26-9 presenting C_{org} characteristics close to the one of terrestrial C_3 plants (Figure 9a).

Looking at the C_{org} versus N_{tot}-content of the sediment (Figure 9b), we can clearly see that most of the sediment of the Amazon shelf fell along a line of slope (106/16) and intercept equal to 0, with station 9-6 and 10-6, in the Para River mouth presenting a higher C_{org} content. Conversely, station 13-3, located in the Amazon River mouth, was described by a line with a similar slope (106/16) but an negative intercept, suggesting a N-content of 0.02 %wt when no C_{org} was measured (Figure 9b).

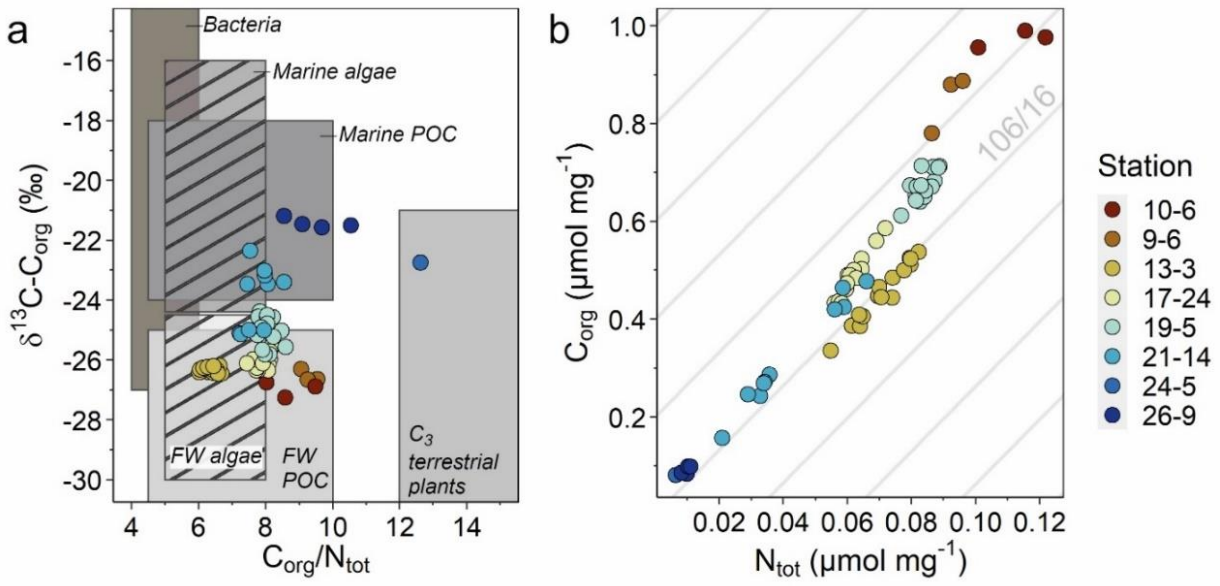

Figure 9. (**a**) The distribution of δ^{13}C-C_{org} versus C_{org}/N_{tot} ratios in the sediments compared to the compilation of typical values in coastal sediments by Lamb et al. (2006) provided more detail on the potential origins of OM on the shelf. FW stands for freshwater and POC for particulate organic carbon. (**b**) The relationship between C_{org} and N_{tot} content of the sediment falling virtually along a line with a slope of 106/16 lines (Redfield ratio) suggests that C_{org} and N_{tot} have similar remineralization pathways.

Porewater nutrient profiles

Maximum nutrient concentrations usually decreased from stations located in the river mouth to stations further off, e.g., with a difference of a factor 10 in the case of NH_4^+ (Figure 10). Aside from NO_3^-, pore water profiles show an increase in concentration with depth, with higher porewater concentration relative to the bottom water ones. $Si(OH)_4$ ranged from ~1200 μM in the Pará River mouth (station 10-6 and 9-6) to 150~300 μM at the other stations. A few $Si(OH)_4$ profiles presented a deviation from the asymptotic shape, typical in continental margin sediments. Instead, altering peaks and decrease in concentration were observed in cores from almost all stations. Station 13-3, in the Amazon River mouth, was presenting a regular $Si(OH)_4$ increase, reaching a maximum concentration of 200 μM at 30 cm depth.

Little to no NO_2^- was measured along transect, and concentrations were in general higher in the first few centimeters, except for stations 10-6 and 9-6, which presented a downcore increase up to 20 μM of NO_2^-. NO_3^- profiles showed a peak (up to 11.50 ± 0.30 μM, Figure 10) and a steep decrease within the first two centimeters within the sediment, reaching values below the detection limit (<0.02 μM). In the river mouth (stations 13-3 and 17-24), NO_3^- concentrations were 3 to 4 μM higher in the top 2 cm of the core compared to overlying water. Some profile at stations 9-6, 13-3, 17-24, 19-5 and 21-14 showed an increase in NO_3^- deeper in the sediment.

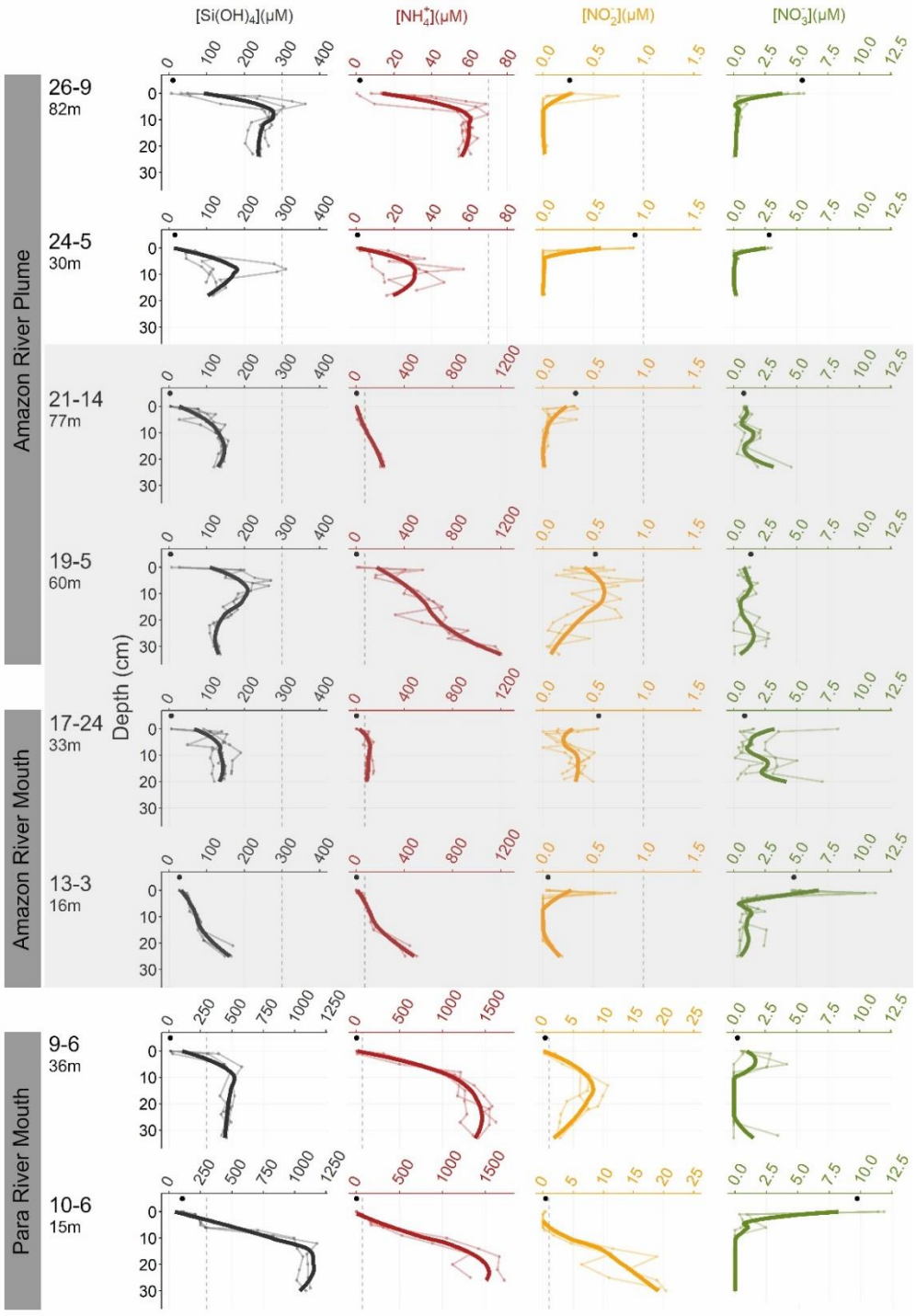

Figure 10. The porewater $Si(OH)_4$ and other nutrient profiles (NH_4^+, NO_2^- and NO_3^-) provide information on the processes at play below the sediment's surface. The shaded profiles are from stations located in regions where high accumulation rates or reworking were observed (see Figure 7). Concentrations are given in μM and each cores is represented by thin lines. The average per station (bold lines), was obtained by fitting multiple local polynomial regressions. The concentrations of each nutrient in the overlying water is represented by a small black marker. The grey dashed line in the $Si(OH)_4$ profiles highlights the 300 μM concentration threshold, value below which fresh phytoplankton usually naturally dissolves (Dixit et al. 2001). In order to facilitate the inter station comparison of other nutrient profiles, the grey dashed line represent the peak nutrient concentration measured at the most distal sites. Note the different scales for the x-axes.

Oxygen demand and benthic N fluxes

High benthic O_2 consumption rates were measurable at every station (ranging between 16.76 and 41.60 mmol m^{-2} d^{-1}, Figure 11a). Comparatively, fluxes of NH_4^+, NO_2^- and NO_3^- measured in both the core incubation experiments and via Fick's diffusion first law were low (ranging between -0.37 and 1.13 mmol m^{-2} d^{-1}; Figure 11b, c, d). The high variability between the three cores sampled for porewater nutrient at a same station results in most diffusion rates not being significantly different from 0 (one sample t-test, $p_{value} > 0.05$), and nutrient fluxes measured with both methods were usually not significantly different between station along transect (Tuckey test, $p_{value} > 0.05$). According to incubation fluxes, sediments appear to be a sink for NO_2^- (-0.06 mmol m^{-2} d^{-1}, Figure 11d).

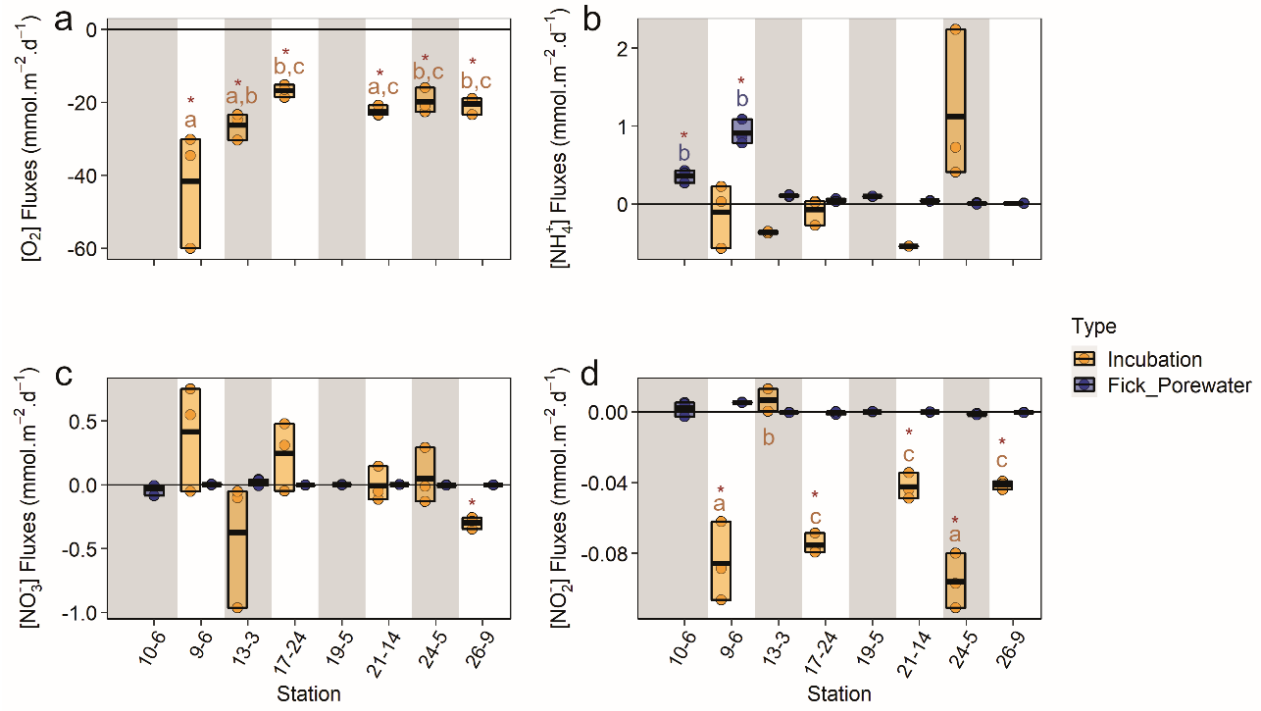

Figure 11. O_2 consumption and DIN fluxes obtained from the cores incubation (yellow) and the pore water profiles (dark blue) revealed that no clear source or sink of NH_4^+ and NO_3^- was detectable on the Amazon shelf, as measurements gathered around the zero-line, which represent the absence of fluxes. A negative flux accounts for a flux into the sediment and a positive flux represents diffusion in the overlying water. The boxes highlight the data range and the average of triplicate measurements. Letters group the stations that are not significantly different from each other (according to a Tuckey test), and red starts highlight fluxes that are significantly different from 0 (according to a one-sample student test).

There were discernable differences in the fluxes calculated from the core incubation and the pore water ones, the latter being on average ten times lower than the former, and in some cases, in the opposite direction. At station 13-3 for instance, in the Amazon River mouth, NH_4^+

and NO_3^- incubation fluxes are measured into the sediments, while out of the sediment according to the porewater profiles at this station (Figure 11c, d).

N_2O concentrations in sediment overlying waters

N_2O concentrations in overlying water were close to saturation (around 7.2 nM N_2O) at most stations on the shelf (Figure 12), with ΔN_2O values only 1 nM above or below zero, which is in the range of measurement uncertainty. Only station 10-6, located in the Para River mouth and station 26-9, at the edge of the shelf, presented an excess N_2O, with resulting ΔN_2O averaging 4 nM (Figure 12a). Otherwise, most stations harboured equilibrated N_2O concentrations, resulting in a weak relationship of ΔN_2O with AOU and NO_3^- on the shelf (Figure 12b, c).

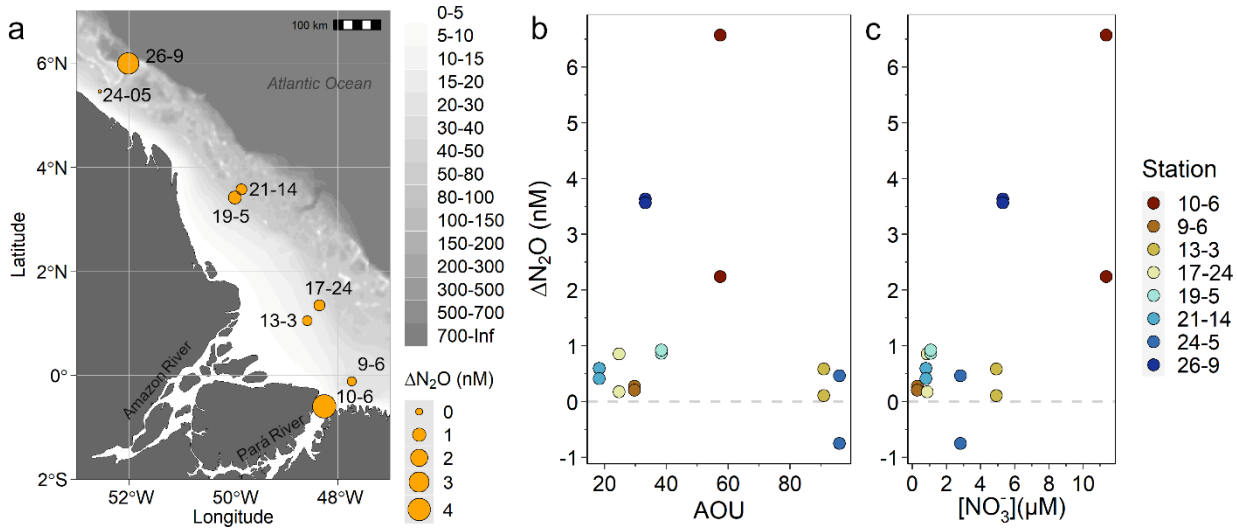

Figure 12. The role of the seabed as a source of N_2O for the water column on the shelf can be shown by (**a**) the variability of ΔN_2O in sediment overlying water along the shelf. The pathways behind the potential N_2O production can be unveiled looking at (**b**) the relationship between ΔN_2O and AOU and (**c**) NO_3^-. The grey dashed line in panel (**b**) and (**c**) highlights the N_2O equilibrium concentration with the atmosphere.

Discussion

Sediments are often considered as a reactor for OM, potentially acting as a net source or sink of dissolved nutrients for the overlying waters. In regions impacted by riverine N inputs such as river plumes, constraining the rates and mechanisms behind OM conversion to DIN is crucial for estimating N pools. Here, we measured benthic respiration and diffusive fluxes of N from the sediments along the Amazon River Plume to examine the behavior of benthic N, its remineralization pathways, and discuss potential consequences on the overlying waters and N budgets as the material moves progressively from the Amazon River mouth along the Amazon–Guianas shelf.

Seabed dynamics and sediment characteristics

From their analysis of several long cores retrieved on the shelf, Kuehl et al. proposed in 1986 a distribution of accumulation rates of sediment, and a distribution of regions where intense reworking occurs on the Amazon shelf. They observed slow accumulation and maximum reworking regions around the 15 m isobaths, resulting from resuspension by shoaling surface waves and tidal currents (Kuehl et al., 1986). After plotting our stations on top of this distribution, it becomes clear that station 13-3 (bottom depth of 16 m, Table 4) was located in a zone of maximum reworking, with a reworked layer thickness of up to 150 cm (Kuehl et al., 1986). While our cores are too short to confirm these numbers, the homogeneity of Hg, ^{210}Pb and ^{137}Cs downcore profiles at these stations suggest the occurrence of recent reworking events (Figure S1, Text S1). Riverine material could be found as far as 300 km away, e.g. at station 21-14, explaining the similarities between the characteristics of some sediments layer of this latter station with the material analyzed at the Amazon River mouth (Figure 8a; Figure 9a). The different sediment layers suggested by solid phase properties, such as at station 21-14 (2-5 cm, Figure S1), could then arise from lateral movements of sediments, leading to a layering of the deposits, a process reviewed recently by Nittrouer et al., (2021). With distance from the mouth, the top 30 cm of the sediment C_{org} and Hg (<10 μg kg^{-1}; S1) gets diluted compared to the river mouth (up to 60 μg kg^{-1}; Figure S1), a sign that little terrestrial material settles there (station 24-5 and 26-9, Figure 7b; Figure S1). This observation was confirmed by the low PSi content of the sediment along the plume, which decreased from 0.6 %wt in the river mouth to nearly 0 at more distal stations (Figure S1).

The terrestrial material delivered by the Amazon River displays a C_{org} fraction of 0.5 to 1.2 %wt with a $\delta^{13}C$-C_{org} value of -26.3 to -26.9 ‰ (Figure 8a), and a $\delta^{15}N$ of 4.7 ± 0.4 ‰ (Table 5), in accordance with previous studies of the region (Hedges et al. 1986; Keil et al. 1997; Mortillaro et al. 2011). The C_{org}/N_{tot} ratios of sediment in the Amazon River mouth ranged between 6.0 and 8.2 (Table 5) and did not vary with depth, an observation consistent with previous studies. While it is a sign for sediment mixing, it also suggests that C_{org} and N have similar recycling patterns (Aller et al., 1996). Sediment from stations located in the Pará River mouth (stations 10-6 and 9-6) had twice the C_{org} content of the material retrieved close to the Amazon River mouth (stations 13-3 and 17-24; Figure 8a) and higher C_{org}/N_{tot} ratios (ranging from 8.0 to 9.5; Table 5). This difference is surprising as stations 10-6 and 13-3, or 9-6 and 17-24 have similar water depths (~16 and ~30 m; Table 4), but could be the result of differences in types or loads of OM delivered (Sioli 1984; Einbock et al. 2023), or recycling efficiency between the two rivers. It is also likely that this difference originates from a difference in distance from the river mouth, as stations 10-6 and 9-6 are located within 60 km from the coast, while station 13-3, our Amazon River end-member, is already 100 km offshore (Figure 7). Station 19-5, which shows a higher C_{org} content than other stations with a similar $^{13}C_{org}$ isotopic composition, is located in a zone previously characterized by high sediment accumulation rates (Figure 7a; Kuehl et al., 1986).

With distance from the river mouth, the isotopic composition of C_{org} gets heavier, and the C_{org} content in the surface sediments lower, reaching values of -21.2 ± 0.2 ‰ and 0.2 wt%, respectively, off French Guyana's coast (Figure 8a). The observed increase in $\delta^{13}C$-C_{org} between the river mouth and more offshore stations could then reflect the addition of a marine component to the sedimentary OM pool (Gearing et al. 1984; Boutton 1991). C_{org}/N_{tot} ratios remain close to the values observed in the river mouth, except at most distal stations (24-5 and 26-9), where C_{org}/N_{tot} ranged between 8.5 and 12.6 (Table 5; Figure 9a). This difference could highlight a difference in OM source, with material originating from marine POC and C_3 plants (Figure 9a). Indeed, station 24-5 is located close to the mangrove belt, an ecosystem populated by C_3 plants (Gontharet et al. 2014), while station 26-9 is the most distal station, therefore most likely to be more influenced by marine OM than other stations. Similarly, while the $\delta^{15}N$ of sediment remains virtually unchanged on the shelf, station 26-9 exhibited slightly lower $\delta^{15}N$ values (3.5 ± 0.3 ‰; Table 5), which could result from a higher contribution of OM derived from dinitrogen fixation in this more marine station. This is also suggested by the lower $\delta^{15}N$-POM at the surface at this site (Carpenter et al. 1997). As expected, a mixing model applied to

this data reveals that marine OM could explain more than 80 % of the observed surface $\delta^{13}C$-C_{org} at the most distal stations (Figure 8b).

Sediments on the Amazon shelf present a variation in their characteristics along the Amazon River Plume, with higher concentrations of terrestrial C_{org} close to the Amazon and Pará River mouths and more marine C_{org} at distal stations. The rapid decrease in C_{org} content with distance from the river mouth could arise from intense reworking and consequent dilution of the sediment's terrestrial C_{org} content. However, the overall increase in C_{org}/N_{tot} while both C_{org} and N_{tot} content decrease with distance from the river mouth Figure 9a b) could also suggest that remineralization occurs, with preferential loss of N relative to C_{org} during the decomposition of OM (Gordon 1971).

The offset from the $\delta^{13}C$-C_{org} versus C_{org} content (Figure 8a) provides additional hints for remineralization. Stations 13-3 and 17-24, located less than 100 km off the river mouth, exhibit a C_{org} content up to 60 % lower compared to station 9-6, which has a similar $\delta^{13}C$-C_{org} (Figure 8a), while also being in an area where sediment accumulation occurs. The distribution of the sediment C_{org} and N_{tot} data, virtually falling along the C/N Redfield ratio slope (Figure 9b), further confirms the occurrence of OM remineralization. Furthermore, sediments at station 13-3 exhibit a $\delta^{15}N$ nearly 3 ‰ lower than the $\delta^{15}N$ of POM observed in surface waters at this station (7.7 ‰; Table 5), hinting towards a significant alteration of terrestrial OM in the river mouth. This station also exhibited the lowest C_{org}/N_{tot} values (Figure 9a). There, the average C_{org}/N_{tot} value of 6.4 ± 0.2 could hint towards the higher activity of bacteria, biomass with a C/N of ~5±1 (Zimmerman et al. 2014). Remineralization could also lead to higher inorganic N concentrations relative to sediments unaffected by this process, explaining the lower C_{org}/N_{tot} ratios observed at this station.

Oxygen consumption at the seabed

We performed core incubations to measure benthic O_2 consumption rates, which often represent an integrated measure of remineralization (Mackin and Swider 1989). However, these measurements only provide information on the sediment's reactivity during stable seabed periods, which is a situation that seldom happens on the Amazon shelf (Kuehl et al. 1995; Nittrouer and DeMaster 1996). During our cruise, which took place during rising or peak river flow, sediment's total O_2 uptake averaged 23 mmol m^{-2} d^{-1} on the shelf (Figure 11a). This value is almost two times higher than respiration rates previously measured during this period (Aller

et al. 1996). The shelf's average for C_{org} remineralization rates, comprising both terrestrial and marine sources, were estimated to be at least of 53 mmol m^{-2} d^{-1} (Aller et al. 1996). In this scenario, our O_2 consumption rates (~ 23 mmol m^{-2} d^{-1} on the shelf) only explain 40 % of C_{org} remineralization.

One major reason for discrepancies between studies may be solely due to the dynamics of the seabed. In fact, sediment reworking has been demonstrated to cause an increase in benthic respiration rates (Almroth et al. 2009; Niemistö et al. 2018). Therefore, it could be hypothesized that even though we sampled during a period already covered in previous studies, some recent resuspension events prior to our sampling led to the higher observed O_2 consumption rates. Furthermore, other processes might lead to an O_2 uptake in our incubation, such as the oxidation of reduced metabolites other than NH_4^+ (like ferrous iron) during episodes of sediment reworking, which are, as discussed earlier, frequent on the Amazon shelf. Described as a main consumption term, reoxidation of reduced compounds, mainly ferrous iron, has been found to lead to O_2 consumption that is in roughly the same proportion as though decomposition with nitrification (O_2/C = 1.3, Aller et al. 1996; Aller and Blair 1996).

However, it is interesting to note that the marginally higher O_2 consumption values were consistently observed at every station, even the more distal ones where Aller et al. (2001) did not measure rates higher than 18 mmol m^{-2} d^{-1}. An increase in POM load could explain the higher O_2 consumption rates in 2021, but despite major changes in the Amazon Basin, Montanher et al. (2018) underlined an overall decreasing trend in suspended sediment transport between 1984 and 2016. Since our incubations also encompass processes in the sediment overlying waters, it is also possible that the higher rates observed reflect a difference in dissolved OM (DOM) or DIN content in the overlying water between 1989-1991 (Aller et al. 1996) and our study. Such an increase could result from the climate-changed-induced increase in maximum discharge during wet seasons (Liang et al. 2020), and (Aquino et al. 2022) reported an increase in DIN over the past decade, which could result in increased O_2 consumption rates. Whether this DIN increase could result in a direct increase in ammonification and nitrification or an increased primary production and subsequent remineralization of POM deposition remains to be determined.

Porewater processes

The impact of climate change and increase in population growth, agriculture and deforestation (Aquino et al. 2022) that the Amazon River basin underwent since the study by Aller et al., (1996) may have resulted in changes in benthic N cycling. We aimed to assess the impact of OM remineralization on benthic N cycling and fluxes on the Amazon shelf by measuring porewater nutrients, as well as nutrient fluxes in sediment incubations. Whereas the solid phase remains homogeneous after reworking, porewaters usually readjust more rapidly (Sloth et al. 1996) and record pathways for OM mineralization in the sediments. However, porewater concentrations can remain at non-steady state conditions when surrounding conditions are altered constantly, e.g., by temperature, salinity changes, bioirrigation and reworking (Huettel et al., 1998; Huettel et al., 2013). It is, therefore, necessary to first define whether the sediment studied is subject to these processes before interpreting the nutrient gradients. This can be achieved by looking at the $Si(OH)_4$ profile in porewater, as this nutrient is not governed by any microbial turnover process, but only by physical mechanisms (Boudreau 1997). Bioirrigation is likely not dominant as the cores contained little to no macrofauna.

Porewater nutrients concentration were 3 to 15 times lower in the Amazon River mouth sediments relative to the Pará stations (Figure 10). While we could discuss potential differences in nutrient sources and processes, the most likely explanation is that, as discussed for C_{org} content, this pattern simply originates from a difference in distance from the river mouth. At inshore stations and as far as 300 km away from the river mouth, $Si(OH)_4$ porewater concentrations were not asymptotic, but presented irregular patterns, a sign for intense reworking of the sediment (Boudreau 1997). At river mouth stations, it is therefore likely that porewater transfer in and out of the sediment by reworking dominates the distribution of dissolved nutrients over microbial degradation.

The maximum $Si(OH)_4$ concentrations were found to be lower than 300 μM (Figure 10) along the Amazon Plume. This value is below the molecular solubility of fresh plankton (Dixit et al. 2001), which could explain the low concentrations of PSi found in the sediment. It could also suggest a loss of $Si(OH)_4$ formed by the dissolution of biogenic opal through the formation of alumino-silicate minerals. Nevertheless, NH_4^+ fixation on clay seems to be of minor importance, as NH_4^+ concentrations mostly increased with depth (Figure 10) as a result of OM degradation (Henrichs and Farrington 1987; Burdige and Martens 1988). The accumulation of NH_4^+ was more intense at the stations located in the Pará (10-6) and Amazon (13-3) River

mouths (Figure 10), as well as at 19-5, the stations with the highest C_{org} content (Figure 8a) compared to distal stations. The higher OM concentrations at inshore relative to distal stations would foster higher ammonification rates and explain the observed trend.

Anoxic conditions are usually encountered within the first millimeters of the sediment on the Amazon shelf (Aller et al. 1996). This characteristic presumably explains the NO_3^- depletion within the first 5 cm of the sediments while some NO_2^- is still present (Figure 10) as a consequence of denitrification, an anaerobic process (Nixon 1981; Aller et al. 1996; DeMaster and Aller 2001; Crowe et al. 2012). Five stations (9-6, 13-3, 19-5, 17-24 and 21-14) also displayed an increase in NO_3^- concentrations in deeper layers of the sediment, and the $Si(OH)_4$ profiles usually appear to be disturbed as well (Figure 10). Since all nutrient profiles of the three sampled cores seem to be affected, it seems unlikely that this is an artifact during sampling. Infiltration of overlying water deeper into the cores because of recent resuspension of the sediments could explain this phenomenon. The deep NO_3^- concentrations observed were usually a few micromoles per liter higher than the concentration measured in the overlying water, which could indicate that seepage of overlying water into the sediment brings in new O_2 and fosters nitrification (Jäntti et al. 2012). Anoxic nitrification via manganese reduction has also been proven to explain NO_3^- increase in sediments (Luther et al. 1997), but this process would lead to a similar change between the production and consumption of NO_3^- and the change in the NH_4^+ concentration gradient (Chong et al. 2018). However, our data shows a much greater change in NH_4^+ than in NO_3^-. Therefore, the hypothesis of a low NH_4^+ oxygenated waters leakage in the sediments that promotes oxic nitrification is more likely.

Nitrification can also be expected in the top sediments, as hinted by the lower NH_4^+ concentrations (Figure 10). While this process would lead to NO_3^- production, it was interesting to note that no clear NO_3^- peak was measured in the top of the sediments. Instead, there was a decrease from more concentrated overlying waters to depletion in the sediments (Figure 10), which could be a sign for NO_3^- reduction (denitrification), as discussed earlier, and that NO_3^- is consumed faster than it is produced. However, several of the individual replicate cores presented NO_3^- peaks at the sediment-water interface. Our sample resolution was probably too low to capture the very superficial peak in every core, and since we observed a NO_3^- release from some cores, (Figure 11), it is credible that the sediment is a source of NO_3^-. The NO_3^- production observed in many incubations could also be due to nitrification in overlying waters instead of in the porewater.

Resulting benthic N fluxes on the Amazon shelf

Core incubations were performed to address the significance of the nutrient release from sediments to the water column. Although fluxes were low and not significantly different from zero at most stations, NH_4^+ fluxes were measured into the sediments in core incubation. Conversely, porewater profiles clearly indicated the possibility for a flux out of the seabed (Figure 10, Figure 11b), suggesting that NH_4^+ diffusing out of the sediment generally undergoes complete nitrification. Interpretation of diffusive fluxes obtained from porewater profiles have to be interpreted with care, since a lot of stations exhibited non-steady state conditions, probably deriving from recent reworking. But with the important NH_4^+ pool in porewater, we can imagine that resuspension events fuel nitrification in the overlying waters, potentially leading to a buildup of NO_3^- at the bottom.

Assuming complete nitrification of the highest NH_4^+ efflux measured (2.5 mmol NH_4^+ m^{-2} d^{-1}; Figure 11b), resulting in no net NH_4^+ flux in our incubations, (Figure 10, Figure 11b), the total benthic O_2 demand should range between 28 and 35 mmol m^{-2} d^{-1}. This range covers the average measured in our incubations at stations near the Pará and Amazon River mouths (26.2 ± 3.7 at station 13-3 and 41.6 ± 16.1 mmol m^{-2} d^{-1} at station 9-6; Figure 11a). However, this does not match the NO_3^- fluxes observed in our incubations. If the entirety of the O_2 was used for nitrification and assuming a N/O ratio of 16/150, we would have expected NO_3^- fluxes of 2.8 to 4.5 mmol m^{-2} d^{-1} in the Amazon and Pará River mouths. The observed NO_3^- fluxes of -0.97 to 0.75 mmol m^{-2} d^{-1} (Figure 11) would then suggest that efficient NO_3^- reduction (potentially denitrification) takes place, with NO_3^- consumption rates ranging between 1.97 and 5.30 mmol m^{-2} d^{-1}.

But nitrification might not be the only process consuming O_2 on the Amazon shelf, and nitrification might not be the only pathway for OM remineralization. Because O_2 consumption rates cover both, the remineralization of OM and the reoxidation of reduced compounds, we combined our data with measurements of N_2O concentrations in bottom waters in a further attempt to unveil the occurrence and link between nitrification and denitrification on the Amazon shelf. Station 10-6 in the Para River mouth and station 26-9 located at the edge of the northern part of the shelf presented a small N_2O source, with ΔN_2O values averaging 4 nM (Figure 12a). These stations also present a higher AOU and NO_3^- concentrations (Figure 12b, c) relative to other stations, implying that nitrification might be dominant over denitrification there.

However, on the rest of the Amazon shelf, N_2O concentrations were close to equilibrium with the atmosphere (Figure 12a), suggesting that little N_2O is produced or consumed in and above the sediments, making them neither a source nor a sink for N_2O. While the absence of a clear trend in AOU and NO_3^- with ΔN_2O at most stations (Figure 12b) could be interpreted as low reactivity, it is more likely that mixing brings new O_2 to overlying water and dilutes the N_2O signal back to atmospheric values. In the case of increased nitrification following a reworking event and subsequent release porewater NH_4^+, we could hypothesize that the AOU would increase, along with ΔN_2O. It could therefore be that episodes of reworking make the Amazon shelf a source of N_2O for the atmosphere.

These results emphasize a strong coupling between NO_3^- production and consumption pathways on the Amazon shelf, as evidenced by the lack of a net DIN flux across the sediment-water interface. The results further suggest that nitrification is occurring, but is overwritten by mixing and denitrification. NO_3^- concentrations did not always increased over time (Figure 11d), and little NO_3^- accumulated in the porewater, which also highlights the balance between nitrification rates and NO_3^- diffusion into the sediments or removal (likely via denitrification).

While the Amazon River basin underwent drastic changes over the past few decades, our results are in accordance with N diffusion rates measured by Aller et al., (1996), who found that little or no DIN escaped from the sediments. Climate change and anthropogenic forcing can have a broad range of effect on OM and DIN inputs to coastal zones. Thus, the absence of a clear difference between our and previous studies gives hope that the buffering capacity of the Amazon discharge has not yet reached its limit. However, further studies could investigate the impact of the intensification of the Amazon's hydrological cycle on the coupling between nitrification and denitrification and resulting consequences on N_2O fluxes.

Conclusions

The Amazon River delivers a high load of fine sediments to the shelf. At the river mouth, the OM reaching the seabed is primarily composed of terrestrial material (>80 %), and with distance from the mouth, marine organic debris increasingly dominates OM's content. Part of the OM seems to undergo ammonification, resulting in NH_4^+ accumulation in the porewater. In the sediment overlying water, as well as in the very first centimeters of the sediment, this NH_4^+ seems to be transformed to NO_3^- via nitrification, which is further reduced by denitrification in deeper sediment. The higher observed O_2 consumption rates in the Amazon

shelf during the study could be attributed to several factors, including sediment reworking (reoxidation of reduced compounds such as ferrous iron) and changes in DIN content and suspended sediment transport. Despite the elevated O_2 consumption rates measured, the absence of clear NH_4^+ and NO_3^- fluxes at the sediments-water interface suggests that there is a tight coupling between production and removal of N species. In fact, the analysis of N_2O concentrations in bottom waters only showed a weak correlation between ΔN_2O and NO_3^-, suggesting that nitrification is overprinted by denitrification or mixing, making the seabed a sink for organic N, while no DIN or N_2O escapes the sediment. While these results are in accordance with studies conducted in the region before it underwent drastic changes, it seems there is still a strong coupling between nitrification and denitrification in sediment of the Amazon shelf, further highlighting the reactivity and buffer capacity of the sediment.

Acknowledgments. The authors thank the research cruise N-Amazon PI: Maren Voss, R/V Meteor. This study was supported by MeNARP Project (Metabolism of Nitrogen in the Amazon River Plume, project number VO 487/14-1) and M174 cruise "N-Amazon" (GPF19-1-13). The authors also thank Christian Burmeister (nutrient analyses), Iris Liskow, Josephin Lemke, Sascha Plewe and Svenja Papenmeier (lab support), Uwe Hehl (field support), Captain and Crew of the R/V Meteor (support at sea). The two anonymous reviewers provided very helpful comments that led to improved presentation and discussion of our data. Open Access funding enabled and organized by Projekt DEAL.

Appendices

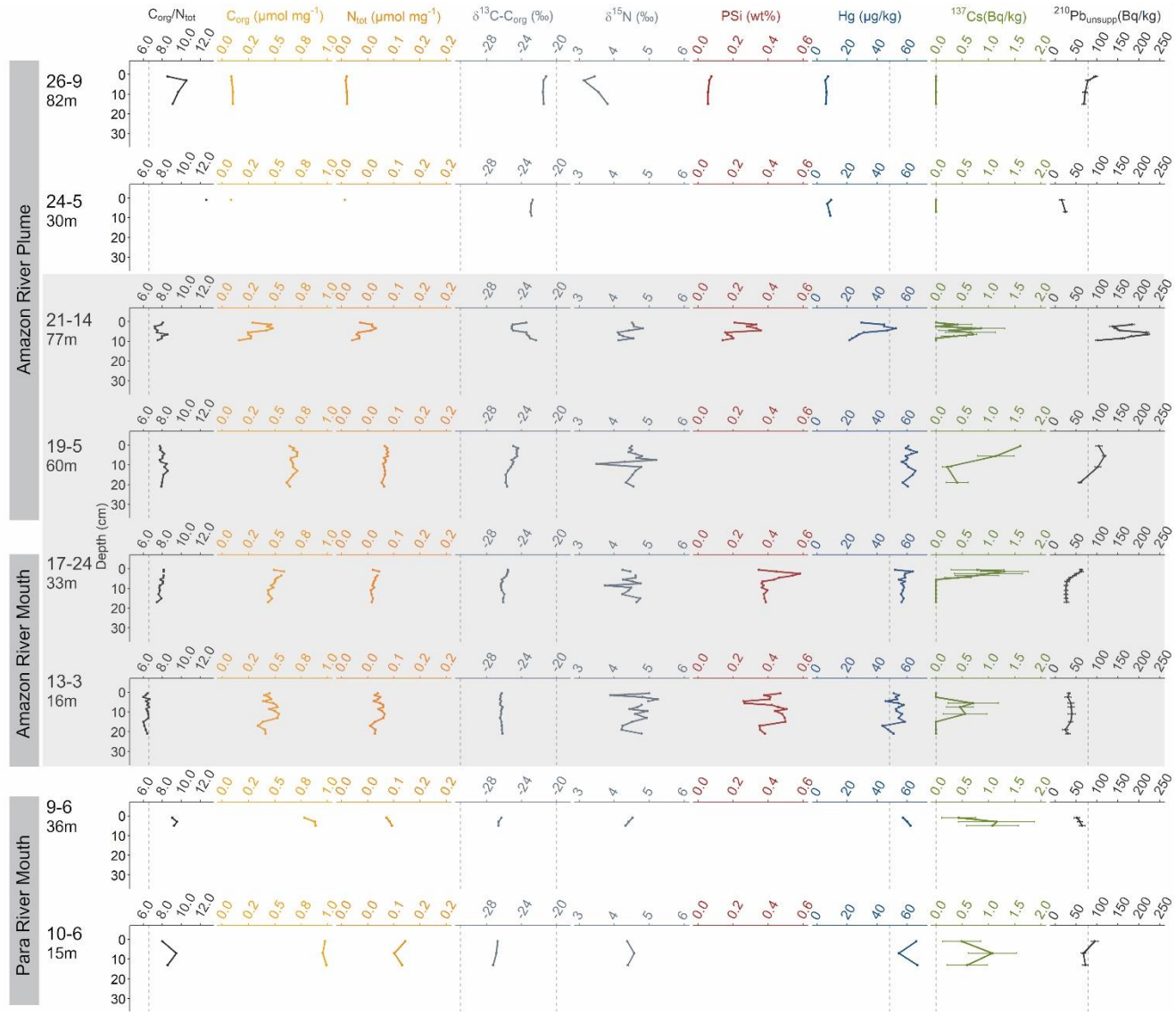

Figure S1. Solid phase characteristics of the sediments (C_{org} content, Psi, C_{org}/N_{tot}, $\delta^{13}C$ and $\delta^{15}N$, Mercury (Hg) and ^{137}Cs and ^{210}Pb activities in Bq/kg) at the sampled stations. The grey dashed line in some profiles highlight some key thresholds for the variable: for the C_{org}/N profiles, the dashed line represent the Redfield ratio, in the $\delta^{13}C$ profiles are highlighted the marine and terrestrial end members used in Figure 8 and Figure 9. 0 is emphasized in the ^{137}Cs profiles. In the Hg and ^{210} Pb profiles, the dashed line represents the average of all data. The shaded profiles are from stations located in regions where high accumulation rates or reworking were observed (see Figure 7 and Figure 10).

Text S1. Text Sedimentation regime

The sedimentation regime is critical for the data interpretation at the respective sites. The sedimentation regime at our sites in the sub-areas, Amazon River Mouth and Amazon River Plume, we characterize based on own short sediment core studies together with the comprehensive results by Kuehl et al. (1986). Kuehl et al. (1986) studied a number of short and long cores from the same general study area. However, data on the Para River Mouth were not obtained by Kuehl et al. (1986).

Sites 26-9 and 24-5: The $^{210}Pb_{unsupp}$ data indicates that the radionuclide ^{210}Pb dating horizon is not reached at 7cm in 24-5 and 15 in 26-9, respectively. No ^{137}Cs could be detected. At these northernmost distal sites Hg is low, as the input/sedimentation of riverine terrestrial material from the Amazon and Para is low. The sites water depths are deeper (with 30 m and 82 m) than the critical water depth of c. 15 m (for sediment re-working) discussed in Kuehl et al. (1986).

Site 21-14 and 19-5: At 21-14 high $^{210}Pb_{unsupp}$ indicates that the sedimentation rate at this site is rather low which is in line with Kuehl et al.'s results. Nuclear weapons testing derived ^{137}Cs is detected down to 7 cm. The ^{210}Pb dating horizon is not reached at 10 cm core depth. High Hg values (lower $^{210}Pb_{unsupp.}$) may indicate the accumulation of material derived from Amazon and Para rivers in the depth interval 2-6 cm. At site 19-5, in accordance with Kuehl et al. (1986) all parameters point to a high sedimentation rate here. Artificial radionuclide ^{137}Cs is present in all samples from the 20cm core interval studied. Kuehl et al. (1986) observed highest sediment accumulation rates in the area of 19-5. The sites water depths with 77 and 60 m are much deeper than the critical water depth of c. 15 m (for sediment re-working) discussed in Kuehl et al. (1986).

Sites 17-24 and 13-3: The $^{210}Pb_{unsupp}$ profiles indicate that the dating horizon is not reached at c. 20 cm in both cores. Hg is still high in the lowermost sample indicative of high terrestrial input. Based on Kuehl et al. (1986)´s results obtained on long sediment cores, our two sites 17-24 and 13-3 are located in an area with a high thickness of re-worked material. This feature needs to be taken into account when interpreting our data obtained at these two sites.

Sites 10-6 / 9-6: Unfortunately, there are no studies on long cores in the Para River Mouth area by Kuehl et al. (1986). However, moderate $^{210}Pb_{unsupp.}$activities, high Hg and ^{137}Cs

detection seem to indicate a high sediment accumulation at the two sites. However, a more solid characterization of the sedimentation regime is not possibly as only the upper 5cm in 9-6 and 15 cm in 10-6, respectively have been studied.

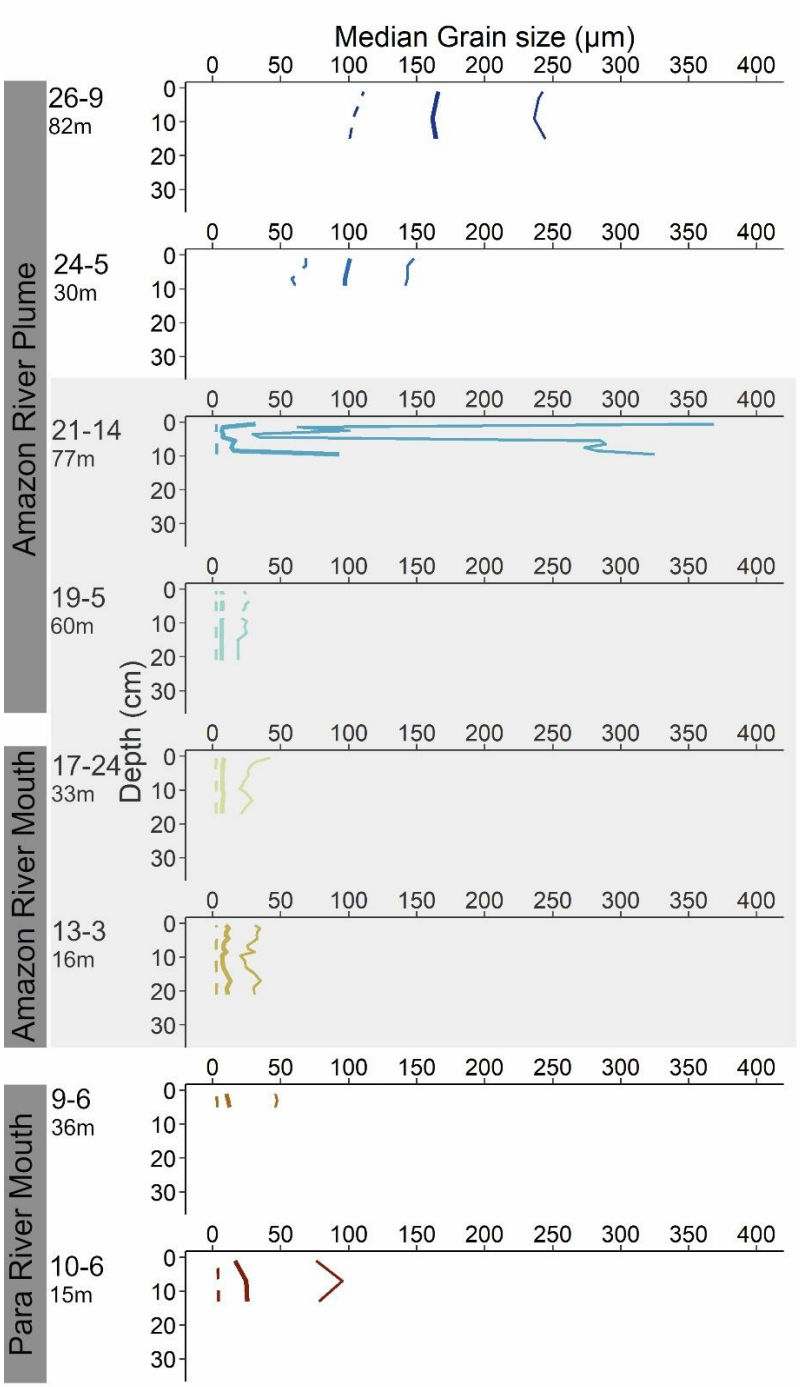

Figure S2. Downcore grain size at each station sampled. The dashed, bold and plain line (from left to right) represent D10, D50 and D90, respectively. It corresponds to the grain size below which 10, 50 and 90% of the particles are measured.

References

Abril, G., S. A. Riou, H. Etcheber, M. Frankignoulle, R. De Wit, and J. J. Middelburg. 2000. Transient, tidal time-scale, nitrogen transformations in an estuarine turbidity maximum-fluid mud system (the Gironde, south-west France). Estuarine, Coastal and Shelf Science **50**: 703–715. doi:10.1006/ecss.1999.0598

Aller, R. C., and N. E. Blair. 1996. Sulfur diagenesis and burial on the Amazon shelf: Major control by physical sedimentation processes. Geo-Marine Letters **16**: 3–10. doi:10.1007/BF01218830

Aller, R. C., and N. E. Blair. 2006. Carbon remineralization in the Amazon–Guianas tropical mobile mudbelt: A sedimentary incinerator. Continental Shelf Research **26**: 2241–2259. doi:10.1016/j.csr.2006.07.016

Aller, R. C., N. E. Blair, Q. Xia, and P. D. Rude. 1996. Remineralization rates, recycling, and storage of carbon in Amazon shelf sediments. Continental Shelf Research **16**: 753–786. doi:10.1016/0278-4343(95)00046-1

Almroth, E., A. Tengberg, J. H. Andersson, S. Pakhomova, and P. O. J. Hall. 2009. Effects of resuspension on benthic fluxes of oxygen, nutrients, dissolved inorganic carbon, iron and manganese in the Gulf of Finland, Baltic Sea. Continental Shelf Research **29**: 807–818. doi:10.1016/j.csr.2008.12.011

Aquino, R., C. Noriega, A. Mascarenhas, and others. 2022. Possible Amazonian contribution to *Sargassum* enhancement on the Amazon Continental Shelf. Science of The Total Environment **853**: 158432. doi:10.1016/j.scitotenv.2022.158432

Benson, B. B., and D. Krause Jr. 1984. The concentration and isotopic fractionation of oxygen dissolved in freshwater and seawater in equilibrium with the atmosphere 1. Limnology and Oceanography **29**: 620–632. doi:10.4319/lo.1984.29.3.0620

Boudreau, B. P. 1997. Diagenetic models and their implementation: Modelling transport and reactions in aquatic sediments, Springer Berlin Heidelberg.

Boutton, T. W. 1991. Stable carbon isotope ratios of natural materials: 2 Atmospheric, terrestrial, marine, and freshwater environments, Academic Press, Inc.

Burdige, D. J., and C. S. Martens. 1988. Biogeochemical cycling in an organic-rich coastal marine basin: 10. The role of amino acids in sedimentary carbon and nitrogen cycling. Geochimica et Cosmochimica Acta **52**: 1571–1584. doi:10.1016/0016-7037(88)90226-8

Carpenter, E. J., H. R. Harvey, B. Fry, and D. G. Capone. 1997. Biogeochemical tracers of the marine cyanobacterium *Trichodesmium*. Deep Sea Research Part I: Oceanographic Research Papers **44**: 27–38. doi:10.1016/S0967-0637(96)00091-X

Chong, L. S., W. M. Berelson, J. McManus, and N. E. Rollins. 2018. Meter-scale early diagenesis of organic matter buried within deep-sea sediments beneath the Amazon River Plume. Front. Mar. Sci. **5**. doi:10.3389/fmars.2018.00250

Coles, V. J., M. T. Brooks, J. Hopkins, M. R. Stukel, P. L. Yager, and R. R. Hood. 2013. The pathways and properties of the Amazon River Plume in the tropical North Atlantic Ocean. J. Geophys. Res. Oceans **118**: 6894–6913. doi:10.1002/2013JC008981

Crowe, S. A., D. E. Canfield, A. Mucci, B. Sundby, and R. Maranger. 2012. Anammox, denitrification and fixed-nitrogen removal in sediments from the Lower St. Lawrence Estuary. Biogeosciences **9**: 4309–4321.

DeMaster, D. J., and R. C. Aller. 2001. Biogeochemical processes on the Amazon shelf: Changes in dissolved and particulate fluxes during river/ocean mixing. The Biogeochemistry of the Amazon Basin 328–357.

Demaster, D. J., and R. H. Pope. 1996. Nutrient dynamics in Amazon shelf waters: Results from AMASSEDS. Continental Shelf Research **16**: 263–289. doi:10.1016/0278-4343(95)00008-O

Dixit, S., P. Van Cappellen, and A. J. van Bennekom. 2001. Processes controlling solubility of biogenic silica and pore water build-up of silicic acid in marine sediments. Marine Chemistry **73**: 333–352. doi:10.1016/S0304-4203(00)00118-3

Einbock, A., E. Burtscher, C. Frey, and F. Conen. 2023. Export of ice-nucleating particles from watersheds: results from the Amazon and Tocantins river plumes. Royal Society Open Science **10**: 220878. doi:10.1098/rsos.220878

Eppley, R. W., and B. J. Peterson. 1979. Particulate organic matter flux and planktonic new production in the deep ocean. Nature **282**: 677–680. doi:10.1038/282677a0

Filizola, N., and J. L. Guyot. 2009. Suspended sediment yields in the Amazon basin: an assessment using the Brazilian national data set. Hydrological Processes **23**: 3207–3215. doi:10.1002/hyp.7394

Froelich Jr, P. N., D. K. Atwood, and G. S. Giese. 1978. Influence of Amazon River discharge on surface salinity and dissolved silicate concentration in the Caribbean Sea. Deep Sea Research **25**: 735–744.

Froelich, P., G. P. Klinkhammer, M. L. Bender, and others. 1979. Early oxidation of organic matter in pelagic sediments of the eastern equatorial Atlantic: Suboxic diagenesis. Geochimica et cosmochimica acta **43**: 1075–1090.

Fry, B. 2006. Stable isotope ecology, Springer.

Gearing, J. N., P. J. Gearing, D. T. Rudnick, A. G. Requejo, and M. J. Hutchins. 1984. Isotopic variability of organic carbon in a phytoplankton-based, temperate estuary. Geochimica et Cosmochimica Acta **48**: 1089–1098. doi:10.1016/0016-7037(84)90199-6

Geyer, W. R. 1995. Tide-induced mixing in the Amazon Frontal Zone. J. Geophys. Res. **100**: 2341. doi:10.1029/94JC02543

Geyer, W. R., R. C. Beardsley, S. J. Lentz, J. Candela, R. Limeburner, W. E. Johns, B. M. Castro, and I. D. Soares. 1996. Physical oceanography of the Amazon shelf. Continental Shelf Research **16**: 575–616.

Gloor, M., R. J. W. Brienen, D. Galbraith, and others. 2013. Intensification of the Amazon hydrological cycle over the last two decades. Geophysical Research Letters **40**: 1729–1733. doi:https://doi.org/10.1002/grl.50377

Goloway, F., and M. Bender. 1982. Diagenetic models of interstitial nitrate profiles in deep sea suboxic sediments 1. Limnology and Oceanography **27**: 624–638.

Gontharet, S., O. Mathieu, J. Lévêque, and others. 2014. Distribution and sources of bulk organic matter (OM) on a tropical intertidal mud bank in French Guiana from elemental and isotopic proxies. Chemical Geology **376**: 1–10. doi:10.1016/j.chemgeo.2014.03.009

Gordon, D. C. 1971. Distribution of particulate organic carbon and nitrogen at an oceanic station in the central Pacific. Deep Sea Research and Oceanographic Abstracts **18**: 1127–1134. doi:10.1016/0011-7471(71)90098-2

Gouveia, N. A., D. F. M. Gherardi, and L. E. O. C. Aragão. 2019. The role of the Amazon River plume on the intensification of the hydrological cycle. Geophys. Res. Lett. **46**: 12221–12229. doi:10.1029/2019GL084302

Grasshoff, K., K. Kremling, and M. Ehrhardt. 1999. Methods of seawater analysis, John Wiley & Sons.

Hammond, D. E., Cummins, K. M., McManus, J., Berelson, W. M., Smith, G., & Spagnoli, F. (2004). Methods for measuring benthic nutrient flux on the California Margin: Comparing shipboard core incubations to in situ lander results. Limnol. Oceanogr. Methods 2(6): 146–159. Portico. https://doi.org/10.4319/lom.2004.2.146

Hedges, J. I., W. A. Clark, P. D. Quay, J. E. Richey, A. H. Devol, and M. Santos. 1986. Compositions and fluxes of particulate organic material in the Amazon River 1. Limnology and Oceanography **31**: 717–738.

Henrichs, S. M., and J. W. Farrington. 1987. Early diagenesis of amino acids and organic matter in two coastal marine sediments. Geochimica et Cosmochimica Acta **51**: 1–15. doi:10.1016/0016-7037(87)90002-0

Howarth, R. W. 1988. Nutrient limitation of net primary production in marine ecosystems. Annu. Rev. Ecol. Syst. **19**: 89–110. doi:10.1146/annurev.es.19.110188.000513

Huettel, M., P. Berg, and J. E. Kostka. 2013. Benthic exchange and biogeochemical cycling in permeable sediments. Annu. Rev. Mar. Sci. **6**: 23–51.

Huettel, M., W. Ziebis, S. Forster, and G. W. Luther. 1998. Advective transport affecting metal and nutrient distributions and interfacial fluxes in permeable sediments. Geochimica et Cosmochimica Acta **62**: 613–631. doi:10.1016/S0016-7037(97)00371-2

Jäntti, H., E. Leskinen, C. F. Stange, and S. Hietanen. 2012. Measuring nitrification in sediments – comparison of two techniques and three ^{15}NO measurement methods. Isotopes in Environmental and Health Studies **48**: 313–326. doi:10.1080/10256016.2012.641543

Keil, R. G., L. M. Mayer, P. D. Quay, J. E. Richey, and J. I. Hedges. 1997. Loss of organic matter from riverine particles in deltas. Geochimica et Cosmochimica acta **61**: 1507–1511.

Kineke, G. C., R. W. Sternberg, J. H. Trowbridge, and W. R. Geyer. 1996. Fluid-mud processes on the Amazon continental shelf. Continental shelf research **16**: 667–696.

Kuehl, S. A., D. J. DeMaster, and C. A. Nittrouer. 1986. Nature of sediment accumulation on the Amazon continental shelf. Continental Shelf Research **6**: 209–225. doi:10.1016/0278-4343(86)90061-0

Kuehl, S. A., T. D. Pacioni, and J. M. Rine. 1995. Seabed dynamics of the inner Amazon continental shelf: temporal and spatial variability of surficial strata. Marine Geology **125**: 283–302.

Lamb, A. L., G. P. Wilson, and M. J. Leng. 2006. A review of coastal palaeoclimate and relative sea-level reconstructions using δ^{13}C and C/N ratios in organic material. Earth-Science Reviews **75**: 29–57. doi:10.1016/j.earscirev.2005.10.003

Leipe, T., M. Moros, A. Kotilainen, H. Vallius, K. Kabel, M. Endler, and N. Kowalski. 2013. Mercury in Baltic Sea sediments—Natural background and anthropogenic impact. Geochemistry **73**: 249–259. doi:10.1016/j.chemer.2013.06.005

Liang, Y.-C., M.-H. Lo, C.-W. Lan, H. Seo, C. C. Ummenhofer, S. Yeager, R.-J. Wu, and J. D. Steffen. 2020. Amplified seasonal cycle in hydroclimate over the Amazon River basin and its plume region. Nature Communications **11**: 4390. doi:10.1038/s41467-020-18187-0

Lohrenz, S. E., M. J. Dagg, and T. E. Whitledge. 1990. Enhanced primary production at the plume/oceanic interface of the Mississippi River. Continental shelf research **10**: 639–664.

Luther, G. W., B. Sundby, B. L. Lewis, P. J. Brendel, and N. Silverberg. 1997. Interactions of manganese with the nitrogen cycle: Alternative pathways to dinitrogen. Geochimica et Cosmochimica Acta **61**: 4043–4052. doi:10.1016/S0016-7037(97)00239-1

Mackin, J. E., and K. T. Swider. 1989. Organic matter decomposition pathways and oxygen consumption in coastal marine sediments. J Mar Res **47**: 681–716. doi:10.1357/002224089785076154

Martinelli, L. A., A. S. Pinto, G. B. Nardoto, J. Ometto, S. Filoso, L. D. Coletta, and E. C. Ravagnani. 2012. Nitrogen mass balance in the Brazilian Amazon: An update. Braz. J. Biol. **72**: 683–690. doi:10.1590/S1519-69842012000400007

Meade, R. H., T. Dunne, J. E. Richey, U. de M. Santos, and E. Salati. 1985. Storage and remobilization of suspended sediment in the lower amazon river of brazil. Science **228**: 488–490. doi:10.1126/science.228.4698.488

Molinier, M., J.-L. Guyot, E. De Oliveira, and V. Guimarães. 1996. Les regimes hydrologiques de l'Amazone et de ses affluents. IAHS publication 209–222.

Montanher, O. C., E. M. L. de M. Novo, and E. E. de Souza Filho. 2018. Temporal trend of the suspended sediment transport of the Amazon River (1984–2016). Hydrological Sciences Journal **63**: 1901–1912. doi:10.1080/02626667.2018.1546387

Mortillaro, J. M., G. Abril, P. Moreira-Turcq, R. L. Sobrinho, M. Perez, and T. Meziane. 2011. Fatty acid and stable isotope (δ^{13}C, δ^{15}N) signatures of particulate organic matter in the lower Amazon River: Seasonal contrasts and connectivity between floodplain lakes and the mainstem. Organic Geochemistry **42**: 1159–1168. doi:10.1016/j.orggeochem.2011.08.011

Mullin, J. B., and J. P. Riley. 1955. The colorimetric determination of silicate with special reference to sea and natural waters. Analytica Chimica Acta **12**: 162–176. doi:10.1016/S0003-2670(00)87825-3

Niemistö, J., M. Kononets, N. Ekeroth, P. Tallberg, A. Tengberg, and P. O. J. Hall. 2018. Benthic fluxes of oxygen and inorganic nutrients in the archipelago of Gulf of Finland,

Baltic Sea – Effects of sediment resuspension measured in situ. Journal of Sea Research **135**: 95–106. doi:10.1016/j.seares.2018.02.006

Nittrouer, C. A., and D. J. DeMaster. 1996. The Amazon shelf setting: tropical, energetic, and influenced by a large river. Continental Shelf Research **16**: 553–573. doi:10.1016/0278-4343(95)00069-0

Nittrouer, C. A., D. J. DeMaster, S. A. Kuehl, and others. 2021. Amazon sediment transport and accumulation along the continuum of mixed fluvial and marine processes. Annu. Rev. Mar. Sci. **13**: 501–536. doi:10.1146/annurev-marine-010816-060457

Nixon, S. W. 1981. Remineralization and nutrient cycling in coastal marine ecosystems, p. 111–138. *In* B.J. Neilson and L.E. Cronin [eds.], Estuaries and Nutrients. Humana Press.

Ometto, J. P., A. P. D. Aguiar, and L. A. Martinelli. 2011. Amazon deforestation in Brazil: Effects, drivers and challenges. Carbon Management **2**: 575–585. doi:10.4155/cmt.11.48

Paerl, H. W., and M. F. Piehler. 2008. Nitrogen and marine eutrophication, p. 529–567. *In* Nitrogen in the Marine Environment. Elsevier.

Ragueneau, O., and P. Tréguer. 1994. Determination of biogenic silica in coastal waters: Applicability and limits of the alkaline digestion method. Marine Chemistry **45**: 43–51. doi:10.1016/0304-4203(94)90090-6

Schulz, H. D., and M. Zabel. 2006. Marine geochemistry, Springer.

Seeberg-Elverfeldt, J., M. Schlüter, T. Feseker, and M. Kölling. 2005. Rhizon sampling of porewaters near the sediment-water interface of aquatic systems: Rhizon porewater sampling. Limnol. Oceanogr. Methods **3**: 361–371. doi:10.4319/lom.2005.3.361

Shepard, F. P. 1954. Nomenclature based on sand-silt-clay ratios. Journal of Sedimentary Research **24**: 151–158. doi:10.1306/D4269774-2B26-11D7-8648000102C1865D

Sioli, H. 1984. The Amazon and its main affluents: Hydrography, morphology of the river courses, and river types, p. 127–165. *In* H. Sioli [ed.], The Amazon: Limnology and landscape ecology of a mighty tropical river and its basin. Springer Netherlands.

Sloth, N. P., B. Riemann, L. P. Nielsen, and T. Blackburn. 1996. Resilience of pelagic and benthic microbial communities to sediment resuspension in a coastal ecosystem, Knebel Vig, Denmark. Estuarine, Coastal and Shelf Science **42**: 405–415. doi:10.1006/ecss.1996.0027

Sternberg, R. W., D. A. Cacchione, B. Paulso, G. C. Kineke, and D. E. Drakez. 1996. Observations of sediment transport on the Amazon subaqueous delta. Continental Shelf Research **16**: 697–715.

Tobias, C., A. Giblin, J. McClelland, J. Tucker, and B. Peterson. 2003. Sediment DIN fluxes and preferential recycling of benthic microalgal nitrogen in a shallow macrotidal estuary. Marine Ecology Progress Series **257**: 25–36. doi:10.3354/meps257025

Tyrrell, T. 1999. The relative influences of nitrogen and phosphorus on oceanic primary production. Nature **400**: 525–531.

Weiss, R. F., and B. A. Price. 1980. Nitrous oxide solubility in water and seawater. Marine Chemistry **8**: 347–359. doi:10.1016/0304-4203(80)90024-9

Zimmerman, A. E., S. D. Allison, and A. C. Martiny. 2014. Phylogenetic constraints on elemental stoichiometry and resource allocation in heterotrophic marine bacteria. Environmental Microbiology **16**: 1398–1410. doi:10.1111/1462-2920.12329

3 | Nitrification in the Amazon River Plume

Authors: Choisnard Noémie, Sperlea Theodor, Liskow Iris, Voss Maren
MEPS (DOI: 10.3354/meps14530).

Author Contribution Statement: NC, MV and TS conceived and designed the research. NC, IL and MV contributed to the collection and compilation of data. NC, MV and TS analyzed the data and NC wrote the manuscript. All authors contributed to content revisions and approved the final text.

Abstract

The Amazon River delivers high concentrations of nitrate (NO_3^-, ~16 μM) to its estuary, shaping phytoplankton community assemblages in the estuary and up to 1,500 km away from the river mouth. Yet, NO_3^- production rates via nitrification, a central process of the nitrogen (N) cycle, have never been studied in this region. By combining nitrification rates and classical oceanographic field measurements with the help of a machine learning model, we highlight for the first time the variability of nitrification rates along the Amazon River plume and discuss potential relationships with environmental variables. The highest nitrification rates observed at the river mouth (up to 302 nmol L^{-1} h^{-1}) co-occurred with high turbidity, nitrite (NO_2^-) and phosphate (PO_4^{3-}) concentrations, consistent with studies documenting high rates in turbid estuaries. Within less than 200 km away from the river mouth, nitrification rates drop to minimum values in the plume and NO_3^- is depleted, likely consumed by phytoplankton when the light limitation constraint is lifted. In addition to climate change, the Amazon River catchment is subject to an array of anthropogenic impacts, such as deforestation, mining and damming. Under these pressures, the riverine discharge, turbidity, nutrient load and nitrification rates will likely be altered. This study gives a baseline for a central N-cycle pathway, also broadening our understanding of its control factors in the region, which is crucial for predicting the future of processes relying on the Amazon River discharge.

Introduction

Nitrogen (N) is essential for primary production (Howarth 1988) and the quantity and speciation of N not only exerts control on phytoplankton growth, but also on the biotic community composition. For instance, N-rich water columns favor diatoms (Margalef 1978), while depletion of surface N promotes nano- and pico-size species (Hallegraeff 2010). An increase in ammonium (NH_4^+) over nitrate (NO_3^-) supply can cause a similar shift in community composition, leading to harmful blooms (Glibert et al. 2016). Additionally, the speciation of N, i.e., the availability of reduced over oxidized and organic versus inorganic forms of N, is also a forcing factor of key microbial pathways (Devol 2015; Hu et al. 2019; Kuenen 2020). A central process of the N cycle controlling the speciation of oxidized and reduced forms of inorganic N is nitrification.

Nitrification begins with the oxidation of NH_4^+ to nitrite (NO_2^-). This step, considered to be rate-limiting, is carried out by ammonia-oxidizing archaea (e.g., *Nitrosopumilus maritimus*) and bacteria (e.g., *Nitrosomonas* spp.). In addition to NH_4^+, these organisms can also use urea, cyanate and polyamines as substrates, making them flexible and thus expanding their role to dissolved organic N cycling (Kitzinger et al. 2019; Damashek et al. 2019). NO_2^--oxidizing bacteria are primarily responsible for the subsequent oxidation of NO_2^- to NO_3^- in the oxic ocean (Ward 2011) and recently, comammox (complete ammonia oxidation) bacteria have been found to be capable of fully oxidizing NH_4^+ in estuaries and coastal waters (Xia et al. 2018; Sun et al. 2020). As nitrification is a recycling pathway, it is a key process in the N cycle, as it produces substrate for assimilation, dissimilatory NO_3^- reduction to NH_4^+, anammox and denitrification, thus determining the distribution of N species among the different dissolved inorganic N (DIN) pools.

Nitrification can be regulated by a wide variety of factors such as temperature, salinity and ambient oxygen concentration, and has long been assumed to only occur below the euphotic zone because of inhibition by light and competition for NH_4^+ in the surface ocean (Merbt et al. 2012; Smith et al. 2014; Wan et al. 2018). But while nitrification is a dominant process in the dark mid-depths of the ocean (Wuchter et al. 2006), there is also increasing proof for nitrifier activity in the euphotic zone, suggesting that new production estimates based on the assumption that NO_3^- is purely allochthonous would be overestimated (Ward 2005; Clark et al. 2007; Smith et al. 2014; Peng et al. 2018; Stephens et al. 2020; Laperriere et al. 2021). Therefore,

constraining the underlying regulatory mechanisms and the significance of nitrification for the euphotic zone N-budget is key to unravelling the controls on primary production.

This is even more crucial in the case of strongly stratified environments, such as estuaries and river plumes, where the nutrient resupply from deeper waters is hampered by the salinity gradient, leading to increasing dependency of surface communities on regenerated forms of N for their growth (Pomeroy 1974; Eppley and Peterson 1979; Azam et al. 1983). But estuaries are diverse ecosystems, with widely varying levels of nutrients (i.e., from low to eutrophic levels), productivity, turbidity, and tidal range, complicating the relationships between N-supply and productivity (Nixon et al. 1986; Paerl et al. 2014). Thus, understanding rates of N cycle processes, such as nitrification, and their role in comparison to riverine N-loads in a variety of estuaries is needed to improve coastal management. But even though nitrification rates have been measured in a variety of regions (Tang et al. 2023), many coastal ecosystems remain understudied.

The Amazon River estuary is no exception, even though the significant freshwater load (6×10^{15} L y^{-1}, 16.8 μM DIN; (DeMaster and Aller 2001) impacts the biotic community structure and its productivity on the entire area of the shelf (Goes et al. 2014), as well as the biochemistry of surface water as far as the Caribbean (Froelich Jr et al. 1978; Muller-Karger et al. 1988; Coles et al. 2013). During periods of maximum discharge in winter and spring, the Amazon River is even potentially responsible for *Sargassum* blooms in the tropical Atlantic (Aquino et al. 2022). Primary production and carbon export were reported to be high in some of the habitats generated by the plume, where dinitrogen fixation is not significant (Subramaniam et al. 2008; Loick-Wilde et al. 2016), underlining the importance of other sources of N for production in the Amazon River Plume. These observations call for improved knowledge about the use and transformation of N species along the river plume, and while biogeochemical models were applied to the region (Stukel et al. 2014; Louchard et al. 2021), there is no proof that remineralization rates are correctly represented. Nitrification rate measurements were carried out in the region in 2019, but only six stations were sampled in the northern plume, beyond 5°N (Starr et al. 2022). Questions regarding the extent of this process at the river mouth and on the entire Brazilian shelf are therefore still unanswered. Still, quantifying remineralization as nitrification and characterizing its environment both remain challenging as nitrification may overlap with NO_3^- assimilation, and its relationship with environmental variables might be highly non-linear.

Machine learning algorithms provide a new tool for exploring the components of an ecosystem describable by a large amount of features with little time and reasonable computing power. Machine learning has been used to describe intricate ecosystems using the microbial community composition (Cordier et al. 2017; Sperlea et al. 2021, 2022), and made it possible to improve water quality prediction in coastal environments (Deng et al. 2021). Machine learning algorithms have also been used in the N-cycle field, notably for predicting dinitrogen fixation rates in the ocean (Tang et al. 2019). This tool has been increasingly used in environmental sciences (Sun and Scanlon 2019), as many machine learning models can handle the highly non-linear relationships prominent in environmental systems.

In the Amazon River Plume, the role of nitrification in DIN speciation has never been investigated. Here, we measured bulk nitrification rates from the Amazon River mouth to the most northern part of the plume for the first time. To highlight the main characteristics of environments with the highest nitrification rates along the plume, we applied seven machine learning models to our dataset. This way, we aimed at 1) quantifying the nitrification rates along the Amazon River Plume, and 2) discussing the role of environmental variables linked to elevated nitrification rates along the Amazon River Plume.

Materials

Study site and sample collection

Samples were collected during the M-174 cruise undertaken in April and May 2021, during maximum river discharge, along the Amazon River Plume aboard the *R/V Meteor* (Figure 1). 18 stations were sampled along the plume, from the river mouth to Bajan waters (15 °N), to explore the variability of nitrification as river waters move northward. That way, we covered several habitats, differing in their sea surface temperature and salinity as well as the depth of the chlorophyll maximum, mixed layer depth and NO_3^- availability (Pham et al. 2024). These habitats were called riverine (RI), young plume core (YPC), western plume margin (WPM), and modified and oceanic sea water (MOW and OSW, respectively; Figure 13). Water samples were obtained using a Seabird Electronics SBE-32 rosette mounted with 21 Free Flow bottles of 10 L. Vertical profiles of temperature and salinity, dissolved oxygen, turbidity and fluorescence were obtained from a Seabird Electronics SBE-911plus (SN-0603) CTD, SBE43 dissolved oxygen sensor, D&A OBS-3 turbidity sensor, and a WETStar fluorometer, respectively, mounted on the rosette.

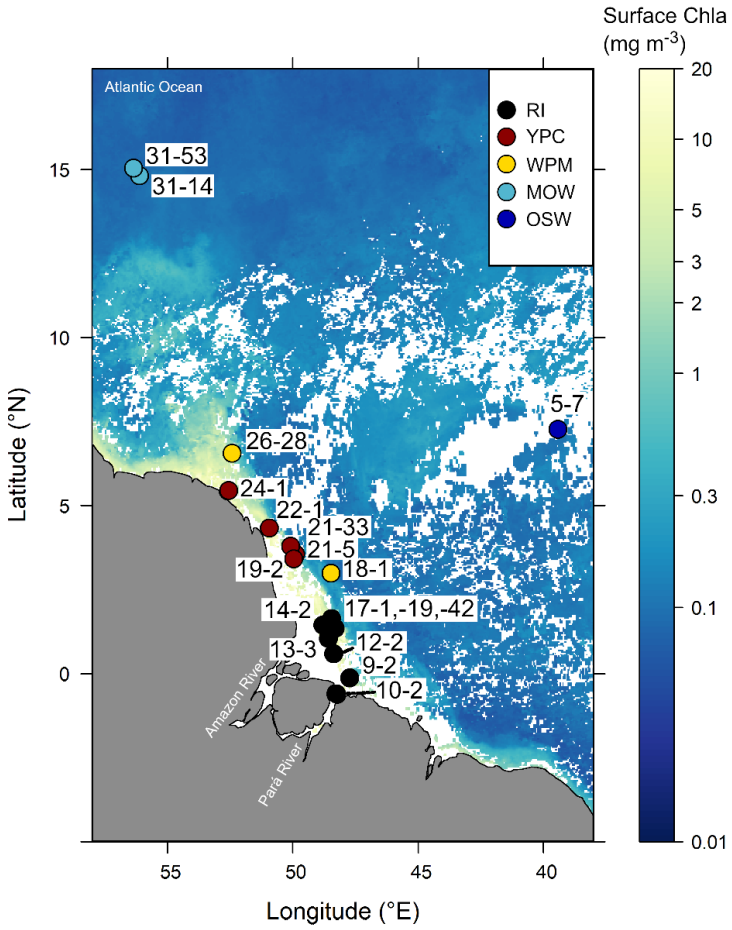

Figure 13. Study site. The Riverine habitat (RI, black markers) is located in front of the River mouth and is followed by the Young Plume Core (YPC, red markers) and Western Plume Margin (WPM, yellow) habitats. Most distal stations are part of the Modified Oceanic Seawater habitat (MOW, cyan). An oceanic seawater reference point was also sampled (OSW habitat; station 5-7). Surface chlorophyll a data (Surface Chla) were obtained for May 2021 from 2014.0 OCI chlorophyll data (AQUA/MODIS, NASA). The plume is discernable, with surface Chl-a values above 5 mg m^{-3}.

Photosynthetically Active Radiation measurements (PAR)

The Seabird Electronics device was used to measure PAR throughout the water column. As some casts were not taken during daylight hours, a first selection of all casts measured between 9:00 AM and 8:30 PM was made. Sixty-seven casts were taken between 8 AM and 8 PM and judged suitable for further %PAR (as a percentage of surface irradiance) calculations. The light attenuation coefficient, K_d(PAR), was calculated from a simple linear fit of log-transformed PAR data versus depth (Kirk 1994). The resulting %PAR was calculated as follows:

$$\%PAR = exp^{(-K_d(PAR)z)} \times 100 \quad (4)$$

The depth where the %PAR reaches 1% is by definition the depth of the euphotic zone.

Nutrients analysis

Samples for nutrient analysis were filtered (0.2 µm pore size) immediately after collection. Nutrient (silicate SiO_2, phosphate PO_4^{3-}, NO_3^-, NO_2^- and NH_4^+) concentrations were determined shortly after on a continuous flow autoanalyser (QuAAtro, SEAL analytics) following (Grasshoff et al. 1999) and HELCOM guidelines (2014) with a precision of 0.3 (SiO_2), 0.01 (PO_4^{3-}), 0.02 (NO_3^-), 0.006 (NO_2^-) and 0.02 μM (NH_4^+).

Nitrification rates measurements

Nitrification rates were measured using the ^{15}N-NH_4^+ tracer incubation method (Santoro et al. 2010; Smith et al. 2014; Damashek et al. 2016). Water was collected at each station from 1 to 3 depths (usually at the surface, mid-depth or chlorophyll maximum and bottom or deeper than the chlorophyll maximum), in triplicates, in 1L PC bottles and immediately amended with ^{15}N-NH_4Cl (ISOTEC, Sigma Aldrich, 98 atom%) at approximately 10 % of the ambient concentration. Samples for the initial conditions (T0) were filtered directly after tracer injection onto precombusted (450 °C for 4 h) 25 mm GF-075 filters (Advantec, GF-075; 25 mm, nominal pore-size 0.3 μm) while endpoint samples were incubated for 3 to 6 h before filtration. One set of endpoints was incubated in the dark, at ambient surface temperature, and one set, when the station was sampled during the day, at *in situ* light intensity and temperature. After filtration, 50 mL aliquots of each sample were collected in Falcon tubes and frozen at -20 °C until analysis. During the incubation, the labelled ^{15}N-NH_4^+ was converted into ^{15}N-NO_2^- and ^{15}N-NO_3^- (^{15}N-NOx), which was analyzed using the bacterial denitrifier method (Sigman et al. 2001). Samples with a NOx concentration above 0.2 μM were run on a Thermo Scientific delta V advantage isotope ratio mass-spectrometer connected to a PAL autosampler and a Finnigan GasBench II. Nitrate standards (IAEA-N3 and USGS34) emulating sample concentrations were used for calibration, with an uncertainty of 0.2 ‰. Nitrification rates depend on the amount of tracer added, the size of the NO_2^-+ NO_3^- pool and the excess ^{15}N-NOx measured during the incubation time (ΔT) and were calculated as follows (Damashek et al. 2016):

$$NR\ (nmol\ L^{-1}h^{-1}) = \frac{\left[{}^{15}N_{NOx}\right] \times \frac{[NH_4^+]_{total}}{\left[{}^{15}NH_4^+\right]_{added}}}{\Delta T} \quad (5)$$

where NR is nitrification rate, ^{15}N-NOx is the difference in ^{15}N-content (AP, in atom%) of the end (T_F) and the beginning (T_0) samples:

$$[{}^{15}N_{NOX}] = \frac{AP_{{}^{15}N_{NOx_{TF}}} - AP_{{}^{15}N_{NOx_{T0}}}}{100} \times [NO_3^- + NO_2^-] \quad (6)$$

This incubation experiment does not discriminate between NH_4^+ oxidation to NO_2^- and further NO_2^- oxidation to NO_3^-. Three samples were re-analyzed after removing all NO_2^- by treatment with sulfamic acid prior to bacterial conversion to N_2O, according to the protocol of Granger and Sigman (2009). We observed that more than 90 % of the labelled NH_4^+ injected ended in the NO_2^- pool (Figure S3). It is therefore likely that the nitrification rates reported here mainly reflect NH_4^+ oxidation rates.

Light and dark incubation experiment

At stations sampled during the day (between 9:00 AM and 8:00 PM), incubations of bottles collected in the euphotic zones (depth <50 m) were performed in two sets. One set was incubated in the dark, to limit potential competition between nitrifiers and phytoplankton, and one set was incubated under in situ light conditions. The aim of the experiment was to study the effect of light on bulk nitrification rates along the Amazon River Plume. Results were grouped by PAR levels, which were arbitrarily chosen to be less than 1 % (outside of the euphotic zone), 1-10 %, 10-50 % and above 50 % PAR. The effect of temperature is assumed to be modest, as little variation (±2 °C) was observed in water temperature between the sampled depths (Figure S4).

Detection limit of nitrification rates

The detection limit of nitrification rates was determined for every incubation following (Santoro et al. 2013) and is dependent on the ^{15}N enrichment of the substrate pool and the concentration of the product pool. Detection limits for nitrification rates ranged from 0.003 to 0.400 nmol L^{-1} h^{-1} at RI stations and from 0.003 to 0.050 nmol L^{-1} h^{-1} at YPC stations. Stations located in the WPM habitat exhibited detection limits ranging from 0.001 to 0.06 nmol L^{-1} h^{-1}, while MOW and the oligotrophic station OSW had detection limits of 0.001-0.01 and 0.001-0.08 nmol L^{-1} h^{-1}, respectively.

Statistical analyses

A total of seven machine learning models from the R package caret (v4.6-14; Kuhn 2008) were used to explore the correlations between a set of environmental variables and bulk, log10 transformed nitrification rates (in nmol L^{-1} h^{-1}): linear model (lm), elasticnet model (enet), Random Forest (rf), extreme gradient boosting (xgbTree), support vector machines with linear and radial kernel (svmLinear, svmRadial) and k-nearest neighbors (knn). Eleven variables were used as input: temperature, oxygen concentrations, fluorescence, turbidity, salinity, particulate organic N (PON), depth and nutrient concentrations (PO_4^{3-}, NO_3^-, NO_2^- and NH_4^+). All variables without missing values were taken into account in this analysis, and two variables were excluded (silica and particulate organic carbon concentrations) as they had the same variability as another variable (with salinity and PON, respectively).

To prevent low (n=45) sample size-related bias and overfitting in algorithm selection, a leave-one-out cross-validation scheme was applied to evaluate models: a separate model was trained for each sample on all the data points except for the sample in question. Then, the fitted model was used to predict the target variable based on the held-out data point. The predictions were collected and compared to the respective measured values to assess the model. As performance metrics, the coefficient of determination (R^2, explained variance), root-mean-square error (RMSE, standard deviation of the residuals) and model average error (MAE, average absolute difference between predicted and original values) were calculated using the postResample function from the R package caret (v4.6-14, Kuhn, 2008).

Two algorithms were selected based on their performance metrics, with a maximal R^2 and minimal RMSE and MAE as indicators of a good fit. For the variable importance analysis, the varImp function (caret package v4.6-14) was used after re-training these two algorithms on the entire dataset. That way, complex and non-linear relationships between measured variables and bulk nitrification rates could be detected, and all the data was included in the ranking of the variables selected for explaining bulk nitrification rates along the Amazon River Plume. The differences among the means of different groups based on the habitats described earlier were explored using a Tukey's test for multiple comparisons.

Results

Environmental variables along the Amazon River Plume

The five plume habitats sampled exhibit different environmental characteristics. Close to the River mouth, the water column showed a strong stratification between 5 and 10 m depth, with potential density increasing from 0 to 25 kg m^{-3} (Figure 14a). With distance from the River Mouth, the water column depth increases and the potential density of the water column becomes more homogeneous with a difference of only ~5 kg m^{-3} between the upper and lower layer of the water column (Figure 14a).

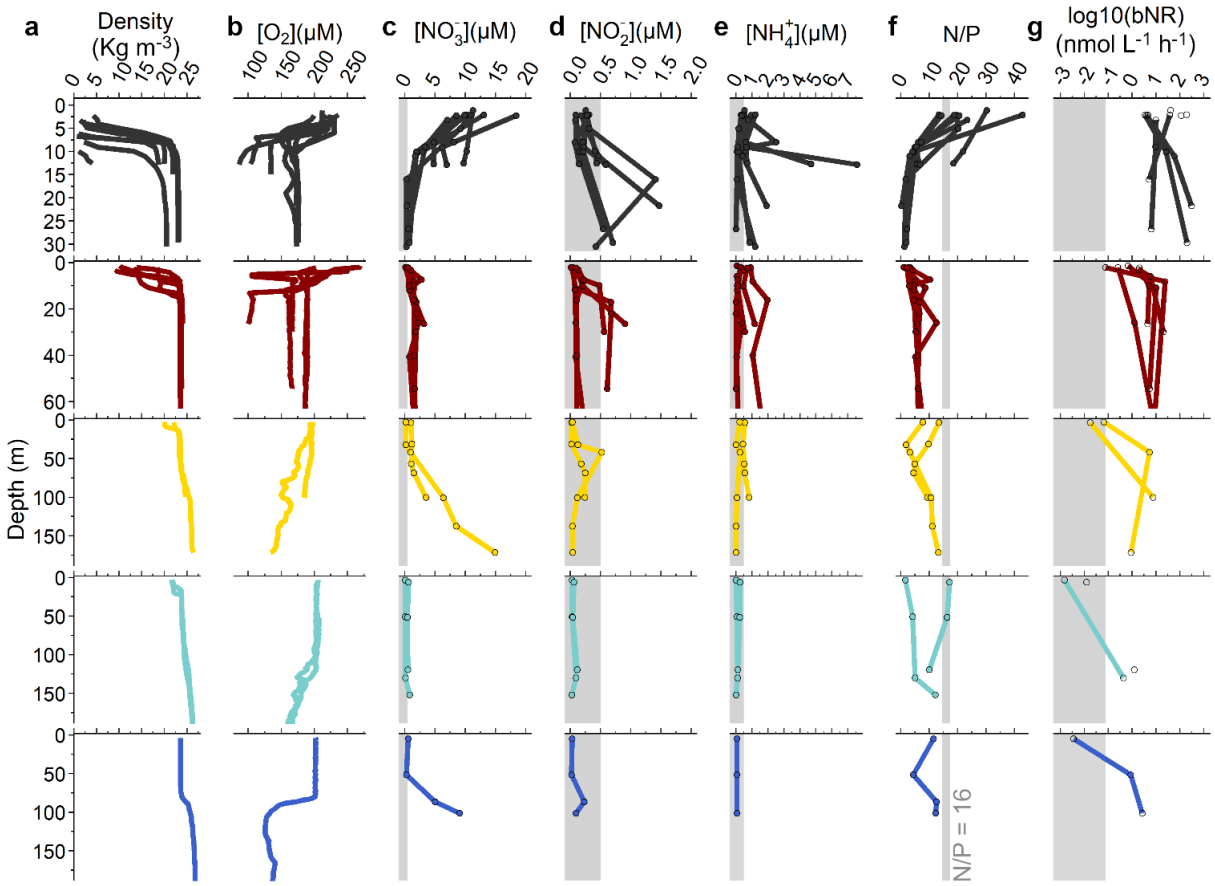

Figure 14. The diversity of different habitats along the plume is shown by the vertical profiles of (**a**) Density (sigma-theta, in kg m^{-3}), (**b**) Dissolved oxygen (in μM), (**c**) NO_3^-, (**d**) NO_2^-, (**e**) NH_4^+ and (**f**) N/P ratios, some variables that might be related to (**g**) log10 transformed bulk nitrification rates (in nmol L^{-1} h^{-1}) at the RI (black), YPC (red), WPM (yellow), MOW (cyan) and OSW (blue) habitats. Rates in the grey area might be below the detection limit of the method (below 0.4 nmol L h^{-1}). Low NO_3^- NO_2^- and NH_4^+ concentrations (below 0.5μM) are highlighted by the grey area. The grey line on the N/P profiles is set at 16, with values above showing excess of NO_3^- and values below a deficit of NO_3^- relative to PO_4^{3-} according to Redfield ratios (see text). Circle markers indicates the sampling depth. For simplification, only the first 30 to 200 m of the water column are presented here.

Oxygen was close to saturation (200 to 250 μM, Figure 14b) in the upper 10 m along the Amazon River Plume. It decreased to 80-100 μM below the halocline (10 m depth) at shallow stations from the RI and YPC habitats, while in other, more distal habitats, oxygen concentrations started decreasing between 80 and 200 m depth (Figure 14b).

N species concentrations (NO_3^-, NO_2^- and NH_4^+) were higher in the River mouth (RI habitat), with NO_3^- being at least 10 times higher (up to 18.4 μM) relative to other habitats, where N concentrations were close to oligotrophic conditions (<0.5 μM). The N/P ratios, calculated from the ratio between NO_3^- and PO_4^{3-} concentrations reveal that NO_3^- gets rapidly depleted, as all but the RI habitats showed N/P values below Redfield (16/1).

Nitrification rates showed a strong spatial variability. In the RI habitat, nitrification rates were homogeneous through the water column, while in other habitats along the plume, nitrification rates were close to 0 at the surface, and up to 100 times lower than in deeper waters (Figure 14g).

Nitrification rates along the Amazon River Plume

Bulk nitrification rates also changed along the Amazon River Plume. Rates were higher in habitats more strongly influenced by the Amazon River as they ranged between 301.6 nmol L^{-1} d^{-1} at the River mouth while reaching 0 at more distal habitats (Figure 15a). The MOW habitat exhibited nitrification rates in the same range as our oceanic reference (OSW habitat) even though the plume's influence was still noticeable at the surface of this habitat, as previously shown in the density profiles (Figure 14a).

Additionally to the apparent spatial variability of bulk nitrification rates, rates also seemed to vary with the light conditions (Figure 15b). In cases where in situ %PAR exceeded 50 %, bulk nitrification rates in both incubations were close to 0. As the %PAR decreased, bulk nitrification rates measured under dark conditions increased, while the in situ light incubation virtually measured no conversion. In light-depleted environments, where %PAR is < 1 %, nitrification rates were maximum and rates measured under in situ light were in the same order of magnitude as the ones measured in dark conditions (Figure 15b).

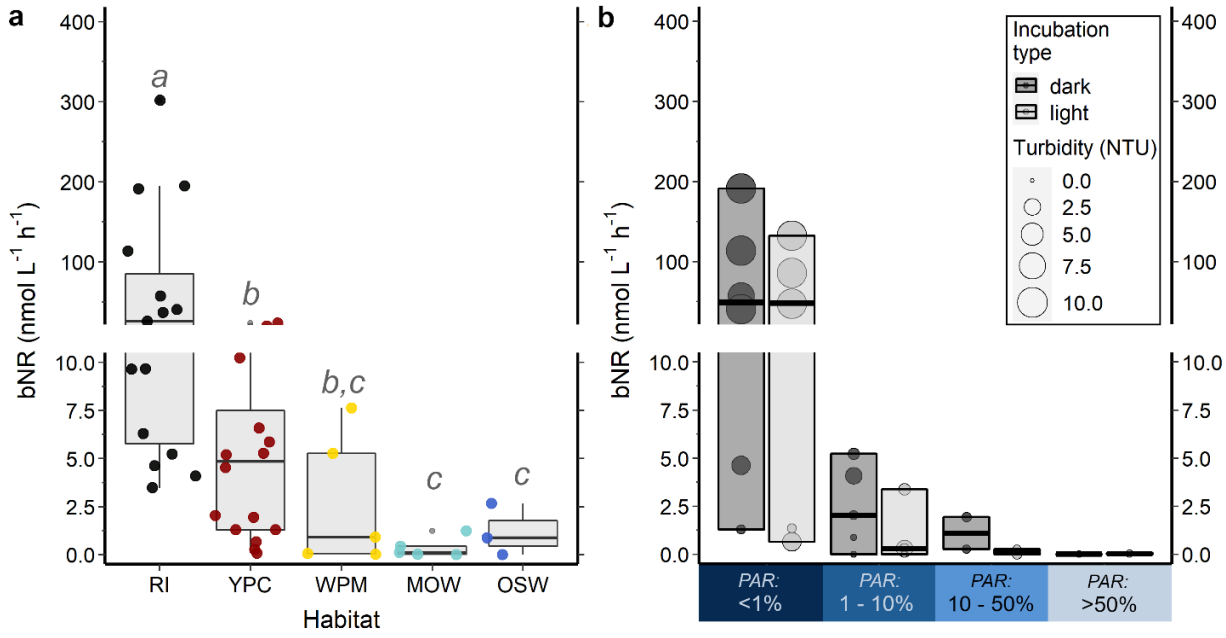

Figure 15. (**a**) Bulk nitrification rates (nmol L^{-1} h^{-1}) are varying along with the habitats. Shared letters above boxes indicate non-significant differences between habitats (Tukey test $p > 0.05$). Boxplots represent the interquartile range. (**b**) Nitrification rates measured under dark (NR dark, dark grey bars) and in situ PAR conditions (NR light, light grey bars). The turbidity (in NTU) of each sample is represented by the size of the marker. In both panels and for each box, the median is represented with a bold line.

Descriptors of habitats with high nitrification rates

To further untangle the relationship between the environmental conditions encountered in each habitat, such as turbidity of the water column, oxygen and nutrient concentrations on the one hand and bulk nitrification rates on the other, we applied a machine learning feature importance analysis. To this end, we first identified machine learning models that best capture this relationship using leave-one-out cross-validation. Models were evaluated using the R^2, RMSE and MAE. The optimal model will produce minimal MAEs and RMSEs and R^2 values close to 1; departures from this optimal value can be either accredited to an ill fit of the model or unobserved variables. We find that the Random Forest (rf), xgbTree, and SVM with a radial kernel (svmRadial) outperform the other models, with the Random Forest being able to explain 68 % of the variation in the nitrification rate based on the environmental parameters (Table 6). In contrast to the other models used here, the models with high performance are known to be able to model highly non-linear relationships. Therefore, our results stress the importance of non-linear processes in the environmental control of nitrification rates.

Table 6. Averaged performance metrics (R^2, RMSE and MAE) of the seven machine learning models applied.

Model	R^2	RMSE (nmol L^{-1} h^{-1})	MAE (nmol L^{-1} h^{-1})
lm	0.39	15.00	7.89
enet	0.42	10.81	6.46
rf	0.68	6.04	3.67
xgbTree	0.65	6.29	3.74
svmLinear	0.30	16.18	8.92
svmRadial	0.59	7.89	4.13
knn	0.33	13.17	6.98

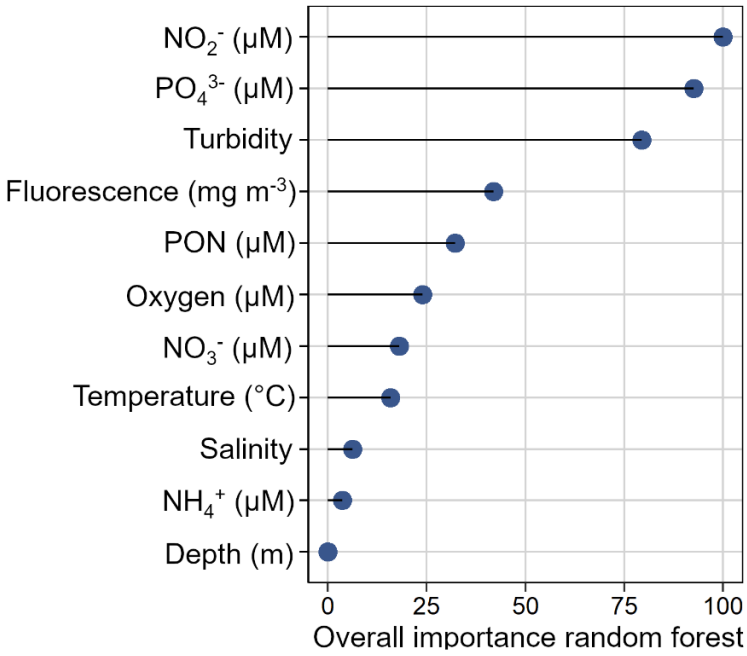

Figure 16. The ranking of variables used in the Random Forest model show which variables are, according to our model, the best predictor for bulk nitrification rates in the Amazon River Plume. The overall importance of each variable was determined by computing the relative influence of each variable on the error of all trees.

Applying a feature importance analysis to the most performant model (rf), we found that NO_2^- and PO_4^{3-} concentrations, as well as turbidity and fluorescence are the variables that best describe environments with high bulk nitrification rates (Figure 16), as higher NO_2^- and PO_4^{3-} concentrations and turbidity co-occur with high bulk nitrification rates (Figure 17). Fluorescence and bulk nitrification rates varied similarly, with nitrification rates increasing

together with fluorescence when the latter one was below 1 mg m^{-3}. Above that threshold, three points were measured with lower nitrification rates (Figure 17). This ranking of variables is in accordance with the important features identified by the xgbTree model, which also presented NO_2^-, Turbidity and PO_4^{3-} as the most important variables (Figure S5).

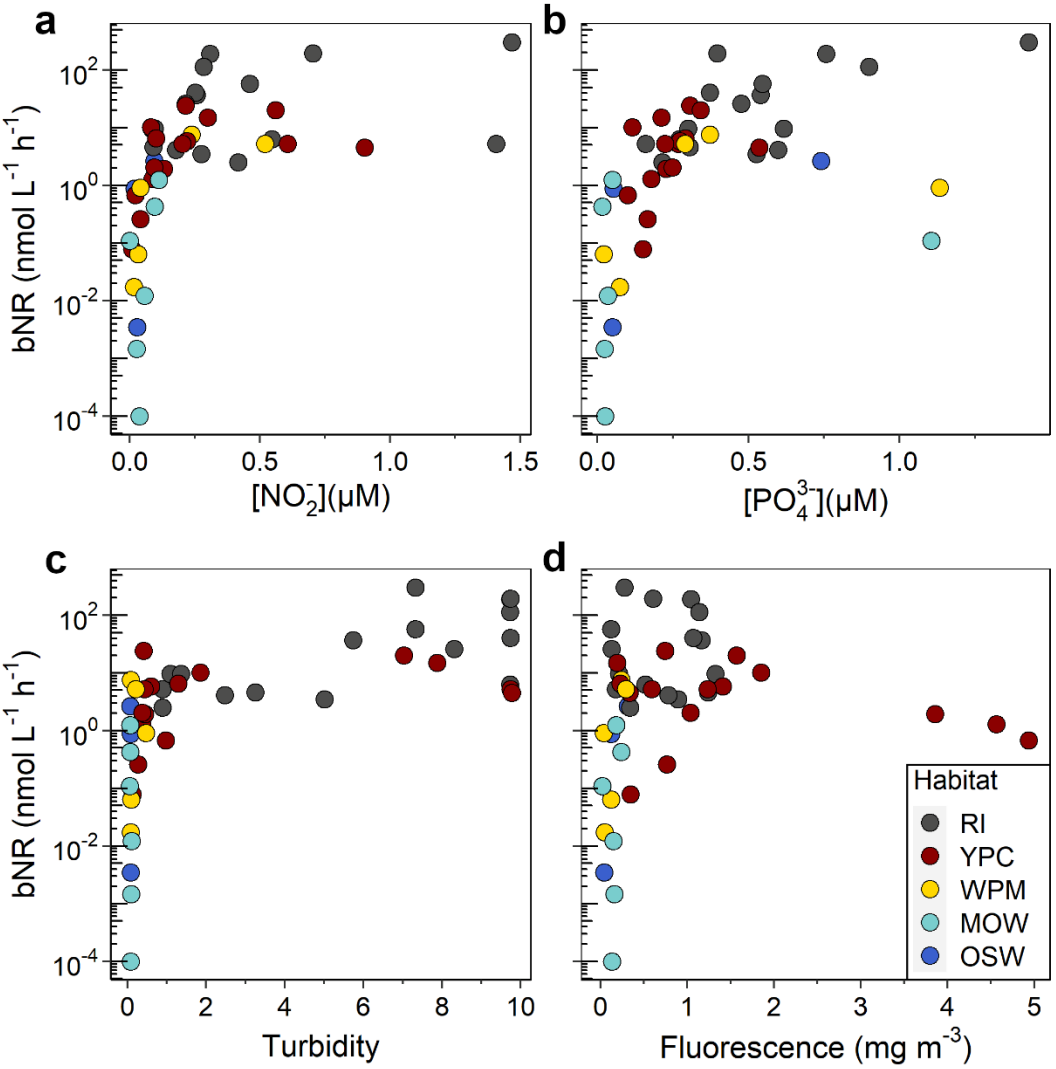

Figure 17. Concentrations of (a) NO_2^- and (b) PO_4^{3-} as well as (c) Turbidity and (d) Fluorescence are the variables that had the highest importance for the Random Forest model. Each of these variable is plotted against bulk nitrification rates and data is colored by habitat. Note the log scale of the y-axis.

Discussion

Nitrification across the Amazon River Plume habitats

The Amazon River delivers large quantities of nutrient-rich, turbid freshwater to the estuary. As it is transported northward along the coast and forms the Amazon River Plume, the Amazon water undergoes alterations, which are visible in the physical and biochemical properties of the water column. With their characterization of several habitats from the river mouth to 16°N (Figure 13), Weber et al. (2019) and Pham et al. (2024) have highlighted this diversity, which might impact the N-cycle along the Amazon River Plume, beyond NO_3^- availability and phytoplankton species composition.

In the RI habitat, the freshwater of the Amazon River was encountered over the first 10 m of the shallow water column and was characterized by high NO_3^- (ranging between 3.4 and 18.4 μM) and NH_4^+ concentrations (up to 1.2 μM), and N/P ratio above 16. As the water travelled and mixed with oceanic waters, the vertical stratification became weaker and the upper water column became depleted in all nutrients, resulting in N/P ratios below Redfield (Figure 14f). The most distal stations, located around 15 °N, belonged to a habitat characterized as MOW (Pham et al. 2024). Despite the presence of a fine layer of less saline water at the very top of the water column, a fingerprint of riverine influence, N species were depleted at the surface (0.07 to 0.92 μM of DIN) and this habitat was otherwise indistinguishable from the oceanic seawater habitat (Figure 14).

Similar to N species, the highest nitrification rates were observed at the river mouth (up to 301.6 nmol L^{-1} h^{-1}; Figure 15a). By contrast, nitrification rates dropped to less than 10 nmol L^{-1} h^{-1} within 100 km of the river mouth, and ranged between 0 and 2.5 nmol $L^{-}1$ h^{-1} at the most distal stations (Figure 15a), in accordance with rates measured in the northern plume (Starr et al. 2022). Even if nitrification rates increased with depth at deeper stations, they were still 2 orders of magnitude lower than those observed in the river mouth (Figure 14g). These results suggest that the Amazon River mouth offers perfect conditions for nitrifiers to thrive, as hypothesized by previous studies (DeMaster and Aller 2001; Aquino et al. 2022).

In fact, nitrification rates measured in the river mouth were as high as those observed in the Chang Jiang River mouth and plume and in the Mississippi River, systems with similar settings (Carini et al. 2010; Hsiao et al. 2014). They were also similar to nitrification rates measured in the Rhône River plume, which had NH_4^+ concentrations about ten times higher at

the time of the study (Bianchi et al. 1999). By contrast, the productive Peruvian upwelling system exhibited nitrification rates about 20 times lower, even though surface NH_4^+ and NO_3^- concentrations were similar to those observed in the Amazon River mouth (Fernández et al. 2009). At more distal, and oceanic stations, nitrification rates were in the range of rates observed in the oligotrophic Atlantic Ocean (0.4 to 7 nmol L^{-1} h^{-1}; Clark et al. 2008). The fairly wide range of nitrification rates along the Amazon River Plume and across sites with similar environmental conditions suggests a strong variability of the factors potentially forcing nitrification rates.

Environmental variables linked to elevated nitrification rates

A myriad of variables might have an effect on nitrification rates and the biogeochemistry of an estuary. For example, Damashek et al. (2016), reported strong positive correlations of NH_4^+ and suspended particulate matter with nitrification rates in San Francisco Bay and across a range of ecosystems (e.g. brackish inland seas, fjords, temperate and tropical estuaries) using linear models. However, controls on nitrification rates might be more complex than simple linear relationships, and these are rarely encountered (Ward 2005; Clark et al. 2008). To overcome this issue, we applied seven machine learning models to our dataset encompassing diverse types of relationships between explanatory and response variables.

As expected, the linear models (lm and svmLinear; Table 6) did not perform well, and had, together with the knn model, the lowest R^2 and highest RMSE and MAE (Table 6). The linear model had a maximum RMSE of 32.36 ± 2.88 nmol L^{-1} h^{-1}, a value above all rates measured outside of the RI habitat (Figure 15a), underlining that this type of model is not adequate here. The model that fitted our data best was the rf model, which had the highest R^2 (0.75 ± 0.10; Table 6). With the 11 explanatory variables used, this model was able to explain nitrification rates with a maximum error of 5.37 ± 1.70 nmol L^{-1} h^{-1}. This error represents less than 2 % and less than 30 % of the maximum nitrification rates measured in the river mouth and YPC habitats, respectively (Figure 15a).

The variable importance function ranks the explanatory variables used in the Random Forest model according to their importance for the prediction of nitrification rates. Altogether, this model highlighted the importance of NO_2^- and PO_4^{3-} concentrations, as well as turbidity and fluorescence as good descriptors for nitrification rates in the Amazon River mouth and Plume (Figure 16). The turbidity of riverine waters provides a particle-rich and light-limited

environment which likely provides an advantage to nitrifiers over phytoplankton for NH_4^+ (Cole and Cloern 1984; Alpine and Cloern 1988; Smith et al. 2014), and in many estuaries, nitrification rates peak in turbid waters (Owens 1986; Berounsky and Nixon 1993; Iriarte et al. 1997; Pakulski et al. 2000; de Wilde and de Bie 2000; Brion et al. 2000; Hsiao et al. 2014). Our extensive analysis indicates that similar conclusions can be drawn in the highly turbid Amazon River mouth environment (Figure 17c). As distance from the river mouth increases and turbidity decreases to values under 5 NTU, nitrification rates drop by up to 5 orders of magnitude and the link between turbidity and rates disappears, as previously reported for the northern part of the Amazon River Plume (Starr et al. 2022).

Turbidity and light are difficult to discriminate, as the concentration of particles leading to elevated turbidity usually results in light attenuation (Figure 15b). An incubation experiment with samples of varying turbidity under both dark and in situ light conditions revealed that elevated nitrification rates were maintained under both dark and in situ light levels when turbidity was high and in situ %PAR was below 1 %, while under low turbidity and high light levels, nitrification rates under in situ light condition dropped to minimum values (Figure 15b). These results underline the strong negative effect of light on nitrification rates along the Amazon River Plume. To determine whether this reflects a light inhibition of nitrifiers or direct competition with phytoplankton for NH_4^+ remains to be assessed. Fluorescence is a proxy for phytoplankton presence, and while some fluorescence was measured at the surface of the most riverine habitat, these measurements were potentially biased by the high concentration of particles. Alternatively, the continuous supply of NH_4^+ from the river mouth could support both the nitrifier and planktonic communities. The highest fluorescence measurements were observed further offshore, in the YPC habitat, and linked to a decrease in nitrification rates by two orders of magnitude (Figure 17d), which could corroborate the hypothesis of competition with phytoplankton at higher light levels and lower substrate concentration.

While the elevated turbidity of the river mouth therefore seems to provide a sufficient light attenuation for nitrification to prevail, the high concentration of particles additionally provides high concentrations of substrate promoting the growth of ammonia-oxidizers, as observed in other contexts (Zheng et al. 2017; Kache et al. 2021). In the river mouth where the highest PON concentrations were found, particle-associated ammonia-oxidizing archaea and nitrite-oxidizing bacteria were at least threefold more abundant than free-living ones (Satinsky et al. 2015, 2017). Further offshore, in the Amazon River Plume, free-living cells accounted

for more than 90 % of the metatranscriptome (Satinsky et al. 2014), and when looking at the PON fraction of particles, no correlation with nitrification rates was found in the non-riverine habitats (YPC, WPM, MOW and OSW). These results suggest that turbidity, or the concentration of particles, holds an additional role in the sole light-protection of nitrifiers in the river mouth, and explains the shift between particle-associated nitrifiers in the river mouth to more free-living communities in the plume, as previously observed (Satinsky et al. 2015, 2017).

NO_2^- is an intermediate of nitrification that usually accumulates just below the deep chlorophyll maximum (Brzezinski 1988; Dore and Karl 1996; Santoro et al. 2013). In oxygenated waters, this accumulation results in NO_2^- concentrations of 0.01-1 μM (Ward 2008), similar in magnitude to the peak concentrations observed across habitats along the Amazon River plume (0.01-1.47 μM; Figure 14d). Nitrifier abundance and nitrification rates often peak at the NO_2^- maximum in the ocean (Ward 1987; Ward et al. 1989; Dore and Karl 1996; Santoro et al. 2010, 2013, 2017; Newell et al. 2011; Buchwald and Casciotti 2013; Smith et al. 2016), though rapid nutrient cycling and mixing in coastal zones tend to conceal this relationship (Hsiao et al. 2014; Bronk et al. 2014; Damashek et al. 2016). It is therefore interesting, though not surprising, to find a similar relationship in our dataset (Figure 16, Figure 17a). The greater NO_2^- concentrations are observed in the RI and YPC habitats (Figure 14d), usually below the plume layer (> 10 m depth) and the euphotic zone, suggesting that neither river runoff nor the excretion of NO_2^- by phytoplankton are likely to explain the relatively high NO_2^- concentrations observed here, as pointed out in other environments (Buchwald and Casciotti 2013; Santoro et al. 2013). Instead, the observed NO_2^- accumulation in these environments could arise from nitrification, influenced by differences in maximum growth rate, loss rate and substrate affinity of nitrite-oxidizers relative to ammonia-oxidizers (Zakem et al. 2018) but also from mesoscale turbulences (Lévy et al. 2014; Liu et al. 2023). In the Amazon River Plume, the increasing mixing between the river plume layer and the more saline water below as the water moves northward could partly explain the decrease in NO_2^--peak between riverine habitats and more oceanic ones.

Another nutrient, PO_4^{3-}, presented a similar variability as nitrification rates, with high concentrations co-occurring with high nitrification rates in the river mouth (Figure 17b). The Amazon River delivers substantial amounts of PO_4^{3-} to the river mouth (~0.7 μM; Demaster and Pope 1996), and release of PO_4^{3-} from particle desorption and degradation during mixing in the estuary supplies similar concentrations to the water column (Chase and Sayles 1980; Fox

et al. 1986). Consequently, most habitats along the Amazon River Plume do not seem to be phosphorus-limited. PO_4^{3-} concentrations range between 0.2 and 1.0 μM (Benitez-Nelson 2000), with the highest concentrations found in the river mouth. While this co-occurrence might solely be a coincidence, nitrifiers have also been shown to have a similar affinity for PO_4^{3-} as bacterioplankton (Tanaka et al. 2003), together with a strong dependency on P turnover rates. Additionally, recent microcosm experiments in a eutrophic lake highlighted the potential of inorganic P as a fuel for nitrification (Zhou et al. 2023), and marine nitrifiers have been reported to assimilate 2 mmol of P per mole of NH_4^+ respired (Meador et al. 2020). The higher P concentrations and lower P turnover rates encountered in the Amazon River mouth (Sohm and Capone 2010; Meador et al. 2020) could thus enhance nitrification rates in this habitat.

Conversely, NO_3^-, NH_4^+ concentration and temperature did not hold a strong explanatory power according to this model. Correlations between NH_4^+ and nitrification rates must be interpreted with care. In fact, competition with phytoplankton aside, a strong coupling between NH_4^+ production and oxidation may result in the occurrence of high nitrification rates at lower NH_4^+ concentrations (Carini et al. 2010; Hsiao et al. 2014; Bronk et al. 2014), potentially explaining the lack of a strong relationship in some habitats of the Amazon River Plume (Figure S6). The absence of a relationship between NO_3^- and nitrification rates is not unexpected either. Even though it was reported in many studies summarized by Wan et al. (2018), others have noted the absence of such a relationship (Damashek et al. 2016). Wan et al. (2018) suggested that nitrifiers can outcompete phytoplankton in NO_3^--rich waters thanks to their higher NH_4^+ affinities relative to eukaryotic phytoplankton which dominate these systems. Unsurprisingly, blooms of large centric diatoms were found at a low-salinity and NO_3^--replete site in the plume, along with the highest expression of the eukaryotic NO_3^- transport gene (Zielinski et al. 2016). It is therefore likely that, similarly to NH_4^+, NO_3^- is subject to rapid cycling or mixing, resulting in a concealing of its relationship with nitrification rates (Middelburg and Nieuwenhuize 2001).

Conclusions

This study highlights, for the first time, the significance of nitrification as a crucial process of N cycling in the Amazon River plume. The river mouth presented nitrification rates comparable to other coastal zones and two orders of magnitude higher than in the open ocean. With high NO_2^- and PO_4^{3-} concentrations, the Amazon River seemed to offer the perfect conditions for nitrifiers to thrive. The high turbidity of its waters probably inhibits

phytoplankton growth and activity, easing potential competition for NH_4^+. Within a few hundreds of kilometers from the river mouth, the NO_3^- produced is depleted, highlighting the importance of nitrification for supporting phytoplankton growth the moment that light limitation constraints are lifted. The Amazon River estuary seems to be a particularly important site for N cycling. Since the Amazon catchment is undergoing drastic changes, this study gives a baseline for a central N-cycle process, also broadening our understanding of its control factors, which is crucial for predicting the future of this ecosystem.

Acknowledgements. The authors thank the Deutsche Forschungsgemeinschaft (DFG) for funding the MeNARP Project (Metabolism of Nitrogen in the Amazon River Plume, project number VO 487/14-1) and the M174 cruise 'N-Amazon' (funding GPF19-1-13, granted to M.aren V.oss) aboard the R/V 'Meteor'. The authors also thank Christian Burmeister (nutrient analyses) and the Captain and Crew of the R/V 'Meteor' (support at sea). The authors are also grateful to Volker Mohrholz, Toralf Heene, Robert Mars, Jens Söder, and Ajit Subramaniam for compiling the hydrographic properties of water masses at each sampled station (Mohrholz et al. 2022).

Appendices

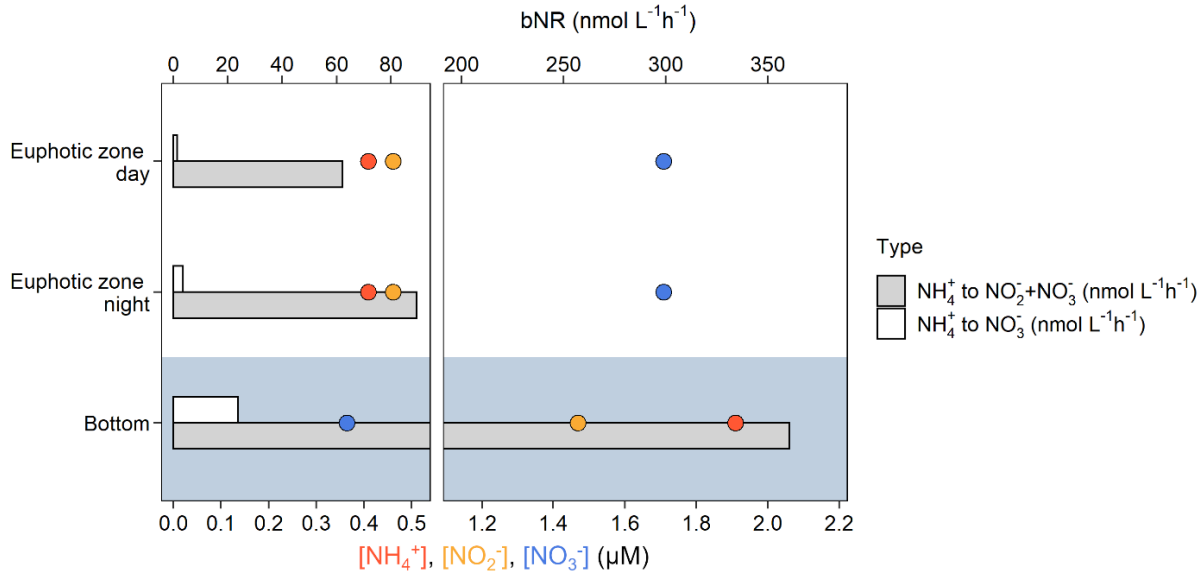

Figure S3. NO_2^- removal in samples from station 17-1 led to a sharp decrease in measured bulk nitrification rates, independently from the in situ light level and whether the incubation was performed under dark (i.e. night) or light (i.e. day) condition.

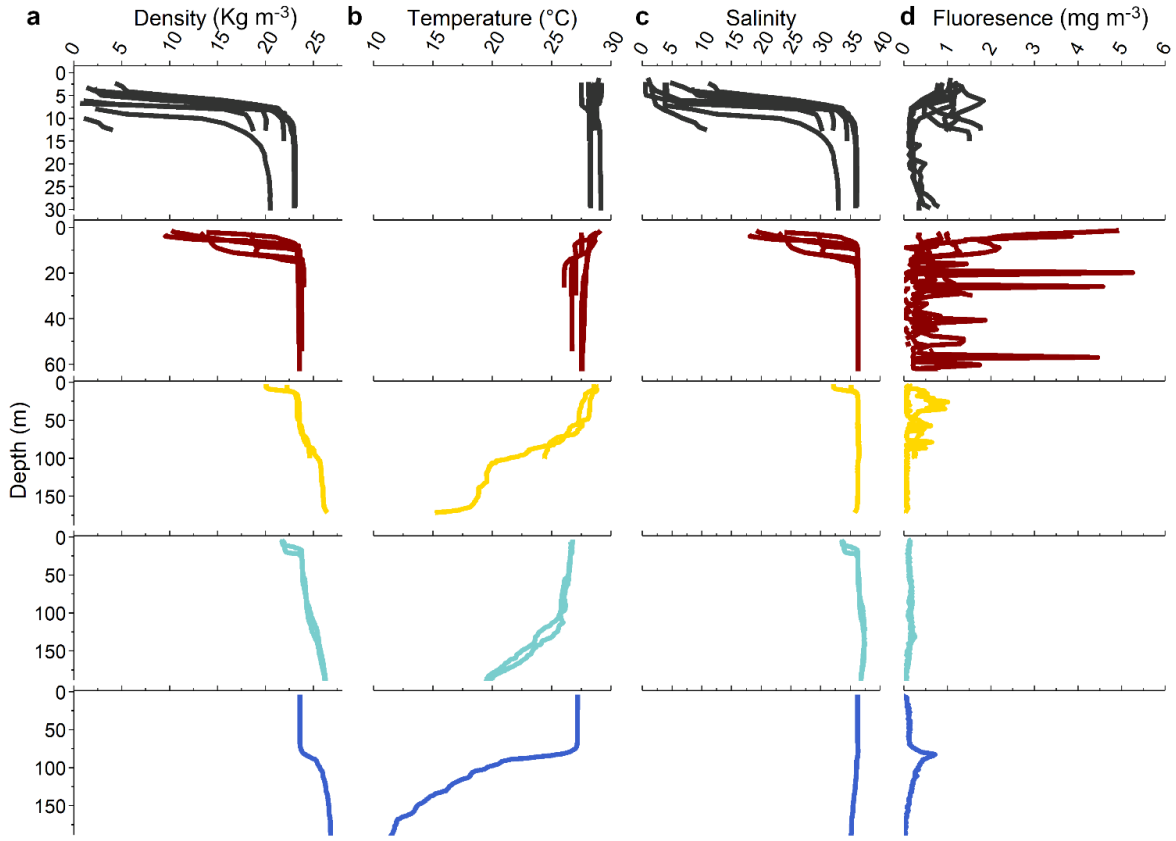

Figure S4. The diversity of different habitats along the plume is shown by the vertical profiles of (**a**) Density (sigma-theta, in kg m^{-3}), (**b**) Temperature (in °C), (**c**) Salinity and (**d**) fluorescence (in mg m^{-3}), at the RI (black), YPC (red), WPM (yellow), MOW (cyan) and OSW (blue) habitats. For simplification, only the first 30 to 200 m of the water column are presented here.

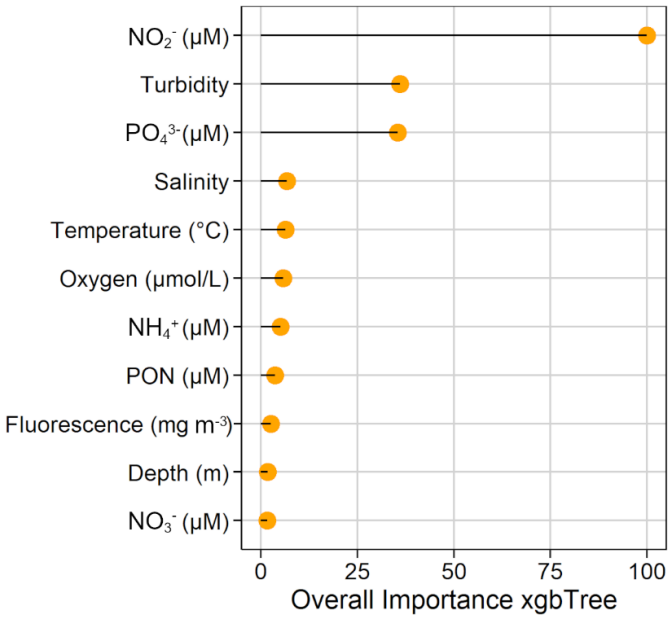

Figure S5. Ranking of variables obtained from the xgbTree model. Similarly to the one obtained via the Random Forest model (see Figure 16), the overall importance of each variable was determined by computing the relative influence of each variable on the error of all trees.

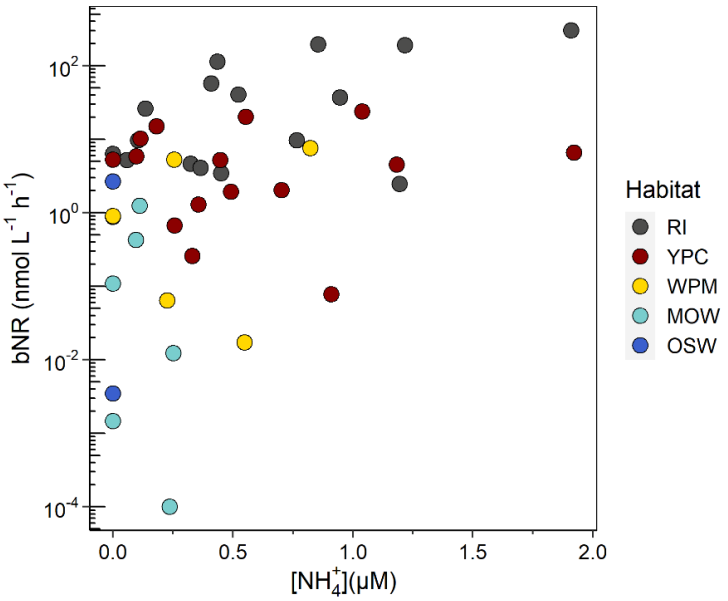

Figure S6. Nitrification rates versus NH_4^+ concentrations, at the different habitat encountered. The occurrence of rates differing by two to four orders of magnitude at a similar NH_4^+ concentrations, independently of the habitat, suggests that nitrifiers are not substrate limited in the Amazon River Plume, but that another process is at play.

References

Alpine, A., and J. Cloern. 1988. Phytoplankton growth rates in a light-limited environment, San Francisco Bay. Mar. Ecol. Prog. Ser. **44**: 167–173. doi:10.3354/meps044167

Aquino, R., C. Noriega, A. Mascarenhas, and others. 2022. Possible Amazonian contribution to *Sargassum* enhancement on the Amazon Continental Shelf. Science of The Total Environment **853**: 158432. doi:10.1016/j.scitotenv.2022.158432

Azam, F., T. Fenchel, J. Field, J. Gray, L. Meyer-Reil, and F. Thingstad. 1983. The ecological role of water-column microbes in the sea. Mar. Ecol. Prog. Ser. **10**: 257–263. doi:10.3354/meps010257

Benitez-Nelson, C. R. 2000. The biogeochemical cycling of phosphorus in marine systems. Earth-Science Reviews **51**: 109–135. doi:10.1016/S0012-8252(00)00018-0

Berounsky, V. M., and S. W. Nixon. 1993. Rates of nitrification along an estuarine gradient in Narragansett Bay. Estuaries **16**: 718–730. doi:10.2307/1352430

Bianchi, M., Feliatra, and D. Lefevre. 1999. Regulation of nitrification in the land-ocean contact area of the Rhône River plume (NW Mediterranean). Aquat. Microb. Ecol. **18**: 301–312. doi:10.3354/ame018301

Brion, N., G. Billen, L. Guézennec, and A. Ficht. 2000. Distribution of nitrifying activity in the Seine River (France) from Paris to the estuary. Estuaries **23**: 669–682. doi:10.2307/1352893

Bronk, D. A., L. Killberg-Thoreson, R. E. Sipler, and others. 2014. Nitrogen uptake and regeneration (ammonium regeneration, nitrification and photoproduction) in waters of the West Florida Shelf prone to blooms of Karenia brevis. Harmful Algae **38**: 50–62. doi:10.1016/j.hal.2014.04.007

Brzezinski, M. A. 1988. Vertical distribution of ammonium in stratified oligotrophic waters. Limnology and Oceanography **33**: 1176–1182. doi:10.4319/lo.1988.33.5.1176

Buchwald, C., and K. L. Casciotti. 2013. Isotopic ratios of nitrite as tracers of the sources and age of oceanic nitrite. Nature Geosci **6**: 308–313. doi:10.1038/ngeo1745

Carini, S. A., M. J. McCarthy, and W. S. Gardner. 2010. An isotope dilution method to measure nitrification rates in the northern Gulf of Mexico and other eutrophic waters. Continental Shelf Research **30**: 1795–1801. doi:10.1016/j.csr.2010.08.001

Chase, E. M., and F. L. Sayles. 1980. Phosphorus in suspended sediments of the Amazon River. Estuarine and Coastal Marine Science **11**: 383–391. doi:10.1016/S0302-3524(80)80063-6

Clark, D. R., A. P. Rees, and I. Joint. 2007. A method for the determination of nitrification rates in oligotrophic marine seawater by gas chromatography/mass spectrometry. Marine Chemistry **103**: 84–96. doi:10.1016/j.marchem.2006.06.005

Clark, D. R., A. P. Rees, and I. Joint. 2008. Ammonium regeneration and nitrification rates in the oligotrophic Atlantic Ocean: Implications for new production estimates. Limnology and Oceanography **53**: 52–62. doi:10.4319/lo.2008.53.1.0052

Cole, B., and J. Cloern. 1984. Significance of biomass and light availability to phytoplankton productivity in San Francisco Bay. Mar. Ecol. Prog. Ser. **17**: 15–24. doi:10.3354/meps017015

Coles, V. J., M. T. Brooks, J. Hopkins, M. R. Stukel, P. L. Yager, and R. R. Hood. 2013. The pathways and properties of the Amazon River Plume in the tropical North Atlantic Ocean. J. Geophys. Res. Oceans **118**: 6894–6913. doi:10.1002/2013JC008981

Cordier, T., P. Esling, F. Lejzerowicz, J. Visco, A. Ouadahi, C. Martins, T. Cedhagen, and J. Pawlowski. 2017. Predicting the ecological quality status of marine environments from eDNA metabarcoding data using supervised machine learning. Environ. Sci. Technol. **51**: 9118–9126. doi:10.1021/acs.est.7b01518

Damashek, J., K. L. Casciotti, and C. A. Francis. 2016. Variable nitrification rates across environmental gradients in turbid, nutrient-rich estuary waters of San Francisco Bay. Estuaries and Coasts **39**: 1050–1071. doi:10.1007/s12237-016-0071-7

Damashek, J., B. B. Tolar, Q. Liu, A. O. Okotie-Oyekan, N. J. Wallsgrove, B. N. Popp, and J. T. Hollibaugh. 2019. Microbial oxidation of nitrogen supplied as selected organic nitrogen compounds in the South Atlantic Bight. Limnol Oceanogr **64**: 982–995. doi:10.1002/lno.11089

DeMaster, D. J., and R. C. Aller. 2001. Biogeochemical processes on the Amazon shelf: Changes in dissolved and particulate fluxes during river/ocean mixing. The Biogeochemistry of the Amazon Basin 328–357.

Demaster, D. J., and R. H. Pope. 1996. Nutrient dynamics in Amazon shelf waters: results from AMASSEDS. Continental Shelf Research **16**: 263–289. doi:10.1016/0278-4343(95)00008-O

Deng, T., K.-W. Chau, and H.-F. Duan. 2021. Machine learning based marine water quality prediction for coastal hydro-environment management. Journal of Environmental Management **284**: 112051. doi:10.1016/j.jenvman.2021.112051

Devol, A. H. 2015. Denitrification, anammox, and N_2 production in marine sediments. Annual Review of Marine Science **7**: 403–423. doi:10.1146/annurev-marine-010213-135040

Dore, J. E., and D. M. Karl. 1996. Nitrification in the euphotic zone as a source for nitrite, nitrate, and nitrous oxide at Station ALOHA. Limnology and Oceanography **41**: 1619–1628. doi:10.4319/lo.1996.41.8.1619

Eppley, R. W., and B. J. Peterson. 1979. Particulate organic matter flux and planktonic new production in the deep ocean. Nature **282**: 677–680. doi:10.1038/282677a0

Fernández, C., L. Farías, and M. E. Alcaman. 2009. Primary production and nitrogen regeneration processes in surface waters of the Peruvian upwelling system. Progress in Oceanography **83**: 159–168. doi:10.1016/j.pocean.2009.07.010

Fox, L. E., S. L. Sager, and S. C. Wofsy. 1986. The chemical control of soluble phosphorus in the Amazon estuary. Geochimica et Cosmochimica Acta **50**: 783–794. doi:10.1016/0016-7037(86)90354-6

Froelich Jr, P. N., D. K. Atwood, and G. S. Giese. 1978. Influence of Amazon River discharge on surface salinity and dissolved silicate concentration in the Caribbean Sea. Deep Sea Research **25**: 735–744.

Glibert, P. M., F. P. Wilkerson, R. C. Dugdale, and others. 2016. Pluses and minuses of ammonium and nitrate uptake and assimilation by phytoplankton and implications for productivity and community composition, with emphasis on nitrogen-enriched conditions. Limnology and Oceanography **61**: 165–197. doi:10.1002/lno.10203

Goes, J. I., H. do R. Gomes, A. M. Chekalyuk, and others. 2014. Influence of the Amazon River discharge on the biogeography of phytoplankton communities in the western tropical north Atlantic. Progress in Oceanography **120**: 29–40. doi:10.1016/j.pocean.2013.07.010

Granger, J., and D. M. Sigman. 2009. Removal of nitrite with sulfamic acid for nitrate N and O isotope analysis with the denitrifier method. Rapid Commun. Mass Spectrom. **23**: 3753–3762. doi:10.1002/rcm.4307

Grasshoff, K., K. Kremling, and M. Ehrhardt. 1999. Methods of seawater analysis, John Wiley & Sons.

Hallegraeff, G. M. 2010. Ocean climate change, phytoplankton community responses, and harmful algal blooms: A formidable predictive challenge 1. Journal of Phycology **46**: 220–235. doi:10.1111/j.1529-8817.2010.00815.x

Howarth, R. W. 1988. Nutrient limitation of net primary production in marine ecosystems. Annu. Rev. Ecol. Syst. **19**: 89–110. doi:10.1146/annurev.es.19.110188.000513

Hsiao, S. S.-Y., T.-C. Hsu, J. -w Liu, and others. 2014. Nitrification and its oxygen consumption along the turbid Chang Jiang River plume. Biogeosciences **11**: 2083–2098. doi:10.5194/bg-11-2083-2014

Hu, Z., H. J. C. T. Wessels, T. van Alen, M. S. M. Jetten, and B. Kartal. 2019. Nitric oxide-dependent anaerobic ammonium oxidation. Nat Commun **10**: 1244. doi:10.1038/s41467-019-09268-w

Iriarte, A., I. de Madariaga, F. Diez-Garagarza, M. Revilla, and E. Orive. 1997. Primary plankton production, respiration and nitrification in a shallow temperate estuary during summer. Journal of Experimental Marine Biology and Ecology **208**: 127–151. doi:10.1016/S0022-0981(96)02672-X

Kache, S., I. Bartl, J. Wäge-Recchioni, and M. Voss. 2021. Influence of organic particle addition on nitrification rates and ammonium oxidiser abundances in Baltic seawater. Marine Ecology Progress Series **674**: 59–72. doi:10.3354/meps13797

Kirk, J. T. O. 1994. Light and Photosynthesis in Aquatic Ecosystems, Cambridge University Press.

Kitzinger, K., C. C. Padilla, H. K. Marchant, and others. 2019. Cyanate and urea are substrates for nitrification by Thaumarchaeota in the marine environment. Nature microbiology **4**: 234–243.

Kuenen, J. G. 2020. Anammox and beyond. Environmental Microbiology **22**: 525–536. doi:10.1111/1462-2920.14904

Kuhn, M. 2008. Building predictive models in R using the caret package. Journal of Statistical Software **28**: 1–26. doi:10.18637/jss.v028.i05

Laperriere, S. M., M. Morando, D. G. Capone, T. Gunderson, J. M. Smith, and A. E. Santoro. 2021. Nitrification and nitrous oxide dynamics in the Southern California Bight. Limnology and Oceanography **66**: 1099–1112. doi:10.1002/lno.11667

Lévy, M., O. Jahn, S. Dutkiewicz, and M. J. Follows. 2014. Phytoplankton diversity and community structure affected by oceanic dispersal and mesoscale turbulence. Limnology and Oceanography: Fluids and Environments **4**: 67–84. doi:10.1215/21573689-2768549

Liu, L., M. Chen, X. S. Wan, and others. 2023. Reduced nitrite accumulation at the primary nitrite maximum in the cyclonic eddies in the western North Pacific subtropical gyre. Science Advances **9**: eade2078. doi:10.1126/sciadv.ade2078

Loick-Wilde, N., S. C. Weber, B. J. Conroy, D. G. Capone, V. J. Coles, P. M. Medeiros, D. K. Steinberg, and J. P. Montoya. 2016. Nitrogen sources and net growth efficiency of

zooplankton in three A mazon River plume food webs. Limnol. Oceanogr. **61**: 460–481. doi:10.1002/lno.10227

Louchard, D., N. Gruber, and M. Münnich. 2021. The impact of the amazon on the biological pump and the air-sea CO_2 balance of the Western Tropical Atlantic. Global Biogeochemical Cycles **35**: e2020GB006818. doi:10.1029/2020GB006818

Margalef, R. 1978. Life-forms of phytoplankton as survival alternatives in an unstable environment. Oceanologica acta **1**: 493–509.

Meador, T. B., N. Schoffelen, T. G. Ferdelman, O. Rebello, A. Khachikyan, and M. Könneke. 2020. Carbon recycling efficiency and phosphate turnover by marine nitrifying archaea. Science Advances **6**: eaba1799. doi:10.1126/sciadv.aba1799

Merbt, S. N., D. A. Stahl, E. O. Casamayor, E. Martí, G. W. Nicol, and J. I. Prosser. 2012. Differential photoinhibition of bacterial and archaeal ammonia oxidation. FEMS Microbiology Letters **327**: 41–46. doi:10.1111/j.1574-6968.2011.02457.x

Middelburg, J. J., and J. Nieuwenhuize. 2001. Nitrogen isotope tracing of dissolved inorganic nitrogen behaviour in tidal estuaries. Estuarine, Coastal and Shelf Science **53**: 385–391. doi:10.1006/ecss.2001.0805

Mohrholz, V., T. Heene, R. Mars, J. Söder, and A. Subramaniam. 2022. Hydrographic properties of water masses in the Amazonas River plume obtained in April/May 2021 by CTD measurements during RV METEOR cruise M174.doi:10.1594/PANGAEA.942346

Muller-Karger, F. E., C. R. McClain, and P. L. Richardson. 1988. The dispersal of the Amazon's water. Nature **333**: 56–59.

Newell, S. E., A. R. Babbin, A. Jayakumar, and B. B. Ward. 2011. Ammonia oxidation rates and nitrification in the Arabian Sea. Global Biogeochemical Cycles **25**. doi:10.1029/2010GB003940

Nixon, S. W., C. A. Oviatt, J. Frithsen, and B. Sullivan. 1986. Nutrients and the productivity of estuarine and coastal marine ecosystems. Journal of the Limnological Society of Southern Africa **12**: 43–71. doi:10.1080/03779688.1986.9639398

Owens, N. J. P. 1986. Estuarine nitrification: A naturally occurring fluidized bed reaction? Estuarine, Coastal and Shelf Science **22**: 31–44. doi:10.1016/0272-7714(86)90022-3

Paerl, H. W., N. S. Hall, B. L. Peierls, and K. L. Rossignol. 2014. Evolving paradigms and challenges in estuarine and coastal eutrophication dynamics in a culturally and climatically stressed world. Estuaries and Coasts **37**: 243–258. doi:10.1007/s12237-014-9773-x

Pakulski, J. D., R. Benner, T. Whitledge, R. Amon, B. Eadie, L. Cifuentes, J. Ammerman, and D. Stockwell. 2000. Microbial metabolism and nutrient cycling in the Mississippi and Atchafalaya River Plumes. Estuarine, Coastal and Shelf Science **50**: 173–184. doi:10.1006/ecss.1999.0561

Peng, X., S. E. Fawcett, N. van Oostende, M. J. Wolf, D. Marconi, D. M. Sigman, and B. B. Ward. 2018. Nitrogen uptake and nitrification in the subarctic North Atlantic Ocean. Limnology and Oceanography **63**: 1462–1487. doi:10.1002/lno.10784

Pham, A. H., N. Choisnard, A. Fernández-Carrera, A. Subramaniam, E. K. Strope, E. J. Carpenter, M. Voss, and J. P. Montoya. 2024. Planktonic habitats in the Amazon Plume region of the Western Tropical North Atlantic. Frontiers in Marine Science. doi:10.3389/fmars.2024.1287497

Pomeroy, L. R. 1974. The ocean's food web, a changing paradigm. BioScience **24**: 499–504. doi:10.2307/1296885

Santoro, A. E., K. L. Casciotti, and C. A. Francis. 2010. Activity, abundance and diversity of nitrifying archaea and bacteria in the central California Current. Environmental Microbiology **12**: 1989–2006. doi:10.1111/j.1462-2920.2010.02205.x

Santoro, A. E., M. A. Saito, T. J. Goepfert, C. H. Lamborg, C. L. Dupont, and G. R. DiTullio. 2017. Thaumarchaeal ecotype distributions across the equatorial Pacific Ocean and their potential roles in nitrification and sinking flux attenuation. Limnology and Oceanography **62**: 1984–2003. doi:10.1002/lno.10547

Santoro, A. E., C. M. Sakamoto, J. M. Smith, and others. 2013. Measurements of nitrite production in and around the primary nitrite maximum in the central California Current. Biogeosciences **10**: 7395–7410. doi:10.5194/bg-10-7395-2013

Satinsky, B. M., C. S. Fortunato, M. Doherty, and others. 2015. Metagenomic and metatranscriptomic inventories of the lower Amazon River, May 2011. Microbiome **3**: 39, s40168-015-0099–0. doi:10.1186/s40168-015-0099-0

Satinsky, B. M., C. B. Smith, S. Sharma, and others. 2017. Expression patterns of elemental cycling genes in the Amazon River Plume. ISME J **11**: 1852–1864. doi:10.1038/ismej.2017.46

Satinsky, B. M., B. L. Zielinski, M. Doherty, C. B. Smith, S. Sharma, J. H. Paul, B. C. Crump, and M. A. Moran. 2014. The Amazon continuum dataset: Quantitative metagenomic and metatranscriptomic inventories of the Amazon River plume, June 2010. Microbiome **2**: 17. doi:10.1186/2049-2618-2-17

Sigman, D. M., K. L. Casciotti, M. Andreani, C. Barford, M. Galanter, and J. K. Böhlke. 2001. A bacterial method for the nitrogen isotopic analysis of nitrate in seawater and freshwater. Anal. Chem. **73**: 4145–4153. doi:10.1021/ac010088e

Smith, J. M., F. P. Chavez, and C. A. Francis. 2014. Ammonium uptake by phytoplankton regulates nitrification in the sunlit ocean. PLOS ONE **9**: e108173. doi:10.1371/journal.pone.0108173

Smith, J. M., J. Damashek, F. P. Chavez, and C. A. Francis. 2016. Factors influencing nitrification rates and the abundance and transcriptional activity of ammonia-oxidizing microorganisms in the dark northeast Pacific Ocean. Limnology and Oceanography **61**: 596–609. doi:10.1002/lno.10235

Sohm, J. A., and D. G. Capone. 2010. Zonal differences in phosphorus pools, turnover and deficiency across the tropical North Atlantic Ocean. Global Biogeochemical Cycles **24**. doi:10.1029/2008GB003414

Sperlea, T., N. Kreuder, D. Beisser, G. Hattab, J. Boenigk, and D. Heider. 2021. Quantification of the covariation of lake microbiomes and environmental variables using a machine learning-based framework. Molecular Ecology **30**: 2131–2144. doi:10.1111/mec.15872

Sperlea, T., J. P. Schenk, H. Dreßler, D. Beisser, G. Hattab, J. Boenigk, and D. Heider. 2022. The relationship between land cover and microbial community composition in European lakes. Science of the Total Environment **825**: 153732. doi:10.1016/j.scitotenv.2022.153732

Starr, L. D., M. J. McCarthy, C. R. Hammerschmidt, A. Subramaniam, M. C. Despins, J. P. Montoya, and S. E. Newell. 2022. Mercury methylation linked to nitrification in the tropical North Atlantic Ocean. Marine Chemistry **247**: 104174. doi:10.1016/j.marchem.2022.104174

Stephens, B. M., S. D. Wankel, J. M. Beman, A. J. Rabines, A. E. Allen, and L. I. Aluwihare. 2020. Euphotic zone nitrification in the California Current Ecosystem. Limnology and Oceanography **65**: 790–806. doi:10.1002/lno.11348

Stukel, M. R., V. J. Coles, M. T. Brooks, and R. R. Hood. 2014. Top-down, bottom-up and physical controls on diatom-diazotroph assemblage growth in the Amazon River plume. Biogeosciences **11**: 3259–3278. doi:10.5194/bg-11-3259-2014

Subramaniam, A., P. L. Yager, E. J. Carpenter, and others. 2008. Amazon River enhances diazotrophy and carbon sequestration in the tropical North Atlantic Ocean. Proc. Natl. Acad. Sci. U.S.A. **105**: 10460–10465. doi:10.1073/pnas.0710279105

Sun, A. Y., and B. R. Scanlon. 2019. How can Big Data and machine learning benefit environment and water management: A survey of methods, applications, and future directions. Environ. Res. Lett. **14**: 073001. doi:10.1088/1748-9326/ab1b7d

Sun, D., X. Tang, M. Zhao, and others. 2020. Distribution and diversity of comammox *Nitrospira* in coastal wetlands of China. Front. Microbiol. **11**: 589268. doi:10.3389/fmicb.2020.589268

Tanaka, T., F. Rassoulzadegan, and T. F. Thingstad. 2003. Measurements of phosphate affinity constants and phosphorus release rates from the microbial food web in Villefranche Bay, northwestern Mediterranean. Limnology and Oceanography **48**: 1150–1160. doi:10.4319/lo.2003.48.3.1150

Tang, W., Z. Li, and N. Cassar. 2019. Machine learning estimates of global marine nitrogen fixation. Journal of Geophysical Research: Biogeosciences **124**: 717–730. doi:10.1029/2018JG004828

Tang, W., B. B. Ward, M. Beman, and others. 2023. Database of nitrification and nitrifiers in the global ocean. Earth System Science Data Discussions, 1–66. Doi: 10.5194/essd-15-5039-2023

Wan, X. S., H.-X. Sheng, M. Dai, and others. 2018. Ambient nitrate switches the ammonium consumption pathway in the euphotic ocean. Nat Commun **9**: 915. doi:10.1038/s41467-018-03363-0

Ward, B. B. 1987. Nitrogen transformations in the Southern California Bight. Deep Sea Research Part A. Oceanographic Research Papers **34**: 785–805. doi:10.1016/0198-0149(87)90037-9

Ward, B. B. 2005. Temporal variability in nitrification rates and related biogeochemical factors in Monterey Bay, California, USA. Marine Ecology Progress Series **292**: 97–109. doi:10.3354/meps292097

Ward, B. B. 2008. Nitrification in marine systems, p. 199–261. *In* Nitrogen in the Marine Environment. Elsevier.

Ward, B. B. 2011. Chapter thirteen - Measurement and distribution of nitrification rates in the oceans, p. 307–323. *In* M.G. Klotz [ed.], Methods in Enzymology. Academic Press.

Ward, B. B., H. E. Glover, and F. Lipschultz. 1989. Chemoautotrophic activity and nitrification in the oxygen minimum zone off Peru. Deep Sea Research Part A. Oceanographic Research Papers **36**: 1031–1051. doi:10.1016/0198-0149(89)90076-9

Weber, S. C., A. Subramaniam, J. P. Montoya, H. Doan-Nhu, L. Nguyen-Ngoc, J. W. Dippner, and M. Voss. 2019. Habitat delineation in highly variable marine environments. Frontiers in Marine Science **6**: 112. doi:10.3389/fmars.2019.00112

de Wilde, H. P. J., and M. J. M. de Bie. 2000. Nitrous oxide in the Schelde estuary: Production by nitrification and emission to the atmosphere. Marine Chemistry **69**: 203–216. doi:10.1016/S0304-4203(99)00106-1

Wuchter, C., B. Abbas, M. J. L. Coolen, and others. 2006. Archaeal nitrification in the ocean. Proceedings of the National Academy of Sciences **103**: 12317–12322. doi:10.1073/pnas.0600756103

Xia, F., J.-G. Wang, T. Zhu, B. Zou, S.-K. Rhee, and Z.-X. Quan. 2018. Ubiquity and diversity of complete ammonia oxidizers (comammox) A.J.M. Stams [ed.]. Appl Environ Microbiol **84**: e01390-18. doi:10.1128/AEM.01390-18

Zakem, E. J., A. Al-Haj, M. J. Church, and others. 2018. Ecological control of nitrite in the upper ocean. Nat Commun **9**: 1206. doi:10.1038/s41467-018-03553-w

Zheng, Z.-Z., X. Wan, M. N. Xu, and others. 2017. Effects of temperature and particles on nitrification in a eutrophic coastal bay in southern China. Journal of Geophysical Research: Biogeosciences **122**: 2325–2337. doi:10.1002/2017JG003871

Zhou, Z., Y. Liu, S. Wang, J. Xiao, X. Cao, Y. Zhou, and C. Song. 2023. Interactions between phosphorus enrichment and nitrification accelerate relative nitrogen deficiency during cyanobacterial blooms in a large shallow eutrophic lake. Environ. Sci. Technol. **57**: 2992–3001. doi:10.1021/acs.est.2c07599

Zielinski, B. L., A. E. Allen, E. J. Carpenter, and others. 2016. Patterns of transcript abundance of eukaryotic biogeochemically-relevant genes in the Amazon River Plume. PLOS ONE **11**: e0160929. doi:10.1371/journal.pone.0160929

4 | N assimilation and recycling in surface waters of the Amazon and Pará Estuaries

Authors: †Choisnard Noémie and †Umbricht Jacqueline, Araujo Moacyr, Böttcher Michael, Burmeister Christian, Liskow Iris, Schmiedinger Iris and Voss Maren.

Journal of Geophysical Research-Oceans.

† These authors contributed equally to this work

Author Contribution Statement: NC, JU and MV conceived and designed the research. All authors contributed to the collection and compilation of data. NC, JU and MV analyzed the data. NC and JU wrote the manuscript. All authors contributed to content revisions and approved the final text.

Abstract

Under increasing anthropogenic impacts, the hydrology, weathering, turbidity, and biogeochemistry of the Amazon and Pará river catchments are changing, potentially affecting the concentration and speciation of nitrogen (N) entering the estuary, as well as the subsequent primary productivity. Primary production and several N-cycling rates have been studied in the northern river plume, and new studies focusing on specific processes in the river mouth emerged. Yet, a general overview is still lacking. For the first time, we provide an overview of primary production along with nitrification, ammonium (NH_4^+), nitrate (NO_3^-), and amino acid uptake rates in the Amazon and Pará river mouths which exhibit different degrees of catchment land use. Our results indicate that the Amazon supplies tenfold more NH_4^+ and NO_3^-, and its nitrification rates are four times higher than in the Pará River. The stable isotope composition of ambient water and NO_3^- confirmed that nitrification is a dominant pathway, with fluxes reaching $8.5x10^8$ mol N d^{-1} in the Amazon. Nutrients are transported to regions with reduced turbidity and nitrification, facilitating NH_4^+ (0.2 to $2.4x10^8$ mol N d^{-1}) and carbon uptake (4.6 and $14.0x10^8$ mol C d^{-1} in the Pará and the Amazon, respectively). The lower N-cycling rates measured in the Pará relative to the Amazon River mouth likely originate from differences in river discharge and watershed characteristics. As such, the Pará River could provide a glimpse of what the Amazon River N budget could become if climate change-induced droughts become more frequent in the future.

Introduction

Estuaries are undeniably subject to an array of perturbations, as their catchments are often densely populated. Increased urbanization or agriculture necessary to meet the needs of a growing population can in turn act on the concentration of nitrogen (N) in rivers and result in harmful consequences for the estuary's health (Rosenberg et al. 1990; Cooper and Brush 1991; Nixon 1995; Jickells 1998; Seitzinger et al. 2010; Paerl et al. 2014). To predict the future of the N supply to the ocean and the associated productivity of both phytoplankton and higher trophic levels, it is, therefore, crucial to quantify the current fluxes of N from rivers to the ocean, starting with a correct quantification of N transformation processes in estuaries.

The amount of N exported to the ocean depends on a complex interplay of factors, such as the physical characteristics of the estuary and in situ biogeochemical processes (Jickells, 1998; Nixon et al., 1996). Ammonification and nitrification (i.e. the production and oxidation of ammonium - NH_4^+ - from organic matter) lead to recycling within the estuary, hence retain N, while other metabolic pathways, such as denitrification (i.e. the reduction of nitrate - NO_3^- - to dinitrogen), remove bioavailable N from the system. As a result, numerous studies have explored nutrient fluxes and budgets through the land-sea continuum to implement estuarine management strategies and reduce and monitor N inputs into coastal ecosystems (Galloway et al. 1996; Dham et al. 2002; Riemann et al. 2016; Lefcheck et al. 2018). But while this effort has been made in many different ecosystems, such as urbanized rivers (Lefcheck et al. 2018), mangroves (Reis et al. 2017) or lagoons (Cabral et al. 2019), other ecosystems, such as the Amazon River estuary, remain understudied and knowledge acquired in one system may not be transferrable to another.

As the world's largest river, the Amazon discharges around 200,000 $m^3\ s^{-1}$ of freshwater into the Western Tropical North Atlantic (WTNA) during the peak discharge season in May and June and forms a large estuarine region, where it meets the ocean (Nittrouer and DeMaster 1996). The Amazon estuary is also influenced by the neighboring Pará River (mean discharge of 20,946 $m^3\ s^{-1}$; Prestes et al., 2020), which receives most of its water from the Tocantins River but also from the Amazon River. The high turbidity of the water hundreds of kilometers away from the coast due to the huge riverine sediment load of 750 Tg yr^{-1} (DeMaster and Aller 2001; Park and Latrubesse 2015) results in light limitation, which is thought to reduce phytoplankton activity in the estuary and promote the export of the roughly 3.0 Tg N y^{-1} supplied by the rivers (Sharples et al. 2017). However, other studies showed that phytoplankton can make use of the

nutrients supplied by the rivers (Gomes et al. 2018), potentially resulting in low export to the open ocean (Izett and Fennel 2018).

This lack of a consensus on the N export and utilization in the estuary of the Amazon and Pará rivers impedes reliable predictions of the future of productivity in both the estuaries and the adjacent coastal ocean. Many studies explored rates of singular processes such as dinitrogen fixation and nitrification or primary production along the Amazon River plume (Smith and Demaster 1996; Cooley et al. 2007; Subramaniam et al. 2008; Choisnard et al. 2024), but other N-cycling rates remain unexplored, and global overviews linking this data are scarce. Earlier studies have been carried out in the region and helped to refine the global N budget on the shelf (DeMaster and Aller 2001; Smoak et al. 2005; Araujo et al. 2014, 2017; Drake et al. 2021). However, these studies were based on N fluxes estimated from nutrient concentrations and river flows and not on measured rates of N cycling pathways. Furthermore, these studies use datasets collected in the 90's to early 2010's. However, like most other rivers, the Amazon catchment area has experienced tremendous anthropogenic impacts for decades. Increasing deforestation (+25 % since 2010; Wang et al., 2019) and agricultural land use (+67 % since 2010; Ometto et al., 2011; Wang et al., 2019), the construction of dams (Latrubesse et al. 2017) and population growth (Martinelli et al. 2010) cause changes in the nutrient load of the Amazon. Current NO_3^- fluxes at Obidos (up to 1600 kg NO_3^- s^{-1} in 2014; Lapointe et al., 2021) can be greater by approximately a factor of ten compared with historical values (Lapointe et al. 2021; Aquino et al. 2022). The N to phosphorus (P) ratio in coastal and open ocean waters could also be altered, as N input from fertilizer use exceeds that of P (Sutton et al. 2013; Glibert et al. 2014), which could in turn impact primary production and the associated N cycle in the estuary and beyond (Wang et al. 2019). As such, updating our knowledge of the Amazon estuary's N budget is relevant.

In this study, we present current nutrient concentrations and the first overview of NO_3^-, NH_4^+, and amino acids (AA) assimilation, nitrification, and primary production rates from the Amazon and Pará estuaries. We combined these results with the measurement of N and oxygen stable isotopes in water (H_2O) and NO_3^-, as these measurements provide further insights on the longer-term dominance of one N cycle process versus the other. The aim was to improve the understanding of N cycling in the region of the world's largest river mouth and present an estimate of the N budget for the shelf. Our findings provide a baseline for N transformation and

export from the Amazon estuary to the WTNA and can help to predict changes in the biogeochemical cycling and associated productivity of the Amazon and its plume in the future.

Materials and Methods

Sample collection

Six stations were sampled during the M-174 cruise undertaken in April and May 2021, during maximum river discharge, in the Amazon and Pará river mouths aboard the *R/V Meteor* (Figure 18; Table 7; Table 7). Water samples were obtained using a Seabird Electronics SBE-32 rosette mounted with 21 Free Flow bottles of 10 L. Vertical profiles of temperature and salinity, dissolved oxygen (O_2), turbidity and fluorescence were obtained from a Seabird Electronics SBE-911plus (SN-0603) CTD, SBE43 dissolved O_2 sensor, D&A OBS-3 turbidity sensor, and a WETStar fluorometer, respectively, mounted on the rosette.

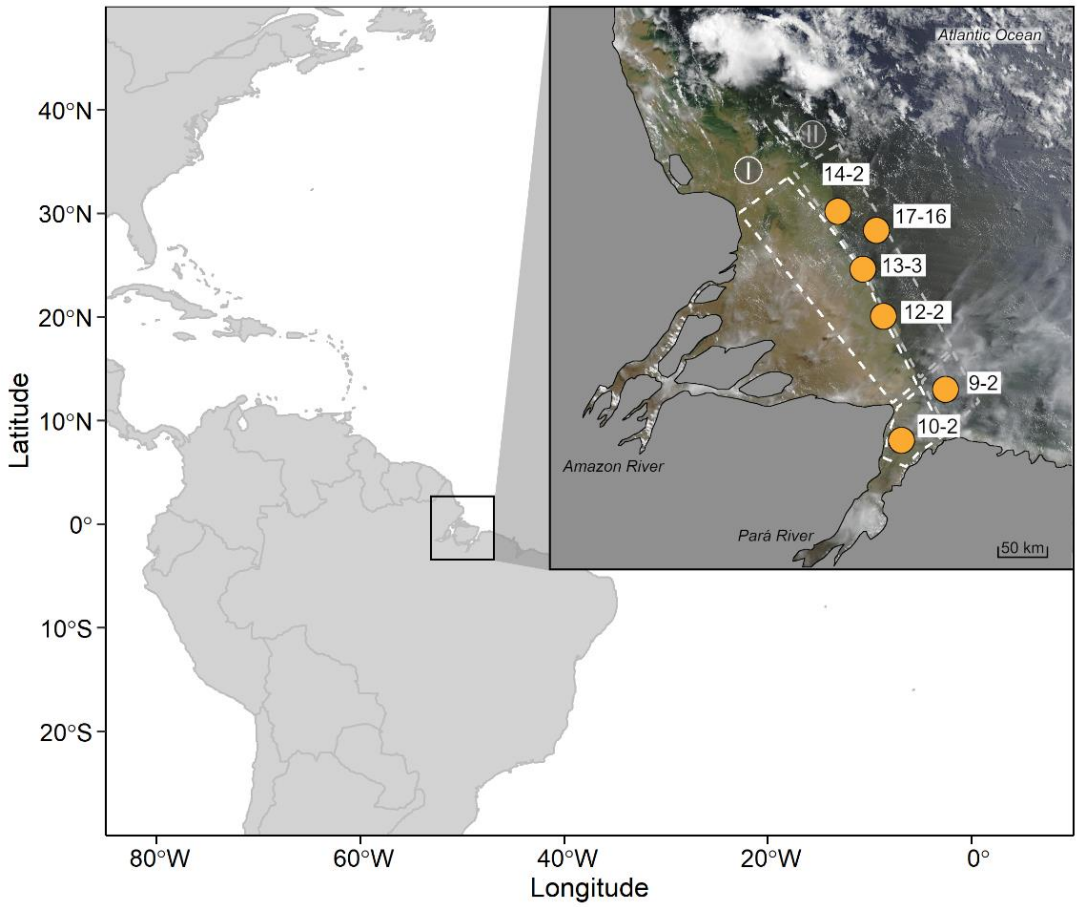

Figure 18. Study site. The map was generated with NASA Worldview, on the day when station 14-2 was sampled. The white and grey dashed boxes represent the areas taken into account for the N budget of the two rivers (see Figure 24). Box (I) is drawn between the 10 m isobaths (thickness of the plume at sampled stations) and the most turbid station sampled (~ 50 km), and across the width of the delta. Box (II) is a 50 km wide box around the stations located at less turbid stations, at the edge of both river plumes.

Table 7. Main characteristics of surface waters at each station sampled, with S being the surface salinity.

Station	Lat (dec)	Long (dec)	Date	Depth (m)	Ez (m)	S	Turbidity (NTU)	PO_4^{3-} (μM)	NO_3^- (μM)	NO_2^- (μM)	NH_4^+ (μM)	PN (μM)	$\delta^{15}N$–PN (mUr)
9-2	-0.122	-47.731	4/23/2021	36	10	3.7	5.7	0.54	10.7	0.26	0.95	2.5	7.3
10-2	-0.598	-48.261	4/23/2021	14	3	0.9	9.7	0.37	11.3	0.25	0.52	15.8	6.6
12-2	0.597	-48.374	4/24/2021	16	3	0.5	9.7	0.76	10.1	0.31	1.22	6.5	5.8
13-3	1.05	-48.584	4/24/2021	16	3	0.9	9.7	0.90	18.4	0.28	0.43	10.3	7.7
14-2	1.613	-48.84	4/25/2021	15	3	4.6	3.3	0.31	13.1	0.09	0.32	3.2	3.3
17-16	1.427	-48.442	4/27/2021	27	10	5.4	2.9	0.60	8.5	0.18	0.36	1.6	5.5

Depth of the euphotic zone

The Seabird Electronics device was used to measure PAR throughout the water column. The light attenuation coefficient, K_d(PAR), was calculated from a simple linear fit of log-transformed PAR data versus depth (Kirk 1994). The resulting %PAR was calculated following:

$$\%PAR = exp^{(-K_d(PAR)z)} \times 100 \quad (7)$$

The depth where the %PAR reaches 1 % is by definition the depth of the euphotic zone.

Nutrient analysis

Samples for nutrient analysis were retrieved at five to six depths and filtered (0.2 µm pore size) immediately after collection. Shortly after, phosphate (PO_4^{3-}), NO_3^-, nitrite (NO_2^-), and NH_4^+ concentrations were determined on a continuous flow autoanalyzer (QuAAtro, Seal analytical) following (Grasshoff et al. 1999) and HELCOM guidelines (2014). The precision on each nutrient was 0.01 (PO_4^{3-}), 0.02 (NO_3^-), 0.006 (NO_2^-), and 0.05 (NH_4^+) μM.

Rates measurements

N uptake and nitrification rates were measured using tracer incubation methods (Dugdale and Goering 1967; Santoro et al. 2010; Damashek et al. 2016). Details on the incubation procedures are given in Table S1. Briefly, water was collected from 1 to 2 depths (usually surface only or surface and 10 m depth, depending on the depth of the euphotic zone)

in triplicates from the CTD rosette into acid-washed 1 L polycarbonate bottles, and spiked with $^{15}NaNO_3$, $^{15}NH_4Cl$ or a dually labeled AA mixture (Table S2). The final tracer concentration was 10 % of ambient concentration for NH_4^+- and NO_3^--uptake. As we did not have a way to measure in situ AA concentrations on board, 10 % AA tracer injections were performed assuming that in situ concentrations equaled 0.5 μM. DIC-uptake rates were measured in conjunction with dissolved inorganic nitrogen (DIN) uptake rates by adding $NaH^{13}CO_3$ to samples in a final concentration of 20 μM. All bottles were incubated in transparent on-deck incubators flooded with sea surface water for two (NH_4^+ and AA uptake) to three hours (NO_3^- uptake), during daylight. In situ, light intensity was simulated by placing the bottles into black gauze bags that matched the light intensity of the sampled depth.

Samples for nitrification rates and microbial NH_4^+ uptake measurements were sealed air-tight, and amended with $^{15}NH_4Cl$, at approximately 10 % of ambient concentration. Initial conditions samples (T0) were filtered directly after tracer injection while end-point samples were split into two batches of three bottles each for their two hours of incubation: one batch was incubated in the dark, and one batch was incubated under in situ light for three hours, as described for uptake rates.

The incubation of all rates was terminated by filtration onto precombusted (450 °C for 4 hours) glass-fiber filters (Advantec, GF-075; 25 mm, nominal pore-size 0.3 μm). Filters were oven-dried (50°C, 48 hours) and analyzed on a continuous flow-isotope ratio mass spectrometer (CF-IRMS, Delta V advantage , Thermo scientific) connected to EA Isolink CN (Thermo scientific) elemental analyser via an open split interface ConFlo IV (Thermo scientific), to calculate phytoplankton NO_3^-, NH_4^+ and AA uptake, as well as microbial NH_4^+ uptake and DIC uptake rates.

For nitrification rates, 50 mL aliquots of the filtrate from each incubation were collected in Falcon tubes and frozen at -20 °C until analysis. During the incubation, the labeled ^{15}N-NH_4^+ is converted into ^{15}N-(NO_3^-+NO_2^-) which was analyzed at the Voss Lab (Institute for Baltic Sea Research, Warnemünde, Germany) using the bacterial denitrifier method described below. Uptake rates were calculated after (Dugdale and Wilkerson 1986) and Collos, (1987), and nitrification rates were calculated following Damashek et al. (2016) (see Text S2 for details). Uptake rates were then integrated over the euphotic zone only, while microbial rates over the freshwater layer (~ 10 m; Figure S7) to properly describe the N cycling in the plume layer. When the euphotic zone was nearly at the surface (3 m, Table 7), measured uptake rates were

assumed to be roughly equal over this depth interval. To get an estimate of daily rates, uptake rates were multiplied by 12 hours. Daily nitrification rates are represented by the sum of the hourly dark and light nitrification rates arbitrarily multiplied by 12. The detection limit of all rates was determined for every incubation following (Santoro et al. 2013) and ranged from 0.01 to 0.50 nmol L^{-1} h^{-1} for nitrification rates, and 0.001 to 0.577 nmol L^{-1} h^{-1} for DIN, AA and DIC uptake rates.

δ^{15}N-PN analysis

Samples for particulate nitrogen (PN) analysis were collected at each station by filtration of approximately 500 mL of water onto precombusted (450 °C for 4 hours) glass-fiber filters (Advantec, GF-075; 25 mm, nominal pore-size 0.3 μm) immediately after collection. Filters were oven-dried (50°C, 48 hours) and analyzed on a continuous flow-isotope ratio mass spectrometer (CF-IRMS, Delta V advantage, Thermo scientific) connected to EA Isolink CN (Thermo scientific) elemental analyser via an open split interface ConFlo IV (Thermo scientific). The ultrapure N_2 reference gas for stable isotope analysis was calibrated using IAEA standards and a Peptone (laboratory standard) is interspersed in each analytical run to control the isotopic composition. The standard error for the PN concentration and its isotopic composition (δ^{15}N-PN) data was < 0.2 mUr. δ^{15}N-PN values were used as T0 for N uptake rate calculations (see Text S2).

δ^{15}N- and δ^{18}O-NO_3^- analysis

Samples for natural abundance stable isotopic composition of NO_3^- (δ^{15}N-NO_3^- and δ^{18}O-NO_3^-) were collected at the surface (depth < 5 m), filtered (0.2 µm pore size), and immediately stored frozen (-20°C) until analysis. Additionally to these samples, one rainwater sample was collected during a rain event at station 12-2. Samples were treated with sulfamic acid to remove NO_2^-, according to the protocol of Granger and Sigman (2009). After treatment, the δ^{15}N and δ^{18}O of NO_3^- were measured in duplicate using the denitrifier method (Sigman et al. 2001; Casciotti et al. 2002) at the Leibniz Institute for Baltic Sea Research (IOW), following the protocols of Weigand et al., (2016). 10 to 20 nmol of NO_3^- were quantitatively converted to nitrous oxide (N_2O) gas by a strain of denitrifying bacteria (*Pseudomonas aureofaciens*) that lacks an active N_2O reductase enzyme. The resulting N_2O was analyzed for stable N and O isotopic composition using a Thermo Scientific Fisher delta-V Advantage isotope ratio mass-spectrometer connected to a PAL autosampler and a Thermo Finnigan GasBench II.

Sets of NO_3^- standards (IAEAN3 and USGS34) emulating our sample concentrations were measured every 10 samples (3 to 4 times per run). These standards were used for calibration and bacteria blank correction, with an uncertainty of less than 0.20 mUr and 0.30 mUr for $\delta^{15}N$ and $\delta^{18}O$ (SD), respectively. $\delta^{15}N$ and $\delta^{18}O$ values are reported on the AIR and V-SMOW scales, respectively.

Water $\delta^{18}O$ analysis

Samples for natural abundance stable isotopic composition of water ($\delta^{18}O$-H_2O) were collected as described for $\delta^{15}N$-NO_3^- and $\delta^{18}O$-NO_3^- samples. $\delta^{18}O$-H_2O values were analyzed in the Böttcher lab at IOW using a laser cavity-ring-down spectroscopy (LCRDS) system (Picarro L2140-i;(Böttcher and Schmiedinger 2021). The reference materials SLAP, VSMOW, and GISP, besides in-house standards, were used to calibrate measured isotope ratios towards the V-SMOW scale. The reproducibility of both in-house standards was better than 0.05 mUr (1SD) for $\delta^{18}O$ over the entire dataset. The given 'mUr' (milliUrey) values are equivalent to the traditional '‰' (Brand and Coplen 2012).

Stable isotope data analysis

NO_3^- concentration and dual isotopic composition are governed by a mixture of N sources and biogeochemical transformations (Middelburg and Nieuwenhuize 2001; Dähnke et al. 2008; Kendall et al. 2010). It is therefore crucial to first define the characteristics of the various NO_3^- sources in the Amazon estuary. To our knowledge, no such data is available in the study area. The riverine end member is therefore represented by the $\delta^{15}N$-NO_3^- and $\delta^{18}O$-NO_3^- values of the stations presenting the lowest salinities and highest turbidity (salinity < 1 and turbidity > 9). The isotopic composition of other putative sources is defined as follows (Table 8):

Table 8. Characteristics of putative NO_3^- end-members in the study area.

NO_3^- source	NO_3^- (μM)	$\delta^{15}N$-NO_3^- (mUr)	$\delta^{18}O$-NO_3^- (mUr)	Reference
NO_3^- precipitation	3.7	1.8	55.9	This study
Seawater	20.0	5.59 ± 0.44	2.14 ± 0.14	Marconi et al., 2019
River	8.2	3.6 ± 0. 2	-0.6 ± 1.0	This Study

The seawater end-member is assumed to be similar to the Atlantic subsurface water (150-400 m depth) collected in the equator along the CLIVAR/GO-SHIP cruise (~-20°E; 0°N;

(Marconi et al. 2019). This water mass should represent adequately marine NO_3^- as it is less influenced than other waters by the addition of new NO_3^- sources and subsequent biological processes. It bears about 20 μM of NO_3^-, with a δ^{15}N- and δ^{18}O-NO_3^- of 5.59 ± 0.44 mUr and 2.14 ± 0.14 mUr, respectively. The δ^{15}N-NO_3^- values of this water mass agree well with the value of 5.8 – 6 mUr reported for the subsurface waters of the North Brazilian Current at a station sampled closer to the Amazon estuary (-38.9°E; 2.54°N; Fripiat et al., 2021).

Mixing between the riverine and seawater end-member is assumed to have a major role in driving NO_3^- isotopic composition. The physical mixing between these two sources was evaluated for both isotopes using a classical mixing model (Fry, 2006):

$$\delta_{mix} = \frac{(f_{river} \times \delta_{river} \times C_{river}) + (f_{seawater} \times \delta_{seawater} \times C_{seawater})}{C_{mixture}} \quad (8)$$

$$C_{mix} = (f_{river} \times C_{river}) + (f_{seawater} \times C_{seawater}) \quad (9)$$

$$f_{river} + f_{seawater} = 1 \quad (10)$$

Where f_{river} and $f_{seawater}$ are the proportion of the riverine and marine end-member calculated from salinity, and C and δ represent the concentration and isotopic composition of each end member as given in Table 8.

Results and Discussion

Sources of DIN in the Pará and Amazon River mouths

While it is fed by a large drainage basin, the Amazon River, part of which diverts to the Pará River, transports low nutrient concentrations relative to other smaller rivers (Bianchi et al. 1999; Hsiao et al. 2014). But these DIN (~ 20 μM) and relatively elevated phosphate concentrations (~1 μM), together with the tremendous freshwater discharge, result in loads of year-round high N, high N/P waters to the estuaries of both rivers (Figure 19, Figure S7; Araujo et al. 2014; Aquino et al. 2022). The Amazon River is reported as the main source of NO_3^- (~3.0 Tg N y^{-1}) and NH_4^+ (~0.3 Tg N y^{-1}) in the estuary (DeMaster and Aller 2001; Smoak et al. 2005; Drake et al. 2021), while advection and surface mixing supply half as much N, with a

flux estimated at 1.6×10^8 mol N d^{-1} (Demaster and Pope 1996; DeMaster and Aller 2001). Other sources of riverine N, such as dissolved (~1.1 Tg N y^{-1}) or particulate organic N (~1 Tg N y^{-1}) are slightly lower than the riverine NO_3^- fluxes, underlining the importance of this inorganic N form as a N-source to the estuary (DeMaster and Aller 2001; Drake et al. 2021).

The dual isotopic composition of NO_3^- has been a widely used tool for better characterizing the origin and fate of NO_3^- in riverine and estuarine environments (Ye et al. 2015; Wong et al. 2018; Archana et al. 2018). Here, we report for the first time the $\delta^{15}N$- and $\delta^{18}O$- values of the NO_3^- delivered to the Pará and the Amazon estuary. In both river mouths, most riverine stations present a similar $\delta^{15}N$-NO_3^- (3.6 and 4.0 mUr; Table 8; Figure 20a; Table S4), in line with previous measurements further upstream in the Amazon River (4.1±0.3 mUr; (Brandes and Devol 2002). $\delta^{18}O$-NO_3^- values are also closely similar to each other in both estuaries (-0.0 – -0.6 mUr; Table 8; Figure 20b). With increasing salinity (ranging between 0.4 and 8.3; Figure 20a), little variation is noticeable in the $\delta^{15}N$-NO_3^- values, which vary between 3.4 and 5.1 mUr. The $\delta^{18}O$-NO_3^- values present more scatter along the salinity gradient, ranging between -4.0 and 1.8 mUr and all Amazon samples fall below the $\delta^{18}O$-NO_3^- range given by the riverine and marine end-members (-0.6 – 2.14 mUr; Figure 20b). Together with the difference in dynamics between $\delta^{15}N$- and $\delta^{18}O$-NO_3^-, these results suggest that mixing between one riverine and one marine end-member cannot be the unique driver of NO_3^- isotopic composition in both estuaries (Archana et al., 2018; Kendall, 1998). Instead, some additional NO_3^- sources might also be at play here.

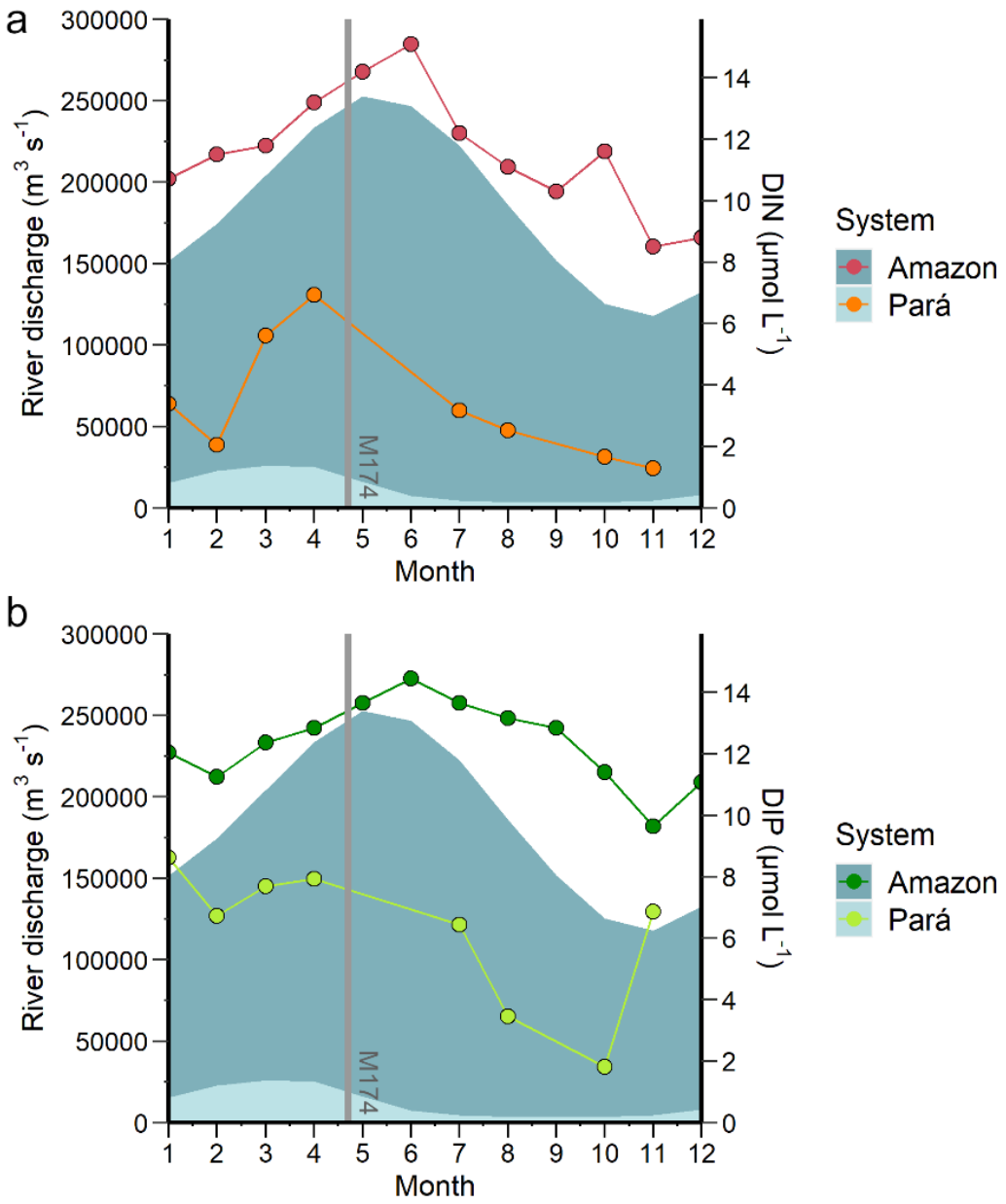

Figure 19. River discharge (blue areas), DIN (**a**), and DIP (**b**) concentrations in the Amazon and Pará river mouths. Data was retrieved in 2014 for the Amazon (Araujo et al. 2014), and in 2018 for the Pará River (Aquino et al. 2022). The grey vertical bar indicates the time of the year at which cruise M174 took place.

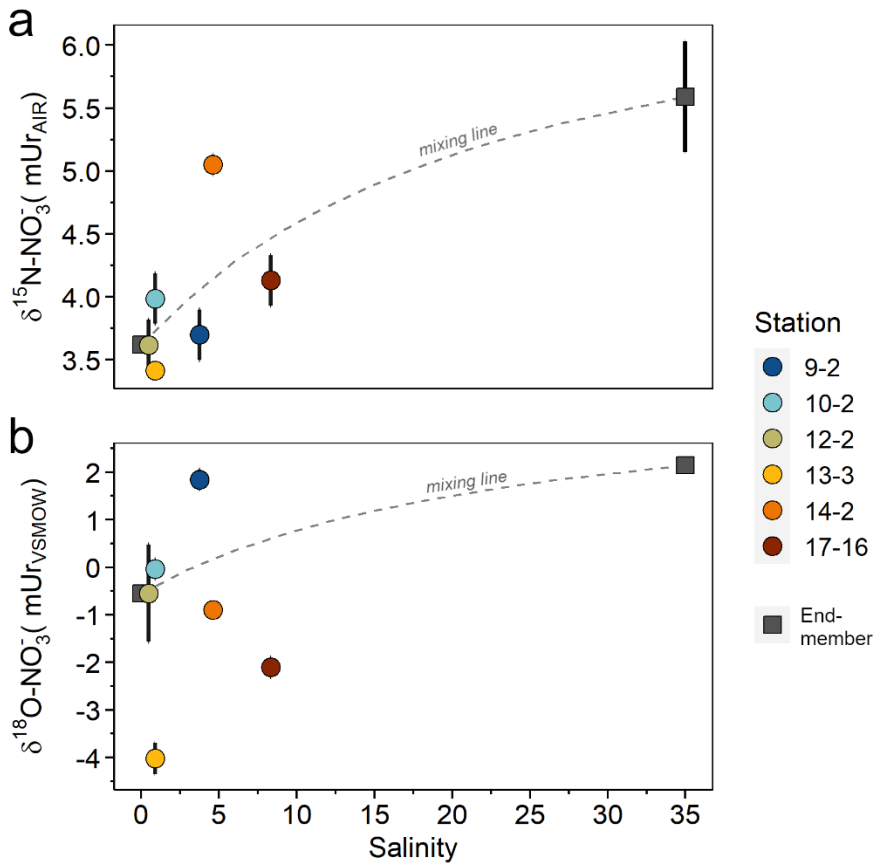

Figure 20. (**a**) δ^{15}N-NO_3^- and (**b**) δ^{18}O-NO_3^- values versus salinity. The square markers represent the isotopic composition of the riverine and marine end members, and the grey dashed line illustrates the physical mixing between them.

The rainwater sample collected at station 12-2 provides us with an additional putative NO_3^- source, with a δ^{15}N- and δ^{18}O-NO_3^- of 1.8 and 55.9 mUr, respectively (Table 8, Figure 21a). However, our measurements are significantly different from this end member, arguing for a modest contribution of rainwater to the NO_3^- pool in the estuaries (at most). We acknowledge that not all NO_3^- sources have been characterized here, and future studies should focus on unraveling the potential of other end-members, such as sewage or groundwater, for explaining the lower δ^{18}O-NO_3^- values of the Amazon estuary samples relative to the ones of the end-members defined here (Figure 21b).

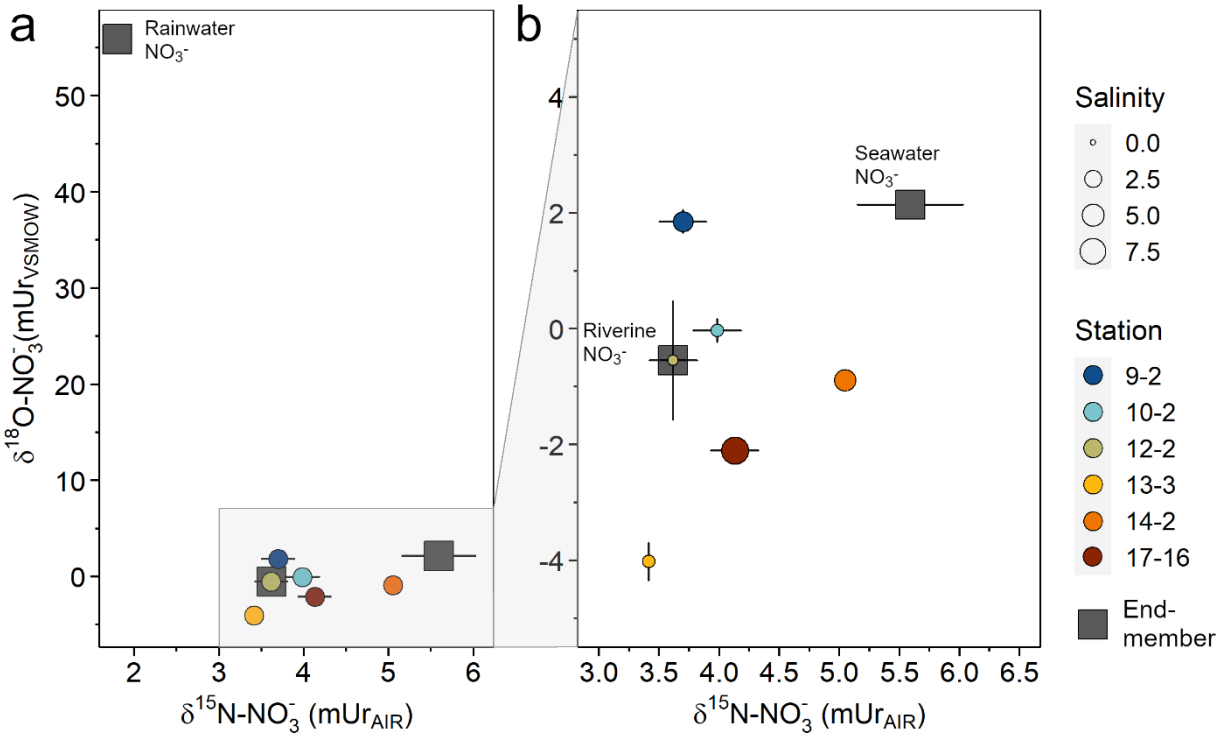

Figure 21. (**a**) δ^{15}N-NO_3^- versus δ^{18}O-NO_3^- at our study sites (circle markers, colored per station) in comparison to the isotopic composition of several putative end-members (square grey markers). Panel (**b**) is a zoomed-in view of panel a. The size of the colored markers represents the salinity of each sample.

In addition to sources mixing, biological N cycling might also impact the isotopic composition of NO_3^-, a hypothesis supported by the lack of linear relationships between salinity and other nutrients in the Amazon and Pará estuaries (Aquino et al. 2022). The rather high NO_3^- concentrations and relatively low δ^{15}N- and δ^{18}O-NO_3^- values measured could suggest that nitrification is at play here. Nitrification imprints the δ^{18}O of both O_2 (which has a δ^{18}O of ~23.5 mUr; (Kroopnick and Craig 1972; Barkan and Luz 2005) and ambient H_2O, and biogeochemical studies usually refer to two end-member scenarios for O atom incorporation during nitrification: (i) ~1/3 O atoms come from O_2 and ~2/3 from H_2O (Andersson and Hooper 1983; Kumar et al. 1983), with some fractionation effects associated with O atoms incorporation during NH_4^+ and NO_2^- oxidation, and equilibrium isotope effect associated with O isotope exchange between NO_2^- and H_2O (Buchwald and Casciotti 2010; Buchwald et al. 2012); Text S3) and (ii) all of the O atoms derive from H_2O, leaving the δ^{18}O of newly nitrified NO_3^- to be 1.1-1.2 mUr higher than that of H_2O (Granger et al. 2013; Marconi et al. 2019). These two scenarios give us a range of theoretical δ^{18}O-NO_3^-, which covered the surface value of one Amazon River station (13-3; Figure 22). This station is characterized by a difference between δ^{18}O-NO_3^- and δ^{18}O-H_2O of less than 1.5 mUr, which argues that nitrification is a

dominant pathway there. In the most turbid part of both estuaries, nitrification rates ranged between 39 and 65 mmol m^{-2} d^{-1} (Amazon River) and 4 to 15 mmol m^{-2} d^{-1} (Pará River; Figure 23), a range of nitrification rates about ten times higher than rates observed in the euphotic zone of less turbid regions of the Amazon River plume (Starr et al. 2022; Choisnard et al. 2024). Within a few hours, nitrification could produce NO_3^- to levels comparable to in situ concentrations, further highlighting the significance of this process as an N-source in both estuaries.

Although the $\delta^{18}O\text{-}NO_3^-$ value at station 13-3 is within the range of expectations, all other stations fall outside of this range, and the differences between $\delta^{18}O\text{-}NO_3^-$ and H_2O of more than 4 mUr at stations 12-2 and 14-2 and 9-2 (Figure 22) could suggest that another process counteracts the effect of nitrification on $\delta^{18}O\text{-}NO_3^-$. During NO_3^- assimilation and denitrification, N and O isotopes are closely coupled, leading to an identical enrichment in both ^{15}N- and $^{18}O\text{-}NO_3^-$ (Granger et al. 2004, 2008). Surface waters were close to O_2 saturation (Figure S7), which together with the slim $\delta^{15}N$ enrichment (0.2-1.7 mUr; Figure 20) compared to the strong N and O isotopic discriminations associated with denitrification (Barford et al. 1999; Granger et al. 2008; Kritee et al. 2012) speaks against the occurrence of denitrification in surface waters of our study area. Instead, the enrichment in $\delta^{18}O\text{-}NO_3^-$ relative to $\delta^{18}O\text{-}H_2O$ at higher salinities could arise from the co-occurrence of nitrification and NO_3^- assimilation (Fawcett et al. 2015).

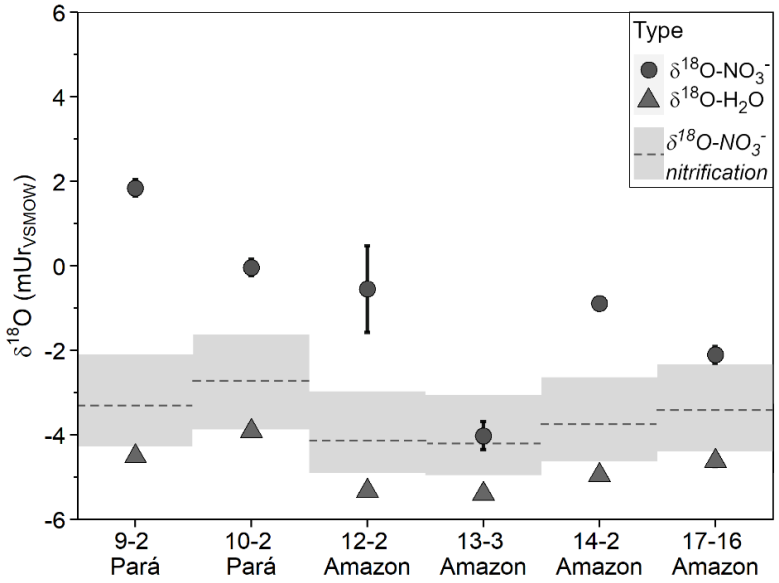

Figure 22. The $\delta^{18}O\text{-}NO_3^-$ values (circle markers) are close to the ambient $\delta^{18}O\text{-}H_2O$ values (triangle markers) at all stations, but only one station is within the range of expected $\delta^{18}O$ values of newly nitrified NO_3^- given by scenario (i) (grey area) and scenario (ii) (grey dashed line) for O atom incorporation during nitrification (see text).

Nitrogen uptake rates

The strong vertical stratification observed in both river mouths (Figure S7) seems to hinder vertical mixing. In combination with the strong North-Eastward currents, the riverine N species, mainly NO_3^- (Figure S7), remain trapped in the upper 10 m of the water column and are likely to be transferred away from the river mouths, to regions where turbidity is reduced, allowing for intense primary and secondary production (Subramaniam et al. 2008; Loick-Wilde et al. 2016).

While at the most turbid stations in the Amazon and Pará river mouths, NH_4^+ uptake by phytoplankton did not exceed 0.60 mmol m^{-2} d^{-1}, it doubled to quadrupled at less turbid stations, and so did NO_3^- and AA uptake rates (Figure 23; Table S3), suggesting that phytoplankton thrives on N species delivered by the rivers when enough light is available. It can thus be expected that the edges of the most turbid part of the estuary host intense primary production supported by NH_4^+ uptake, as rates were up to 22.7 mmol m^{-2} d^{-1} (Figure 23; Table S3), a value in the same range as the one observed in the Chesapeake Bay in spring (Bronk et al. 1998). Since NO_3^- production via nitrification was a dominant process at turbid stations, one could have hypothesized that NO_3^- uptake would be a major N-source used by phytoplankton in clearer waters. However, NO_3^- uptake rates were five times lower than NH_4^+ uptake (Figure 23; Table S3), making NH_4^+ the main N-source for phytoplankton growth at our study sites, as observed in most estuaries (Middelburg and Nieuwenhuize 2001; Voss et al. 2011; Burford et al. 2012). NH_4^+ was detected at all stations. At the light-replete, most saline stations, NH_4^+ concentrations still ranged between 0.32 and 0.95 μM, a range sufficiently high to result in a reduced NO_3^- uptake in favor of NH_4^+ assimilation (Paasche and Kristiansen 1982; Dortch 1990; L'Helguen et al. 1996). Phytoplankton thus favors NH_4^+ and wins the competition for it over nitrifiers when light constraints are lifted (Merbt et al. 2012; Smith et al. 2014; Wan et al. 2018).

Additionally, the presence of low levels of NH_4^+ in surface waters at all stations suggests that even though nitrification rates in the river mouths were high (up to 65.3 mmol m^{-2} d^{-1}, Figure 23; Table S3) they likely did not equal NH_4^+ production pathways (e.g. ammonification), underlining the importance of in situ NH_4^+ production in both estuaries, as observed in the Mississippi River plume (Wawrik et al. 2004). Conversely, since the colossal amount of NO_3^- produced via nitrification is not matched by NO_3^- uptake (Figure 23), this N-form is likely transported along the Amazon River plume, potentially supporting primary

production beyond the limits of the estuary. A decrease in DIN uptake rates could however be expected with distance from the river mouth, as the maximum uptake rates measured here were seventy-four (NO_3^- uptake), eight (AA uptake), and four (NH_4^+ uptake) times higher than the DIN uptake rates measured in the Diatom Diazotrophs Association blooms of the northern Amazon River plume (Carpenter et al. 1999).

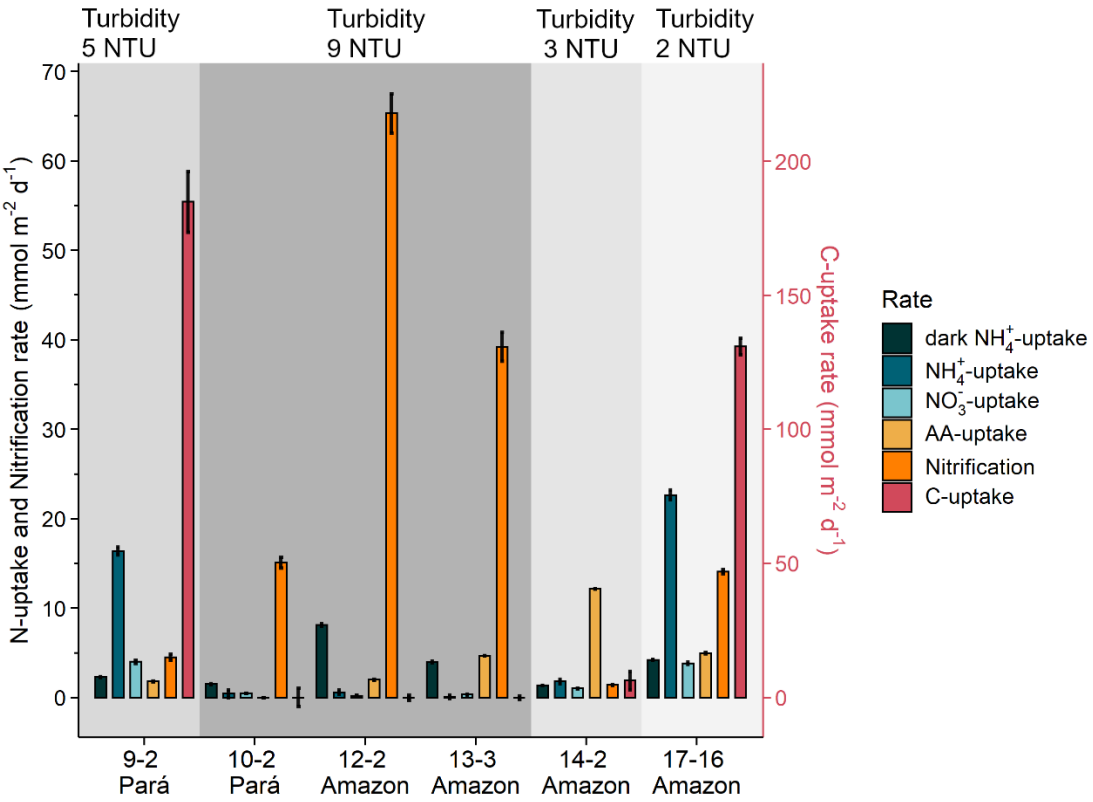

Figure 23. DIN and DIC uptakes, as well as bulk nitrification rates, in mmol m^{-2} d^{-1}, in the Amazon and Pará river mouths. The grey-shaded areas represent the surface turbidity measured at each station (in nephelometric turbidity unit). DIC uptake rates are represented on the right y-axis (in red), while other rates are represented on the left y-axis.

Carbon uptake

Incubation experiments with labeled DIC corroborate the conclusions drawn above, as DIC-uptake rates, nearly zero at the most turbid stations, reached values of up to 180 mmol m^{-2} d^{-1} at less turbid stations, where N-uptake rates were also high (Figure 23; Table S3). These rates were three to five times higher than the ones reported further north, in mesohaline and oceanic regions of the Amazon River plume (Cooley et al. 2007; Subramaniam et al. 2008), although lower than the average productivity of turbid and nutrient-rich waters near the mouth (~230 mmol m^{-2} d^{-1}; (Smith and Demaster 1996). Assuming that the conversion between N uptake and DIC uptake rates can be made according to a C/N ratio of 106/16, we could compare

measured and theoretical DIC uptake rates. In the case of both, stations 9-2 (Pará estuary) and 17-16 (Amazon estuary), measured and theoretical uptake were similar, suggesting that at these stations, the DIN uptake rates measured support all primary production observed. At station 14-2 on the other hand, theoretical DIC uptake rates were twice as high as the measured ones, suggesting that the DIN uptake measured at this station might not be performed by photo- and autotrophs only. This would be in accordance with previous observations of the microbial community composition in the Amazon River mouth and plume, which hinted towards intense microbial activity as well as mixotrophy in this environment (Satinsky et al. 2017; Pinto et al. 2020).

Microbial activity is also highlighted by the dark NH_4^+ uptake rates which were measured at all stations, with depth integrated rates of up to 8.1 mmol m^{-2} d^{-1} in the most turbid part of the Amazon River mouth and comprised between 1.4 and 4.2 mmol m^{-2} d^{-1} at the less turbid stations (Figure 23; Table S3). The Amazon and Pará River mouths thus seem to offer optimal conditions for intense remineralization in light-limited environments, and high uptake and productivity in less turbid habitats. The proportion of nitrification, NH_4^+, NO_3^-, and AA uptake rates therefore determines whether nutrients can be exported away from the estuaries, and subsequently, to what extent these N species could fuel productivity in the Amazon River plume.

Nitrogen balance for the Pará and Amazon River mouths

Nitrification and DIN uptake rates integrated over the euphotic zone (down to 3 or 10 m, Table 1) or the freshwater layer (~ 10 m; Figure S7) and extrapolated over the area of the Pará and Amazon River mouths (Table S5) were combined to draw an improved N-budget of both estuaries (Figure 24). The Amazon and Pará rivers deliver about 3.0 and $0.2x10^8$ mol DIN d^{-1}, respectively (Figure 24), more than 90 % of this DIN being in the form of NO_3^-. This value is in agreement with previous riverine DIN flux estimations from the Amazon River ($2.5x10^8$ mol DIN d^{-1}; (DeMaster and Aller 2001). Near-river mouth processing, or recycling, was thought to be a dominant process with a mass balance to be about $16x10^8$ mol DIN d^{-1} (DeMaster and Aller 2001). Our results agree with this observation, as recycling fluxes via nitrification are one order of magnitude higher than other processes in the most turbid part of the Amazon estuary (Figure 24a). Recycling fluxes measured here are nonetheless lower than the estimate of DeMaster and Aller (2001), ranging between 5.1 and $8.5x10^8$ mol d^{-1} (Figure 24a). However, this difference might simply arise from the higher primary productivity of the

region, as well as the larger study area considered by (DeMaster and Aller 2001) for their calculation. The recycling estimate presented here is also likely underestimating total recycling fluxes, as other mineralization pathways, such as NH_4^+ production via ammonification, were not measured in the present study. This in situ NH_4^+ production is likely supported by the great amount of particulate and dissolved organic nitrogenous compounds delivered by the Amazon River (~1.5 and $2.2x10^8$ mol d^{-1}, respectively; (DeMaster and Aller 2001) and by autochthonous primary production (up to $4.6x10^8$ mol d^{-1}; Figure 24b). Summing up to about $8x10^8$ mol d^{-1}, these N sources could support the nitrification fluxes observed in the Amazon estuary.

As previously highlighted, a shift from a nitrification-dominated to a NH_4^+ assimilation-dominated system is noticeable between the high and low turbidity regions of both river mouths (Figure 23). The obvious preference of phytoplankton for NH_4^+ likely allows the NO_3^- produced in the most turbid area of the estuaries to be transported further along the plume. The sum of all N uptake fluxes in the Amazon estuary (~$3.4x10^8$ mol d^{-1}; Figure 24b) is again much lower than the estimate of DeMaster and Aller (2001) for the extended study region, as turbidity in our study area is likely still too high to allow for maximal primary productivity. By comparing the amount of NO_3^- recycled via NH_4^+ oxidation to the amount of riverine NO_3^- delivered and the NO_3^- demand for phytoplankton growth, assuming that little denitrification is at play in the freshwater layer, we could calculate the potential NO_3^- export from both river mouths. Again, the NO_3^- export from the most turbid part of the Amazon River mouth (8.0-$11.4x10^8$ mol d^{-1}, or 4-6 Tg N y^{-1}; Figure 24a) is much higher than in the Pará River (0.56 $x10^8$ mol d^{-1} or 0.3 Tg N y^{-1}; Figure 24b). With decreasing turbidity, light becomes available but nitrification is still greater than NO_3^- uptake in both river estuaries, resulting in higher NO_3^- export (Figure 24c, d), mainly supported by nitrification.

The Amazon NO_3^- export flux is three to five times higher than that previously given by (DeMaster and Aller 2001). As previously discussed, the total N-uptake associated with primary production in their study ($27x10^8$ mol d^{-1}; (DeMaster and Aller 2001) is also significantly higher than in the present one. But even in regions of the Amazon River plume with maximal productivity, NO_3^- uptake is small (11.3 mmol m^{-2} d^{-1}; Umbricht, personal communication), and most of the productivity is supported by NH_4^+ uptake. Exported to the area of regions of maximal plankton abundance (~$2.8x10^{10}$ m^2; (Smith and Demaster 1996) the maximal biotic NO_3^- demand that could be expected would be of about $3.2x10^8$ mol d^{-1}. The NO_3^- export flux would remain roughly between 6 and $10x10^8$ mol d^{-1}, allowing for NO_3^- export

beyond 5 °N, more than 500 km away from the river mouth. Even taking this maximal NO_3^- uptake into account, the yearly export of NO_3^- could be up to 5 Tg N y^{-1}, almost two times the estimates based on freshwater export and nutrient concentrations (Sharples et al. 2017; Izett and Fennel 2018). These differences likely highlight the limits of the methods used for estimating DIN export rather than inter-annual variability associated with changes in the Amazon River catchment area. Nevertheless, the present study also highlights the strength of remineralization processes, such as nitrification, in increasing the NO_3^- export from the river mouth, advocating for its inclusion in future N-budgets of the region.

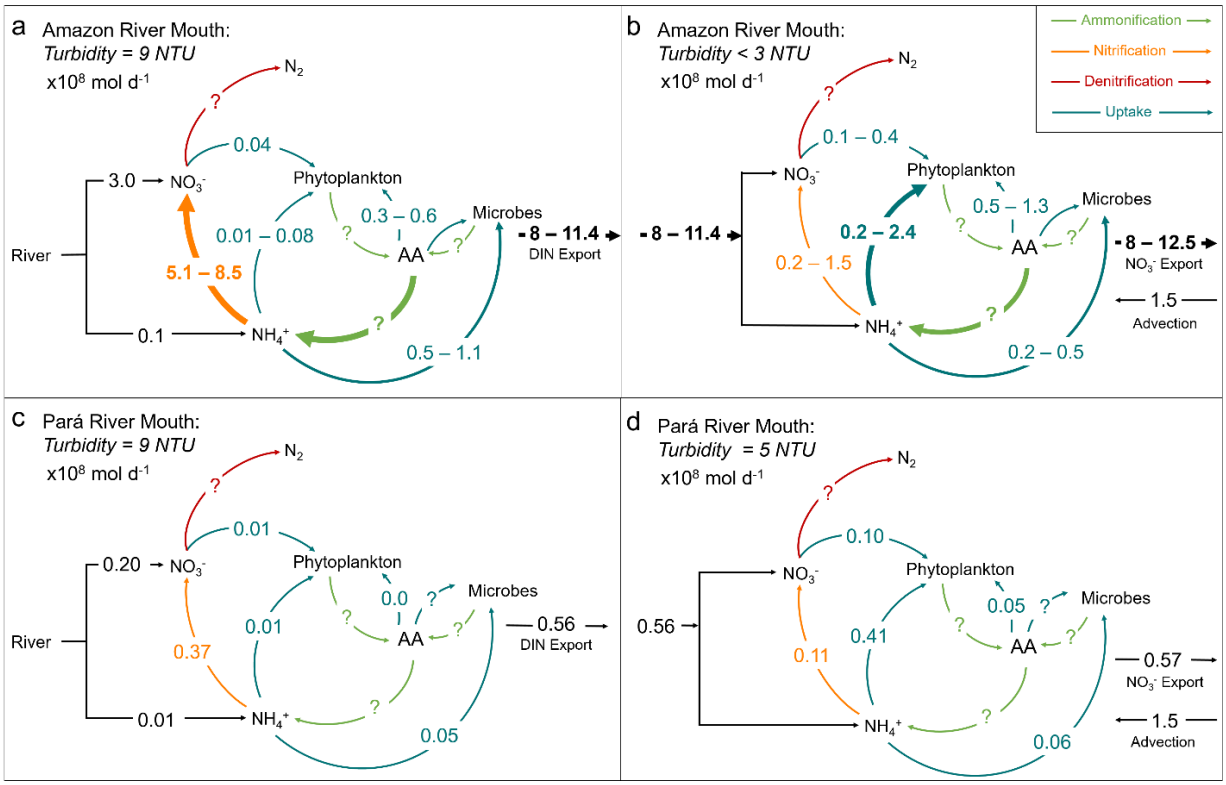

Figure 24. N-budget of the Amazon and Pará river mouths, first in the most turbid area of the Amazon (**a**) and Pará (**c**) rivers, and in the second box defined in Figure 1, where light limitation is eased (**b**, **d**).

Another evident feature of the budgets calculated here is the higher fluxes in the Amazon River mouth relative to the Pará River mouth, by more than a factor of 10 for nitrification, bacterial NH_4^+ assimilation (Figure 24a, c), and phytoplankton NH_4^+ assimilation (Figure 24b, d). Other fluxes were also substantially higher in the Amazon River, highlighting that the characteristics of the Amazon River mouth result in an overall greater reactor compared to the Pará River mouth. These results could underline the differences in both rivers' watersheds, discharge, and subsequently in the amount and type of particles and dissolved material reaching the estuary (Wagner et al. 2015). This difference in river catchment has

already been hypothesized to explain the difference in ice nucleating particle type and concentrations in both river plumes (Einbock et al. 2023). In fact, the Pará River is mainly influenced by the Tocantins River, whose watershed is drier, and more damaged by deforestation than the whole Amazon catchment area (Bullock et al. 2020). However, with the continuous increase of droughts and land use in the Amazon region (Swann et al. 2015; Rodrigues 2023; Clarke et al. 2024), it could be that the future Amazon estuary will be close to today's Pará River mouth, in terms of N cycling and budgets. In this scenario, we could expect reduced productivity in the Amazon River plume, as the N supply via remineralization processes in the estuary could decrease. Accordingly, phytoplankton productivity and the associated carbon export to the deep ocean in less light-limited regions of the river plume via the biological pump could decrease.

Conclusions

Here, we used stable isotope partitioning and N-cycling rate measurements in the Amazon and Pará river mouths to provide an updated budget for N-cycling and export. Our results demonstrated the significance of nitrification as the main source of NO_3^- to regions where light-limitation constraints are eased, and NH_4^+ assimilation becomes the dominant pathway. NO_3^- is likely exported even further from the river mouths, highlighting the potential of the Amazon River as a NO_3^- source to the open ocean. This study provides a snapshot of the N-budget for both estuaries at maximum discharge. As both rivers are characterized by high annual variability in discharge and nutrient concentrations, future studies in the regions will have to address different seasons to complete the annual budget. Nevertheless, the overall decreased reactivity measured in the Pará relative to the Amazon River mouth, in terms of N-cycling rates, likely originates from differences in discharge between the two rivers, reflecting further watershed characteristics. Therefore, the Pará River N-budget potentially provides a glimpse of what the Amazon River N-budget could develop into if deforestation and ongoing climate change-induced droughts increase in the future.

Acknowledgements. We are grateful to the DFG for funding the MeNARP Project (Metabolism of Nitrogen in the Amazon River Plume, project number VO 487/14-1) and the M174 cruise "N-Amazon" (funding GPF19-1-13), and BNP Paribas for funding the NOTION project, all led by principal investigator Maren Voss. We acknowledge the support received from the Brazilian Research Network on Global Climate Change - Rede CLIMA (FINEP-CNPq 437167/2016-0)

and the Brazilian National Institute of Science and Technology for Tropical Marine Environments - INCT AmbTropic (CNPq/FAPESB 565054/2010-4 and 8936/2011). Special thanks go to the Captain and Crew of the R/V Meteor for their support at sea.

Appendices

Table S1. Depths collected and tracer incubation performed at each station. NH_4^+ uptake by phytoplankton and microbes was measured using $^{15}NH_4Cl$ tracer spiked at 10 % of ambient concentration. NO_3^- uptake by phytoplankton was measured similarly, using a $^{15}NaNO_3$ tracer. AA uptake was measured by spiking 50 nM of a labeled custom ^{15}N-AA mixture (Table S2). DIC uptake rates were measured by adding $NaH^{13}CO_3$ to samples in a final concentration of 20 μM, representing < 10 % of estimated in situ DIC concentrations.

Station	Depth (m)	Depths sampled	Depth Ez (m)	Time start incubation (UTC)	$^{15}NH_4Cl$ (μM)	$^{15}NaNO_3$ (μM)	^{15}N-AA (nM)	$NaH^{13}CO_3$ (μM)
9-2	36	2 m	10	2021-04-23 08:15:00	0.095	1.074	0.050	20
9-2	36	10 m	10	2021-04-23 08:15:00	0.006	0.026	0.050	20
10-2	14	1 m	3	2021-04-23 14:50:00	0.052	1.125	0.50	20
12-2	16	2 m	3	2021-04-24 10:40:00	0.122	1.012	0.50	20
13-3	16	2 m	3	2021-04-24 16:15:00	0.043	1.844	0.50	20
14-2	15	2 m	3	2021-04-25 09:30:00	0.032	1.305	0.50	20
17-16	27	2 m	10	2021-04-27 10:20:00	0.036	0.850	0.50	20
17-16	27	11 m	10	2021-04-27 10:40:00	0.041	0.171	0.50	20

Table S2. Composition of the custom ^{15}N, ^{13}C-AA mixture used for AA uptake rates incubations.

Amino Acid	Item Number CIL	Concentration (mg/L)
L-ALANINE (1-^{13}C, 99%; ^{15}N, 98%)	CNLM-6993-PK	1.378
GLYCINE (1-^{13}C, 99%; ^{15}N, 98%+)	CNLM-507-PK	1.676
L-THREONINE (1-^{13}C, 99%, ^{15}N, 98%)	CNLM-7811-0	0.767
L-SERINE (1-^{13}C, 99%; ^{15}N, 98%)	CNLM-7814-0.25	1.162
L-VALINE (1-^{13}C, 99%; ^{15}N, 98%)	CNLM-3466-PK	0.536
L-LEUCINE (1-^{13}C, 99%; ^{15}N, 98%+)	CNLM-615-PK	0.516
L-ISOLEUCINE (1-^{13}C, 99%; ^{15}N, 98%)	CNLM-7810-PK	0.366
L-PROLINE (1-^{13}C, 99%; ^{15}N, 98%)	CNLM-7822-PK	0.586
L-ASPARTIC ACID (1,4-$^{13}C_2$, 99%; ^{15}N, 98%)	CNLM-7817-PK	1.497
L-METHIONINE (1-^{13}C, 99%; ^{15}N, 98%)	CNLM-7807-PK	0.227
L-GLUTAMIC ACID (1-^{13}C, 99%; ^{15}N, 98%)	CNLM-7812-PK	1.398

Text S2. Detail of rates calculations.

To calculate rates, we first transformed δ values, to atom % and atom % excess. Nitrate uptake rates were then calculated after (Dugdale and Wilkerson 1986):

$$V_N\,(t) = \frac{{}^{15}N_{xs,\ sample}}{\left({}^{15}N_{xs,\ pool} - F\right) \times \mathrm{t}} \qquad (11)$$

Where V_N (t) is the specific uptake rate (N taken up per unit particulate N per unit time), $^{15}N_{xs}$, sample is the atom% excess in the sample ($^{15}N_{xs,\ sample} = {}^{15}N_s - F$ with $^{15}N_s$ being the atom% ^{15}N in the sample), $^{15}N_{xs,\ pool}$ is the atom% ^{15}N in the initially labeled fraction, F is the natural abundance of ^{15}N and t is the incubation time. Rates were calculated assuming a nitrate concentration of 0.001 μM when nitrate concentrations were below the detection limit.

The volumetric rate ρN(t) (N uptake in concentration units) was then calculated using V(t) and the δ values of particulate organic nitrogen (PON) at the end of the incubation (PON (t)):

$$\rho_N\,(t) = V(t) \times PON\,(t) \qquad (12)$$

Calculation of carbon uptake rates is the same as that of nitrate uptake as follows (Collos 1987):

$$V_C\,(t) = \frac{(^{13}C_{final} - {}^{13}C_{initial})}{\left(DIC - {}^{13}C_{initial}\right) \times t} \quad (13)$$

V_C is the specific uptake rate (C uptake per unit particulate C per unit time), $^{13}C_{final}$ is the concentration of ^{13}C in atom% in the sample after incubation, $^{13}C_{initial}$ is the concentration of ^{13}C in atom% at the beginning of the incubation, hence the natural abundance of ^{13}C in the sample, DIC – ^{13}Cinitial is the concentration of ^{13}C in the dissolved phase, and t is the incubation time.

Nitrification rates depend on the amount of tracer added, the size of the nitrite+ nitrate pool (NO_2^-+ NO_3^- pool, or NOx), and the excess ^{15}N-NOx measured during the incubation time (ΔT) and were calculated as follows (Damashek et al. 2016):

$$NR\ (nmol\ L^{-1}h^{-1}) = \frac{\left[{}^{15}N_{NOx}\right] \times \frac{[NH_4^+]_{total}}{\left[{}^{15}NH_4^+\right]_{added}}}{\Delta T} \quad (14)$$

Where ^{15}N-NOx is the difference in ^{15}N-content (AP, in atom%) of the end (TF) and the beginning (T0) samples:

$$\left[{}^{15}N_{NOx}\right] = \frac{AP_{{}^{15}N_{NOx_{TF}}} - AP_{{}^{15}N_{NOx_{T0}}}}{100} \times [NO_3^- + NO_2^-] \quad (15)$$

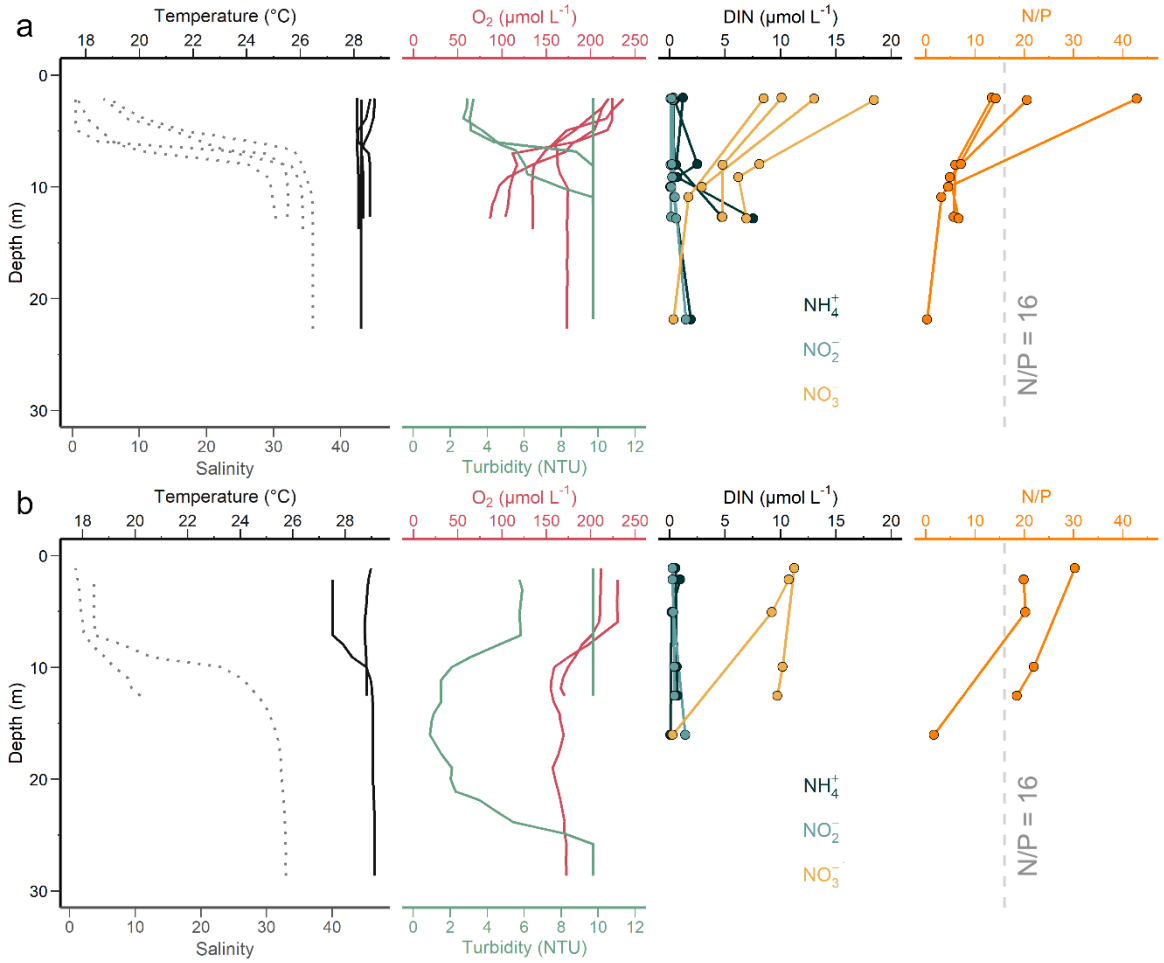

Figure S7. Environmental variables in (**a**) the Amazon River Mouth and (**b**) the Pará River Mouth. Salinity (grey dotted line) is shown on the bottom axis on the Temperature plot (black line). Oxygen concentrations (red) and turbidity (green) vary with depth. The DIN concentrations panel shows NO_3^- (yellow), NO_2^- (light blue), and NH_4^+ concentrations (dark blue), and N/P ratios are shown in orange. The grey dashed-line highlights the Redfield N/P ratio.

Text S3. Estimating $\delta^{18}O\text{-}NO_3^-$ values of nitrified NO_3^-.

Nitrified $\delta^{18}O\text{-}NO_3^-$ values depend on the $\delta^{18}O$- values of ambient water ($\delta^{18}O\text{-}H_2O$) and dissolved oxygen ($\delta^{18}O\text{-}O_2$). During ammonia oxidation, the first step of nitrification, O atoms are incorporated from H_2O and dissolved oxygen with a kinetic isotope fractionation ($^{18}\varepsilon k\text{-}H_2O$, 1 and $^{18}\varepsilon k\text{-}O_2$). During NO_2^- oxidation, the second step of nitrification, O atoms are incorporated from ambient H_2O with the kinetic isotope fractionation $^{18}\varepsilon k\text{-}H_2O$, 2. Nitrified $\delta^{18}O\text{-}NO_3^-$ values also depend on the fraction of NO_2^- oxygen atoms exchanged with H_2O during ammonia oxidation (x_{AO}) and the associated equilibrium isotope effect ($^{18}\varepsilon_{eq}$). The resulting calculation can be written as follows (Casciotti et al. 2010; Buchwald et al. 2012):

$$\delta^{18}O_{NO_3^-} = \left(\frac{2}{3} + \frac{1}{3}x_{AO}\right)\delta^{18}O_{H_2O} + \frac{1}{3}\left[\left(\delta^{18}O_{O_2} - {}^{18}\varepsilon_{k,O_2} - {}^{18}\varepsilon_{k,H_2O,1}\right)(1 - x_{AO}) - {}^{18}\varepsilon_{k,H_2O,2}\right] + \frac{2}{3}{}^{18}\varepsilon_{eq}x_{AO} \quad (16)$$

With $^{18}\varepsilon_{eq}$ calculated from in situ temperature (in Kelvin) according to (Buchwald and Casciotti 2013):

$${}^{18}\varepsilon_{eq} = -0.12T + 48.79 \quad (17)$$

Culture studies have reported that (^{18}εk-O_2 + ^{18}εk-H_2O, 1) ranges between 17.9 and 37.6 mUr (Casciotti et al. 2010), while ^{18}εk-H_2O, 2 ranged between 12.8 and 18.2 mUr (Buchwald and Casciotti 2010). We assumed that ammonia was fully oxidized to NO_3^- as less than 0.3 μM of NO_2^- was measured at our study sites, and that the exchange of oxygen isotope between NO_2^- and H_2O during ammonia oxidation (x_{AO}) ranged between 0.22 and 1, as observed in field experiments (Buchwald et al. 2012). This calculation gave us a range of possible nitrified δ^{18}O-NO_3^- values between -5.0 and -1.6 mUr.

Table S3. Volumetric and depth-integrated uptake rates measured at our study sites. The incubation type refers to dark or in situ light incubation for nitrification rates.

Station	Depth (m)	Depth Ez (m)	Incubation type	System	Nitrification (nM h^{-1})	SD	NO_3^- uptake (nM h^{-1})	SD	NH_4^+ uptake (nM h^{-1})	SD	AA uptake (nM h^{-1})	SD	DIC uptake (µM h-1)	SD	microb. NH_4^+ uptake (nM h^{-1})	SD
M174_9-2	2	10	dark	Pará	37	13.8									31.7	2.8
M174_9-2	2	10	light	Pará	17	5.6	27.6	13.6	112.8	35.3	4	1.7	1.7	0.9		
M174_9-2	10	10	dark	Pará	5.2	1.8	19.5	1.5	80.1	3.8	13.1	2.6	0.7	0	3.3	0.9
M174_10-2	2	3	dark	Pará	40.8	11.7									21	6.3
M174_10-2	2	3	light	Pará	0	14.2	13.1	1.6	66.2	34.7	0	0	0	0.3		
M174_10-2	10	3	dark	Pará												
M174_12-2	2	3	dark	Amazon	191.1	52.7									112.8	11.1
M174_12-2	2	3	light	Amazon	132.5	5.1	5.8	2.2	40.9	18.6	16.3	6.8	0	0.1		
M174_12-2	10	3	dark	Amazon												
M174_13-3	2	3	dark	Amazon	113.5	16.5									55	7.2
M174_13-3	2	3	light	Amazon	85.9	61.1	9.1	3.1	14.2	16.2	21.1	1.8	0	0		
M174_13-3	10	3	dark	Amazon												
M174_14-2	2	3	dark	Amazon	4.6	1.3									18.9	1.2
M174_14-2	2	3	light	Amazon	0.6	0.2	27.8	3.1	463	21.8	77.6	1.7	1.9	0.3		
M174_14-2	10	3	dark	Amazon												
M174_17-16	2	10	dark	Amazon	4.1	1.5									50.1	2.4
M174_17-16	2	10	light	Amazon	0.3	0.3	58.2	10	337.6	48.1	51.2	5.8	2.2	0.3		
M174_17-16	11	10	dark	Amazon	57.6	7.7	2.7	0.7	19.9	1.3	15.7	1.4	0	0.1	9.8	3.3

					Nitrification (mmol m^{-2} d^{-1})	SD	NO_3^- uptake (mmol m^{-2} d^{-1})	SD	NH_4^+ uptake (mmol m^{-2} d^{-1})	SD	AA uptake (mmol m^{-2} d^{-1})	SD	DIC uptake (mmol m^{-2} d^{-1})	SD	microb. NH_4^+ uptake (mmol m^{-2} d^{-1})	SD
M174_9-2	Integrated	10		Pará	4.5	0.4	4	0.2	16.4	0.4	1.8	0	184.7	11	2.3	0
M174_10-2	Integrated	3		Pará	12.2	0.6	0.5	0	0.4	0.4	0	0	0	3.4	1.5	0.1
M174_12-2	Integrated	3		Amazon	65.3	2.2	0.2	0	0.6	0.2	2	0.1	0	1	8.1	0.1
M174_13-3	Integrated	3		Amazon	39.2	1.6	0.3	0	0.1	0.2	4.7	0	0	0.6	4	0.1
M174_14-2	Integrated	3		Amazon	1.4	0.1	1	0	1.8	0.3	12.2	0	6.4	3.4	1.4	0
M174_17-16	Integrated	10		Amazon	14.1	0.3	3.8	0.1	22.7	0.6	5	0.1	130.9	3.1	4.2	0

Table S4. Isotopic composition of ambient NO_3^- and H_2O at each station.

Station	Depth (m)	T (°C)	S	NO_3^- (μM)	SD NO_3^-	$\delta^{15}N$-NO_3^- (mUr)	SD $\delta^{15}N$-NO_3^-	$\delta^{18}O$-NO_3^- (mUr)	SD $\delta^{18}O$-NO_3^-	$\delta^{18}O$-H_2O (mUr)	SD $\delta^{18}O$-H_2O
17-16	3.191	28.9	8.3	9.00	0.01	4.1	0.2	-2.1	0.2	-4.62	0.13
14-2	2.106	28.6	4.6	12.30	0.78	5.1	0.1	-0.9	0.1	-4.95	0.03
13-3	2.225	28.3	0.9	19.70	1.72	3.4	0.2	-4.0	0.3	-5.40	0.04
12-2	2.018	28.1	0.5	8.20	0.29	3.6	0.2	-0.6	1.0	-5.33	0.07
10-2	1.101	28.9	0.9	9.70	0.01	4.0	0.2	0.0	0.2	-3.91	0.01
9-2	2.145	27.5	3.8	12.10	0.01	3.7	0.2	1.8	0.2	-4.50	0.04

Table S5. Values used for Amazon Shelf budget calculations. The area of the two river mouths was arbitrarily defined as the area between the two sampling points for the Pará River, and the area between the 10 m isobaths and the most turbid station for the Amazon River mouth (see Figure 18).

Data used in calculations	Value	Reference
Amazon riverine discharge	1.6×10^{13} L d^{-1}	(Nittrouer and DeMaster 1996)
Pará riverine discharge	1.8×10^{12} L d^{-2}	(Prestes et al. 2020)
Area of Amazon River mouth	3×10^{10} m^2	This study
Area of Pará River mouth	4×10^{9} m^2	This study
Riverine water layer	10 m	This study
NH_4^+ (Amazon)	0.9 μM	This study
NH_4^+ (Pará)	0.3 μM	This study
NO_2^- (Amazon)	0.3 μM	This study
NO_2^- (Pará)	0.1 μM	This study
NO_3^- (Amazon)	18.4 μM	This study
NO_3^- (Pará)	8.5 μM	This study

References

Andersson, K. K., and A. B. Hooper. 1983. O_2 and H_2O are each the source of one O in NO_2^- produced from NH_3 by *Nitrosomonas*: ^{15}N-NMR evidence. FEBS Letters **164**: 236–240. doi:10.1016/0014-5793(83)80292-0

Aquino, R., C. Noriega, A. Mascarenhas, and others. 2022. Possible Amazonian contribution to *Sargassum* enhancement on the Amazon Continental Shelf. Science of the Total Environment **853**: 158432. doi:10.1016/j.scitotenv.2022.158432

Araujo, M., C. Noriega, G. A. Hounsou-gbo, and others. 2017. A synoptic assessment of the Amazon River-ocean *continuum* during Boreal Autumn: From physics to plankton communities and carbon flux. Frontiers in Microbiology **8**.

Araujo, M., C. Noriega, and N. Lefèvre. 2014. Nutrients and carbon fluxes in the estuaries of major rivers flowing into the tropical Atlantic. Frontiers in Marine Science **1**.

Archana, A., B. Thibodeau, N. Geeraert, M. N. Xu, S.-J. Kao, and D. M. Baker. 2018. Nitrogen sources and cycling revealed by dual isotopes of nitrate in a complex urbanized environment. Water Research **142**: 459–470. doi:10.1016/j.watres.2018.06.004

Barford, C. C., J. P. Montoya, M. A. Altabet, and R. Mitchell. 1999. Steady-state nitrogen isotope effects of N_2 and N_2O production in *Paracoccus denitrificans*. Applied and Environmental Microbiology **65**: 989–994. doi:10.1128/AEM.65.3.989-994.1999

Barkan, E., and B. Luz. 2005. High precision measurements of $^{17}O/^{16}O$ and $^{18}O/^{16}O$ ratios in H_2O. Rapid Communications in Mass Spectrometry **19**: 3737–3742. doi:10.1002/rcm.2250

Bianchi, M., Feliatra, and D. Lefevre. 1999. Regulation of nitrification in the land-ocean contact area of the Rhône River plume (NW Mediterranean). Aquat. Microb. Ecol. **18**: 301–312. doi:10.3354/ame018301

Böttcher, M. E., and I. Schmiedinger. 2021. The impact of temperature on the water isotope ($^2H/^1H$, $^{17}O/^{16}O$, $^{18}O/^{16}O$) fractionation upon transport through a low-density polyethylene membrane. Isotopes in Environmental and Health Studies **57**: 183–192. doi:10.1080/10256016.2020.1845668

Brand, W. A., and T. B. Coplen. 2012. Stable isotope deltas: Tiny, yet robust signatures in nature. Isotopes in Environmental and Health Studies **48**: 393–409. doi:10.1080/10256016.2012.666977

Brandes, J. A., and A. H. Devol. 2002. A global marine-fixed nitrogen isotopic budget: Implications for Holocene nitrogen cycling. Global Biogeochemical Cycles **16**: 67-1-67–14. doi:10.1029/2001GB001856

Bronk, D. A., P. M. Glibert, T. C. Malone, S. Banahan, and E. Sahlsten. 1998. Inorganic and organic nitrogen cycling in Chesapeake Bay: Autotrophic versus heterotrophic processes and relationships to carbon flux. Aquatic Microbial Ecology **15**: 177–189. doi:10.3354/ame015177

Buchwald, C., and K. L. Casciotti. 2010. Oxygen isotopic fractionation and exchange during bacterial nitrite oxidation. Limnology and Oceanography **55**: 1064–1074. doi:10.4319/lo.2010.55.3.1064

Buchwald, C., and K. L. Casciotti. 2013. Isotopic ratios of nitrite as tracers of the sources and age of oceanic nitrite. Nature Geosci **6**: 308–313. doi:10.1038/ngeo1745

Buchwald, C., A. E. Santoro, M. R. McIlvin, and K. L. Casciotti. 2012. Oxygen isotopic composition of nitrate and nitrite produced by nitrifying cocultures and natural marine assemblages. Limnol. Oceanogr. **57**: 1361–1375. doi:10.4319/lo.2012.57.5.1361

Bullock, E. L., C. E. Woodcock, C. Souza Jr., and P. Olofsson. 2020. Satellite-based estimates reveal widespread forest degradation in the Amazon. Global Change Biology **26**: 2956–2969. doi:10.1111/gcb.15029

Burford, M. A., I. T. Webster, A. T. Revill, R. A. Kenyon, M. Whittle, and G. Curwen. 2012. Controls on phytoplankton productivity in a wet–dry tropical estuary. Estuarine, Coastal and Shelf Science **113**: 141–151. doi:10.1016/j.ecss.2012.07.017

Cabral, A., M. V. Bercovich, and A. Fonseca. 2019. Implications of poor-regulated wastewater treatment systems in the water quality and nutrient fluxes of a subtropical coastal lagoon. Regional Studies in Marine Science **29**: 100672. doi:10.1016/j.rsma.2019.100672

Carpenter, E., J. Montoya, J. Burns, M. Mulholland, A. Subramaniam, and D. Capone. 1999. Extensive bloom of a N_2-fixing diatom/cyanobacterial association in the tropical Atlantic Ocean. Mar. Ecol. Prog. Ser. **185**: 273–283. doi:10.3354/meps185273

Casciotti, K. L., M. McIlvin, and C. Buchwald. 2010. Oxygen isotopic exchange and fractionation during bacterial ammonia oxidation. Limnology and Oceanography **55**: 753–762. doi:10.4319/lo.2010.55.2.0753

Casciotti, K. L., D. M. Sigman, M. G. Hastings, J. K. Böhlke, and A. Hilkert. 2002. Measurement of the oxygen isotopic composition of nitrate in seawater and freshwater using the denitrifier method. Anal. Chem. **74**: 4905–4912. doi:10.1021/ac020113w

Choisnard, N., T. Sperlea, I. Liskow, and M. Voss. 2024. Nitrification in the Amazon River plume. Mar. Ecol. Prog. Ser. doi:10.3354/meps14530

Clarke, B., C. Barnes, R. Rodrigues, and others. 2024. Climate change, not El Niño, main driver of exceptional drought in highly vulnerable Amazon River Basin.

Collos, Y. 1987. Calculations of ^{15}N uptake rates by phytoplankton assimilating one or several nitrogen sources. International Journal of Radiation Applications and Instrumentation. Part A. Applied Radiation and Isotopes **38**: 275–282. doi:10.1016/0883-2889(87)90038-4

Cooley, S. R., V. J. Coles, A. Subramaniam, and P. L. Yager. 2007. Seasonal variations in the Amazon plume-related atmospheric carbon sink. Global Biogeochemical Cycles **21**. doi:10.1029/2006GB002831

Cooper, S. R., and G. S. Brush. 1991. Long-term history of Chesapeake Bay anoxia. Science **254**: 992–996. doi:10.1126/science.254.5034.992

Dähnke, K., E. Bahlmann, and K. Emeis. 2008. A nitrate sink in estuaries? An assessment by means of stable nitrate isotopes in the Elbe estuary. Limnology and Oceanography **53**: 1504–1511. doi:10.4319/lo.2008.53.4.1504

Damashek, J., K. L. Casciotti, and C. A. Francis. 2016. Variable nitrification rates across environmental gradients in turbid, nutrient-rich estuary waters of San Francisco Bay. Estuaries and Coasts **39**: 1050–1071. doi:10.1007/s12237-016-0071-7

DeMaster, D. J., and R. C. Aller. 2001. Biogeochemical processes on the Amazon shelf: Changes in dissolved and particulate fluxes during river/ocean mixing. The Biogeochemistry of the Amazon Basin 328–357.

Demaster, D. J., and R. H. Pope. 1996. Nutrient dynamics in Amazon shelf waters: Results from AMASSEDS. Continental Shelf Research **16**: 263–289. doi:10.1016/0278-4343(95)00008-O

Dham, V. V., A. M. Heredia, S. Wafar, and M. Wafar. 2002. Seasonal variations in uptake and in situ regeneration of nitrogen in mangrove waters. Limnol. Oceanogr. **47**: 241–254. doi:10.4319/lo.2002.47.1.0241

Dortch, Q. 1990. The interaction between ammonium and nitrate uptake in phytoplankton. Mar. Ecol. Prog. Ser. **61**: 183–201. doi:10.3354/meps061183

Drake, T. W., J. D. Hemingway, M. R. Kurek, and others. 2021. The pulse of the Amazon: Fluxes of dissolved organic carbon, nutrients, and ions from the world's largest river. Global Biogeochemical Cycles **35**: e2020GB006895. doi:10.1029/2020GB006895

Dugdale, R. C., and J. J. Goering. 1967. Uptake of new and regenerated forms of nitrogen in primary productivity. Limnol. Oceanogr. **12**: 196–206. doi:10.4319/lo.1967.12.2.0196

Dugdale, R. C., and F. P. Wilkerson. 1986. The use of ^{15}N to measure nitrogen uptake in eutrophic oceans; experimental considerations. Limnology and Oceanography **31**: 673–689. doi:10.4319/lo.1986.31.4.0673

Einbock, A., E. Burtscher, C. Frey, and F. Conen. 2023. Export of ice-nucleating particles from watersheds: results from the Amazon and Tocantins river plumes. Royal Society Open Science **10**: 220878. doi:10.1098/rsos.220878

Fawcett, S. E., B. B. Ward, M. W. Lomas, and D. M. Sigman. 2015. Vertical decoupling of nitrate assimilation and nitrification in the Sargasso Sea. Deep Sea Research Part I: Oceanographic Research Papers **103**: 64–72. doi:10.1016/j.dsr.2015.05.004

Fripiat, F., A. Martínez-García, D. Marconi, and others. 2021. Nitrogen isotopic constraints on nutrient transport to the upper ocean. Nat. Geosci. **14**: 855–861. doi:10.1038/s41561-021-00836-8

Galloway, J. N., R. W. Howarth, A. F. Michaels, S. W. Nixon, J. M. Prospero, and F. J. Dentener. 1996. Nitrogen and phosphorus budgets of the North Atlantic Ocean and its watershed, p. 3–25. *In* R.W. Howarth [ed.], Nitrogen Cycling in the North Atlantic Ocean and its Watersheds. Springer Netherlands.

Glibert, P. M., F. P. Wilkerson, R. C. Dugdale, A. E. Parker, J. Alexander, S. Blaser, and S. Murasko. 2014. Phytoplankton communities from San Francisco Bay Delta respond differently to oxidized and reduced nitrogen substrates—even under conditions that would otherwise suggest nitrogen sufficiency. Frontiers in Marine Science **1**.

Gomes, H. do R., Q. Xu, J. Ishizaka, E. J. Carpenter, P. L. Yager, and J. I. Goes. 2018. The influence of riverine nutrients in niche partitioning of phytoplankton communities – A contrast between the Amazon River Plume and the Changjiang (Yangtze) River diluted water of the East China Sea. Frontiers in Marine Science **5**.

Granger, J., M. G. Prokopenko, C. W. Mordy, and D. M. Sigman. 2013. The proportion of remineralized nitrate on the ice-covered eastern Bering Sea shelf evidenced from the oxygen isotope ratio of nitrate. Global Biogeochemical Cycles **27**: 962–971. doi:10.1002/gbc.20075

Granger, J., and D. M. Sigman. 2009. Removal of nitrite with sulfamic acid for nitrate N and O isotope analysis with the denitrifier method. Rapid Commun. Mass Spectrom. **23**: 3753–3762. doi:10.1002/rcm.4307

Granger, J., D. M. Sigman, M. F. Lehmann, and P. D. Tortell. 2008. Nitrogen and oxygen isotope fractionation during dissimilatory nitrate reduction by denitrifying bacteria. Limnology and Oceanography **53**: 2533–2545.

Granger, J., D. M. Sigman, J. A. Needoba, and P. J. Harrison. 2004. Coupled nitrogen and oxygen isotope fractionation of nitrate during assimilation by cultures of marine phytoplankton. Limnol. Oceanogr. **49**: 1763–1773. doi:10.4319/lo.2004.49.5.1763

Grasshoff, K., K. Kremling, and M. Ehrhardt. 1999. Methods of seawater analysis, John Wiley & Sons.

Hsiao, S. S.-Y., T.-C. Hsu, J. -w Liu, and others. 2014. Nitrification and its oxygen consumption along the turbid Chang Jiang River plume. Biogeosciences **11**: 2083–2098. doi:10.5194/bg-11-2083-2014

Izett, J. G., and K. Fennel. 2018. Estimating the cross-shelf export of riverine materials: Part 2. Estimates of global freshwater and nutrient export. Global Biogeochemical Cycles **32**: 176–186. doi:10.1002/2017GB005668

Jickells, T. D. 1998. Nutrient biogeochemistry of the coastal zone. Science **281**: 217–222. doi:10.1126/science.281.5374.217

Kendall, C. 1998. Chapter 16 - Tracing nitrogen sources and cycling in catchments, p. 519–576. *In* C. Kendall and J.J. McDonnell [eds.], Isotope Tracers in Catchment Hydrology. Elsevier.

Kendall, C., M. B. Young, and S. R. Silva. 2010. Applications of stable isotopes for regional to national-scale water quality and environmental monitoring programs, p. 89–111. *In* J.B. West, G.J. Bowen, T.E. Dawson, and K.P. Tu [eds.], Isoscapes. Springer Netherlands.

Kirk, J. T. O. 1994. Light and photosynthesis in aquatic ecosystems, Cambridge University Press.

Kritee, K., D. M. Sigman, J. Granger, B. B. Ward, A. Jayakumar, and C. Deutsch. 2012. Reduced isotope fractionation by denitrification under conditions relevant to the ocean. Geochimica et Cosmochimica Acta **92**: 243–259. doi:10.1016/j.gca.2012.05.020

Kroopnick, P., and H. Craig. 1972. Atmospheric oxygen: Isotopic composition and solubility fractionation. Science **175**: 54–55. doi:10.1126/science.175.4017.54

Kumar, S., D. J. D. Nicholas, and E. H. Williams. 1983. Definitive ^{15}N NMR evidence that water serves as a source of 'O' during nitrite oxidation by *Nitrobacter agilis*. FEBS Letters **152**: 71–74. doi:10.1016/0014-5793(83)80484-0

Lapointe, B. E., R. A. Brewton, L. W. Herren, and others. 2021. Nutrient content and stoichiometry of pelagic Sargassum reflects increasing nitrogen availability in the Atlantic Basin. Nat Commun **12**: 3060. doi:10.1038/s41467-021-23135-7

Latrubesse, E. M., E. Y. Arima, T. Dunne, and others. 2017. Damming the rivers of the Amazon basin. Nature **546**: 363–369. doi:10.1038/nature22333

Lefcheck, J. S., R. J. Orth, W. C. Dennison, and others. 2018. Long-term nutrient reductions lead to the unprecedented recovery of a temperate coastal region. Proceedings of the National Academy of Sciences **115**: 3658–3662. doi:10.1073/pnas.1715798115

L'Helguen, S., C. Madec, and P. Le Corre. 1996. Nitrogen uptake in permanently well-mixed temperate coastal waters. Estuarine, Coastal and Shelf Science **42**: 803–818. doi:10.1006/ecss.1996.0051

Loick-Wilde, N., S. C. Weber, B. J. Conroy, D. G. Capone, V. J. Coles, P. M. Medeiros, D. K. Steinberg, and J. P. Montoya. 2016. Nitrogen sources and net growth efficiency of zooplankton in three Amazon River plume food webs. Limnology and Oceanography **61**: 460–481. doi:10.1002/lno.10227

Marconi, D., M. A. Weigand, and D. M. Sigman. 2019. Nitrate isotopic gradients in the North Atlantic Ocean and the nitrogen isotopic composition of sinking organic matter. Deep Sea Research Part I: Oceanographic Research Papers **145**: 109–124. doi:10.1016/j.dsr.2019.01.010

Martinelli, L. A., R. Naylor, P. M. Vitousek, and P. Moutinho. 2010. Agriculture in Brazil: Impacts, costs, and opportunities for a sustainable future. Current Opinion in Environmental Sustainability **2**: 431–438. doi:10.1016/j.cosust.2010.09.008

Merbt, S. N., D. A. Stahl, E. O. Casamayor, E. Martí, G. W. Nicol, and J. I. Prosser. 2012. Differential photoinhibition of bacterial and archaeal ammonia oxidation. FEMS Microbiology Letters **327**: 41–46. doi:10.1111/j.1574-6968.2011.02457.x

Middelburg, J. J., and J. Nieuwenhuize. 2001. Nitrogen isotope tracing of dissolved inorganic nitrogen behaviour in tidal estuaries. Estuarine, Coastal and Shelf Science **53**: 385–391. doi:10.1006/ecss.2001.0805

Nittrouer, C. A., and D. J. DeMaster. 1996. The Amazon shelf setting: Tropical, energetic, and influenced by a large river. Continental Shelf Research **16**: 553–573. doi:10.1016/0278-4343(95)00069-0

Nixon, S. W. 1995. Coastal marine eutrophication: A definition, social causes, and future concerns. Ophelia **41**: 199–219. doi:10.1080/00785236.1995.10422044

Nixon, S. W., J. W. Ammerman, L. P. Atkinson, and others. 1996. The fate of nitrogen and phosphorus at the land-sea margin of the North Atlantic Ocean. Biogeochemistry **35**: 141–180. doi:10.1007/BF02179826

Ometto, J. P., A. P. D. Aguiar, and L. A. Martinelli. 2011. Amazon deforestation in Brazil: Effects, drivers and challenges. Carbon Management **2**: 575–585. doi:10.4155/cmt.11.48

Paasche, E., and S. Kristiansen. 1982. Nitrogen nutrition of the phytoplankton in the Oslofjord. Estuarine, Coastal and Shelf Science **14**: 237–249. doi:10.1016/S0302-3524(82)80014-5

Paerl, H. W., N. S. Hall, B. L. Peierls, and K. L. Rossignol. 2014. Evolving paradigms and challenges in estuarine and coastal eutrophication dynamics in a culturally and climatically stressed world. Estuaries and Coasts **37**: 243–258. doi:10.1007/s12237-014-9773-x

Park, E., and E. M. Latrubesse. 2015. Surface water types and sediment distribution patterns at the confluence of mega rivers: The Solimões-Amazon and Negro Rivers junction. Water Resources Research **51**: 6197–6213. doi:10.1002/2014WR016757

Pinto, O. H. B., T. F. Silva, C. S. Vizzotto, R. H. Santana, F. A. C. Lopes, B. S. Silva, F. L. Thompson, and R. H. Kruger. 2020. Genome-resolved metagenomics analysis provides insights into the ecological role of Thaumarchaeota in the Amazon River and its plume. BMC Microbiol **20**: 13. doi:10.1186/s12866-020-1698-x

Prestes, Y. O., T. A. da C. Borba, A. C. da Silva, and M. Rollnic. 2020. A discharge stationary model for the Pará-Amazon estuarine system. Journal of Hydrology: Regional Studies **28**: 100668. doi:10.1016/j.ejrh.2020.100668

Reis, C. R. G., G. B. Nardoto, and R. S. Oliveira. 2017. Global overview on nitrogen dynamics in mangroves and consequences of increasing nitrogen availability for these systems. Plant Soil **410**: 1–19. doi:10.1007/s11104-016-3123-7

Riemann, B., J. Carstensen, K. Dahl, and others. 2016. Recovery of danish coastal ecosystems after reductions in nutrient loading: A holistic ecosystem approach. Estuaries and Coasts **39**: 82–97. doi:10.1007/s12237-015-9980-0

Rodrigues, M. 2023. The Amazon's record-setting drought: How bad will it be? Nature **623**: 675–676. doi:10.1038/d41586-023-03469-6

Rosenberg, R., R. Elmgren, S. Fleischer, P. Jonsson, G. Persson, and H. Dahlin. 1990. Marine eutrophication case studies in Sweden. Ambio **19**: 102–108.

Santoro, A. E., K. L. Casciotti, and C. A. Francis. 2010. Activity, abundance and diversity of nitrifying archaea and bacteria in the central California Current. Environmental Microbiology **12**: 1989–2006. doi:10.1111/j.1462-2920.2010.02205.x

Santoro, A. E., C. M. Sakamoto, J. M. Smith, and others. 2013. Measurements of nitrite production in and around the primary nitrite maximum in the central California Current. Biogeosciences **10**: 7395–7410. doi:10.5194/bg-10-7395-2013

Satinsky, B. M., C. B. Smith, S. Sharma, and others. 2017. Expression patterns of elemental cycling genes in the Amazon River Plume. ISME J **11**: 1852–1864. doi:10.1038/ismej.2017.46

Seitzinger, S. P., E. Mayorga, A. F. Bouwman, and others. 2010. Global river nutrient export: A scenario analysis of past and future trends. Global Biogeochemical Cycles **24**. doi:10.1029/2009GB003587

Sharples, J., J. J. Middelburg, K. Fennel, and T. D. Jickells. 2017. What proportion of riverine nutrients reaches the open ocean? Global Biogeochem. Cycles **31**: 39–58. doi:10.1002/2016GB005483

Sigman, D. M., K. L. Casciotti, M. Andreani, C. Barford, M. Galanter, and J. K. Böhlke. 2001. A bacterial method for the nitrogen isotopic analysis of nitrate in seawater and freshwater. Anal. Chem. **73**: 4145–4153. doi:10.1021/ac010088e

Smith, J. M., F. P. Chavez, and C. A. Francis. 2014. Ammonium uptake by phytoplankton regulates nitrification in the sunlit ocean. PLOS ONE **9**: e108173. doi:10.1371/journal.pone.0108173

Smith, W. O., and D. J. Demaster. 1996. Phytoplankton biomass and productivity in the Amazon River plume: Correlation with seasonal river discharge. Continental Shelf Research **16**: 291–319. doi:10.1016/0278-4343(95)00007-N

Smoak, J. M., J. M. Krest, and P. W. Swarzenski. 2005. Geochemistry of the Amazon Estuary, p. 71–90. *In* P.J. Wangersky [ed.], Estuaries. Springer Berlin Heidelberg.

Starr, L. D., M. J. McCarthy, C. R. Hammerschmidt, A. Subramaniam, M. C. Despins, J. P. Montoya, and S. E. Newell. 2022. Mercury methylation linked to nitrification in the tropical North Atlantic Ocean. Marine Chemistry **247**: 104174. doi:10.1016/j.marchem.2022.104174

Subramaniam, A., P. L. Yager, E. J. Carpenter, and others. 2008. Amazon River enhances diazotrophy and carbon sequestration in the tropical North Atlantic Ocean. Proc. Natl. Acad. Sci. U.S.A. **105**: 10460–10465. doi:10.1073/pnas.0710279105

Sutton, M. A., A. Bleeker, C. M. Howard, and others. 2013. Our nutrient world. The challenge to produce more food & energy with less pollution. Centre for Ecology & Hydrology.

Swann, A. L. S., M. Longo, R. G. Knox, E. Lee, and P. R. Moorcroft. 2015. Future deforestation in the Amazon and consequences for South American climate. Agricultural and Forest Meteorology **214–215**: 12–24. doi:10.1016/j.agrformet.2015.07.006

Voss, M., N. Wannicke, B. Deutsch, D. Bronk, R. Sipler, R. Purvaja, R. Ramesh, and T. Rixen. 2011. 5.07 - Internal cycling of nitrogen and nitrogen transformations, p. 231–259. *In* E. Wolanski and D. McLusky [eds.], Treatise on Estuarine and Coastal Science. Academic Press.

Wagner, S., T. Riedel, J. Niggemann, A. V. Vähätalo, T. Dittmar, and R. Jaffé. 2015. Linking the molecular signature of heteroatomic dissolved organic matter to watershed characteristics in world rivers. Environ. Sci. Technol. **49**: 13798–13806. doi:10.1021/acs.est.5b00525

Wan, X. S., H.-X. Sheng, M. Dai, and others. 2018. Ambient nitrate switches the ammonium consumption pathway in the euphotic ocean. Nat Commun **9**: 915. doi:10.1038/s41467-018-03363-0

Wang, M., C. Hu, B. B. Barnes, G. Mitchum, B. Lapointe, and J. P. Montoya. 2019. The great Atlantic *Sargassum* belt. Science **365**: 83–87. doi:10.1126/science.aaw7912

Wawrik, B., J. H. Paul, D. A. Bronk, D. John, and M. Gray. 2004. High rates of ammonium recycling drive phytoplankton productivity in the offshore Mississippi River plume. Aquatic Microbial Ecology **35**: 175–184. doi:10.3354/ame035175

Weigand, M. A., J. Foriel, B. Barnett, S. Oleynik, and D. M. Sigman. 2016. Updates to instrumentation and protocols for isotopic analysis of nitrate by the denitrifier method. Rapid Commun. Mass Spectrom. **30**: 1365–1383. doi:10.1002/rcm.7570

Wong, W. W., J. Pottage, F. Y. Warry, P. Reich, K. L. Roberts, M. R. Grace, and P. L. M. Cook. 2018. Stable isotopes of nitrate reveal different nitrogen processing mechanisms in streams across a land use gradient during wet and dry periods. Biogeosciences **15**: 3953–3965. doi:10.5194/bg-15-3953-2018

Ye, F., Z. Ni, L. Xie, G. Wei, and G. Jia. 2015. Isotopic evidence for the turnover of biological reactive nitrogen in the Pearl River Estuary, south China. Journal of Geophysical Research: Biogeosciences **120**: 661–672. doi:10.1002/2014JG002842

5 | Conclusions and perspectives

Large river plumes, such as the Amazon River Plume, are complex systems that shape the biological, chemical, and physical characteristics of the marine environments into which they discharge. They are constantly changing, due to natural climate variability and anthropogenic impacts. Depending on the balance between sources and removal pathways, the riverine N is either processed in the river mouth or transported (Mulholland et al. 2008; Wells and Eyre 2019), influencing the primary productivity and associated carbon export in coastal zones. This equilibrium between retention and export is largely driven by the degradation of organic matter which is a dominant process in the seabed or turbid water columns (Jørgensen and Revsbech 1989).

In the context of this thesis, three studies were carried out to investigate the sources and fates of N on the Amazon shelf and along the river plume. The first study evaluates the significance of organic matter remineralization in the sediment as a source of DIN for overlying waters. In the oxygenated waters of the Amazon River Plume, the NH_4^+ produced during organic matter breakdown rarely accumulates, as it is rapidly assimilated by plankton or oxidized to NO_2^- and NO_3^- (i.e. nitrification). The second study thus focuses on nitrification in the water column along the Amazon River Plume, and the last study uses parts of these results, along with DIN and AA uptake rates measurements to calculate the balance between N inputs and N retention or removal processes in the surface waters at the river mouth. These studies are based on results from the cruise M174 which took place in April/May 2021, during rising to maximum river discharge. The dates of the cruise allowed the characterization of the riverine N end-member and study its maximal northward export.

The results highlight the high sedimentation and organic matter processing at the seabed on the shelf, and the significance of nitrification as a source of NO_3^- for turbid surface waters. At the seabed, the net impact of nitrification following organic matter degradation may be buffered due to the occurrence of N loss processes such as denitrification. In light-replete environments, surface water nitrification rates decrease, and NH_4^+ is rather assimilated by phytoplankton, but more NO_3^- is produced in the river mouth than is removed by NO_3^- uptake. Near the river mouth, the stable vertical stratification due to freshwater inflow is maintained despite the tidal forcing (Figure 25). The NO_3^- produced thus likely remains in the surface layer (8-10 m) and is be exported further along the Amazon River Plume.

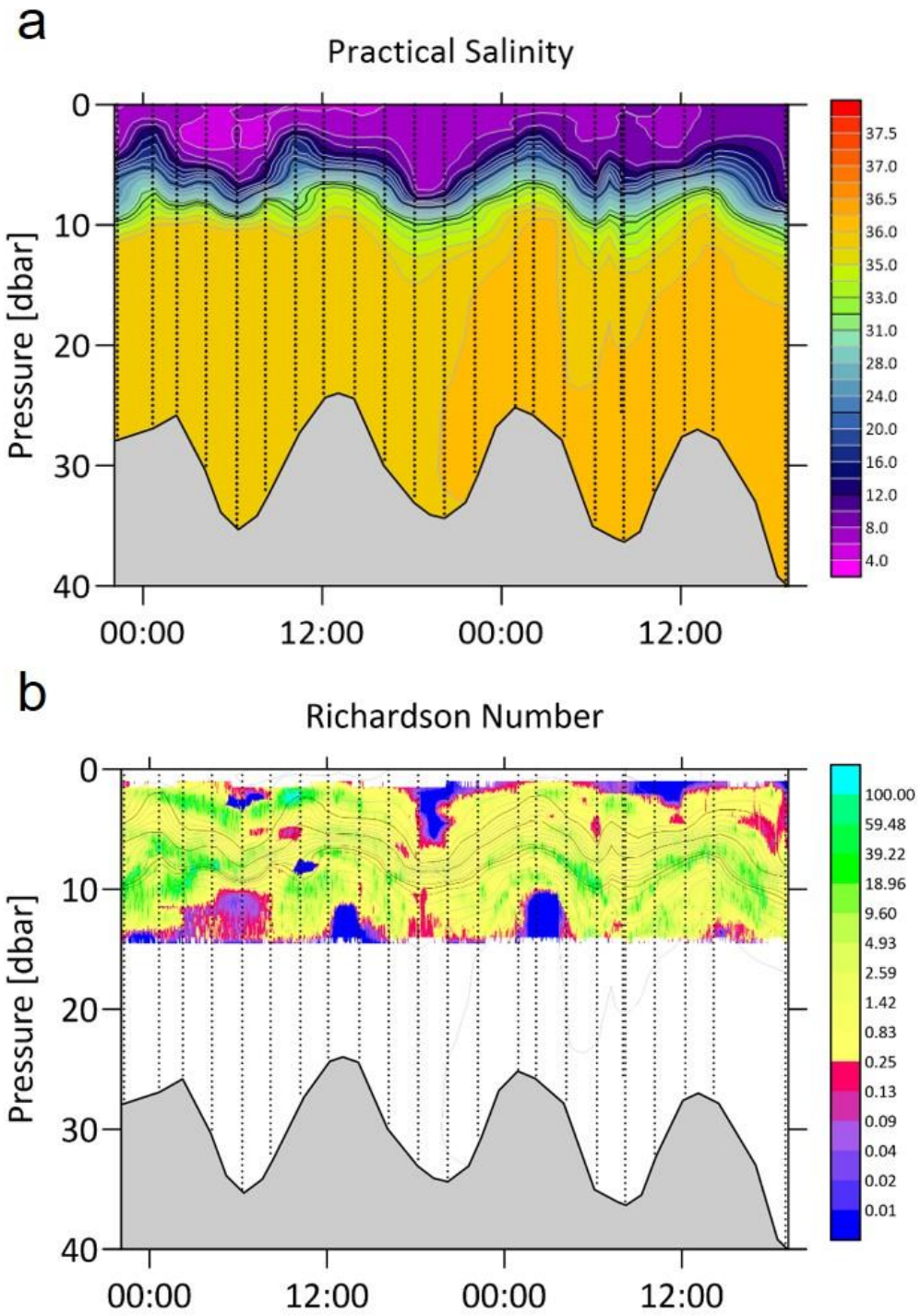

Figure 25. A microstructure-turbulence profiler MSS 90-S was deployed near the Amazon River mouth on a drifter (starting position: 01° 20.97'N; 048° 18.99'W), and enabled resolving (**a**) the strong vertical stratification from the salinity profiles, and (**b**) the limited turbulences in the halocline, as indicated by the Richardson number above 0.25 throughout the salinity gradient. The grey area shows the bottom depth, which captures the tidal impact on the drifter's trajectory. Figure by Volker Mohrholz.

Organic matter mineralization at the sediment-water interface

Past studies on the Amazon shelf indicated that the seabed primarily acted as a sink for N, where organic matter degradation is followed with denitrification, resulting in no net source or sink of DIN for the overlying water column (Aller et al. 1996; DeMaster and Aller 2001). With the continuous and substantial changes due to climate change, deforestation, and damming in the Amazon Basin, updating our understanding of benthic remineralization processes in this region was necessary. The analysis of eight short cores on the shelf, in areas influenced to varying degrees by the Amazon River Plume (Chapter 2) revealed intense recycling of terrestrial material in the river mouth. These results emphasize the importance of the seabed as a sink for particulate N, as previously measured in the region (Aller et al. 1996; DeMaster and Aller 2001). Sediment $\delta^{13}C\text{-}C_{org}$ and C_{org}/N_{tot} ratios showed a transition along the Amazon River Plume, between a terrestrial end-member at the river mouth (-26.3 mUr; 6.4 for $\delta^{13}C\text{-}C_{org}$ and C_{org}/N_{tot}, respectively) and a marine end member (-21.2 mUr; 8.5 for $\delta^{13}C\text{-}C_{org}$ and C_{org}/N_{tot}, respectively) at more distal stations, which suggests that the different sediment characteristics lead to differences in recycling efficiency. Similarly to a previous study, no clear source or sink of DIN was measured along the transect, suggesting a balance between DIN production (e.g. ammonification, nitrification) and consumption processes (e.g. denitrification, anammox). A key difference to the earlier study by Aller et al (2001), was a two-fold increase in sediment oxygen demand, providing insights into the processes driving ammonification and nitrification.

The notable increase in respiration rates between studies could be interpreted as an increased reactivity of the seabed, presumably originating from increased particulate and dissolved organic matter delivered to the estuary. However, there is no proof that the quantity of particles and dissolved organic matter transported by the Amazon River and reaching the sediment has increased over the last decades (Martinez et al. 2009; Montanher et al. 2018). The difference in oxygen consumption rates could also be the result of the occurrence of a resuspension event shortly before the sampling campaign (Kuehl et al. 1986), as signatures of such events were found in the $Si(OH)_4$ porewater profiles as well as in the solid phase of sediment located near the river mouth. Nevertheless, despite changes in the Amazon Basin, the balance between nitrification and denitrification remains, with no significant DIN diffusion in or out of the sediment. Benthic DIN is likely lost via complete denitrification (N_2 production), as no clear N_2O excess (i.e. relative to atmospheric values) was measured on the shelf. Overall,

these results underline the resilience of the sediment on the Amazon shelf, likely because despite the land-use changes in the Amazon catchment, little change in the sediment flux of the Amazon River is measureable (Montanher et al. 2018). The contrasting effects of deforestation and damming on erosion rates might be at play here, as the former has the potential of increasing erosion rates while the latter traps sediments. But this "buffer capacity" of the Amazon ecosystem is likely not endless, highlighting the need for continued monitoring in the face of ongoing environmental changes in the region.

Nitrification in the water column

The second chapter of this thesis underlines the reactor function of the sediment and overlying waters for PN remineralization, mainly via ammonification and nitrification. In the water column, it is also expected that nitrification is the dominant process, due to the large quantities of PN and DIN, mainly NO_3^-, delivered by the river. The use of the $^{15}N\text{-}NH_4^+$ tracer method (Damashek et al. 2016) for nitrification rate measurements alongside traditional oceanographic measurements allowed for the first comprehensive examination of nitrification along the Amazon River Plume, detailed in Chapter 3 of this thesis. The analysis of the environmental controls on nitrification rates was performed with the help of a random forest algorithm. Several habitats have been defined along the Amazon River Plume, based on the physical (i.e. sea surface temperature, sea surface salinity, mixed layer depth) and biochemical characteristics (i.e. NO_3^- availability, depth of the chlorophyll-a maximum), which explain the distribution of phytoplankton and cyanobacteria communities along the plume (Weber et al. 2019; Pham et al. 2024). During cruise M174, eight habitats were defined, five of which were sampled for nitrification rate analysis. Nevertheless, measured nitrification rates did not seem to follow such a fine variability, and were rather split into three groups as only two of the habitats (riverine and young plume core) exhibited nitrification rates significantly higher than the most oceanic habitat.

Variability in nitrification rates was observed, with the highest rates (302 nmol L^{-1} h^{-1}; Figure 26) measured at the river mouth, an region with high turbidity, NO_2^- and PO_4^{3-} concentrations. With distance from the river mouth, surface turbidity decreases, allowing for phytoplankton growth. These organisms outcompete nitrifiers for NH_4^+ in surface waters, leading to a drop in surface nitrification rates by at least two orders of magnitude. In deeper waters and close to the seabed, where light is still absent, nitrification rates are still as high as at the river mouth, further highlighting the role of the sediment overlying water as a reactor for

N. While nitrification rates in the Amazon River mouth were comparable to those in other river plumes worldwide, such as the Chang Jiang and Mississippi Rivers, at the least turbid stations of the Amazon River Plume, surface nitrification rates dropped to oceanic values (0-2.5 nmol L^{-1} h^{-1}). At these most distal stations, the nitrification rate maximum was found at or just below the chlorophyll-a maximum, as observed by a previous study of the Northern plume (Starr et al. 2022).

Fluorescence, a proxy for phytoplankton presence, exhibited patterns consistent with the hypothesis of competition of nitrifiers with phytoplankton. NO_2^- concentrations, known to accumulate below the deep chlorophyll-a maximum, displayed a similar spatial pattern to nitrification rates. The NO_2^--peak observed in the river mouth and YPC habitats, below the euphotic zone, indicated a potential role of nitrification in generating this intermediate product (Zakem et al. 2018). Additionally, the mesoscale turbulences resulting from the mixing between river plume and oceanic waters could further contribute to the accumulation of NO_2^- in regions of the plume with elevated nitrification rates (Lévy et al. 2014; Liu et al. 2023). The positive correlation between PO_4^{3-} concentrations and nitrification rates, also highlighted by the machine learning model, could also suggest a link between P availability and nitrification, as mentioned in other studies (Zhou et al. 2023), although this link remains to be proven.

Re-evaluating the N-budget of surface waters at the Amazon River mouth

The Amazon River is the dominant source of NO_3^- (3.0×10^8 mol N d^{-1}) and NH_4^+ (0.1×10^8 mol N d^{-1}) for the Amazon shelf, a source that is one order of magnitude greater than the inputs of the neighboring Pará River. Advection and surface mixing contribute additional N fluxes, totaling 1.6×10^8 mol N d^{-1}. NO_3^- concentrations in riverine waters are moderate compared to concentrations measured in less pristine rivers, such as the Seine (Brion et al. 2000) or the Pearl River (Dai et al. 2008). The main driver behind the great N inputs observed in the Amazon River is therefore the magnitude of the river discharge.

The NO_3^- delivered by the Amazon and the Pará rivers have a similar isotopic composition (3.7-4.0 and -0.6-1.8 mUr for $\delta^{15}N$ and $\delta^{18}O$, respectively; Figure 26), suggesting that similar sources or processes influence this nutrient in both estuaries. But while the $\delta^{15}N$-NO_3^- values remain unchanged with increasing salinity in the estuaries, the $\delta^{18}O$-NO_3^- is more variable. At most stations, $\delta^{18}O$-NO_3^- values were a couple of mUr greater than the $\delta^{18}O$ of

ambient water at the river mouth, although at one, the measured value was within the range of $\delta^{18}O$ values that could be expected if nitrification was the dominant pathway at the river mouth, in the plume layer: about 1.2 mUr above the $\delta^{18}O$ of ambient water (Granger et al. 2013; Marconi et al. 2019). As discussed in Chapter 3, at the river mouth, where it is too turbid for primary production (Figure 26), nitrification rates were ten to a hundred times higher than measured in any other part of the Amazon River Plume (Figure 26). This variability is likely explained by the particulate and dissolved organic N delivered by the river or by primary production close to the river mouth (DeMaster and Aller 2001; Drake et al. 2021), which provides the ecosystem with a source of organic matter that can be converted to NH_4^+, the substrate for nitrification.

The resulting nitrification rates presented in Chapter 3 and 4 are so high, ranging from 99 to 162 nmol L^{-1} h^{-1} in the Amazon River and 27 to 44 nmol L^{-1} h^{-1} in the Pará River, that the resulting NO_3^- production calculated in Chapter 4 exceeds riverine NO_3^- fluxes (Figure 26). When turbidity decreases with distance from the river mouth, primary producers become active, but preferentially consume NH_4^+ as this compound is easier to process than NO_3^-, and is still present at sufficient levels (Paasche and Kristiansen 1982; Dortch 1990; L'Helguen et al. 1996). The nitrified NO_3^- is therefore not consumed and is exported further along the Amazon River Plume, where it gets diluted by mixing with oceanic waters. Many recent studies have hypothesized that this NO_3^- could reach the most northern parts of the plume, 16 °N and beyond at high river discharge, and could be a cause of the great *Sargassum* blooms observed in the region (Wang et al. 2019; Aquino et al. 2022). The enhancement of the riverine NO_3^- discharged by nitrification shown in Chapters 3 and 4 of this thesis indicates that the impact of the Amazon River reaches regions far beyond the limits of the estuary.

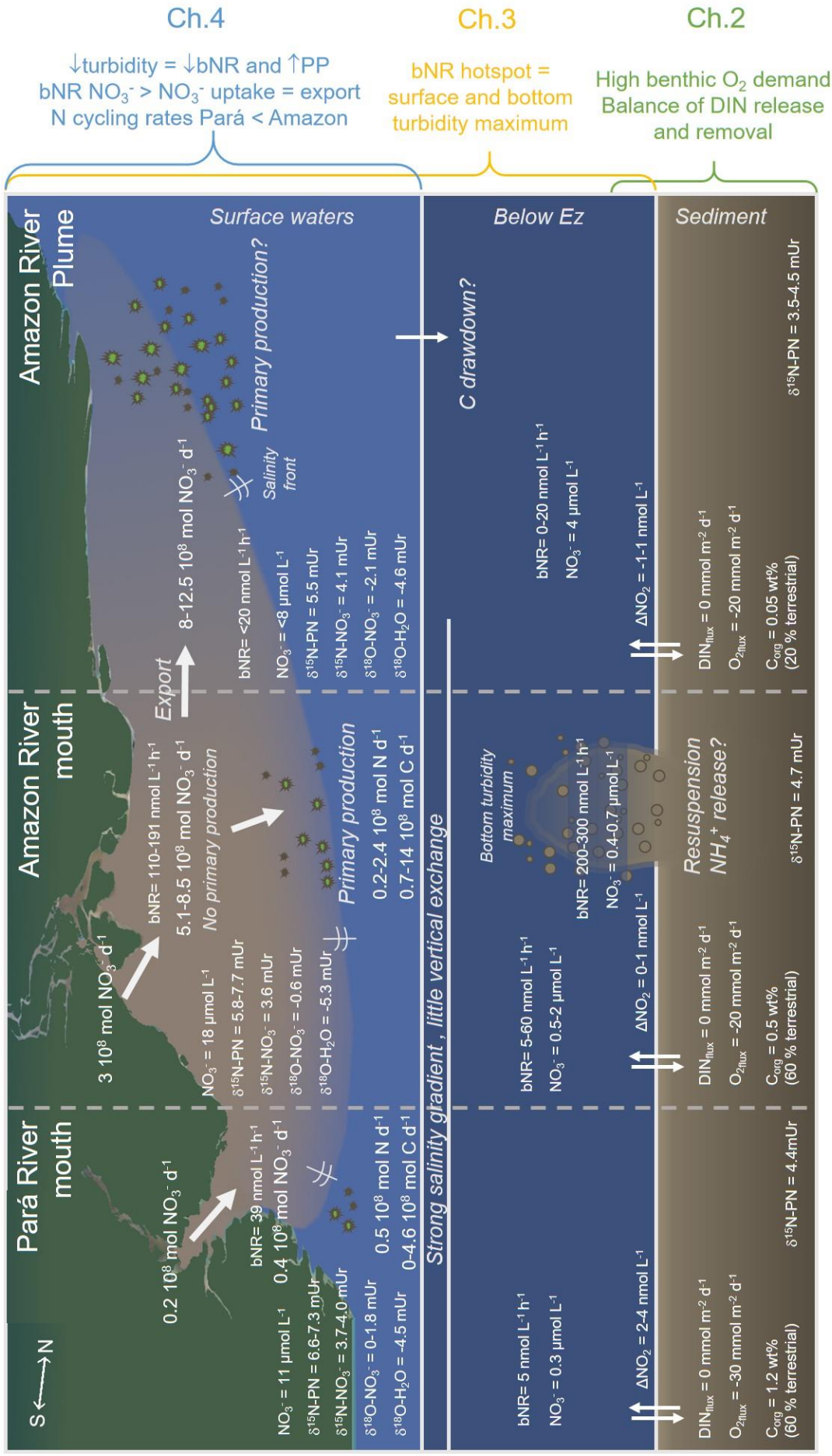

Figure 26. Summary of the main findings of this thesis, discussed in Chapters 2, 3 and 4. bNR stands for nitrification rates and bNR NO_3^- is the nitrified NO_3^-. PP stands for primary production. The arrows show the input, export, and diffusion of N between reservoirs.

Outlook

The relationship between the N and the carbon cycle is twofold. In the most shallow and turbid parts of the river mouth, the intense remineralization processes affecting the various N forms also impact the carbon cycle. The strong reworking of the sediment generates an extensive microbial reactor, as described in Chapter 2, leading to most of the POC to be recycled and resupplied to the water column as DIC (DeMaster and Aller 2001). As a result, only around 35 % of the terrigenous and marine POC is buried on the Amazon shelf ($13x10^8$ mol d^{-1}, or 5.7 Tg y^{-1}; (DeMaster and Aller 2001). The rest is mostly regenerated as dissolved inorganic and organic carbon which is in turn exported to the open ocean. At the surface along the Amazon River Plume, sea-air CO_2 exchange can reach values as high as 47.2±20.8 Tg y^{-1} during high water seasons (Valerio et al. 2021).In light-replete regions of the river plume, the DIN delivered by the river or produced by mineralization processes is assimilated into plankton biomass, in conjunction with DIC, as discussed in Chapter 4 of this thesis. The NH_4^+ uptake (337.6±48.1 nmol L^{-1} h^{-1}), NO_3^- (58.2±10.0 nmol L^{-1} h^{-1}), and AA uptake rates (51.2±5.8 nmol L^{-1} h^{-1}) and associated DIC uptake (2200±300 nmol L^{-1} h^{-1}) in the least turbid region of the most riverine habitat of the plume only result in a C burial of 0.2 Tg y^{-1}, assuming that only 3 % of marine biomass is buried on the shelf (DeMaster and Aller 2001). As a comparison, the much higher primary productivity in mesohaline waters of the plume, further away from the river mouth, could foster a C drawdown of up to 20 Tg y^{-1} (Cooley et al. 2007; Subramaniam et al. 2008). These results further highlight the importance of DIN production via mineralization processes in the river mouth and its export for the efficiency of the biological pump in the Amazon River Plume.

In the context of increasing anthropogenic changes in the region, this thesis underlines the necessity of understanding the interplay between N sources, remineralization processes, and N export on the Amazon/Pará shelf. While remineralization processes at the sediment-water interface and in the sediment seem to have remained unchanged over the last decades, as discussed in Chapter 2, data on N cycling rates is scarce in the region, especially in the Amazon River estuary. Chapter 2 highlighted the significance of nitrification and denitrification at the seabed for buffering the DIN release from the sediment. In Chapter 3, we demonstrated that nitrification was occurring at high rates in the most turbid parts of the Amazon River Plume, that is, in the river mouth and close to the seabed on the shelf. However, no denitrification rates data is available for the shelf so far. This data would be necessary to refine N burial calculations

on the shelf (DeMaster and Aller 2001). Furthermore, the impact and extent of sediment resuspension on the N cycling at the river mouth needs to be properly assessed, as many studies state that such events likely constitute a major source of NH_4^+ and organic matter to the water column (Chapter 2; (Kuehl et al. 1995; DeMaster and Aller 2001).

Chapter 3 and 4 of this thesis provide a comprehensive overview of nitrification and DIN uptake and export, at high river discharge. Nevertheless, the variability of the Amazon River Discharge requires continued research covering different seasons, to understand the potential long-term impacts of human alterations on the processes investigated here. During low discharge season, the water residence time in the estuary increases, which should lead to increased sedimentation rates and thus increase benthic organic matter degradation rates, which should overall increase N removal and reduce N export to the open ocean (Seitzinger et al. 2006). N cycle monitoring could be done by measuring the same N cycling rates reported here at different seasons. It would be critical to also measure NH_4^+ production rates, and as mentioned above, denitrification rates. Snapshots of the dominant N cycle processes could also be given by studying the variability of NO_3^- stable isotopes in time and space along the Amazon River Plume, a type of study made possible by the characterization of the isotopic composition of the Amazon River NO_3^- source in Chapter 4 of this thesis.

References

Aller, R. C., N. E. Blair, Q. Xia, and P. D. Rude. 1996. Remineralization rates, recycling, and storage of carbon in Amazon shelf sediments. Continental Shelf Research **16**: 753–786. doi:10.1016/0278-4343(95)00046-1

Alongi, D. M. 2013. Cycling and global fluxes of nitrogen in mangroves. Global Environmental Research 173–182.

Aquino, R., C. Noriega, A. Mascarenhas, and others. 2022. Possible Amazonian contribution to *Sargassum* enhancement on the Amazon Continental Shelf. Science of The Total Environment **853**: 158432. doi:10.1016/j.scitotenv.2022.158432

Araujo, M., C. Noriega, G. A. Hounsou-gbo, and others. 2017. A synoptic assessment of the Amazon River-ocean continuum during Boreal Autumn: From physics to plankton communities and carbon flux. Frontiers in Microbiology **8**.

Araujo, M., C. Noriega, and N. Lefèvre. 2014. Nutrients and carbon fluxes in the estuaries of major rivers flowing into the tropical Atlantic. Frontiers in Marine Science **1**.

Asmala, E., J. Carstensen, D. J. Conley, C. P. Slomp, J. Stadmark, and M. Voss. 2017. Efficiency of the coastal filter: Nitrogen and phosphorus removal in the Baltic Sea. Limnology and Oceanography **62**: S222–S238. doi:10.1002/lno.10644

Atkinson, S. J., C. G. Mowat, G. A. Reid, and S. K. Chapman. 2007. An octaheme c-type cytochrome from *Shewanella oneidensis* can reduce nitrite and hydroxylamine. FEBS letters **581**: 3805–3808.

Azam, F., T. Fenchel, J. Field, J. Gray, L. Meyer-Reil, and F. Thingstad. 1983. The ecological role of water-column microbes in the sea. Mar. Ecol. Prog. Ser. **10**: 257–263. doi:10.3354/meps010257

Babbin, A. R., R. G. Keil, A. H. Devol, and B. B. Ward. 2014. Organic matter stoichiometry, flux, and oxygen control nitrogen loss in the ocean. Science **344**: 406–408. doi:10.1126/science.1248364

Babbin, A. R., and B. B. Ward. 2013. Controls on nitrogen loss processes in Chesapeake Bay sediments. Environ. Sci. Technol. **47**: 4189–4196. doi:10.1021/es304842r

Bandekar, M., N. Ramaiah, and R. M. Meena. 2018. Diversity and abundance of denitrifying and anammox bacteria from the Arabian Sea oxygen minimum zone. Deep Sea Research Part II: Topical Studies in Oceanography **156**: 19–26. doi:10.1016/j.dsr2.2018.08.008

Barbosa, V. A., J. C. Nabout, and H. F. da Cunha. 2023. Spatial and temporal deforestation in the Brazilian Savanna: The discrepancy between observed and licensed deforestation in the state of Goiás. Land Use Policy **131**: 106730. doi:10.1016/j.landusepol.2023.106730

Beardsley, R. C., J. Candela, R. Limeburner, W. R. Geyer, S. J. Lentz, B. M. Castro, D. Cacchione, and N. Carneiro. 1995. The M_2 tide on the Amazon Shelf. Journal of Geophysical Research: Oceans **100**: 2283–2319. doi:10.1029/94JC01688

Bentzon-Tilia, M., S. J. Traving, M. Mantikci, H. Knudsen-Leerbeck, J. L. Hansen, S. Markager, and L. Riemann. 2015. Significant N_2 fixation by heterotrophs, photoheterotrophs and heterocystous cyanobacteria in two temperate estuaries. The ISME journal **9**: 273–285.

Bernhard, J. M., K. L. Casciotti, M. R. McIlvin, D. J. Beaudoin, P. T. Visscher, and V. P. Edgcomb. 2012. Potential importance of physiologically diverse benthic foraminifera in sedimentary nitrate storage and respiration. Journal of Geophysical Research: Biogeosciences **117**. doi:10.1029/2012JG001949

Bernhardt, E. S., J. R. Blaszczak, C. D. Ficken, M. L. Fork, K. E. Kaiser, and E. C. Seybold. 2017. Control points in ecosystems: moving beyond the hot spot hot moment concept. Ecosystems **20**: 665–682. doi:10.1007/s10021-016-0103-y

Bonnet, S., J. Dekaezemacker, K. A. Turk-Kubo, T. Moutin, R. M. Hamersley, O. Grosso, J. P. Zehr, and D. G. Capone. 2013. Aphotic N_2 fixation in the eastern tropical South Pacific Ocean. PloS one **8**: e81265.

Bourbonnais, A., R. T. Letscher, H. W. Bange, V. Échevin, J. Larkum, J. Mohn, N. Yoshida, and M. A. Altabet. 2017. N_2O production and consumption from stable isotopic and concentration data in the Peruvian coastal upwelling system. Global Biogeochemical Cycles **31**: 678–698. doi:10.1002/2016GB005567

Bowles, M. W., L. M. Nigro, A. P. Teske, and S. B. Joye. 2012. Denitrification and environmental factors influencing nitrate removal in Guaymas Basin hydrothermally altered sediments. Frontiers in Microbiology **3**: 377.

Brandsma, J., J. van de Vossenberg, N. Risgaard-Petersen, and others. 2011. A multi-proxy study of anaerobic ammonium oxidation in marine sediments of the Gullmar Fjord, Sweden. Environmental Microbiology Reports **3**: 360–366. doi:10.1111/j.1758-2229.2010.00233.x

Brion, N., G. Billen, L. Guézennec, and A. Ficht. 2000. Distribution of nitrifying activity in the Seine River (France) from Paris to the estuary. Estuaries **23**: 669–682. doi:10.2307/1352893

Bristow, L. A., N. Sarode, J. Cartee, A. Caro-Quintero, B. Thamdrup, and F. J. Stewart. 2015. Biogeochemical and metagenomic analysis of nitrite accumulation in the Gulf of Mexico hypoxic zone. Limnol. Oceanogr. **60**: 1733–1750. doi:10.1002/lno.10130

Byrne, N., M. Strous, V. Crépeau, and others. 2009. Presence and activity of anaerobic ammonium-oxidizing bacteria at deep-sea hydrothermal vents. ISME J **3**: 117–123. doi:10.1038/ismej.2008.72

Caffrey, J. M. 2004. Factors controlling net ecosystem metabolism in U.S. estuaries. Estuaries **27**: 90–101. doi:10.1007/BF02803563

Caffrey, J. M., S. Bonaglia, and D. J. Conley. 2019. Short exposure to oxygen and sulfide alter nitrification, denitrification, and DNRA activity in seasonally hypoxic estuarine sediments. FEMS microbiology letters **366**: fny288.

Cai, W.-J., X. Hu, W.-J. Huang, and others. 2011. Acidification of subsurface coastal waters enhanced by eutrophication. Nature Geosci **4**: 766–770. doi:10.1038/ngeo1297

Canuel, E. A., and A. K. Hardison. 2016. Sources, ages, and alteration of organic matter in estuaries. Annual Review of Marine Science **8**: 409–434. doi:10.1146/annurev-marine-122414-034058

Capone, D. G., J. A. Burns, J. P. Montoya, A. Subramaniam, C. Mahaffey, T. Gunderson, A. F. Michaels, and E. J. Carpenter. 2005. Nitrogen fixation by *Trichodesmium* spp.: An important source of new nitrogen to the tropical and subtropical North Atlantic Ocean. Global Biogeochem. Cycles **19**: n/a-n/a. doi:10.1029/2004GB002331

Caranto, J. D., and K. M. Lancaster. 2017. Nitric oxide is an obligate bacterial nitrification intermediate produced by hydroxylamine oxidoreductase. Proc. Natl. Acad. Sci. U.S.A. **114**: 8217–8222. doi:10.1073/pnas.1704504114

Chang, B. X., J. R. Rich, A. Jayakumar, H. Naik, A. K. Pratihary, R. G. Keil, B. B. Ward, and A. H. Devol. 2014. The effect of organic carbon on fixed nitrogen loss in the eastern tropical South Pacific and Arabian Sea oxygen deficient zones. Limnology and Oceanography **59**: 1267–1274. doi:10.4319/lo.2014.59.4.1267

Coles, V. J., M. T. Brooks, J. Hopkins, M. R. Stukel, P. L. Yager, and R. R. Hood. 2013. The pathways and properties of the Amazon River Plume in the tropical North Atlantic Ocean. J. Geophys. Res. Oceans **118**: 6894–6913. doi:10.1002/2013JC008981

Cooley, S. R., V. J. Coles, A. Subramaniam, and P. L. Yager. 2007. Seasonal variations in the Amazon plume-related atmospheric carbon sink. Global Biogeochemical Cycles **21**. doi:10.1029/2006GB002831

Dai, M., L. Wang, X. Guo, W. Zhai, Q. Li, B. He, and S.-J. Kao. 2008. Nitrification and inorganic nitrogen distribution in a large perturbed river/estuarine system: The Pearl River Estuary, China. Biogeosciences **5**: 1227–1244. doi:10.5194/bg-5-1227-2008

Daims, H., S. Lücker, and M. Wagner. 2016. A new perspective on microbes formerly known as nitrite-oxidizing bacteria. Trends in microbiology **24**: 699–712.

Dalsgaard, T., F. J. Stewart, B. Thamdrup, L. De Brabandere, N. P. Revsbech, O. Ulloa, D. E. Canfield, and E. F. DeLong. 2014. Oxygen at nanomolar levels reversibly suppresses process rates and gene expression in anammox and denitrification in the oxygen minimum zone off Northern Chile. mBio **5**: 10.1128/mbio.01966-14. doi:10.1128/mbio.01966-14

Damashek, J., K. L. Casciotti, and C. A. Francis. 2016. Variable nitrification rates across environmental gradients in turbid, nutrient-rich estuary waters of san francisco bay. Estuaries and Coasts **39**: 1050–1071. doi:10.1007/s12237-016-0071-7

Damashek, J., and C. A. Francis. 2018. Microbial nitrogen cycling in estuaries: From genes to ecosystem processes. Estuaries and Coasts **41**: 626–660. doi:10.1007/s12237-017-0306-2

Damashek, J., B. B. Tolar, Q. Liu, A. O. Okotie-Oyekan, N. J. Wallsgrove, B. N. Popp, and J. T. Hollibaugh. 2019. Microbial oxidation of nitrogen supplied as selected organic nitrogen compounds in the South Atlantic Bight. Limnol Oceanogr **64**: 982–995. doi:10.1002/lno.11089

Day, J. W., R. Ramachandran, L. Giosan, J. Syvitski, and G. Paul Kemp. 2019. Chapter 9 - Delta winners and losers in the Anthropocene, p. 149–165. *In* E. Wolanski, J.W. Day, M. Elliott, and R. Ramachandran [eds.], Coasts and Estuaries. Elsevier.

DeMaster, D. J., and R. C. Aller. 2001. Biogeochemical processes on the Amazon shelf: Changes in dissolved and particulate fluxes during river/ocean mixing. The Biogeochemistry of the Amazon Basin 328–357.

Demaster, D. J., and R. H. Pope. 1996. Nutrient dynamics in Amazon shelf waters: Results from AMASSEDS. Continental Shelf Research **16**: 263–289. doi:10.1016/0278-4343(95)00008-O

Dortch, Q. 1990. The interaction between ammonium and nitrate uptake in phytoplankton. Mar. Ecol. Prog. Ser. **61**: 183–201. doi:10.3354/meps061183

Drake, T. W., J. D. Hemingway, M. R. Kurek, and others. 2021. The pulse of the Amazon: Fluxes of dissolved organic carbon, nutrients, and ions from the world's largest river. Global Biogeochemical Cycles **35**: e2020GB006895. doi:10.1029/2020GB006895

Duce, R. A., J. LaRoche, K. Altieri, and others. 2008. Impacts of atmospheric anthropogenic nitrogen on the open ocean. Science **320**: 893–897. doi:10.1126/science.1150369

Dugdale, R. C., and J. J. Goering. 1967. Uptake of new and regenerated forms of nitrogen in primary productivity. Limnol. Oceanogr. **12**: 196–206. doi:10.4319/lo.1967.12.2.0196

Dugdale, R. C., D. W. Menzel, and J. H. Ryther. 1961. Nitrogen fixation in the Sargasso Sea. Deep Sea Research (1953) **7**: 297–300. doi:10.1016/0146-6313(61)90051-X

Eady, R. R. 1996. Structure−function relationships of alternative nitrogenases. Chem. Rev. **96**: 3013–3030. doi:10.1021/cr950057h

Edmond, J. M., E. A. Boyle, B. Grant, and R. F. Stallard. 1981. The chemical mass balance in the Amazon plume I: The nutrients. Deep Sea Research Part A. Oceanographic Research Papers **28**: 1339–1374. doi:10.1016/0198-0149(81)90038-8

Eppley, R. W., and B. J. Peterson. 1979. Particulate organic matter flux and planktonic new production in the deep ocean. Nature **282**: 677–680. doi:10.1038/282677a0

Eyre, B. D., D. T. Maher, and P. Squire. 2013. Quantity and quality of organic matter (detritus) drives N_2 effluxes (net denitrification) across seasons, benthic habitats, and estuaries. Global Biogeochemical Cycles **27**: 1083–1095. doi:10.1002/2013GB004631

Falkowski, P. G. 1997. Evolution of the nitrogen cycle and its influence on the biological sequestration of CO_2 in the ocean. Nature **387**: 272–275.

Falkowski, P., R. J. Scholes, E. Boyle, J. Canadell, D. Canfield, J. Elser, N. Gruber, and K. Hibbard. 2000. The global carbon cycle: A test of our knowledge of Earth as a system. **290**.

Fearnside, P. M. 2015. Amazon dams and waterways: Brazil's Tapajós Basin plans. Ambio **44**: 426–439. doi:10.1007/s13280-015-0642-z

Foster, R. A., M. M. Kuypers, T. Vagner, R. W. Paerl, N. Musat, and J. P. Zehr. 2011. Nitrogen fixation and transfer in open ocean diatom–cyanobacterial symbioses. The ISME journal **5**: 1484–1493.

Fowler, D., M. Coyle, U. Skiba, and others. 2013. The global nitrogen cycle in the twenty-first century. Phil. Trans. R. Soc. B **368**: 20130164. doi:10.1098/rstb.2013.0164

Fricke, A. T., C. A. Nittrouer, A. S. Ogston, D. J. Nowacki, N. E. Asp, and P. W. M. Souza Filho. 2019. Morphology and dynamics of the intertidal floodplain along the Amazon tidal river. Earth Surface Processes and Landforms **44**: 204–218. doi:10.1002/esp.4545

Gaby, J. C., and D. H. Buckley. 2015. Assessment of nitrogenase diversity in the environment, p. 209–216. *In* F.J. De Bruijn [ed.], Biological Nitrogen Fixation. Wiley.

Galloway, J. N., J. D. Aber, J. W. Erisman, S. P. Seitzinger, R. W. Howarth, E. B. Cowling, and B. J. Cosby. 2003. The nitrogen cascade. BioScience **53**: 341–356. doi:10.1641/0006-3568(2003)053[0341:TNC]2.0.CO;2

Galloway, J. N., F. J. Dentener, D. G. Capone, and others. 2004. Nitrogen cycles: Past, present, and future. Biogeochemistry **70**: 153–226. doi:10.1007/s10533-004-0370-0

Galloway, J. N., W. H. Schlesinger, H. Levy, A. Michaels, and J. L. Schnoor. 1995. Nitrogen fixation: Anthropogenic enhancement-environmental response. Global Biogeochem. Cycles **9**: 235–252. doi:10.1029/95GB00158

Galy, V., B. Peucker-Ehrenbrink, and T. Eglinton. 2015. Global carbon export from the terrestrial biosphere controlled by erosion. Nature **521**: 204–207. doi:10.1038/nature14400

Gandy, E. L., and D. C. Yoch. 1988. Relationship between nitrogen-fixing sulfate reducers and fermenters in salt marsh sediments and roots of *Spartina alterniflora*. Appl Environ Microbiol **54**: 2031–2036. doi:10.1128/aem.54.8.2031-2036.1988

Geyer, W. R., R. C. Beardsley, S. J. Lentz, J. Candela, R. Limeburner, W. E. Johns, B. M. Castro, and I. D. Soares. 1996. Physical oceanography of the Amazon shelf. Continental Shelf Research **16**: 575–616.

Geyer, W. R., and G. C. Kineke. 1995. Observations of currents and water properties in the Amazon Frontal Zone. Journal of Geophysical Research: Oceans **100**: 2321–2339. doi:10.1029/94JC02657

Gibbs, R. J. 1967. The geochemistry of the Amazon River System: Part I. The factors that control the salinity and the composition and concentration of the suspended solids. GSA Bulletin **78**: 1203–1232. doi:10.1130/0016-7606(1967)78[1203:TGOTAR]2.0.CO;2

Gier, J., C. R. Löscher, A. W. Dale, S. Sommer, U. Lomnitz, and T. Treude. 2017. Benthic dinitrogen fixation traversing the oxygen minimum zone off Mauritania (NW Africa). Frontiers in Marine Science **4**: 390.

Glibert, P. M., F. P. Wilkerson, R. C. Dugdale, and others. 2016. Pluses and minuses of ammonium and nitrate uptake and assimilation by phytoplankton and implications for productivity and community composition, with emphasis on nitrogen-enriched conditions. Limnology and Oceanography **61**: 165–197. doi:10.1002/lno.10203

Gloor, M., R. J. W. Brienen, D. Galbraith, and others. 2013. Intensification of the Amazon hydrological cycle over the last two decades. Geophysical Research Letters **40**: 1729–1733. doi:https://doi.org/10.1002/grl.50377

Goes, J. I., H. do R. Gomes, A. M. Chekalyuk, and others. 2014. Influence of the Amazon River discharge on the biogeography of phytoplankton communities in the western tropical north Atlantic. Progress in Oceanography **120**: 29–40. doi:10.1016/j.pocean.2013.07.010

Goreau, T. J., W. A. Kaplan, S. C. Wofsy, M. B. McElroy, F. W. Valois, and S. W. Watson. 1980. Production of NO_2^- and N_2O by nitrifying bacteria at reduced concentrations of oxygen. Appl Environ Microbiol **40**: 526–532. doi:10.1128/aem.40.3.526-532.1980

Gouveia, N. A., D. F. M. Gherardi, and L. E. O. C. Aragão. 2019. The Role of the Amazon River Plume on the Intensification of the Hydrological Cycle. Geophys. Res. Lett. **46**: 12221–12229. doi:10.1029/2019GL084302

van de Graaf, A. A., A. Mulder, P. de Bruijn, M. S. Jetten, L. A. Robertson, and J. G. Kuenen. 1995. Anaerobic oxidation of ammonium is a biologically mediated process. Applied and Environmental Microbiology **61**: 1246–1251. doi:10.1128/aem.61.4.1246-1251.1995

Graf, D. R., C. M. Jones, and S. Hallin. 2014. Intergenomic comparisons highlight modularity of the denitrification pathway and underpin the importance of community structure for N_2O emissions. PloS one **9**: e114118.

Granger, J., M. G. Prokopenko, C. W. Mordy, and D. M. Sigman. 2013. The proportion of remineralized nitrate on the ice-covered eastern Bering Sea shelf evidenced from the oxygen isotope ratio of nitrate. Global Biogeochemical Cycles **27**: 962–971. doi:10.1002/gbc.20075

Gruber, N. 2004. The Dynamics of the Marine Nitrogen Cycle and its Influence on Atmospheric CO_2 Variations, p. 97–148. *In* M. Follows and T. Oguz [eds.], The Ocean Carbon Cycle and Climate. Springer Netherlands.

Gruber, N. 2008. The marine nitrogen cycle: Overview and challenges, p. 1–50. *In* Nitrogen in the marine environment.

Gruber, N., and J. L. Sarmiento. 1997. Global patterns of marine nitrogen fixation and denitrification. Global Biogeochem. Cycles **11**: 235–266. doi:10.1029/97GB00077

Gruber, N., and J. L. Sarmiento. 2002. Large-scale biogeochemical-physical interactions in elemental cycles. The sea **12**: 337–399.

Harris, S. J., D. I. Cendón, S. I. Hankin, M. A. Peterson, S. Xiao, and B. F. J. Kelly. 2022. Isotopic evidence for nitrate sources and controls on denitrification in groundwater beneath an irrigated agricultural district. Science of the Total Environment **817**: 152606. doi:10.1016/j.scitotenv.2021.152606

Hong, Y.-G., M. Li, H. Cao, and J.-D. Gu. 2011. Residence of habitat-specific anammox bacteria in the deep-sea subsurface sediments of the South China Sea: Analyses of marker gene abundance with physical chemical parameters. Microb Ecol **62**: 36–47. doi:10.1007/s00248-011-9849-0

Howarth, R. W., and R. Marino. 2006. Nitrogen as the limiting nutrient for eutrophication in coastal marine ecosystems: Evolving views over three decades. Limnology and Oceanography **51**: 364–376. doi:10.4319/lo.2006.51.1_part_2.0364

Hutchins, D. A., and S. A. Sañudo-Wilhelmy. 2022. The enzymology of ocean global change. Annu. Rev. Mar. Sci. **14**: 187–211. doi:10.1146/annurev-marine-032221-084230

Hylén, A., S. Bonaglia, E. Robertson, U. Marzocchi, M. Kononets, and P. O. J. Hall. 2022. Enhanced benthic nitrous oxide and ammonium production after natural oxygenation of long-term anoxic sediments. Limnology & Oceanography **67**: 419–433. doi:10.1002/lno.12001

IBGE, I.-B. I. of G. and S. 2018. Pesquisa Nacional de Saneamento Básico | IBGE.

Ittekkot, V. 1988. Global trends in the nature of organic matter in river suspensions. Nature **332**: 436–438. doi:10.1038/332436a0

Jäntti, H., and S. Hietanen. 2012. The effects of hypoxia on sediment nitrogen cycling in the Baltic Sea. Ambio **41**: 161–169.

Jetten, M. S. M., L. van Niftrik, M. Strous, B. Kartal, J. T. Keltjens, and H. J. M. Op den Camp. 2009. Biochemistry and molecular biology of anammox bacteria. Critical Reviews in Biochemistry and Molecular Biology **44**: 65–84. doi:10.1080/10409230902722783

Ji, B., K. Yang, L. Zhu, Y. Jiang, H. Wang, J. Zhou, and H. Zhang. 2015. Aerobic denitrification: a review of important advances of the last 30 years. Biotechnology and bioprocess engineering **20**: 643–651.

Jickells, T. D., E. Buitenhuis, K. Altieri, and others. 2017. A reevaluation of the magnitude and impacts of anthropogenic atmospheric nitrogen inputs on the ocean. Global Biogeochemical Cycles **31**: 289–305. doi:10.1002/2016GB005586

Johnston, D. T., B. C. Gill, A. Masterson, E. Beirne, K. L. Casciotti, A. N. Knapp, and W. Berelson. 2014. Placing an upper limit on cryptic marine sulphur cycling. Nature **513**: 530–533.

Jones, C. M., D. R. Graf, D. Bru, L. Philippot, and S. Hallin. 2013. The unaccounted yet abundant nitrous oxide-reducing microbial community: a potential nitrous oxide sink. The ISME journal **7**: 417–426.

Jones, C. M., B. Stres, M. Rosenquist, and S. Hallin. 2008. Phylogenetic analysis of nitrite, nitric oxide, and nitrous oxide respiratory enzymes reveal a complex evolutionary history for denitrification. Molecular biology and evolution **25**: 1955–1966.

Jørgensen, B. B., and D. C. Nelson. 2004. Sulfide oxidation in marine sediments: Geochemistry meets microbiology, p. 0. *In* J.P. Amend, K.J. Edwards, and T.W. Lyons [eds.], Sulfur Biogeochemistry - Past and Present. Geological Society of America.

Jørgensen, B. B., and N. P. Revsbech. 1989. Oxygen uptake, bacterial distribution, and carbon-nitrogen-sulfur cycling in sediments from the baltic sea - North sea transition. Ophelia **31**: 29–49. doi:10.1080/00785326.1989.10430849

Kamp, A., D. De Beer, J. L. Nitsch, G. Lavik, and P. Stief. 2011. Diatoms respire nitrate to survive dark and anoxic conditions. Proc. Natl. Acad. Sci. U.S.A. **108**: 5649–5654. doi:10.1073/pnas.1015744108

Kamp, A., S. Høgslund, N. Risgaard-Petersen, and P. Stief. 2015. Nitrate storage and dissimilatory nitrate reduction by eukaryotic microbes. Frontiers in microbiology **6**: 1492.

Karl, D., R. Letelier, L. Tupas, J. Dore, J. Christian, and D. Hebel. 1997. The role of nitrogen fixation in biogeochemical cycling in the subtropical North Pacific Ocean. Nature **388**: 533–538.

Kartal, B., J. T. Keltjens, and M. S. M. Jetten. 2011. Metabolism and genomics of anammox bacteria, p. 179–200. *In* Nitrification. John Wiley & Sons, Ltd.

Kelso, B., R. V. Smith, R. J. Laughlin, and S. D. Lennox. 1997. Dissimilatory nitrate reduction in anaerobic sediments leading to river nitrite accumulation. Appl Environ Microbiol **63**: 4679–4685. doi:10.1128/aem.63.12.4679-4685.1997

Kennish, M. J., and V. N. de Jonge. 2011. 8.05 - Chemical introductions to the systems: Diffuse and nonpoint source pollution from chemicals (nutrients: eutrophication), p. 113–148. *In* E. Wolanski and D. McLusky [eds.], Treatise on Estuarine and Coastal Science. Academic Press.

King, D., and D. B. Nedwell. 1985. The influence of nitrate concentration upon the end-products of nitrate dissimilation by bacteria in anaerobic salt marsh sediment. FEMS Microbiology Letters **31**: 23–28. doi:10.1111/j.1574-6968.1985.tb01127.x

Kitzinger, K., C. C. Padilla, H. K. Marchant, and others. 2019. Cyanate and urea are substrates for nitrification by Thaumarchaeota in the marine environment. Nature microbiology **4**: 234–243.

Koch, H., S. Lücker, M. Albertsen, and others. 2015. Expanded metabolic versatility of ubiquitous nitrite-oxidizing bacteria from the genus *Nitrospira*. Proc. Natl. Acad. Sci. U.S.A. **112**: 11371–11376. doi:10.1073/pnas.1506533112

Könneke, M., A. E. Bernhard, J. R. de La Torre, C. B. Walker, J. B. Waterbury, and D. A. Stahl. 2005. Isolation of an autotrophic ammonia-oxidizing marine archaeon. Nature **437**: 543–546.

Kosuth, P., J. Callède, A. Laraque, N. Filizola, J. L. Guyot, P. Seyler, J. M. Fritsch, and V. Guimarães. 2009. Sea-tide effects on flows in the lower reaches of the Amazon River. Hydrological Processes **23**: 3141–3150. doi:10.1002/hyp.7387

Kozlowski, J. A., M. Stieglmeier, C. Schleper, M. G. Klotz, and L. Y. Stein. 2016. Pathways and key intermediates required for obligate aerobic ammonia-dependent chemolithotrophy in bacteria and Thaumarchaeota. The ISME journal **10**: 1836–1845.

Kuehl, S. A., D. J. DeMaster, and C. A. Nittrouer. 1986. Nature of sediment accumulation on the Amazon continental shelf. Continental Shelf Research **6**: 209–225. doi:10.1016/0278-4343(86)90061-0

Kuehl, S. A., T. D. Pacioni, and J. M. Rine. 1995. Seabed dynamics of the inner Amazon continental shelf: Temporal and spatial variability of surficial strata. Marine Geology **125**: 283–302.

Kuypers, M. M., H. K. Marchant, and B. Kartal. 2018. The microbial nitrogen-cycling network. Nature Reviews Microbiology **16**: 263–276.

Latrubesse, E. M., E. Y. Arima, T. Dunne, and others. 2017. Damming the rivers of the Amazon basin. Nature **546**: 363–369. doi:10.1038/nature22333

Leigh, J. A., and J. A. Dodsworth. 2007. Nitrogen regulation in bacteria and archaea. Annu. Rev. Microbiol. **61**: 349–377. doi:10.1146/annurev.micro.61.080706.093409

Lévy, M., O. Jahn, S. Dutkiewicz, and M. J. Follows. 2014. Phytoplankton diversity and community structure affected by oceanic dispersal and mesoscale turbulence. Limnology and Oceanography: Fluids and Environments **4**: 67–84. doi:10.1215/21573689-2768549

L'Helguen, S., C. Madec, and P. Le Corre. 1996. Nitrogen uptake in permanently well-mixed temperate coastal waters. Estuarine, Coastal and Shelf Science **42**: 803–818. doi:10.1006/ecss.1996.0051

Lin, B., Z. Liu, T. I. Eglinton, S. Kandasamy, T. M. Blattmann, N. Haghipour, and G. J. de Lange. 2019. Perspectives on provenance and alteration of suspended and sedimentary organic matter in the subtropical Pearl River system, South China. Geochimica et Cosmochimica Acta **259**: 270–287. doi:10.1016/j.gca.2019.06.018

Lisa, J. A., B. Song, C. R. Tobias, and K. A. Duernberger. 2014. Impacts of freshwater flushing on anammox community structure and activities in the New River Estuary, USA. Aquatic Microbial Ecology **72**: 17–31. doi:10.3354/ame01682

Liu, L., M. Chen, X. S. Wan, and others. 2023. Reduced nitrite accumulation at the primary nitrite maximum in the cyclonic eddies in the western North Pacific subtropical gyre. Science Advances **9**: eade2078. doi:10.1126/sciadv.ade2078

Loick-Wilde, N., S. C. Weber, B. J. Conroy, D. G. Capone, V. J. Coles, P. M. Medeiros, D. K. Steinberg, and J. P. Montoya. 2016. Nitrogen sources and net growth efficiency of zooplankton in three A mazon River plume food webs. Limnol. Oceanogr. **61**: 460–481. doi:10.1002/lno.10227

Löscher, C. R., A. Kock, M. Könneke, J. LaRoche, H. W. Bange, and R. A. Schmitz. 2012. Production of oceanic nitrous oxide by ammonia-oxidizing archaea. Biogeosciences **9**: 2419–2429. doi:10.5194/bg-9-2419-2012

MacPherson, I. 2007. Evolution of copper-containing nitrite reductase. PhD Thesis. University of British Columbia.

Malone, T. C., and A. Newton. 2020. The globalization of cultural eutrophication in the coastal ocean: Causes and consequences. Frontiers in Marine Science **7**.

Marconi, D., M. A. Weigand, and D. M. Sigman. 2019. Nitrate isotopic gradients in the North Atlantic Ocean and the nitrogen isotopic composition of sinking organic matter. Deep Sea Research Part I: Oceanographic Research Papers **145**: 109–124. doi:10.1016/j.dsr.2019.01.010

Martikainen, P. J. 2022. Heterotrophic nitrification–An eternal mystery in the nitrogen cycle. Soil Biology and Biochemistry **168**: 108611.

Martinez, J. M., J. L. Guyot, N. Filizola, and F. Sondag. 2009. Increase in suspended sediment discharge of the Amazon River assessed by monitoring network and satellite data. CATENA **79**: 257–264. doi:10.1016/j.catena.2009.05.011

Martínez-Espinosa, C., S. Sauvage, A. Al Bitar, P. A. Green, C. J. Vörösmarty, and J. M. Sánchez-Pérez. 2021. Denitrification in wetlands: A review towards a quantification at global scale. Science of The Total Environment **754**: 142398. doi:10.1016/j.scitotenv.2020.142398

McRose, D. L., X. Zhang, A. M. L. Kraepiel, and F. M. M. Morel. 2017. Diversity and activity of alternative nitrogenases in sequenced genomes and coastal environments. Frontiers in Microbiology **8**.

Milliman, J. D., and K. L. Farnsworth. 2013. River discharge to the coastal ocean: A global synthesis, Cambridge University Press.

Montanher, O. C., E. M. L. de M. Novo, and E. E. de Souza Filho. 2018. Temporal trend of the suspended sediment transport of the Amazon River (1984–2016). Hydrological Sciences Journal **63**: 1901–1912. doi:10.1080/02626667.2018.1546387

Moore, C. M., M. M. Mills, K. R. Arrigo, and others. 2013. Processes and patterns of oceanic nutrient limitation. Nature Geosci **6**: 701–710. doi:10.1038/ngeo1765

Moreno-Vivián, C., P. Cabello, M. Martínez-Luque, R. Blasco, and F. Castillo. 1999. Prokaryotic nitrate reduction: molecular properties and functional distinction among bacterial nitrate reductases. J Bacteriol **181**: 6573–6584. doi:10.1128/JB.181.21.6573-6584.1999

Mulholland, P. J., A. M. Helton, G. C. Poole, and others. 2008. Stream denitrification across biomes and its response to anthropogenic nitrate loading. Nature **452**: 202–205. doi:10.1038/nature06686

Nicholls, J., and M. Trimmer. 2009. Widespread occurrence of the anammox reaction in estuarine sediments. Aquat. Microb. Ecol. **55**: 105–113. doi:10.3354/ame01285

Nittrouer, C. A., and D. J. DeMaster. 1996. The Amazon shelf setting: tropical, energetic, and influenced by a large river. Continental Shelf Research **16**: 553–573. doi:10.1016/0278-4343(95)00069-0

Nixon, S. W. 1981. Remineralization and nutrient cycling in coastal marine ecosystems, p. 111–138. *In* B.J. Neilson and L.E. Cronin [eds.], Estuaries and Nutrients. Humana Press.

Nixon, S. W., C. A. Oviatt, J. Frithsen, and B. Sullivan. 1986. Nutrients and the productivity of estuarine and coastal marine ecosystems. Journal of the Limnological Society of Southern Africa **12**: 43–71. doi:10.1080/03779688.1986.9639398

Paasche, E., and S. Kristiansen. 1982. Nitrogen nutrition of the phytoplankton in the Oslofjord. Estuarine, Coastal and Shelf Science **14**: 237–249. doi:10.1016/S0302-3524(82)80014-5

Paerl, H. W. 2009. Controlling eutrophication along the freshwater–marine continuum: Dual nutrient (N and P) reductions are essential. Estuaries and Coasts **32**: 593–601. doi:10.1007/s12237-009-9158-8

Paerl, H. W., N. S. Hall, B. L. Peierls, and K. L. Rossignol. 2014. Evolving paradigms and challenges in estuarine and coastal eutrophication dynamics in a culturally and climatically stressed world. Estuaries and Coasts **37**: 243–258. doi:10.1007/s12237-014-9773-x

Pajares, S., and R. Ramos. 2019. Processes and microorganisms involved in the marine nitrogen cycle: Knowledge and gaps. Frontiers in Marine Science **6**: 739.

Peng, X., and D. L. Valentine. 2021. Diversity and N_2O production potential of fungi in an oceanic oxygen minimum zone. Journal of Fungi **7**: 218. doi:10.3390/jof7030218

Pham, A. H., N. Choisnard, A. Fernández-Carrera, A. Subramaniam, E. K. Strope, E. J. Carpenter, M. Voss, and J. P. Montoya. 2024. Planktonic habitats in the Amazon Plume region of the Western Tropical North Atlantic. Frontiers in Marine Science. doi:10.3389/fmars.2024.1287497

Piña-Ochoa, E., S. Høgslund, E. Geslin, and others. 2010. Widespread occurrence of nitrate storage and denitrification among Foraminifera and Gromiida. Proceedings of the National Academy of Sciences **107**: 1148–1153. doi:10.1073/pnas.0908440107

Pomeroy, L. R. 1974. The Ocean's Food Web, A Changing Paradigm. BioScience **24**: 499–504. doi:10.2307/1296885

Preisler, A., D. De Beer, A. Lichtschlag, G. Lavik, A. Boetius, and B. B. Jørgensen. 2007. Biological and chemical sulfide oxidation in a *Beggiatoa* inhabited marine sediment. The ISME journal **1**: 341–353.

Prokopenko, M. G., D. M. Sigman, W. M. Berelson, D. E. Hammond, B. Barnett, L. Chong, and A. Townsend-Small. 2011. Denitrification in anoxic sediments supported by biological nitrate transport. Geochimica et Cosmochimica Acta **75**: 7180–7199. doi:10.1016/j.gca.2011.09.023

Qin, W., S. A. Amin, W. Martens-Habbena, and others. 2014. Marine ammonia-oxidizing archaeal isolates display obligate mixotrophy and wide ecotypic variation. Proc. Natl. Acad. Sci. U.S.A. **111**: 12504–12509. doi:10.1073/pnas.1324115111

Rees, J. A., R. Bjornsson, J. Schlesier, D. Sippel, O. Einsle, and S. DeBeer. 2015. The Fe–V Cofactor of vanadium nitrogenase contains an interstitial carbon atom. Angewandte Chemie International Edition **54**: 13249–13252. doi:10.1002/anie.201505930

Richey, J. E., J. I. Hedges, A. H. Devol, P. D. Quay, R. Victoria, L. Martinelli, and B. R. Forsberg. 1990. Biogeochemistry of carbon in the Amazon River. Limnology and Oceanography **35**: 352–371. doi:10.4319/lo.1990.35.2.0352

Richey, J. E., R. H. Meade, E. Salati, A. H. Devol, C. F. Nordin, and U. D. Santos. 1986. Water discharge and suspended sediment concentrations in the Amazon River: 1982-1984. Water Resour. Res. **22**: 756–764. doi:10.1029/WR022i005p00756

Rios-Del Toro, E. E., E. I. Valenzuela, N. E. López-Lozano, M. G. Cortés-Martínez, M. A. Sánchez-Rodríguez, O. Calvario-Martínez, S. Sánchez-Carrillo, and F. J. Cervantes. 2018. Anaerobic ammonium oxidation linked to sulfate and ferric iron reduction fuels nitrogen loss in marine sediments. Biodegradation **29**: 429–442. doi:10.1007/s10532-018-9839-8

Risgaard-Petersen, N., A. M. Langezaal, S. Ingvardsen, and others. 2006. Evidence for complete denitrification in a benthic foraminifer. Nature **443**: 93–96. doi:10.1038/nature05070

Robertson, E. K., K. L. Roberts, L. D. W. Burdorf, P. Cook, and B. Thamdrup. 2016. Dissimilatory nitrate reduction to ammonium coupled to Fe(II) oxidation in sediments of a periodically hypoxic estuary: DNRA Coupled to Fe(II) oxidation. Limnol. Oceanogr. **61**: 365–381. doi:10.1002/lno.10220

Rysgaard, S., R. N. Glud, N. Risgaard-Petersen, and T. Dalsgaard. 2004. Denitrification and anammox activity in Arctic marine sediments. Limnology and Oceanography **49**: 1493–1502. doi:10.4319/lo.2004.49.5.1493

Sanford, R. A., D. D. Wagner, Q. Wu, and others. 2012. Unexpected nondenitrifier nitrous oxide reductase gene diversity and abundance in soils. Proc. Natl. Acad. Sci. U.S.A. **109**: 19709–19714. doi:10.1073/pnas.1211238109

Santos, I. R., X. Chen, A. L. Lecher, and others. 2021. Submarine groundwater discharge impacts on coastal nutrient biogeochemistry. Nat Rev Earth Environ **2**: 307–323. doi:10.1038/s43017-021-00152-0

Sarmiento, J. L., and N. Gruber. 2006. Ocean biogeochemical dynamics, Princeton University Press.

Seefeldt, L. C., B. M. Hoffman, and D. R. Dean. 2009. Mechanism of Mo-dependent nitrogenase. Annu. Rev. Biochem. **78**: 701–722. doi:10.1146/annurev.biochem.78.070907.103812

Seitzinger, S., J. A. Harrison, J. K. Böhlke, A. F. Bouwman, R. Lowrance, B. Peterson, C. Tobias, and G. V. Drecht. 2006. Denitrification accross landscapes and waterscapes: A synthesis. Ecological Applications **16**: 2064–2090. doi:10.1890/1051-0761(2006)016[2064:DALAWA]2.0.CO;2

Seitzinger, S. P., and C. Kroeze. 1998. Global distribution of nitrous oxide production and N inputs in freshwater and coastal marine ecosystems. Global Biogeochemical Cycles **12**: 93–113. doi:10.1029/97GB03657

Seitzinger, S. P., E. Mayorga, A. F. Bouwman, and others. 2010. Global river nutrient export: A scenario analysis of past and future trends. Global Biogeochemical Cycles **24**. doi:10.1029/2009GB003587

Senga, Y., K. Mochida, R. Fukumori, N. Okamoto, and Y. Seike. 2006. N_2O accumulation in estuarine and coastal sediments: The influence of H_2S on dissimilatory nitrate reduction. Estuarine, Coastal and Shelf Science **67**: 231–238. doi:10.1016/j.ecss.2005.11.021

Sharples, J., J. J. Middelburg, K. Fennel, and T. D. Jickells. 2017. What proportion of riverine nutrients reaches the open ocean? Global Biogeochem. Cycles **31**: 39–58. doi:10.1002/2016GB005483

Simon, J., and M. G. Klotz. 2013. Diversity and evolution of bioenergetic systems involved in microbial nitrogen compound transformations. Biochimica et Biophysica Acta (BBA)-Bioenergetics **1827**: 114–135.

Sioli, H. 1984. The Amazon and its main affluents: Hydrography, morphology of the river courses, and river types, p. 127–165. *In* H. Sioli [ed.], The Amazon: Limnology and landscape ecology of a mighty tropical river and its basin. Springer Netherlands.

Sippel, D., and O. Einsle. 2017. The structure of vanadium nitrogenase reveals an unusual bridging ligand. Nat Chem Biol **13**: 956–960. doi:10.1038/nchembio.2428

Slobodkina, G. B., A. V. Mardanov, N. V. Ravin, A. A. Frolova, N. A. Chernyh, E. A. Bonch-Osmolovskaya, and A. I. Slobodkin. 2017. Respiratory ammonification of nitrate coupled to anaerobic oxidation of elemental sulfur in deep-sea autotrophic thermophilic bacteria. Frontiers in microbiology **8**: 87.

Smith, E. M., and R. Benner. 2005. Photochemical transformations of riverine dissolved organic matter: effects on estuarine bacterial metabolism and nutrient demand. Aquatic Microbial Ecology **40**: 37–50. doi:10.3354/ame040037

Smith, W. O., and D. J. Demaster. 1996. Phytoplankton biomass and productivity in the Amazon River plume: Correlation with seasonal river discharge. Continental Shelf Research **16**: 291–319. doi:10.1016/0278-4343(95)00007-N

Sohm, J. A., E. A. Webb, and D. G. Capone. 2011. Emerging patterns of marine nitrogen fixation. Nature Reviews Microbiology **9**: 499–508.

Starr, L. D., M. J. McCarthy, C. R. Hammerschmidt, A. Subramaniam, M. C. Despins, J. P. Montoya, and S. E. Newell. 2022. Mercury methylation linked to nitrification in the

tropical North Atlantic Ocean. Marine Chemistry **247**: 104174. doi:10.1016/j.marchem.2022.104174

Stein, L. Y. 2019. Insights into the physiology of ammonia-oxidizing microorganisms. Current opinion in chemical biology **49**: 9–15.

Strous, M., E. Pelletier, S. Mangenot, and others. 2006. Deciphering the evolution and metabolism of an anammox bacterium from a community genome. Nature **440**: 790–794.

Subramaniam, A., P. L. Yager, E. J. Carpenter, and others. 2008. Amazon River enhances diazotrophy and carbon sequestration in the tropical North Atlantic Ocean. Proc. Natl. Acad. Sci. U.S.A. **105**: 10460–10465. doi:10.1073/pnas.0710279105

Sun, D., X. Tang, M. Zhao, and others. 2020. Distribution and diversity of comammox *Nitrospira* in coastal wetlands of China. Front. Microbiol. **11**: 589268. doi:10.3389/fmicb.2020.589268

Sunda, W. G., and W.-J. Cai. 2012. Eutrophication induced CO_2-Acidification of subsurface coastal waters: Interactive effects of temperature, salinity, and atmospheric PCO_2. Environ. Sci. Technol. **46**: 10651–10659. doi:10.1021/es300626f

Syvitski, J. P. M., A. J. Kettner, A. Correggiari, and B. W. Nelson. 2005. Distributary channels and their impact on sediment dispersal. Marine Geology **222–223**: 75–94. doi:10.1016/j.margeo.2005.06.030

Thamdrup, B. 2012. New pathways and processes in the global nitrogen cycle. Annual Review of Ecology, Evolution, and Systematics **43**: 407–428. doi:10.1146/annurev-ecolsys-102710-145048

Tikhonova, T. V., A. Slutsky, A. N. Antipov, K. M. Boyko, K. M. Polyakov, D. Y. Sorokin, R. A. Zvyagilskaya, and V. O. Popov. 2006. Molecular and catalytic properties of a novel cytochrome c nitrite reductase from nitrate-reducing haloalkaliphilic sulfur-oxidizing bacterium *Thioalkalivibrio nitratireducens*. Biochimica et Biophysica Acta (BBA)-Proteins and Proteomics **1764**: 715–723.

Trimmer, M., and P. Engström. 2011. Distribution, activity, and ecology of anammox bacteria in aquatic environments, p. 201–235. *In* Nitrification. John Wiley & Sons, Ltd.

Trowbridge, J. H., and G. C. Kineke. 1994. Structure and dynamics of fluid muds on the Amazon Continental Shelf. Journal of Geophysical Research: Oceans **99**: 865–874. doi:10.1029/93JC02860

Vajrala, N., W. Martens-Habbena, L. A. Sayavedra-Soto, A. Schauer, P. J. Bottomley, D. A. Stahl, and D. J. Arp. 2013. Hydroxylamine as an intermediate in ammonia oxidation by

globally abundant marine archaea. Proc. Natl. Acad. Sci. U.S.A. **110**: 1006–1011. doi:10.1073/pnas.1214272110

Valerio, A. M., M. Kampel, N. D. Ward, H. O. Sawakuchi, A. C. Cunha, and J. E. Richey. 2021. CO_2 partial pressure and fluxes in the Amazon River plume using in situ and remote sensing data. Continental Shelf Research **215**: 104348. doi:10.1016/j.csr.2021.104348

Van De Vossenberg, J., J. E. Rattray, W. Geerts, and others. 2008. Enrichment and characterization of marine anammox bacteria associated with global nitrogen gas production. Environmental Microbiology **10**: 3120–3129. doi:10.1111/j.1462-2920.2008.01643.x

Voss, M., N. Choisnard, M. Bartoli, and others. 2023. Coastal nitrogen cycling – Biogeochemical processes and the impacts of human activities and climate change, p. B9780323907989000421. *In* Reference Module in Earth Systems and Environmental Sciences. Elsevier.

Walker, C. B., J. R. De La Torre, M. G. Klotz, and others. 2010. *Nitrosopumilus maritimus* genome reveals unique mechanisms for nitrification and autotrophy in globally distributed marine crenarchaea. Proc. Natl. Acad. Sci. U.S.A. **107**: 8818–8823. doi:10.1073/pnas.0913533107

Wang, H., X. Ran, A. F. Bouwman, and others. 2022. Damming alters the particulate organic carbon sources, burial, export and estuarine biogeochemistry of rivers. Journal of Hydrology **607**: 127525. doi:10.1016/j.jhydrol.2022.127525

Wang, M., C. Hu, B. B. Barnes, G. Mitchum, B. Lapointe, and J. P. Montoya. 2019. The great Atlantic *Sargassum* belt. Science **365**: 83–87. doi:10.1126/science.aaw7912

Ward, B. B. 1996. Nitrification and denitrification: Probing the nitrogen cycle in aquatic environments. Microbial Ecology **32**: 247–261.

Ward, B. B. 2008. Nitrification in marine systems, p. 199–261. *In* Nitrogen in the Marine Environment. Elsevier.

Ward, B. B. 2013. How nitrogen is lost. Science **341**: 352–353. doi:10.1126/science.1240314

Ward, B. B., A. H. Devol, J. J. Rich, B. X. Chang, S. E. Bulow, H. Naik, A. Pratihary, and A. Jayakumar. 2009. Denitrification as the dominant nitrogen loss process in the Arabian Sea. Nature **461**: 78–81. doi:10.1038/nature08276

Weber, S. C., E. J. Carpenter, V. J. Coles, P. L. Yager, J. Goes, and J. P. Montoya. 2017. Amazon River influence on nitrogen fixation and export production in the western tropical North Atlantic. Limnol. Oceanogr. **62**: 618–631. doi:10.1002/lno.10448

Weber, S. C., A. Subramaniam, J. P. Montoya, H. Doan-Nhu, L. Nguyen-Ngoc, J. W. Dippner, and M. Voss. 2019. Habitat delineation in highly variable marine environments. Frontiers in Marine Science **6**: 112. doi:10.3389/fmars.2019.00112

Wells, N. S., and B. D. Eyre. 2019. δ^{15}N patterns in three subtropical estuaries show switch from nitrogen "reactors" to "pipes" with increasing degradation. Limnology and Oceanography **64**: 860–876. doi:10.1002/lno.11080

Wells, N. S., D. T. Maher, D. V. Erler, M. Hipsey, J. A. Rosentreter, and B. D. Eyre. 2018. Estuaries as sources and sinks of N_2O Across a land use gradient in Subtropical Australia. Global Biogeochemical Cycles **32**: 877–894. doi:10.1029/2017GB005826

West, T. A. P., and P. M. Fearnside. 2021. Brazil's conservation reform and the reduction of deforestation in Amazonia. Land Use Policy **100**: 105072. doi:10.1016/j.landusepol.2020.105072

Wilson, S. T., D. A. del Valle, M. Segura-Noguera, and D. M. Karl. 2014. A role for nitrite in the production of nitrous oxide in the lower euphotic zone of the oligotrophic North Pacific Ocean. Deep Sea Research Part I: Oceanographic Research Papers **85**: 47–55. doi:10.1016/j.dsr.2013.11.008

Wrage, N., G. L. Velthof, M. L. Van Beusichem, and O. Oenema. 2001. Role of nitrifier denitrification in the production of nitrous oxide. Soil biology and Biochemistry **33**: 1723–1732.

Wu, L., X. Chen, W. Wei, Y. Liu, D. Wang, and B.-J. Ni. 2020. A critical review on nitrous oxide production by ammonia-oxidizing archaea. Environ. Sci. Technol. **54**: 9175–9190. doi:10.1021/acs.est.0c03948

Wuchter, C., B. Abbas, M. J. L. Coolen, and others. 2006. Archaeal nitrification in the ocean. Proceedings of the National Academy of Sciences **103**: 12317–12322. doi:10.1073/pnas.0600756103

Xia, F., J.-G. Wang, T. Zhu, B. Zou, S.-K. Rhee, and Z.-X. Quan. 2018. Ubiquity and diversity of complete ammonia oxidizers (comammox) A.J.M. Stams [ed.]. Appl Environ Microbiol **84**: e01390-18. doi:10.1128/AEM.01390-18

Yang, W. H., B. H. Traut, and W. L. Silver. 2015. Microbially mediated nitrogen retention and loss in a salt marsh soil. Ecosphere **6**: art7. doi:10.1890/ES14-00179.1

Zakem, E. J., A. Al-Haj, M. J. Church, and others. 2018. Ecological control of nitrite in the upper ocean. Nat Commun **9**: 1206. doi:10.1038/s41467-018-03553-w

Zehr, J. P., and R. M. Kudela. 2011. Nitrogen cycle of the open ocean: From genes to ecosystems. Annu. Rev. Mar. Sci. **3**: 197–225. doi:10.1146/annurev-marine-120709-142819

Zehr, J. P., M. Mellon, S. Braun, W. Litaker, T. Steppe, and H. W. Paerl. 1995. Diversity of heterotrophic nitrogen fixation genes in a marine cyanobacterial mat. Appl Environ Microbiol **61**: 2527–2532. doi:10.1128/aem.61.7.2527-2532.1995

Zehr, J. P., and P. J. Turner. 2001. Nitrogen fixation: Nitrogenase genes and gene expression. Methods in microbiology **30**: 271–286.

Zhang, X., B. B. Ward, and D. M. Sigman. 2020. Global nitrogen cycle: Critical enzymes, organisms, and processes for nitrogen budgets and dynamics. Chem. Rev. **120**: 5308–5351. doi:10.1021/acs.chemrev.9b00613

Zhou, Z., Y. Liu, S. Wang, J. Xiao, X. Cao, Y. Zhou, and C. Song. 2023. Interactions between phosphorus enrichment and nitrification accelerate relative nitrogen deficiency during cyanobacterial blooms in a large shallow eutrophic lake. Environ. Sci. Technol. **57**: 2992–3001. doi:10.1021/acs.est.2c07599

Zumft, W. G. 1997. Cell biology and molecular basis of denitrification. Microbiol Mol Biol Rev **61**: 533–616. doi:10.1128/mmbr.61.4.533-616.1997

Scientific outreach

Publications in peer-reviewed journals

Choisnard, N, Sperlea, T., Liskow, I., & Voss, M. (2024). Nitrification in the Amazon River plume. Marine Ecology Progress Series. https://doi.org/10.3354/meps14530

Pham, A. H., Choisnard, N., Fernández-Carrera, A., Subramaniam, A., Strope, E. K., Carpenter, E. J., et al. (2024). Planktonic habitats in the Amazon Plume region of the Western Tropical North Atlantic. Frontiers in Marine Science. https://doi.org/10.3389/fmars.2024.1287497

Choisnard, N, Duprey, N. N., Wald, T., Thibault, M., Houlbrèque, F., Foreman, A. D., et al. (2024). Tracing the fate of seabird-derived nitrogen in a coral reef using nitrate and coral skeleton nitrogen isotopes. Limnology and Oceanography, n/a(n/a). https://doi.org/10.1002/lno.12485

Choisnard, N, Burtscher, E., Forster, S., Frey, C., Moros, M., & Voss, M. (2023). The Amazon shelf sediments, a reactor that fuels intense nitrogen cycling at the seabed. Limnology and Oceanography, 68(10), 2211–2226. https://doi.org/10.1002/lno.12416

Thibault, M., Houlbreque, F., Duprey, N. N., Choisnard, N., Gillikin, D. P., Meunier, V., et al. (2022). Seabird-derived nutrients supply modulates the trophic strategies of mixotrophic corals. Frontiers in Marine Science, 8, 790408. https://doi.org/10.3389/fmars.2021.790408

Non peer-reviewed publications

Voss, M., Choisnard, N., Bartoli, M., Bonaglia, S., Bourbonnais, A., Frey, C., et al. (2023). Coastal nitrogen cycling – Biogeochemical processes and the impacts of human activities and climate change. In Reference Module in Earth Systems and Environmental Sciences (p. B9780323907989000421). Elsevier. https://doi.org/10.1016/B978-0-323-90798-9.00042-1

Manuscript submitted or in preparation

N. Choisnard, J. Umbricht, M. Araujo, M. E. Böttcher,C. Burmeister, I. Liskow, I. Schmiedinger, M. Voss. Nitrogen assimilation and recycling in surface waters of the Amazon and Pará Estuaries. Submitted to Journal of Geophysical Research - Oceans

Talk and poster presentations

Choisnard N., Mohrholz V., Heene T., Mars R., Umbricht J., Voss M. Nitrate dual isotopes reveal the source and cycling of Nitrate in the Amazon River Mouth. Talk at the Aquatic Science meeting, 2023.

Voss M., Choisnard N., Loick-Wilde N., Mohrholz V., Subramaniam A. , Umbricht J., Montoya JP. Physical observations and fate of nutrients in the Amazon River plume. Talk at the Aquatic Science meeting, 2023.

Umbricht J., Benavides M., Choisnard N., Montoya J. P., Subramaniam A., Voss M. Ammonium fuels a large proportion of the primary production in the Amazon River plume. Talk at the Aquatic Science meeting, 2023.

Choisnard, N., Umbricht J., Liskow I., Mohrholz V., Voss M. N-cycling in the Amazon Estuary. Poster at the Leibniz Institute for Baltic Sea Research, midterm audits, August 29-31 2023, Warnemuende, Germany

Umbricht J., Burmeister C., Choisnard N., Liskow I., Montoya JP., Subramaniam A., Voss M. An evaluation of the nitrogen sources supporting phytoplankton production in the Amazon River plume. Talk at the Ocean Science Meeting, 2022.

Choisnard N., Umbricht J., Voss M. Nitrification contribution to the N-budget of the Amazon Estuary. Talk at the Ocean Science Meeting, 2022.

Datasets

Choisnard, Noémie; Umbricht, Jacqueline; Voss, Maren: Contibution of various Nitrogen cycle processes to the nitrogen budget of the Amazon and Pará estuaries of METEOR cruise M174. PANGAEA, https://doi.pangaea.de/10.1594/PANGAEA.965416

Choisnard, Noémie; Umbricht, Jacqueline; Voss, Maren: Updated pelagic nitrogen budget of the Amazon and Pará estuaries of METEOR cruise M174. PANGAEA, https://doi.pangaea.de/10.1594/PANGAEA.965427

Choisnard, Noémie; Böttcher, Michael Ernst; Liskow, Iris; Schmiedinger, Iris; Voss, Maren: Nitrate $\delta^{15}N$ and $\delta^{18}O$, and water $\delta^{2}H$ and $\delta^{18}O$ stable isotopes of METEOR cruise M174. PANGAEA, https://doi.pangaea.de/10.1594/PANGAEA.965429

Choisnard, Noémie; Moros, Matthias; Voss, Maren (2023): Porewater nutrients in sediment cores from the Amazon shelf obtained in April/May 2021 during RV METEOR cruise M174. PANGAEA, https://doi.org/10.1594/PANGAEA.961274

Choisnard, Noémie; Moros, Matthias; Voss, Maren (2023): Sediment solid phase characteristics on the Amazon shelf obtained in April/May 2021 during RV METEOR cruise M174. PANGAEA, https://doi.org/10.1594/PANGAEA.961264

Choisnard, Noémie; Moros, Matthias; Voss, Maren (2023): Nutrient fluxes at the sediment-water interface in the Amazon shelf obtained in April/May 2021 during RV METEOR cruise M174. PANGAEA, https://doi.org/10.1594/PANGAEA.961275

Choisnard, Noémie; Duprey, Nicolas N; Wald, Tanja; Houlbrèque, Fanny; Foreman, Alan D; Cuet, Pascale; Guillaume, Mireille MM; Vonhof, Hubert; Sigman, Daniel M; Haug, Gerald H; Maguer, Jean Francois; L'Helguen, Stephane; Martínez-García, Alfredo; Lorrain, Anne, 2023, "Replication Data for: Tracing the fate of seabird-derived-nitrogen in a coral reef using nitrate and coral skeleton nitrogen isotopes", https://doi.org/10.7910/DVN/QSHDVR, Harvard Dataverse

Thibault, Martin; Houlbreque, Fanny; Duprey, Nicolas N; Choisnard, Noémie; Gillikin, David; Meunier, Valentine; Benzoni, Francesca; Ravache, Andreas; Lorrain, Anne, 2021, "Data for: Seabird-derived nutrients supply modulates the trophic strategies of mixotrophic corals", https://doi.org/10.23708/INWSD6, DataSuds

Author contribution

The three scientific papers that are part of this thesis are either accepted or submitted to peer-reviewed journals. Chapter two and three are first author papers, where I conceived and designed the research, and contributed to the data collection and interpretation. Chapter four is a shared first authorship, I contributed 50 % to the study design, data collection and interpretation. I authored the initial drafts for all three manuscripts.

.....	.....	.....
(Place)	(Date)	(Signature of the author)

.....	.....	.....
(Place)	(Date)	(Signature of the supervisor)

Declaration of authorship

I hereby declare the following:

1. The opportunity for this PhD project was not communicated commercially to me. In particular, I have not engaged any organization that, for money, seeks supervisors for the drawing up of dissertations or that performs, entirely or partially on my behalf, the duties incumbent upon me regarding the examinations.

2. I hereby declare under oath that I have completed the work submitted here independently and have composed it without outside assistance. Furthermore, I have not used anything other than the resources and sources stated. In cases where I have incorporated content or text from these works, I have duly acknowledged it.

.....	.....	.....
(Place)	(Date)	(Signature)